Functional genomic screening to unravel mechanisms underlying resistance to conventional induction therapy in T-cell acute lymphoblastic leukaemia

Melanie Beckett

Doctor of Philosophy

Wolfson Childhood Cancer Research Centre

Northern Institute for Cancer Research

Faculty of Medical Sciences, Newcastle University

Abstract

Long term cure is achieved in more than 80% of children with T-cell acute lymphoblastic leukaemia (T-ALL), which can be attributed to the refinement of intensive, MRD driven, chemotherapy regimens. However, poor response to induction therapy is associated with unfavourable outcomes. Vincristine, Dexamethasone, Asparaginase and Daunorubicin (VXLD) form the cornerstone of T-ALL induction therapy. Identifying mechanism of resistance to induction chemotherapy could help us improve the efficacy of treatment and outcomes for patients with poor response to current therapy.

This project aimed to develop a preclinical model which allowed the identification of pathways underlying drug resistance to T-ALL induction therapy and inform the development of a more targeted approach to reduce disease burden in refractory disease.

This thesis describes the optimisation of a 4 drug treatment regimen in Rag2$^{-/-}$ gamma c$^{-/-}$ mice that mirrors the clinical induction protocol. This preclinical *in vivo* model has utility both as a model to explore drug resistance as well as a benchmark to assess efficacy and toxicity of new compounds or drug combinations. In this work the established *in vivo* model of induction therapy was combined with CRISPR screening to identify mechanisms of chemo-resistance.

The MAGeCKFlute algorithm was used to identify differential representation of CRISPR guide RNAs under VXLD treatment pressure, and identified several interconnecting pathways in the generation of chemo-resistance. The role of the apoptotic regulator BCL-X was further investigated, as gene specific guides were depleted (suggestive of drug target). Targeted inhibition of BCL-X has already entered the clinical arena, and may provide a means to overcome induction resistance.

The successful development of this preclinical model incorporating VXLD chemotherapy has increased our understanding of T-ALL biology and identified potential drug resistance mechanisms. Further work will focus on the validation of these putative drug targets which may revert induction failure in future therapeutic approaches.

Dedication

To

my family

both old

new

and

furry

Acknowledgments

Firstly, I would like to thank my supervisor Dr Frederik van Delft for his encouragement, patience, advice and his ability to tackle everything with a smile. Secondly, I would like to thank the other members of our T-cell leukaemia team both past and present for their guidance on various laboratory techniques. I would like to thank Professor Dr Olaf Heidenreich for his amazing ability to troubleshoot any issues and the vast array of knowledge he imparted.

I would like to acknowledge the generosity and patience of Dr Helen Blair who taught me every technique I needed for my *in vivo* work. She has been my unofficial supervisor for everything mouse related and more. She has been both role model and friend, and I am incredibly grateful to have worked with her. I would also like to thank Mankaran Singh and Philip Berry for very kindly giving up their time running my pharmacokinetic samples for me. Next, I would like to thank Chris, Jill and Huw for performing IV injections for me. Furthermore, I would like to thank all the members of the leukaemia stem cell group who helped harvest tissues and count cells, without a group effort I would not have managed to collect all my *in vivo* samples.

I am grateful to Katie, Matt, Ruth and Kasia for all their CRISPR screening related advice. I would like to thank Rin for bioinformatics support, and Amir and Matt for their advice on using R. A special thank you to Ed for helping correct my grammar and setting me straight when it comes to synergy. Thanks also to my fellow PhD students: Ricky, Asmida and Yuzhe for PCR, lentivirus, flow cytometry and emotional support.

I would like to thank those people who inspired me to do research both when things were going well, and most importantly when they were not. Thank you, Vicky, Vikki and Deepali. Lastly, I would like to thank my parents and partner for standing by me throughout this process

Abbreviation	description
ALL	Acute lymphoblastic leukaemia
AML	Acute myeloid leukaemia
Asp	Asparaginase
B-ALL	B-cell acute lymphoblastic leukaemia
BLI	Bioluminescent imaging
CI	Combination index
CLL	Chronic lymphocytic leuakemia
CLP	Common lymphoid progenitor
C_{max}	maximum concentration
CRISPR	Clustered regularly interspaced short palindromic repeats
Dauno	Daunborubicin
Dex	Dexamethasone
DN	CD4-CD8- double negative T-cell
DSB	Double stranded break
GC	Glucocorticoid
GI	Growth inhibtion
GR	Glucocorticoid Receptor
IF	Intrafemoral
indels	Insertions and deletions
IP	Intraperitoneal
IV	Intravenous
IVIS	*In vivo* imaging system
mRNA	Messenger RNA

NHEJ	Non-homolgous end joining
PAM	Protospacer adjacent motif
PBS	Phosphate buffered saline
PDX	Patient derived xenograft
PK	Pharmacokinetic
preTCR	pre T-cell receptor
qRT-PCR	Quantitative Reverse Transcription PCR
RNAi	RNA interfernce
ROS	Reactive oxygen species
sgRNA	single guide RNA
shRNA	Short-hairpin RNA
siRNA	Small interfering RNA
T-ALL	T-cell acute lymphoblastic leukaemia
TCR	T-cell receptor
Vinc	Vincristine
VXLD	Vincristine, Dexamethasone, Asparaginase and Daunorubicin

Contents

Table of figures

Table of tables

Chapter 1. Introduction

1.1 Acute lymphoblastic leukaemia

Acute lymphoblastic leukaemia or ALL is a cancer of immature lymphocytes and can occur in both adults and paediatric patients. Patients present with bone pain, frequent infections, bruising and anaemia with high white blood cell counts. ALL more commonly originates from B-cells and this is known as B-ALL. In 10-15% of children and 25% of adults ALL is derived from T-cells (Lustosa de Sousa et al., 2015, Chiaretti et al., 2014, Vora et al., 2014). ALLs derived from T-cells display characteristics of immature T-lymphocytes (which is determined at diagnosis) and this type of ALL is known as T-ALL.

T-ALL and B-ALL have many similarities in presenting symptoms and treatment strategies. However, they exhibit differences in their common mutations, median age range at presentation and risk of relapse, which is not unexpected considering the divergent development of B and T cells.

1.2 T-cell acute lymphoblastic leukaemia

T-ALL can originate from any of the stages of T-cell development from common lymphoid progenitors (CLPs) through to $CD4^+CD8^+$ double positive T-cells. A basic overview of T-cell development is shown in figure 1.1. CLPs derived from haematopoietic stem cells in the bone marrow travel to the thymus. In the thymus, NOTCH signalling helps drive progenitors towards the T-cell lineage. Lymphoid progenitor cells move to the thymus where their development into T-cells continues. The immature T-cells undergo rearrangement of their t-cell receptor (TCR) genes. The alpha and beta chain loci each consist of variable, diversity, junctional and constant gene segments flanked by recombination signal sequences (Krangel, 2009). Segments are joined by somatic recombination. Successfully rearranged beta chains are expressed alongside a surrogate alpha chain (the preTCRα), and together they form the pre-T-cell receptor (preTCR). Expression of preTCR confirms correct rearrangement of pre-T-cell receptor beta and provides survival signals to the cell. Rearranged alpha and beta chain form a heterodimer known as the αβ T-cell receptor (TCR). TCRs and preTCRs are important signalling complexes in developing T-cells. A small number of T-cells have a TCR composed of gamma and delta chains and are referred to as gamma delta (γδ) T-cells. The δ locus is found

between the V and J segments of the TCR α locus, and rearrangements of α locus leads to loss of the δ locus (Krangel, 2009).

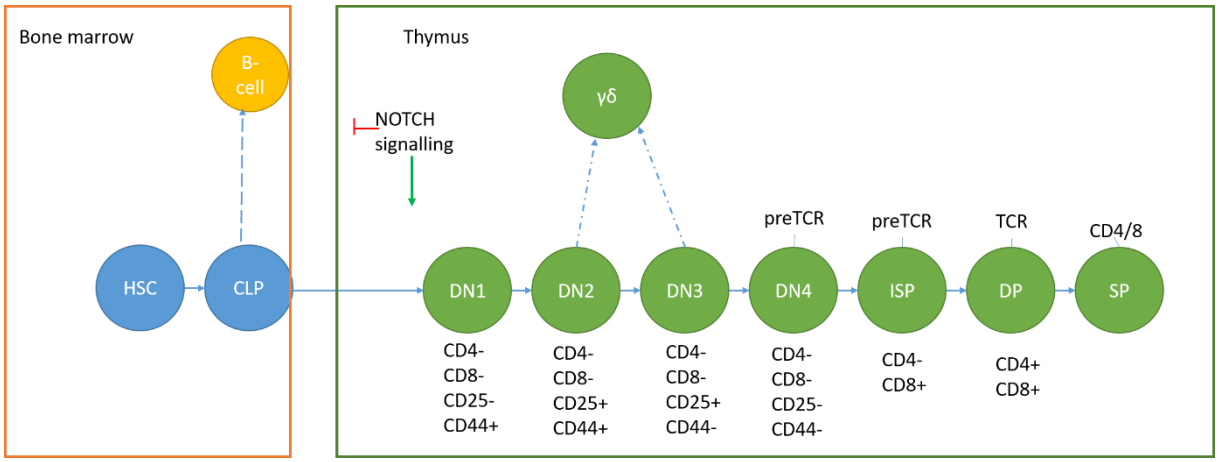

Figure 1.1 T-cell development. Initiated in the bone marrow, common lymphoid progenitors (CLPs) derived from haematopoietic stem cells (HSCs), migrate to the thymus where their development continues. NOTCH signalling pushes cells toward a T-cell route of development. The immature T-cells undergo rearrangement of their t-cell receptor (TCR) genes. Expression of a pre-T-cell receptor (preTCR) confirms correct rearrangement of the T-cell receptor beta chain locus. The alpha chain is then rearranged before formation of the mature T-cell receptor. In a minority of T-cells TCR is formed from γ and δ chains. Both preTCR and TCR are important signalling complexes in developing T-cells. The stage of development of a T-cell can also be determined by expression of cluster of differentiation genes (Rosewicz et al.).

The rearrangement of T-cell receptor genes can be utilised to study clonality in T-ALL(Hodges et al., 2003). TCR and pre-TCR status combined with cluster of differentiation expression, can be used to identify the differentiation stage of the T-cell from which T-ALL developed.

T-ALL can be divided into subgroups based on aberrant transcription factor expression, which is often generated by chromosomal rearrangements. The most common chromosomal re-arrangements are translocation of a transcription factor to a t-cell receptor (TCR) gene locus. Nearly 80% of T-ALL patients have oncogenic rearrangements, but aberrant transcription factor expression can also be attributed to duplication, amplification, or generation of novel enhancers via mutations (van der Zwet et al., 2019). Commonly altered transcription factors in T-ALL are: T-Cell Acute Lymphocytic Leukemia Protein 1 (TAL1), T Cell Leukemia Homeobox 1 (TLX1), T Cell Leukemia Homeobox 1 (TLX3), MYB, LIM domain only 2 (LMO2), Homeobox

cluster A (HOXA) and NK2 homeobox 1/ NK2 homeobox 2 (NKX2.1/NKX2.2). Their relative frequencies are shown in figure 1.2. Ectopic transcription factor expression can be an initiating event in T-ALL development or contribute to self-renewal properties and differentiation arrest prior to the acquisition of required additional mutations to lead to leukaemia (Dadi et al., 2012, Gerby et al., 2014, De Keersmaecker et al., 2010).

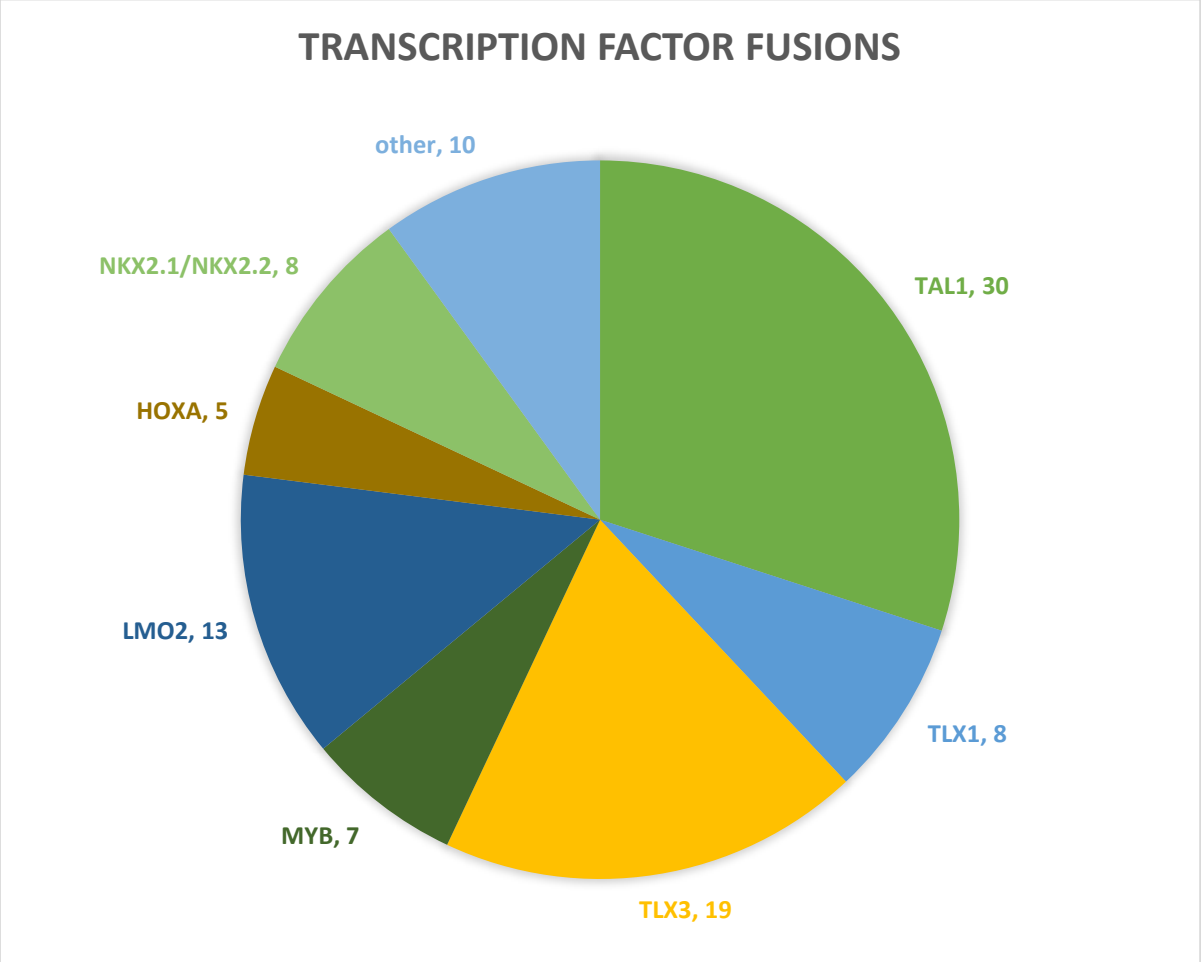

Figure 1.2 Transcription factor aberrations in T-ALL. T-ALL can be grouped according to altered expression of transcription factors due to translocations. Shown are the most common translocations and their relative percentages (Chen et al., 2018, Downing et al., 2012, Girardi et al., 2017, Neumann et al., 2015)

Genome-wide expression analysis has helped broaden our understanding of ectopic transcription factor expression in T-ALL and helped categorise the T-ALL into subgroups. Ectopic expression of LYL1 was identified through such studies as T-ALL patients with LYL1 expression do not have rearrangements of *LYL1* (Ferrando et al., 2002).

Recent studies categorise T-ALL into 4 main subgroups: immature, TLX, proliferative and TALLMO (van der Zwet et al., 2019). The immature group also referred to as early T-cell precursor (ETP) is associated with high expression of self-renewal genes found in haematopoietic stem cells. This group is characterised by high BCL2, LYL1, LMO2, HHEX and MEF2C expression (Homminga et al., 2011, McCormack et al., 2010).

The second key subgroup is the TLX group. Most patients in the TLX group have a chromosomal rearrangement involving TLX3. The most common fusion partner for TLX3 is BCL11B- which is involved in the commitment of T cell progenitors to the αβ lineage. TLX3 is placed near the BCL11B enhancer, both driving TLX3 expression and inactivating one copy of BCL11B. TLX3-BCL11B rearrangements may impair αβ lineage development and therefore drive a γδ lineage, which is consistent with the finding that patients with this fusion normally either express γδ TCR or lack TCR surface expression. This group also contains patients with events that activate HOXA such as: *SET-NUP214, PCALM-MLLT10* and *MLL* fusions.

Although researchers have previously grouped *TLX3* rearrangements with *TLX1* rearrangements, *TLX1* rearranged patients have a distinct expression patterns to *TLX3* rearranged patients and are now considered a separate subtype -referred to as the proliferative type (Dadi et al., 2012, van der Zwet et al., 2019). A proliferative gene signature also encompasses patients with *NKX2-1* translocations.

The last and largest subtype is the TALLMO. TAL1 and TAL2 form transcription complexes with E2A/HEB, RUNX1, GATA3 and MYB co-factors in normal erythroid precursors. In T-ALL these cofactors bridged by LMO1 or LMO2 drive expression of cell cycle genes (such as CDK6*)*, cell survival genes (such as TRIB2*)* and genes associated with transcriptional control (such as ETS family members) (Tan et al., 2019). In addition to recurrent translocations to *TAL1*, small insertion deletion mutations have been seen upstream of *TAL1, LMO1 and LMO2* creating a *MYB* binding site and resulting in the assembly of a super enhancer complex (Mansour et al., 2014).

In addition, to the aberrations and mutations driving the gene expression changes which separate T-ALL subgroups there are a number of other common mutations found in T-ALL patients , a list of the most common are given in table 1.1 (Liu et al., 2017).

Mutation	Frequency % (Liu et al., 2017)	Pathway
NOTCH1	Translocation- rare less than 1% Mutation- 75%	T-cell lineage commitment
FBXW7	24%	NOTCH signalling
PHF6	19%	Transcriptional regulation
USP7	12%	Regulation of P53
DNM2	11%	Vesicle formation and endocytosis
BCL11B	10%	Transcription factor, T-cell differentiation and survival
NRAS	8%	Cell division and differentiation
JAK3	18% in adults	Type 1 cytokine receptor signalling
IL7R	7%	T-cell development and homeostasis
CDKN2A	70-80%	Cell cycle regulation
P53	5%	Cell cycle and apoptosis
PTEN	14%	Regulator of PI3K-AKT pathway

Table 1.1 Common gene mutations in T-ALL. Mutations found in T-ALL their frequencies, and the pathways affected are listed.

Although frequencies differ between age groups and specific studies, there are always two frequently identified mutations, namely in *NOTCH1* and *CDKN2A* (Liu et al., 2017, Girardi et al., 2017, Marks et al., 2009).

1.2.1 NOTCH signalling

NOTCH1 is a class 1 transmembrane glycoprotein that binds to the delta-like and serrate family of ligands on neighbouring cells. NOTCH1 has an N-terminal extracellular domain with epidermal like growth factor repeats, which is where ligands bind (figure 1.3) (Steinbuck and Winandy, 2018). NOTCH1 has two cleavage sites, one in the homology domain where cleavage is by extracellular metalloproteinases such as integrin and metalloproteinase domain-containing proteins 10 and 17 (ADAM10 and ADAM17) (Brou et al., 2000). The second site is at the membrane, cleaved by γ-secretase complex to release NOTCH1 from the membrane (De Strooper et al., 1999, Tosello and Ferrando, 2013). The cleaved intracellular NOTCH1 can translocate to the nucleus, where via binding with signalling complexes; it regulates transcription of target genes. The NOTCH1 protein contains a PEST domain which limits NOTCH signalling by targeting the receptor for proteasome mediated degradation via F-box/WD repeat-containing protein 7 (FBXW7) mediated ubiquitination (Wu et al., 2001, Thompson et al., 2007, O'Neil et al., 2007, Akhoondi et al., 2007).

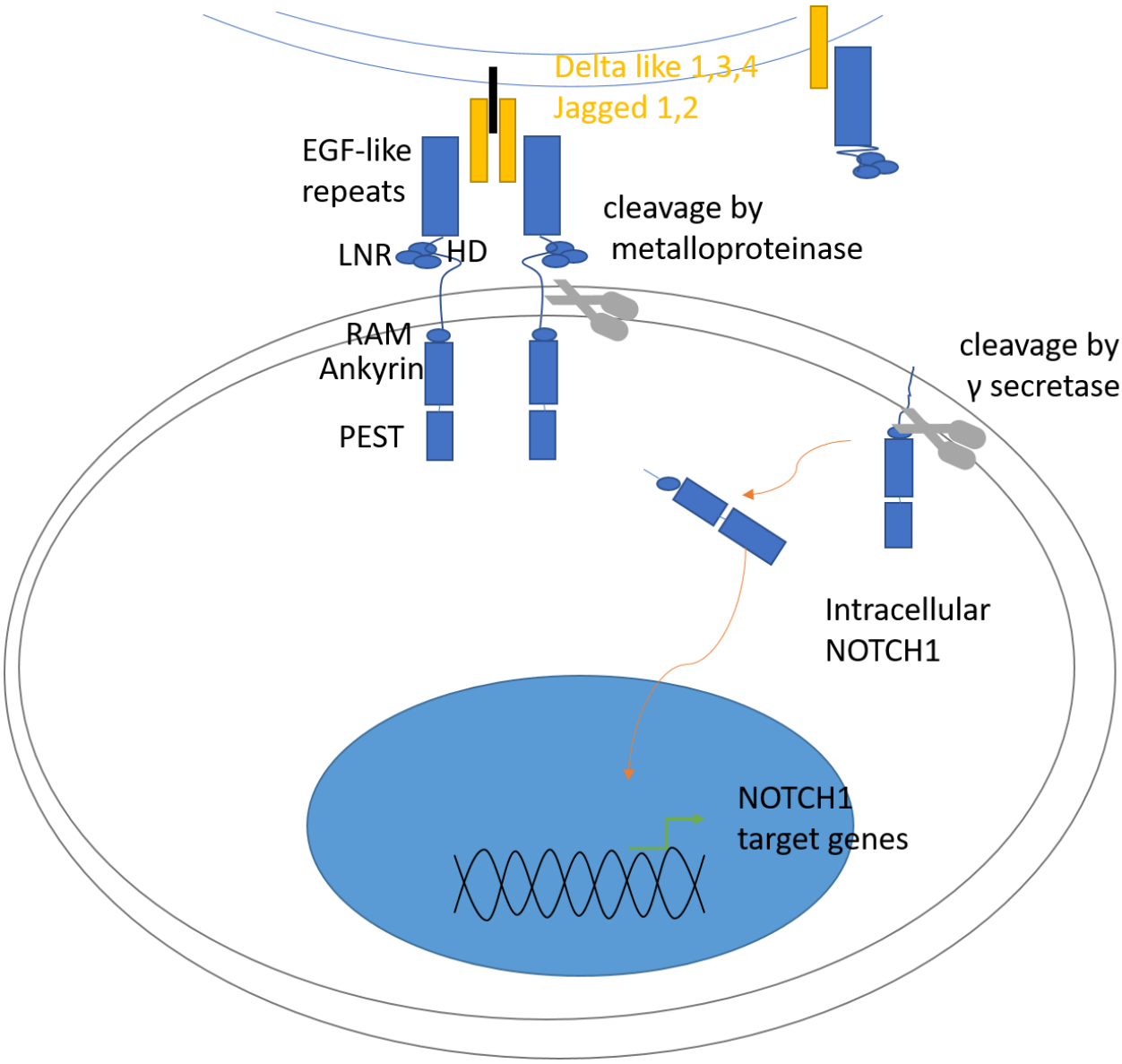

Figure 1.3 NOTCH1 signalling. *NOTCH1 consists of a domain with EGF-like repeats where ligands such as delta like 1,3 and 4 or Jagged 1 and 2, a heterodimerization domain (HD), 3 LIN-12/NOTCH repeats (LNR), a RAM domain (RAM), ankyrin repeats (ankyrin), transactivation domain (Saigusa et al.) and PEST domain (PEST). Interaction of NOTCH1 with ligand triggers a conformational change exposing a cleavage site for metalloproteinases. The cleavage by metalloproteinase leaves a truncated protein with a short extracellular domain. Subsequently a second cleavage by γ secretase releases the intracellular part of NOTCH1. NOTCH1 (ICN1) can then translocate to the nucleus where it interacts with co-activators to activate expression of target genes (Tosello and Ferrando, 2013).*

NOTCH1 is an important driver in T-ALL. Constitutive activation of NOTCH1 was first observed due to a translocation that juxtaposed NOTCH1 (without the extracellular domains) next to the T-cell receptor beta gene (TCRB) (Ellisen et al., 1991). NOTCH1 translocation has since been found to be a relatively rare occurrence in T-ALL (1%), however activating mutations in NOTCH1 are very common (75%) and occur most frequently in the heterodimerisation and PEST domains (Weng et al., 2004a). NOTCH1 controls the transcription of many different genes contributing to a vast range of effects, ultimately leading to increased survival, growth and proliferation (figure 1.4) (Leong and Karsan, 2006, Ferrando, 2009).

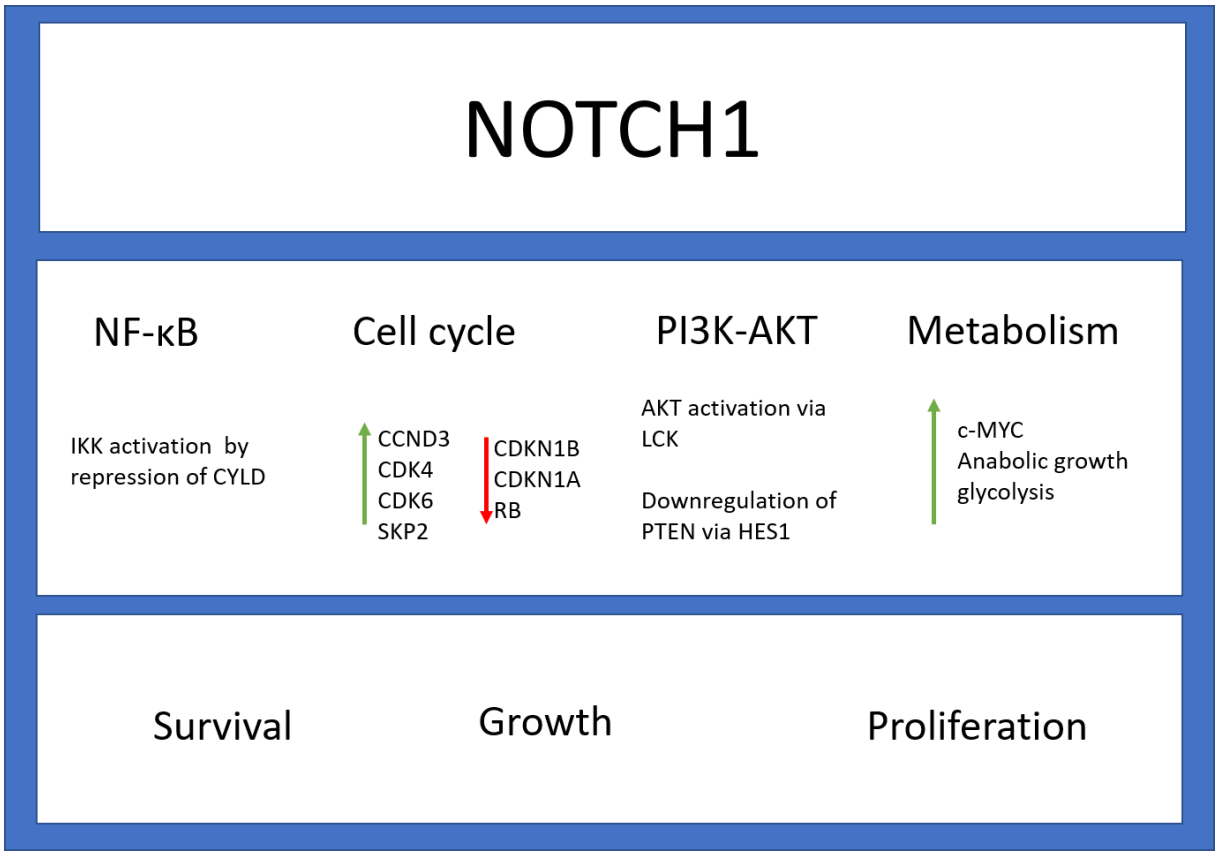

Figure 1.4 **Common pathways associated with NOTCH1 signalling.** Some of the key pathway associated with downstream signalling of NOTCH1 are summarised (Ferrando, 2009, Leong and Karsan, 2006, Tosello and Ferrando, 2013)

1.2.2 CDKN2A

Like *NOTCH1, CDKN2A* is commonly mutated in T-ALL. Located at 9p21.3, copy number alterations are frequently found in this region in many cancer types. *CDKN2A* encodes $P16^{INK4A}$ also known as P16 (Genescà et al., 2018) and $P14^{ARF}$. P16 discovered in 1993 as an interactor with CDK4, it is now one of the most highly studied genes due to its role in cancer (Serrano et al., 1993, Kamb et al., 1994). P16 inhibits cyclin dependant kinases (CDK) 4 and 6, preventing the phosphorylation of retinoblastoma protein (RB) causing a halt in cell cycle progression (Shapiro et al., 1995, Li et al., 2011(Topacio et al., 2019). P16 also acts to inhibit the phosphorylation of the carboxy-terminal domain of RNA polymerase II via its interaction with the TFIIH (Transcription factor II Human) complex (involved in transcription of protein coding genes and nucleotide excision repair) (Nishiwaki et al., 2000, Serizawa, 1998). Lastly, P16 has also been reported to suppress the kinase activity of c-jun N-terminal kinases (JNK) 1 and 3 (Choi et al., 2005). P14 is also involved in cell cycle regulation and inhibits Mouse double minute 2 homolog (MDM2), which consequently increases the action of P53 (Xirodimas et al., 2002). P14 is also found in the nucleolus. It was originally thought its function there was sequestering MDM2 but it is now thought that it has a role in ribosome biogenesis (Rizos et al., 2006). Despite the importance of P16 and P14, adult patients with *CDKN2A* copy number aberrations have actually been shown to respond better to induction therapy than those without (Genescà et al., 2018).

1.3 T-ALL treatment and treatment resistance

Standard treatment for ALL is based around the Berlin-Frankfurt-Münster (BFM) backbone; it includes induction, consolidation, interim maintenance, delayed intensification and maintenance periods with each stage comprising different chemotherapeutics and doses (figure 1.5).

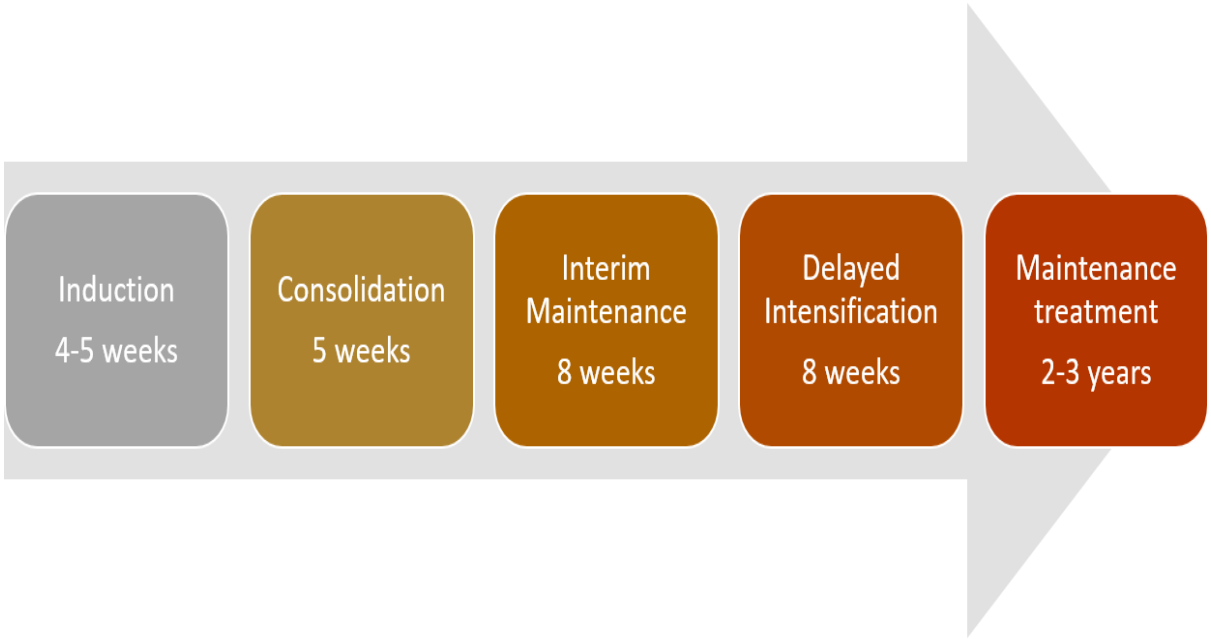

Figure 1.5 Treatment phases for paediatric ALL. Treatment starts with an induction phase, followed by consolidation, interim maintenance, delayed intensification and concludes with a maintenance treatment. Approximate timescales for each phase are given.

The core chemotherapeutic agents have remained relatively unchanged, with a focus on better stratification of patients and improved dosing schedules providing the greatest improvement in outcome (Cooper and Brown, 2015). Historically, T-ALL had a worse prognosis than B-ALL, although this is no longer the case; a T-cell immunophenotype alone puts patients into an intermediate risk group with more intensive chemotherapy than is used for good risk B-ALL (Seibel et al., 2008). Table 1.2 summarises the most recent UK-based clinical trials that T-ALL patients were treated on. These trials all have similarities in the chemotherapy backbone and share most of the same core chemotherapeutics, with additional agents being added to an existing regimen including in relapse trail ALLR3.

Trial	Eligibility	Treatment trailed	Outcome	References
UKALL2003	Children/ young adults with ALL	Treatment modification according to risk status to assign to regimen A,B or C which have increasing intensities	Reduction is feasible for ALL with low risk of relapse and rapid clearance of MRD Patients with end of induction MRD of 0·01% or more can benefit from augmented therapy	(Goulden et al., 2017) (Vora et al., 2013)
UKALL2011	Children /young adults with ALL, NHL or LBL	14-day high dose dexamethasone v. 28 day lower dose in induction. Changes to maintenance therapy to improve CNS prophylactic treatment	No statistically significant difference in steroid related toxicity, MRD response or relapse free survival between arms	(Jackson et al., 2019)
Interfant-06	365 days or younger with ALL	Consolidation with myeloid-style v lymphoid-style chemotherapy, on the backbone of Interfant chemotherapy	Post-induction myeloid-type chemotherapy courses did not significantly improve outcome for infant ALL	(Pieters et al., 2019)
UKALL14	Adults with ALL	Nelarabine or no nelarabine with induction (for T-ALL)		(NIH, 2019)
ALLR3	Children with refractory or relapsed ALL	Idarubicin or mitoxantrone alongside the usual chemotherapy drugs in induction for relapsed ALL	Mitoxantrone better than idarubicin (OS 3 years) 69% mitoxantrone 45.2% Idarubicin)	(Parker et al., 2010)
EsPhALL	Children /adolescents with Philadelphia positive ALL	Post induction imatinib treatment	4 year disease free survival good risk ALL with imatinib:72.9% Without imatinib : 61.7%	(Biondi et al., 2012)

Table 1.2 Recent trials recruiting T-ALL patients in the UK. For each trial the eligibility, key treatment and outcome are summarised and where data is available that outcome is also given.

Current treatment protocols achieve overall survival rates in children of over 80% and around 50% in adults (Patrick et al., 2014, Winter et al., 2018, Marks et al., 2009, Vora et al., 2014). Relapsed and refractory ALL on the other hand offers a very poor prognosis (Raetz et al., 2008, Bartram et al., 2019). Considering all the stages of chemotherapy, response to induction (as measured by MRD) is the most predictive of outcome (Gaynon et al., 1997, Goldberg et al., 2003, Schrappe et al., 2012, Ratei et al., 2008 (Bartram et al., 2019).

1.3.1 Induction therapy in ALL

Prior to commencement of therapy, children are stratified by their risk categorisation to different treatment regimens. Risk is determined by factors such as age, white blood cell count, immunophenotype and cytogenetic abnormalities. There are 3 main treatment regimens: A, B and C which have increasing intensity. Risk stratification was introduced in the ALL97/99 trial and has since become more refined (Mitchell et al., 2009, Goulden et al., 2017). Most T-ALL patients are allocated to regimen B. The first stage in the treatment of childhood ALL is induction therapy. Part of the treatment schedule for a patient on regimen B from UKALL2003 is shown in figure 1.6 below. Regimen B follows a 4-drug induction protocol with the addition of daunorubicin to the 3-drug induction found in regimen A (which consists of dexamethasone, vincristine and asparaginase).

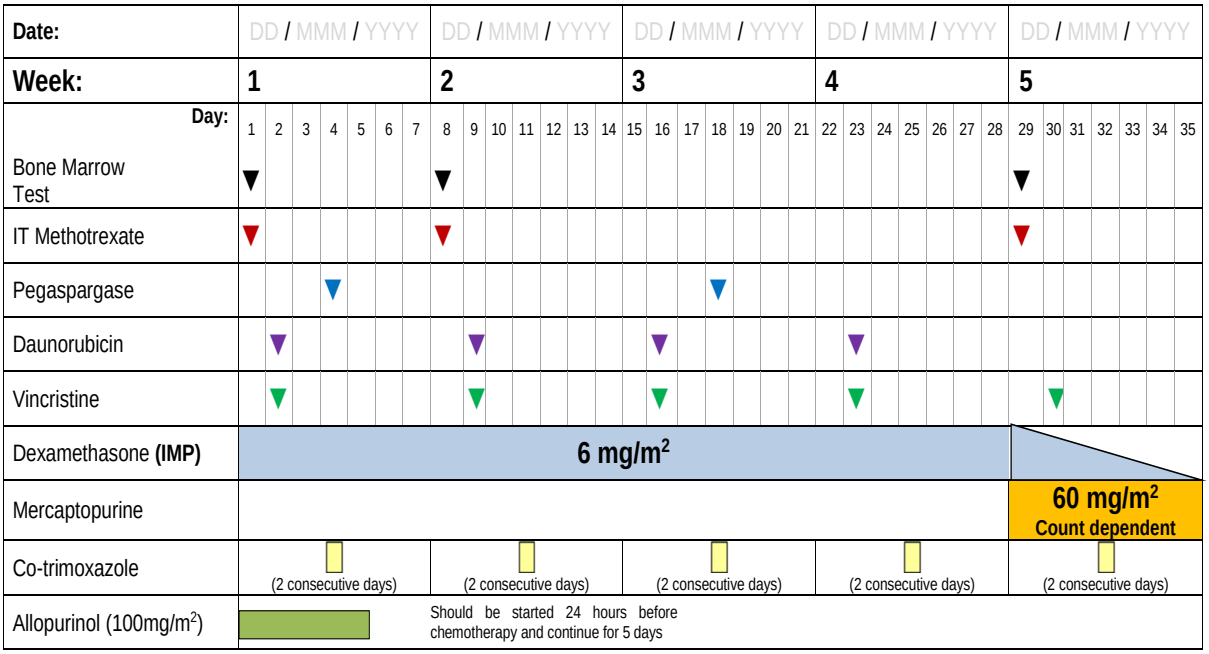

Figure 1.6 UKALL2003 regimen B induction. The first 5 weeks of therapy on regimen B are shown on a day by day basis. Key chemotherapeutics and the days they are given, and where additional medications such as Co-trimaxazole to treat infection and Allopurinol for high uric acid levels are also given. Multiple bone marrow tests were performed as indicated by the black triangles to measure minimal residual disease.

Response to induction therapy (as measured by minimal residual disease (MRD)) is a predictor of outcome, therefore resistance to induction therapy drugs- vincristine, dexamethasone, asparaginase and daunorubicin (VXLD) is of significant interest (Gaynon et al., 1997, Goldberg et al., 2003, Schrappe et al., 2012, Ratei et al., 2008).

1.3.2 Vincristine

Vincristine is a vinca alkaloid, a family of compounds comprised of 2 multi-ringed units. Vinca alkaloids tumour killing properties were identified in 1959 and vinca alkaloids have been used in the clinic since the 1960s (Bohannon et al., 1963, Johnson et al., 1963). The dose-limiting side effect of vincristine is neurotoxicity; other side effects include bone pain and constipation (Sandler et al., 1969, Rosenthal and Kaufman, 1974, Legha, 1986, Gidding et al., 1999).The mechanism of action of vinca alkaloids is primarily through inhibition of tubulin polymerisation by binding to beta tubulin (figure 1.7). Without tubulin polymerisation, the cell cannot separate the chromosomes during metaphase, and this ultimately leads to apoptosis.

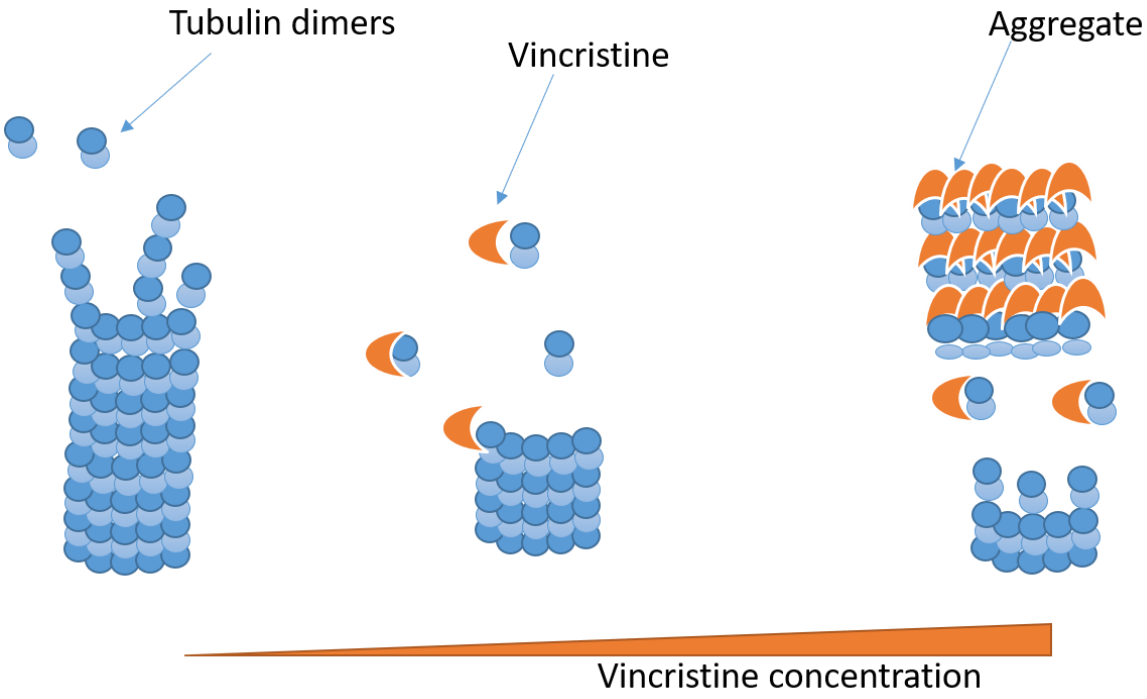

Figure 1.7 Mechanism of action of vincristine. Vincristine binds to tubulin dimers preventing microtubule assembly. At higher concentrations aggregates are formed causing depolymerisation of microtubules. Adapted from (Martino et al., 2018)

Cells can become resistant to vincristine by various methods, some of which are specific to vincristine and some are shared mechanisms of resistance with other chemotherapeutics. ABC (ATP-binding cassette) transporters and multidrug resistance associated proteins are prime candidates for resistance to various chemotherapeutic and vincristine is no exception, with p-glycoprotein and multi drug resistance associated protein 1 (MRP1) shown to offer protection from vincristine-induced toxicity (Chien and Moasser, 2008, Zhang et al., 2017, Van Tellingen et al., 2003). Two other common drug resistance mechanisms thought to contribute to various different chemotherapeutics are changes in apoptotic response and regulation of response to oxidative stress: both of these may play a role in resistance to vincristine (Simonian et al., 1997). In particular, the expression and activity of aldo-keto reductase enzymes (ARK) which form part of the signalling pathway that helps to protect cells from oxidative stress, have been shown to be upregulated by use of chemotherapeutics in T-ALL (Bortolozzi et al., 2018). Modulation of ARK1C1-3 expression could sensitise cells to vincristine (Bortolozzi et al., 2018). Increased tubulin isoform expression, stabilisation by microtubule associated proteins and

changes in mitotic checkpoint signalling are other mechanisms of resistance for tubulin-targeted drugs like vincristine (Zhang et al., 2017, Wang et al., 2003).

1.3.3 Dexamethasone

Dexamethasone is the steroid of choice in the UK for treatment of ALL due to its greater efficacy over prednisolone (Teuffel et al., 2011). A synthetic glucocorticoid, dexamethasone binds to the glucocorticoid receptor (GR), which is encoded by *NR3C1*. Upon glucocorticoid binding, the GR translocates to the nucleus, where it acts upon transcriptional target genes, which have a pleiotropic mode of action, but in the context of ALL, ultimately results in cell death (figure 1.8).

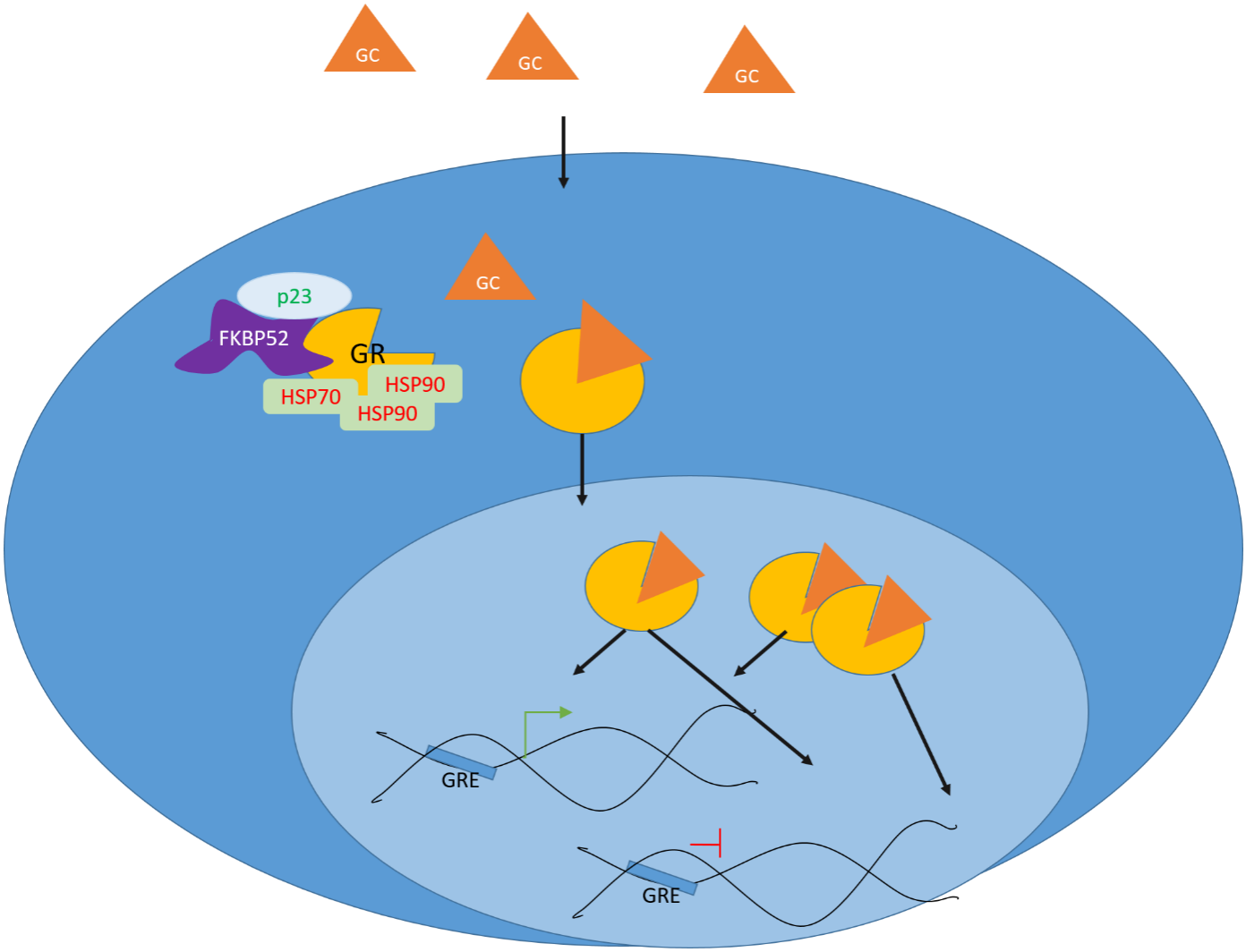

Figure 1.8 Glucocorticoid (GC) mechanism of action. GCs enter the cell and bind to glucocorticoid receptors (GR). The GRs are bound by heat shock proteins such as HSP90 and HSP70 and immunophillins like FKBP5 and its co-chaperone p23. The GC bound GR translocate to the nucleus where it acts (singularly or as dimers) to activate and repress transcription by binding at glucocorticoid response elements (Bernard et al.) (Bernard et al., Oakley and Cidlowski, 2013).

In vitro assays show relapsed ALL to be more resistant to steroids, and far higher levels of resistance was seen to steroids, than to other induction regimen drugs (Klumper et al., 1995). There are many proposed methods to generation of resistance to dexamethasone occurs. Mutations in the nuclear receptor subfamily 3, group C, member 1(*NR3C1*) gene are found in steroid resistant ALL cell lines and have also been identified in relapsed ALL patients, and this provides one explanation for resistance to dexamethasone (Schmidt et al., 2006, Hillmann et al., 2000, Hogan et al., 2011). Others question the role of *NR3C1* mutations due to the low frequency identified in ALL patients (0 out of 57 ALL samples analysed , and 1 out of 50 relapsed ALL analysed)(Tissing et al., 2005, Irving et al., 2005). Glucocorticoid resistance may occur further downstream, and not at the level of glucocorticoid receptor (GR) binding (Bachmann et al., 2005, Beesley et al., 2009). One example of this is through caspase 1 (and it activator cryopyrin) which are upregulated in steroid resistant B-ALL, and overexpression of caspase 1 resulted in GR cleavage and subsequently reduction of GR associated signalling in a B-ALL cell line (Paugh et al., 2015). In T-ALL, activation of AKT has been shown to provide resistance to glucocorticoids via phosphorylation of NR3C1, preventing its nuclear translocation (Piovan et al., 2013).

Upregulation of anti-apoptotic proteins can contribute to resistance, for instance upregulation of B-cell lymphoma 2 (BCL2) contributed to both decreased dexamethasone-induced apoptosis and increased autophagy leading to greater survival in lymphoma lines (Swerdlow et al., 2008). This again highlights the importance of apoptotic regulation in response to chemotherapeutics. Lastly, dexamethasone is a known P-glycoprotein substrate (Ueda et al., 1992). Removal of dexamethasone by p-glycoprotein or via detoxification by glutathione-S-transferases may contribute to resistance. Glutathione S-transferases catalyse the conjugation of reduced glutathione to xenobiotic substrates like dexamethasone increasing water solubility and making them easier to eliminate (Townsend and Tew, 2003).

1.3.4 Asparaginase

Asparaginase is an enzyme that breaks down asparagine into aspartic acid and ammonia. Asparagine is a non-essential amino acid and can be synthesised in normal cells from oxaloacetate, via transamination using the ammonium groups from glutamate. Leukaemia cells depend upon large amounts of asparagine and rely on extracellular sources of asparagine for survival (Broome, 1968). Asparaginase

deprives the leukaemic cells of their asparagine source and leads to cell death (as summarised in figure 1.9 below) (Ueno et al., 1997, Haskell and Canellos, 1969)(Takahashi et al., 2017). Asparaginase also influences glutamine, which is also required for leukemic cell survival; the glutaminase activity is thought to be of more importance in cells expressing asparagine synthetase (ASNS), the enzyme required for asparagine synthesis (Chan et al., 2019).

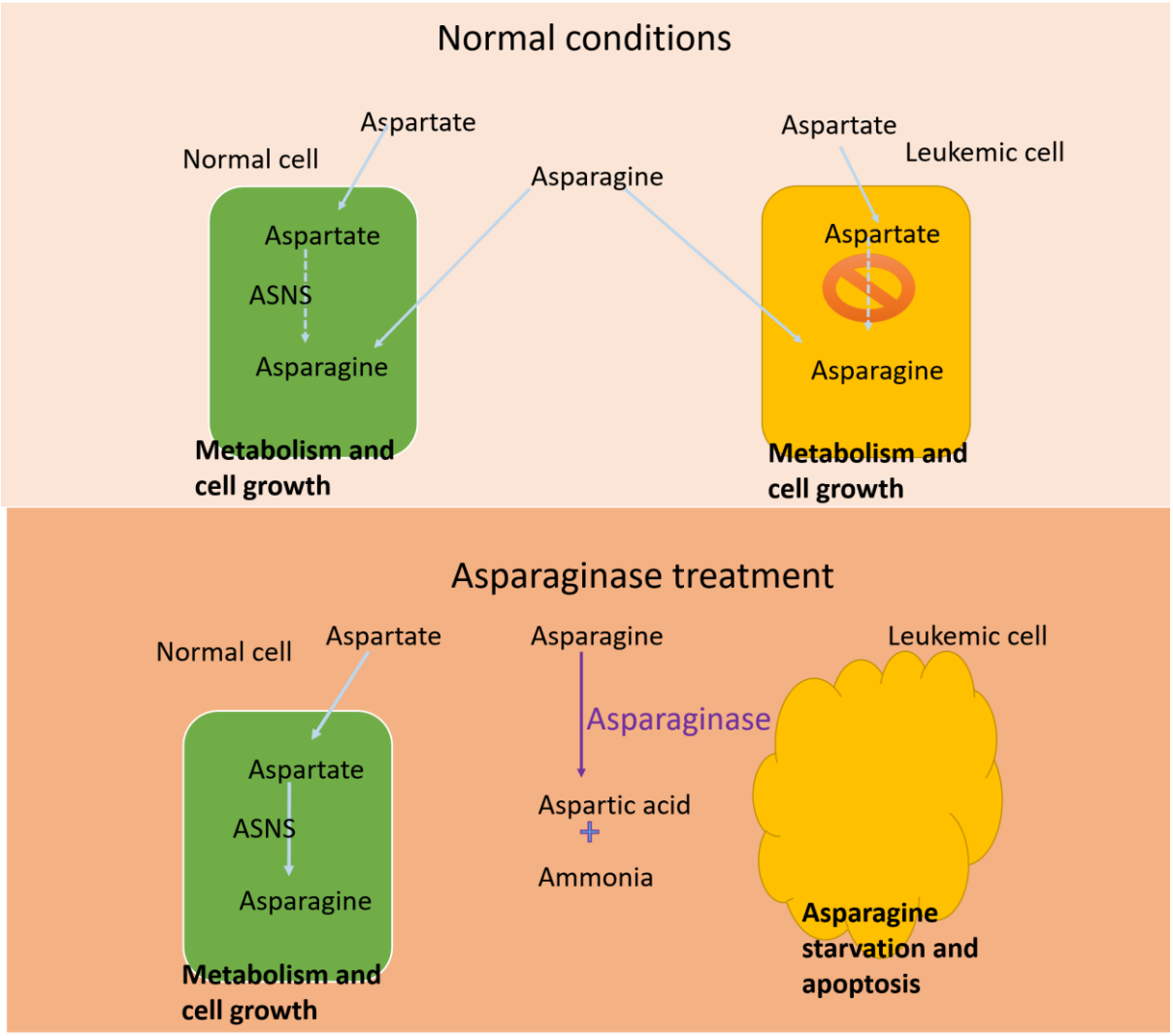

Figure 1.9 Mechanism of action of asparaginase. Normal cells can produce asparagine from aspartate using asparaginase synthetase enzyme (ASNS). Leukaemic cells cannot produce sufficient asparagine from aspartate and require asparagine from the environment. When asparaginase breaks down available asparagine into aspartic acid and ammonia leukaemic cells can no longer meet asparagine requirement and undergo apoptosis. Adapted from (Fung and Chan, 2017)

Historically upregulation of *ASNS* in response to low amino acid availability was thought to be the main means by which cells became asparaginase resistant (Hutson et al., 1997, Aslanian et al., 2001). Whilst some groups data still support a link between *ASNS* and asparaginase resistance, contradictory data suggests there to be no relationship between ASNS upregulation and response to asparaginase (Su et al., 2008, Krejci et al., 2004, Stams et al., 2005, Appel et al., 2006, Hermanova et al., 2012). This has led to the search for other mechanisms of resistance. Changes in apoptotic response due to nuclear factor kappa-light-chain-enhancer of activated B cells (NF-κB) signalling has been shown to be connected with asparaginase response (Chien et al., 2015). RNAi screening identified a reduction in calpain-1-Bid-caspase-3/12 pathway via loss of huntingtin associated protein 1 (HAP1) as a mechanism of asparaginase resistance (Lee et al., 2019). Calpain inhibition increases autophagy, and with calpain mediated cleavage of autophagy related gene 5 (Atg5) being shown to switch cells from autophagy to apoptosis, the role of autophagy in chemo-resistance is of interest (Yousefi et al., 2006). It has been demonstrated that induction of autophagy in response to amino acid depletion helps cells survive asparaginase treatment (Takahashi et al., 2017).

The formation of antibodies against asparaginase, has been reported in some patients, this leads to a more rapid clearance of asparaginase, and may also contribute to resistance (Panosyan et al., 2004). Other cells within the leukamic niche such as the mesenchymal stromal cells can synthesise asparagine, asparagine secretion from the niche may provide some protection from the effects os asparaginase treatment on the leukaemic cells (Iwamoto et al., 2007, Laranjeira et al., 2011).

The protective effect of the bone marrow niche is not restricted to asparaginase. The niche can provide resistance to various chemotherapeutics including vincristine, dexamethasone and daunorubicin for instance via cytokine release (Chen et al., 2019, Polak et al., 2014, Li et al., 2004).

1.3.5 Daunorubicin

Daunorubicin belongs within a class of drugs known as anthracyclines which also includes doxorubicin, epirubicin and idarubicin. There are several proposed mechanisms of actions of anthracyclines including: inhibition of topoisomerase II,

production of reactive oxygen species (ROS), inhibition of synthesis of macromolecules , DNA cross-link formation and histone eviction (Gewirtz, 1999, Marinello et al., 2018, Al-Aamri et al., 2019, Pang et al., 2013). The most widely accepted mechanism of action at clinical concentrations is through inhibition of topoisomerase II, whilst generation of ROS is the main mechanism of action thought to be responsible for cardiotoxic side effects (Gewirtz, 1999, Marinello et al., 2018). The action of topoisomerase II is given in figure 1.10. Daunorubicin is a vesicant (blister causing) drug and is given intravenously to avoid damage to muscles and skin. Its effect on the cardiac tissue is dose limiting, and can lead to cardiomyopathy during, or many years after, treatment (Rahman et al., 2007, McGowan et al., 2017).

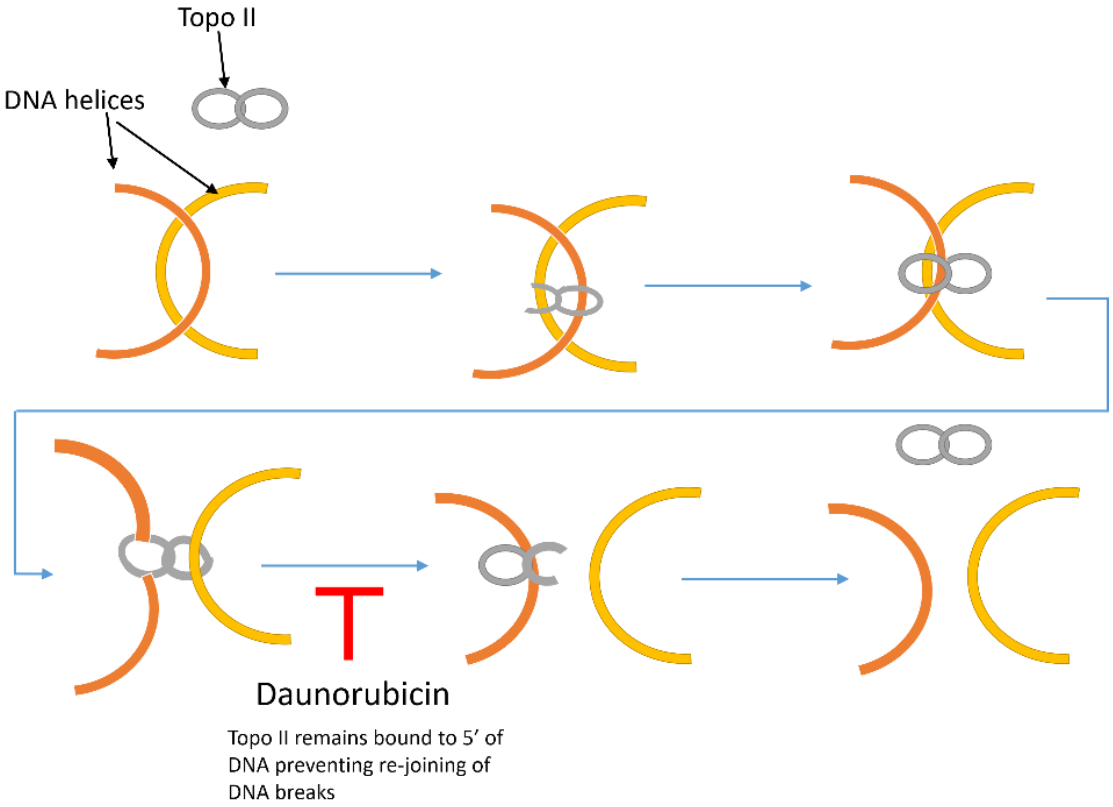

Figure 1.10 Action of topoisomerase II (topo II). Topo II allows for unwinding for DNA helices by generating double stranded breaks. It works by a two gate mechanism, one strand of DNA coloured orange is bound by a binding gate in topo II. A second strand of DNA shown in yellow is captured by an ATPase domain. Hydrolysis of ATP provides the energy to cut the first strand of DNA generating a double stranded break. The other strand can then pass through, the break in the first strand is repaired. Daunorubicin causes topo II to remain bound to DNA after cleavage and prevents re-joining of the break (Nitiss, 2009).

The main mechanism of resistance is thought to be through the ABC transporters: in particular ABCB1 (ATP-binding cassette sub-family B member 1), also known as P-glycoprotein (Kosztyu et al., 2014). Other mechanisms of resistance include alleviation of oxidative stress via change in signalling/ support from other cell types, and modulation of topoisomerase activity via post-translational modification (Sheng et al., 2016, Heasman et al., 2011, Ganapathi and Ganapathi, 2013).

DNA (cytosine-5)-methyltransferase 3A (*DNMT3A*) mutations found in T-ALL and l., are associated with reduced probability of achieving remission and reduced survival (Aref et al., 2016). In acute myeloid leukaemia (AML) *DNMT3A* mutations are associated with daunorubicin resistance *DNMT3A* mutations may also confer chemo resistance in T-ALL leading to poor outcome in these patients (Guryanova et al., 2016).

1.3.6 `Summary of mechanisms of resistance to chemotherapeutics

Resistance can occur to a single chemotherapeutic or to multiple, through numerous mechanisms. Resistance to individual agents can arise through alterations of pathways relating to the drugs mechanism of action, through increased expression, acquisitions or selection for specific mutations, chromatin remodelling and via cell to cell interactions. Resistance can also occur via changes to drug efflux like in the case of the multidrug transporters. Changes in apoptotic signalling pathways is another common mechanism of drug resistance, by upregulation of anti-apoptotic proteins the cells escape drug-induced apoptosis

1.4 The study of relapsed and refractory T-ALL.

Unlike T-ALL at first diagnosis that has overall survival rates in paediatrics at 80%, relapsed T-ALL (occurring in 15-20% of children), has an overall survival closer to 50% (Tallen et a2010, Parker et al., 2010, Bertaina et al., 2017, Bhojwani and Pui, 2013). Similarly, after induction failure (approximately 10% of paediatric T-ALL) outcome is poor with less than 50% event free survival at 5 years (O'Connor et al., 2017).

Treatment choices for relapsed ALL or after induction failure are limited and will include high dose chemotherapy and/or allogenic stem cell transplantation (Balduzzi et al., 2005, Gaynon et al., 2006). Presently there is only a single approved drug

specifically for treatment of relapsed T-ALL- nelarabine (Cohen et al., 2006). Approved for use when patients have relapsed or not responded to two chemotherapy regimens, it is a soluble pro-drug of Ara-G a nucleoside analogue that works by inhibition of DNA synthesis (Gandhi et al., 2006). With a response rate of around 40% there are still many patients in need of alternative options and a better understanding of resistance to induction regimen drugs. (Zwaan et al., 2017, DeAngelo et al., 2007)

With poor response to induction chemotherapeutics leading to poorer outcome, along with the increased chemo-resistance found in relapse understanding the mechanisms behind chemo-resistance is imperative to improving outcomes for T-ALL (Styczynski et al., 2007a, Styczynski et al., 2002, Klumper et al., 1995, Schrappe et al., 2012).

1.4.1 Chemo-resistance in T-ALL:

There are currently limited studies specific to the development of chemoresistance in T-ALL. Most of our current understanding comes from a publication by Li et al. Li et al performed targeted exome sequencing and whole genome sequencing on T-ALL patients. They then correlated mutation data with clinical data to identify that mutations in JAK1 and KRAS are associated with steroid resistance and poor outcome. Further analysis demonstrated a link between Il7R pathway mutations and *in vitro* steroid sensitivity. Introduction of selected mutants into T-ALL cell lines SUPT1 and P12 Ichikawa and subsequent steroid sensitivity assessment confirmed a role for a cysteine mutant of the IL7R -IL7R^{RFCPH} and JAK1 mutants (JAK1^{R724H} and JAK1^{T901A}) in steroid responsiveness, and further identified a role for both NRAS (NRAS^{G12D} and wild-type NRAS) and wild-type AKT.(Li et al., 2016)

Another study also highlighted a role for IL7 receptor signalling in steroid responsiveness and identify subsets of patients that have Il7 dependent steroid resistance (Delgado-Martin et al., 2017). Steroid induced cell death could be reduced by the modulation of cytokine IL7 levels, and with JAK1/2 inhibitor Ruxolitnib (Delgado-Martin et al., 2017).

The studies discussed above focused primarily on steroid resistance. Resistance to other commonly used therapeutics such as asparaginase, daunorubicin and vincristine was also assessed during an investigation into the expression of AKR1C enzymes in T-ALL, an idea inspired by work in solid tumours (Bortolozzi et al., 2018).

The authors identify that T-ALL patients who are resistant to therapy express increased levels of ARK1C enzymes and demonstrate modulation of these enzymes can increase sensitivity of T-ALL cell lines to vincristine. However, the increase in sensitivity to vincristine wasn't replicated with other chemotherapeutic agents tested (including daunorubicin and asparaginase).

The ABC family of membrane transporters including multi-drug resistance protein 1 (MDR1) also known as P-glycoprotein, are involved in the efflux of substances including drugs from cells, and have long been implicated in development of multidrug resistance in many conditions (Chen and Tiwari, 2011, Sui et al., 2012). T-ALL is no different with drug efflux and transporters such as MDR1 being associated with both chemoresistance and poor outcome (Hoofd et al., 2016, Del Principe et al., 2003).

1.4.2 Genetics of relapsed T-ALL

The study of relapsed disease can help us understand the genetics responsible for relapse and help identify ways in which leukaemic cells escape therapy. By comparison of copy number aberrations, mutation frequencies, gene expression, epigenetic changes or a combination of these between diagnostic and relapsed samples, we can enhance our understanding of how relapse occurs and what the drivers of relapse are. This approach has been relatively successful in B-ALL and many genes have been identified as associated with relapsed disease from transcription factors such as *EBF1* to metabolic genes such as *TYMS* (Bhojwani and Pui, 2013). A study published by Mullighan et al, on copy number aberrations in matched diagnosis and relapse samples highlights one of the issues in this approach to T-ALL. Where in B-ALL copy number aberration could be used to identify the clonal origins of relapse in T-ALL this approach was hampered by the low frequency of copy number aberrations (Mullighan et al., 2008). Whilst Kunz et al also note the low frequency of copy number alterations, they did observe increased mutational load at relapse and suggest this could be due to use of chemotherapeutics and highlight cytarabine use as the most likely (Kunz et al., 2015). One of the genes found mutated at relapse was NT5C2, which has similarly been seen by Tzoneva to be mutated in relapsed ALL and induce resistance to 6-mercaptopurine and 6-thioguanine (Kunz et al., 2015, Tzoneva et al., 2013).

These approaches have provided some insight into the mechanism of relapse, however T-ALL still lags behind B-ALL and the only reliable predictor of relapse currently in MRD (O'Connor et al., 2017) The other limitation of this approach is the requirement for large numbers of patient samples, which can be particularly difficult to obtain in T-ALL due to the lower incidence, especially in a relapsed setting. A different approach in the identification of genes important in ALL has been through RNAi based screening.

1.5 Screening approaches to identify drug targets

Screens can be used to identify genes that are important in the progression of disease as well as the treatment response when combined with therapeutics. Prior to the availability of clustered regularly interspaced short palindromic repeats (CRISPR) -based libraries, loss of function screening was predominantly carried out using RNA interference (RNAi). The main limitation of an RNAi approach was the incomplete depletion of gene products and off target effects (Qiu et al., 2005, Moore et al., 2010). For editing at a gene level to achieve knockout, zinc finger like exonucleases (ZFNs) and transcription activator like effector nucleases (TALENs) can be used, but these were not easily amenable to screening due to the large amount of cloning involved. CRISPR technology has allowed for editing at a gene level and is also scalable for large screens.

1.5.1 CRISPR technology and CRISPR screens

Part of the prokaryotic adaptive immune system, CRISPR provide protection from viruses and foreign plasmid DNA by cleaving the DNA sequence as directed by small CRISPR RNA (crRNA) sequences, which are derived from the bacterial genome (Jansen et al., 2002). Sequences from the bacterial genome are integrated into the CRISPR locus separated by short repeat sequences (protospacers). The bacterial sequences are transcribed as a longer pre-crRNA transcript before cleavage at protospacers to form mature crRNA that can be loaded into Cas enzymes (Bolotin et al., 2005). There are 3 types of CRISPR-Cas systems each with different Cas proteins (Haft et al., 2005). It is the type 2 system which uses Cas9 which has been repurposed for use in genome editing. The lentiCRISPR system uses *Streptococcus pyrogene* Cas9 and a short guide RNA (sgRNA) sequence on a single plasmid (Shalem et al., 2014). Along with the Cas9 and sgRNA, promoter sequences and

lentiviral packaging elements allow CRISPR to be introduced into mammalian cells by lentiviral transduction.

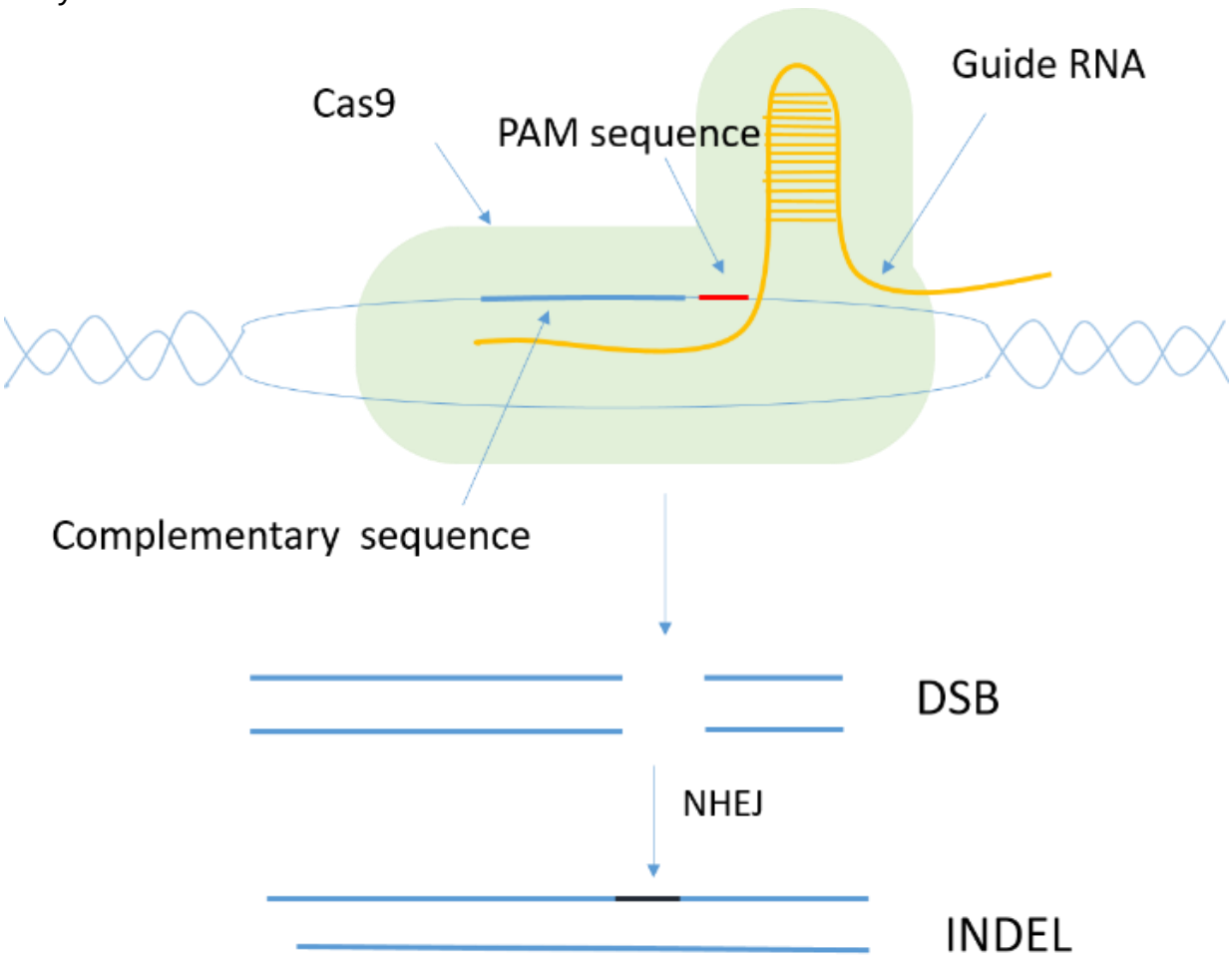

Figure 1.11 The mechanism of action of CRISPR-cas9. The Cas 9 nuclease and guide RNA act to generate double stranded breaks (DSB) in DNA. The guide RNA contains a sequence to direct the site of cleavage. The guide RNA binds to a complementary target site in DNA that is upstream of a protospacer adjacent motif (PAM). For the Streptococcus pyrogenes derived Cas9 this is 3'NGG. Repair of the double stranded breaks by the non-homologous end joining pathway (NHEJ) generates insertions and deletions (indels) which can lead to premature stop codons, frameshifts and nonsense mediated decay of the transcript.

CRISPR knockout screening relies upon the generation of double stranded breaks and repair by non-homologous end joining, and the generation of insertions and deletions which can cause frameshifts and premature stop codon formation, leading to nonsense mediated decay of the transcript (figure 1.11).

The first large commercially available CRISPR library was the GeCKO library a genome wide knock-out library, it is constructed from a single vector containing both cas9 and guide RNA sequence (Shalem et al., 2014). Since the release of this library many other libraries have been generated both knock out and silencing and activation based (Sanjana et al., 2014, Hart et al., 2015, Konermann et al., 2015, Sanson et al., 2018). CRISPR screens have been successfully employed in a number of settings, screening of protein domains, screening of primary immune cells, and in mouse models of cancer (Shi et al., 2015, Parnas et al., 2015, Chen et al., 2015).

1.6 Screens in T-ALL

At the time of designing the project there were no publications on CRISPR screens in T-ALL. Since that time a number of T-ALL cell lines were screened with a CRISPR library as part of the cancer dependencies project known as project Achilles (Cowley et al., 2014). Recently the results of a CRISPR screen in a T-ALL cell line treated with asparaginase were published (Hinze et al., 2019). Through this screen they identified Wnt pathway activation to be required for asparaginase sensitivity.

RNAi-based screens have been performed in T-ALL. A screen for genes phenocopying the oncogenic role of microRNA (miR) 19 was performed in a Notch-driven murine model of T-ALL; this identified *Bcl2L11* (also known as Bim), *Prkaa1*, *Pten* and *Ppp2r5e* to be enriched (Mavrakis et al., 2010). A screen specifically looking at miRs capable of promoting T-ALL development was performed by the same group a year later (Mavrakis et al., 2011). This time a two-step screen was employed to first identify miRs that allowed cells to resist c-MYC driven apoptosis, then a second stage for miRs capable of allowing cytokine independent growth of lymphocytes. They identified 5 miRs that had cooperative effects with known tumour suppressors which included *BIM* and *PTEN* but also *IKZF1, PHF6, NF1* and *FBXW7* (Mavrakis et al., 2011). Other groups focus on kinases, with both siRNA screen in T-ALL patient cells and shRNA screens in T-ALL cell lines together identifying tyrosine

kinase TYK2 and a T-ALL dependence on a TYK2-STAT1-BCL2 pathway (Sanda et al., 2013).

T-ALL screening was also combined with drug treatment in a shRNA screen of chromatin regulators. Screening was performed in DND41 cells persisting after gamma secretase treatment. Bromodomain-containing protein 4 *(BRD4)* was identified, and they suggest the use of epigenetically targeted drugs such as JQ1 (which acts on BRD4) to overcome resistance (Knoechel et al., 2014).

When it comes to performing the screen, the technology used for screening is important but so is the model of choice. The different screens model T-ALL in different ways; from *in vitro* cell line culture, to *ex vivo* patient material, to murine models.

1.7 **Models of T-ALL**

In order to screen for targets to treat T-ALL, an appropriate model of T-ALL is required. There are both *in vitro* and *in vivo* models of T-ALL. *In vitro* models include T-ALL cell lines and patient-derived cells. T-ALL cell lines are immortalised cells derived from patients with T-ALL. These are human cells with human relevant genetics but there is debate over how well these accurately reflect patient disease (Gillet et al., 2013). T-ALL blasts isolated directly from patients or after propagation in mice can be cultured *ex vivo*. However, these cells often do not actively proliferate and die in continuous culture making long terming screening more complex. A feeder layer can be used to help support the survival and proliferation of these cells (Holmes and Zuniga-Pflucker, 2009, Chiu et al., 2010).

In addition to *in vitro* and *ex vivo* models, *in vivo* models are also available for T-ALL. The most used animal to model T-ALL is mice, but zebrafish models also exist (Langenau et al., 2003, Langenau et al., 2005). Murine models of T-ALLs include Notch driven, *IKAROS* and *PTEN*-deleted and T-ALL associated transcription factor driven models such as TAL1 (Kastner and Chan, 2011, Hagenbeek et al., 2004, Pear et al., 1996, Jacoby et al., 2014). An alternative to transgenic models is the use of xenografts. Xenografts have the human relevant mutations which are not always reflected in transgenic murine models. T-ALL cell lines or primary cells from patients can proliferate in immune compromised mice (Agliano et al., 2008). One group even modelled relapse using a xenograft model and the chemotherapeutic treatment used in T-ALL induction therapy (Samuels et al., 2014b).

1.8 Selecting appropriate drug concentrations for *in vitro* an *in vivo* studies

When selecting drug concentrations, it is important to consider clinically relevant concentrations. As pointed out by Smith and Houghton, there is often a disconnect between *in vitro* testing concentrations and clinically achievable concentrations leading to claims of efficacy of drugs from *in vitro* studies that do not hold up in the clinic (Smith and Houghton, 2013). This point was again emphasised by Liston and Davis in the review of clinically relevant concentrations of anticancer drugs (Liston and Davis, 2017). Since vincristine, dexamethasone, asparaginase and daunorubicin have been used for many years in the clinic, pharmacokinetic data is available for patients who receive these drugs. Pharmacokinetic parameters for each of the 4 drugs are summarised in the relevant sections below.

1.8.1 Vincristine

Vincristine is given intravenously as a bolus dose, in the most recent UK ALL trials (UKALL2003 and UKALL2011) a dose of 1.5mg/m^2 is used. The median pharmacokinetic parameters for children receiving cancer treatment including an average vincristine dose of 1.5mg/m^2 were as follows: maximum plasma concentration of 3.5µg/L, area under the curve of 49.7µg/L/hour and a clearance of 482mL/min/m^2. This data is mostly consistent with similar studies, but area under the curve values reported are slightly lower than the 4.4mg/L/min reported by Lonnerholm *et al* which use a dose of 2mg/m^2 (Moore et al., 2011a, Lonnerholm et al., 2008). Vincristine is metabolised in the liver by cytochrome P450 enzyme CYP3A5 (Dennison et al., 2007).

1.8.2 Dexamethasone

Dexamethasone is given orally due to its good bioavailability (90%)(Queckenberg et al., 2011). The following pharmacokinetic parameters have been determined for children treated for ALL: maximum plasma concentration of around 80ng/ml or 200nM, a half-life of around 3 hours and 7l/h/m^2 clearance (Jackson, 2017). Pharmacokinetic studies show large inter-patient variability in drug exposure. Co-administration with asparaginase, which is given alongside dexamethasone in ALL therapy, is predicted to reduce clearance of dexamethasone (Yang et al., 2008). Dexamethasone is metabolised by cytochrome P450 enzymes in particular CYP3A4 and CYP17. Single nucleotide polymorphisms in these genes may also explain

interpatient variability in pharmacokinetic profiles (Tomlinson et al., 1997, Jackson et al., 2016b).

1.8.3 Asparaginase

Asparaginase is produced in bacteria, predominantly *Escherichia coli (E.coli)*. Previously, asparaginase was used in its native form and needed to be given daily due to a short half-life (26 hours). A newer poly-ethylene glycol (PEG) form has since been introduced (Avramis et al., 2002). In the PEGylated form, PEG groups are added to the asparaginase, which increases its half-life in the body (5.5 days) and the dosing frequency has consequently been reduced. Asparaginase can be given by intravenous or intramuscular routes. In the UK protocols it is given intramuscularly. The key issue with asparaginase is the trigger of allergic responses leading to anything from rashes to anaphylaxis (Woo et al., 1998, Ebeid et al., 2008). Other notable side effects are impaired liver function linked to reduced production of plasma proteins in the liver due to depleted asparagine and glutamine levels (Ollenschlager et al., 1988). Different formulations of asparaginase have different pharmacokinetic profiles (Boos et al., 1996, Asselin et al., 1993). For native *E.coli* asparaginase, data suggests maximum activity after a single dose of 2U/ml at around 4 hours (Avramis et al., 2002). The average peak and trough levels have been measured for patients treated with *E.coli*-derived asparaginase with peaks from 7500 to 8000 U/l and troughs of 400-700 U/l (Müller et al., 2001). Although the optimal length and degree of asparagine depletion is uncertain, generally a trough level of 0.1U/ml is set as an adequate activity level to ensure asparagine is depleted (Rizzari et al., 2000, Angiolillo et al., 2014). Antibodies against asparaginase are associated with more rapid clearance of asparaginase (Panosyan et al., 2004).

1.8.4 Daunorubicin

Daunorubicin is given as an intravenous infusion at a dose of 25mg/m^2 over an hour as part of the 4- drug induction used for patients on regimen B. Standard daunorubicin kinetics show two phases of decline after infusion, a rapid decline followed by a slower elimination. Daunorubicin is metabolised to the less cytotoxic daunorubiciol; both daunorubicin and daunorubiciol can then be further metabolised to non-active compounds (Thompson et al., 2014). A study into daunorubicin pharmacokinetics from the Children's Oncology Group show volume of distribution of 68.1 L/m^2 ± 24 % and clearance of 116 L/m^2/h ± 14 % for daunorubicin and 232 L/m^2

± 10 %, and 26.8 L/m^2/h ± 5.6 % for daunorubinicol, for unspecified doses and varying infusion times (Thompson et al., 2014). Another study using 50 mg/m2 infusion over 10 min in adult leukaemia patients showed clearance times of 168L/h. In this study, the majority of maximum plasma concentrations recorded varied between 80 and 300ng/ml, which had reduced to 10ng/ml within 12 hours (Callies et al., 2004). For infants receiving 30mg/m^2 over a 6 hour infusion predicted parameters were volume of distribution of 16.4 L/m^2 ± 46% and clearance of 43.9 L/ h/m^2 ± 65% for daunorubicin and 228 L /m^2 ± 80% and 19.1 L/h/m^2 ± 32% for daunorubiciniol (Hempel et al., 2010a). The approximate peak plasma concentrations for daunorubicin was around 100ng/ml (Hempel et al., 2010a).

1.8.5 Drug concentrations summary

These parameters, particularly the peak achievable plasma concentrations, are important to consider when designing drug treatments. *In vitro* drug concentrations exceeding C_{max}, or at C_{max} for a prolonged period, do not accurately reflect a clinical setting. For *in vivo* dosing we can extrapolate from human doses to mice, or ideally base it on already available pharmacokinetic studies in mice, like that published by Szymanska et al to achieve a pharmacokinetic profile reflecting that found in ALL patients (Nair and Jacob, 2016, Szymanska et al., 2012a).

1.9 Aims and objectives

A crucial step to improving current T-ALL therapy is to identify a treatment that can be used in relapsed and refractory ALL to improve efficacy of induction and outcome for these patients. Since new drugs are normally introduced alongside current chemotherapy, ideally the new treatments should be able to either complement current chemotherapy or help overcome resistance to current chemotherapy. The ultimate goal should therefore be identification of a therapeutically actionable target to treat relapsed and refractory T-ALL that could be used in conjunction with concurrent chemotherapy. The research undertaken should move forward our understanding and bring us closer to this ultimate goal.

Aim of project

- Determine which genes or pathways may drive resistance to the chemotherapy combination of vincristine, dexamethasone, l-asparaginase and daunorubicin in T-ALL.

Performing a screen under chemotherapeutic pressure will allow us to identify genes important in resistance to current chemotherapy. Induction chemotherapy is the first stage of treatment and most predictive of outcome, so we chose to focus on the chemotherapeutics used at induction in T-ALL, namely vincristine, dexamethasone, l-asparaginase and daunorubicin (VXLD).The main aim will be addressed by a number objectives:

Primary objective:

- Design and implement a suitable screening strategy to identify genes conferring resistance to T-ALL induction therapy

This primary objective can be broken down into smaller specific objectives which will be addressed in different chapters.

Specific objectives

- Identify a suitable screening model (Chapters 3 and 4)
- Establish appropriate dose of each induction drug for use in in vitro screening (Chapter 3)
- Create a VXLD dosing regimen that can be used for screening in vivo (chapter 4)
- Ensure a streamlined screening process from introduction of library through to obtaining data (chapter 5)
- Use screening data to identify genes and pathways associated with resistance to VXLD chemotherapy (chapter 6)

Chapter 2. Materials and methods

2.1 Equipment and software

Category	Equipment	Manufacturer	Software
Centrifuges	Optima L-100 XP ultracentrifuge	Beckman Coulter, UK	
	MSE Mistral	MSE, UK	
	Multifuge 35R	Thermo fisher Scientific, UK	
	Centrifuge 5418	Eppendorf, UK	
Spectrophotometers	FLUOstar Omega	BMG labtech	MARS Data Analysis Software
	Nanodrop 1000 spectrophotometer	Thermo Fisher Scientific, UK	
	Qubit 3.0 Fluorometer	Thermo Fisher Scientific, UK	
Flow cytometers	FACSCalibur	Beckton Dickinson, UK	FlowJo v10.0.8
	FACSCanto II	Beckton Dickinson, UK	FlowJo v10.0.8
	ATTUNE NxT	Thermo Fisher Scientific	FlowJo v10.0.8
Thermal cyclers	ViiA™ 7 Real-Time PCR System	Applied Biosystems, USA	ViiA™ 7

Electroporators	EPI 2500 Elektroporations-impulsgenerator	EPI, Germany	
	MicroPulser Electroporator	Bio-Rad, UK	
Imaging systems	G:BOX	Syngene	GeneSys
	GelDoc	Bio-Rad, UK	ImageLab
	IVIS	Caliper Ltd., USA	Living image®
Tissue culture	Inverted microscope, CKX53	Olympus optical, UK	
	BioMAT2 class 2 Microbiological Safety Cabinets	Contained air solutions	
	MCO-230AICUVL-PE CO_2 Incubator	Panasonic, Japan	

Table 2.1 Equipment list. The equipment used throughout this work, the manufacturer and software used to analyse the data produced (where applicable)

2.1.1 Consumables

Standard lab ware was used except where specified

Consumable	Company
Pollyallomer Konical™	Beckman Coulter, USA
0.45µm Acrodisc® syringe filters	Sigma Aldrich, UK
Stericup-HV Sterile Vacuum Filtration System 0.45µm pore size	Merck, UK
Flowgen electroporation cuvettes 1mm	SLS, UK
BD microfine 29G insulin syringes	Beckton Dickinson, UK
Spreaders, triangle shaped, disposable, sterile	VWR International, Vienna
EasyStrip™ Plus Tube Strip	Thermo Fisher Scientific, UK
DNA Lobind Eppendorf tubes	Eppendorf, UK
Nunc™ Square BioAssay Dishes	Thermo Fisher Scientific, UK

Table 2.2 Project specific consumables. Consumables ordered for the purpose of the project and the company that supplied them

2.2 Reagents

Standard chemicals and reagents were purchased from Sigma unless otherwise stated. UltraPure™ Agarose was purchased from Invitrogen and GelRed from Biotum.

2.1.2 Buffers and solutions

PBA

- 0.5% BSA
- 100 µl Sodium Azide
- PBS up to 500ml

Red cell lysis 10x

- 8.3g NH_4Cl_2
- 1.00g $KHCO_3$
- 0.38g Na_2EDTA
- 100ml H_2O

HeBS, 2x

- 16.36g NaCl
- 11.9g HEPES
- 0.213g Na_2HPO_4

pH to 7.00

make up to 1000ml deionized water

HEPES buffered water

- 125ul 1M HEPES (pH 7.3)
- 50ml deionized water

Sterile filtered

0.5M $CaCl_2$

- 36.7g $CaCl_2.2H_2O$
- Volume to 500ml with deionized water

Sterile filtered

Polybrene

- 80mg Hexadimethrine Bromide
- 10ml 0.9% NaCl solution

Sterile filtered

5 x DNA Loading dye

- 40% (v/v) glycerol
- 0.01%(w/v) bromophenol blue
- 10mM EDTA pH 8.0

100ml of 50X TAE buffer

- 24.2gTris base
- 5.71ml of glacical acetic acid
- 10ml 0.5M EDTA(pH 8.0)
- pH to 8.3
- Water to 100ml

Luria-Bertani (LB) broth

- 25g LB broth powder

Contains: 10g/L Tryptone

10g/L NaCl

5g/L yeast extract

- 1 litre DI H_2O

Autoclaved

SOC media

Prepare solution 1:

- 6g Bacto-tryptone
- 1.5g yeast Extract
- 1ml 3M NaCl
- 0.25ml 3M KCl

Adjust to 291ml with water and autoclave

Prepare solution 2

- 3ml 2M Mg^{2+} from $MgSO_4.7H_20$ sterile filtered
- 6ml 1M glucose sterile filtered

Combine solution 1 and 2

LB agar

- 25g LB broth powder
- 12.5g Bacto-agar
- 1L DI H_2O

Autoclaved

10ml Freezing media

- 9ml FBS
- 1ml DMSO

2.1.3 Antibodies

Epitope	Fluorochrome	Clone	Manufacturer
hCD45	APC	H130	BD Biosciences
muCD45	BV421	30F11	BD Biosciences
hCD3	PE	UCHT1	BD Biosciences
LIVE/DEAD™ fixable aqua			Thermo Fischer
phosphoH2AX	PE	N1-431	BD Biosciences
phosphatidylserine	PE	Annexin V	Biolegend

Table 2.3 Antibodies used for flow cytometry. Antibody epitope, clone, manufacturer and conjugated fluorochrome are given.

2.1.4 Drugs/Inhibitors

Drug/Inhibitor	Solvent	Company	Stock concentrations
Dexamethasone	DMSO	Caymen chemicals	30mg/ml
Daunorubicin Hydrochloride	DMSO	Caymen chemicals	10mg/ml
Vincristine sulphate	Methanol	Caymen chemicals	20mg/ml
Asparaginase	Water	Santa Cruz biotechnology	2000U/ml

Table *2.4* Drugs and inhibitors All drugs and inhibitors used in vitro during project.

2.1.5 Brunello library

Human Brunello CRISPR knockout pooled library was a gift from David Root and John Doench (Addgene #73178). The library was provided as a plasmid pool with a lentiCRISPRv2 backbone. LentiCRISPRv2 is a 3rd generation lentiviral vector containing ampicillin resistance for bacterial selection, puromycin for selection in mammalian cells, S. pyogenes Cas9, as well as a guide sequence. The Brunello library targets 19,114 human genes with 76,441 guides (including 1000 controls). There is 4 guides per gene, whereas a similar library- GeCKOv2 has 6 per gene, the number of guides per gene was deduced by subsampling analysis to reduce total library size while maintaining hits. The guides were designed using optimised design rules to increase activity and reduce off-target effects (Doench et al., 2016).

Dug	Product Details	Company	Solvents (for further dilution)	Administration route	Dose	Frequency
Vincristine	Vincristine Sulfate 1 mg/ml solution for injection	Hospira	0.9% sodium chloride	Intra-peritoneal	0.15mg/kg	Once weekly
Dexamethasone	Dexamethasone 3.3 mg/ml Solution for Injection 3.3 mg dexamethasone (as sodium phosphate)	Lameln Pharmaceuticals	Sterile water	Intra-peritoneal	5mg/kg or 2.5mg/kg (as stated in relevant method section)	5 times weekly , once daily
L-asparaginase	Spectrilla 10000units	Medac	0.9% sodium chloride	Intra-peritoneal	1000U/kg	5 times weekly , once daily
Daunorubicin	20mg powder for IV injection 21.4 mg daunorubicin hydrochloride (equivalent to 20 mg as base)	Cenexi laboratories	0.9% sodium chloride	Intra-venous	0.45mg/kg	Once weekly
Luciferin	VivoGlow™	Promega, USA	Dulbeccos phosphate buffered saline	Intra-peritoneal		

Table 2.5 Drugs used for *in vivo* studies. Product details and manufacturing company of drugs used for *in vivo* studies

2.3 Commercial kits

Kit	Manufacturer
Buffer ATL	QIAGEN
Cell Counting Kit-8 WST-8 Cell proliferation Cytotoxicity assay kit	Dojindo
Endofree Plasmid Maxi Kit	QIAGEN
Phusion® High-Fidelity PCR Master Mix	NEB, USA
Proteinase K	QIAGEN
Platinum® SYBR® Green SuperMix UDG	Applied Biosystems
QIAamp DNA Blood Midi kit	QIAGEN
QIAamp DNA Blood Maxi kit	QIAGEN
QIAquick Gel Extraction Kit	QIAGEN
QIAquick PCR Purification Kit	QIAGEN
RevertAid™ H Minus cDNA Synthesis Kit	Thermo Fisher Scientific
RNase-free DNase set	QIAGEN
RNeasy®Mini kit	QIAGEN
RNeasy®Micro kit	QIAGEN
TaKaRa Ex Taq™	Clontech

Table 2.6 Commercial kit and manufacturer list.

2.4 Primers

Primers were either designed with Primer Express v3.0™ Software (ABI), Primer-BLAST software (NCBI) or were taken from published work (where primers are based on published sequences references are given). Primers were ordered from Sigma-Aldrich as desalted oligonucleotides.

Gene	Forward 5' to 3'	Reverse 5' to 3'	Ref
***NR3C1* for mutation screening**	GCTGGAATGAACCTGGAA	TACCTGAAGCCTGTGTAAC	
Glucocorticoid receptor	GAACTTCCCTGGTCGAACAGTT	GAGCTGGATGGAGGAGAGCTT	
GILZ	CATGGAGGTGGCGGTCTA	TTACACCGCAGAACCACCAG	
FKBP5	CATTATCCGGAGAACCAAAC	AATTGGAATGTCGTGGTCTT	
Human *GAPDH*	GAAGGTGAAGGTCGGAGTC	GAAGATGGTGATGGGATTTC	
Cas9	AGTGCGCGAGATCAACAACT	TGTAGTCGCCGTACACGAAC	
TLX3	TCTGCGAGCTGGAAAA	GATGGAGTCGTTGAGGC	
BCL-X 1A	CTGAGCTTCGCAATTCC	GGTCTCCATCTCCGATTC	(Willimott et al., 2011)
BCL-X 1B	AAGTGACTGAGCTTGCAAGT	GGTCTCCATCTCCGATTC	(Willimott et al., 2011)
BCL-XL/S	GGGTCTAGAAGTGGATGGTCAGTGTCTGGT	GGGGAATTCTTGGACAATGGACTGGTTGA	(Willimott et al., 2011)
HECTD2	ATCCGAAATGAAGGCCCCAG	TGAGGCAGTGGCATCTTTCT	
PIAS1	GCGGACAGTGCGGAACTAAA	ATGCAGGGCTTTTGTAAGAAGT	(Liu et al., 2013)

Table 2.7 Oligonucleotide sequences. Oligonucleotides ordered for amplification of cDNA for Sanger sequencing, qRT-PCR and PCR. Where sequences are taken from published work references are given.

2.5 Cloning enzymes and buffers

All enzymes and buffers used for cloning were ordered from Thermo Fisher Scientific, UK unless otherwise stated.

2.6 Bacteria

Two bacterial strains were used in this work:

Stbl3 (Invitrogen) - used for propagation of plasmids. Has recA13 mutation which reduces recombination of cloned DNA.

ElectroMAX™ Stbl4™ (Invitrogen) –electrocompetent cells with high transformation efficiency used to amplify Brunello library.

2.7 Cell culture consumables and reagents

Tissue culture consumables were purchased from Corning, UK unless stated otherwise.

Reagent	Company
RPMI-1640 (R8758)	Sigma-Aldrich, UK
RPMI-1640 (R5886)	Sigma-Aldrich, UK
DMEM (D6171)	Sigma-Aldrich, UK
L-Glutamine	Sigma-Aldrich, UK
Sodium pyruvate	Sigma-Aldrich, UK
Trypsin-EDTA 10X solution	Sigma-Aldrich, UK
GIBCO™ Foetal bovine serum	Thermo Fisher Scientific, UK

Table 2.8 List of cell culture reagents used and suppliers

2.8 Cell line information

2.8.1 Source and authentication of cell lines

Cell lines were thawed from Liquid Nitrogen or -150°C freezer stocks held by the van Delft and Heidenreich groups. The cell lines were authenticated by short tandem repeat profiling by NewGene Ltd (Newcastle University, UK).

2.8.2 Cell culture conditions

Suspension cells were cultured in RPMI-1640 media with 10% FBS (20% for MOLT-16). 293T cells were cultured in DMEM high glucose with 10% FBS. Cell lines were not kept in culture for greater than 3 months.

Cell line	Origin	Link to source and culture information
HPB-ALL	Diagnostic T-ALL age 14	https://www.dsmz.de/collection/catalogue/details/culture/ACC-483
HSB-2	T-ALL from lymphosarcoma	https://www.dsmz.de/collection/catalogue/details/culture/ACC-435
LOUCY	T-ALL primary resistant age 38	https://www.dsmz.de/collection/catalogue/details/culture/ACC-394
CUTLL-1	Paediatric Relapsed T-cell lymphoblastic disease	https://www.ncbi.nlm.nih.gov/pubmed/16688224
DU.528	Diagnostic T-ALL age 16	https://www.ncbi.nlm.nih.gov/pmc/articles/PMC2187926/
MOLT-16	Relapsed T-ALL age 5	https://www.dsmz.de/collection/catalogue/details/culture/ACC-29
PEER	T-ALL at second relapse age 4	https://www.dsmz.de/collection/catalogue/details/culture/ACC-6
RPMI-8402	T-ALL age 16	https://www.dsmz.de/collection/catalogue/details/culture/ACC-290
SUP-T1	Relapsed T-LL age 8	https://www.dsmz.de/collection/catalogue/details/culture/ACC-140
ALL-SIL	Relapsed T-ALL age 17	https://www.dsmz.de/collection/catalogue/details/culture/ACC-511
CCRF-CEM	Relapsed T-ALL age 3	https://www.dsmz.de/collection/catalogue/details/culture/ACC-240
JURKAT	Relapsed T-ALL age 14	https://www.dsmz.de/collection/catalogue/details/culture/ACC-282
KARPAS-45	Diagnostic T-ALL age 2	https://www.sigmaaldrich.com/catalog/product/sigma/cb_06072602?lang=en&region=GB
MOLT4	Relapsed T-ALL age 19	https://www.dsmz.de/collection/catalogue/details/culture/ACC-362
KOPT-K1	Diagnostic T-ALL	https://www.ncbi.nlm.nih.gov/pubmed/7475267
SUP-T1	Relapsed T-ALL age 8	https://www.dsmz.de/collection/catalogue/details/culture/ACC-140
DND41	T-ALL age 13	https://www.dsmz.de/collection/catalogue/details/culture/ACC-525
CTV-1	T-ALL	https://www.dsmz.de/collection/catalogue/details/culture/ACC-40
PF-382	T-ALL at second relapse age 6	https://www.dsmz.de/collection/catalogue/details/culture/ACC-38
P12/ICHIKAWA	T-ALL age 7	https://www.dsmz.de/collection/catalogue/details/culture/ACC-34
697	B-ALL	https://www.dsmz.de/collection/catalogue/details/culture/ACC-42
293T	human embryonic kidney	https://www.dsmz.de/collection/catalogue/details/culture/ACC-635

Table 2.9 Cell line information. Information on disease and age of patient from which cell lines are derived and the medium used in their routine culture

2.8.3 Safety

All cell culture work was performed in a class II microbiological safety cabinet (BIOMAT-2, Medical Air technology Ltd., Oldham, UK).

Lentivirus work was carried out in accordance with ACGM Compendium of Guidance 2000, Part 2A, Annex VI, and BioCOSHH assessments, all lentivirus work was carried out at containment level 2 using microbiological safety cabinets. Only second generation lentivirus derived from FIV and HIV were used. They are both replication in-competent and self-inactivating.

2.9 Cell culture methods

2.9.1 Preservation of cell lines at -150°

Cells were counted, washed and pelleted and re-suspended in a freezing media consisting of FBS with 10% DMSO and aliquoted into cryovials (0.5 million to 10 million cells per vial). Cells were placed in a CoolCell® container (Biocision) and placed at -80°C for 24 hours before transfer to -150°C for long term storage.

2.9.2 Resurrection of cell lines

Cryovials containing cells were removed from the freezer and warmed in water bath at 37°C. Cells were transferred into a tube containing warm media. Cells were pelleted by centrifugation at 350g and DMSO containing media aspirated off. Cells were then re-suspended in further warm media and transferred to an appropriate sized flask

2.9.3 Cell counting

Principle

The trypan blue exclusion assay (Strober, 2001) is used to assess the number of viable cells. Cells with intact cell membranes will exclude the trypan blue dye. Cells with compromised membranes cannot exclude the dye and it is visible within the cytoplasm. Cells with a blue cytoplasm are excluded during counting, only cells of normal shape and size with clear cytoplasm are counted as viable cells. To count cells, they are placed onto a haemocytometer which has a grid with known sizes, so that the concentration of cells can be determined.

Reagents and equipment

- Improved Neubauer haemocytometer
- Trypan blue

Procedure

Cells were mixed well before taking an aliquot of cells which was mixed in 1:1 ratio with trypan blue before applying to an improved Neubauer haemocytometer. Viable cell count was determined by counting the cells excluding the blue dye lying in the 4 larger outer squares and concentration calculated using the following equation.

Counted cells /2 = cell number $x10^4$ per ml

2.9.4 Maintenance of suspension cells

Cells were counted and passaged 3-4 times weekly. Cells were kept at a density of $0.5x10^6$/ml to $2x10^6$/ml.

2.9.5 Maintenance of adherent cells

Principle

Since these cells adhere to the surface of the flask their passage differs to suspension cells. Trypsin catalyses the hydrolysis of peptide bonds, it helps remove focal adhesions that anchor cells to the culture dish. EDTA chelates calcium, the removal of calcium helps break cadherins which hold cells together and separates cells from one another. FBS contains proteins that act as a competitive inhibitor to trypsin.

Reagents and equipment

- Sterile PBS
- Cell culture medium
- Trypsin-EDTA (0.05% Trypsin, 0.02% EDTA)

Procedure

Cells were counted and passaged 2-4 times weekly. Spent media is removed from the flask, cells are washed with warm PBS. Trypsin-EDTA solution is then added to promote detachment of cells from the flask. Once cells had dissociated, the trypsin was inactivated by addition of media. Cells were then counted and seeded at a density of $1x10^5$/ml to $4x10^5$/ml.

2.10 Generation of recombinant lentivirus

In order to express, knock down or knockout genes of interest, the required complementary sequences were cloned into appropriate plasmids, these were then amplified, transfected into 293T cells to produce lentivirus. Lentivirus was then used to introduce the plasmids into mammalian cells.

2.10.1 Cloning of shRNA sequences into pLKO5.d vector

Principle

In order to knockdown BCL-X and HECT2 shRNA vectors were created that target these genes. To create these vectors cloning was performed to introduce the required sequences into the pLKO5.d vector. The vector is cut with a restriction enzyme to allow insertion of sequences with corresponding overhangs.

Reagents

- shRNA oligonucleotides (table 2.10)
- pLKO5d.SFFV.miR30n (pLKO5.d)
- BsmB1
- T4 DNA ligase
- T4 PNK
- T4 DNA ligase buffer
- Buffer Tango

shRNA sequences

Gene	Sense	Antisense
NTC1	AGCGATCTCGCTTGGGCGAGAGTA AGTAGTGAAGCCACAGATGTACTTA CTCTCGCCCAAGCGAGAG	GGCACTCTCGCTTGGGCGAGAGTAAGTA CATCTGTGGCTTCACTACTTACTCTCGCC CAAGCGAGAT
NTC2 (RE)	AGCGAAACCTCGAAATCGTACTGA GATAGTGAAGCCACAGATGTATCTC AGTACGATTTCGAGGTTC	GGCAGAACCTCGAAATCGTACTGAGATA CATCTGTGGCTTCACTATCTCAGTACGAT TTCGAGGTTT
BCL-X	AGCGCCCTTGTGAAGATGATATACT ATAGTGAAGCCACAGATGTATAGTA TATCATCTTCACAAGGA	GGCATCCTTGTGAAGATGATATACTATAC ATCTGTGGCTTCACTATAGTATATCATCTT CACAAGGG
HECTD2	AGCGCGCAGTACATGATTTTTATCT ATAGTGAAGCCACAGATGTATAGAT AAAAATCATGTACTGCT	GGCAAGCAGTACATGATTTTTATCTATAC ATCTGTGGCTTCACTATAGATAAAAATCA TGTACTGCG

Table 2.10 Sense and antisense sequences for cloning of shRNA into pLKO5.d. Sequences include Bsmb1 sites, sense strand, guide strand and hairpin loop. Designed using the mirN shRNA online design tool (Adams et al., 2017).

Procedure

Oligonucleotides were reconstituted to a concentration of 100µM. The sense and antisense oligonucleotides were phosphorylated and annealed. The reaction given in table 2.11 was heated to 37°C for 30 minutes for phosphorylation. Then denatured at 95°C for 5 minutes before being gradually cooled to allow annealing.

Component	Volume (µl)
100µM sense oligonucleotide	1
100µM antisense oligonucleotide	1
T4 DNA ligase buffer	1
Water	6.5
T4 PNK (10U/µl)	0.5

Table 2.11 Constituents of reaction for phosphorylation and annealing of oligonucleotides for shRNA cloning

Component	Volume (µl)
Vector	volume required for 40ng
Oligonucleotide duplex	1
T4 DNA ligase buffer	1
T4 ligase (5U/ µl)	0.5
Water	Up to 10

Table 2.12 Ligation reaction

The vector was provided with Bsmb1 ligation sites by cutting the vector with BsmB1 in buffer tango, checking for linearized vector by agarose gel electrophoresis and purify the vector with a gel extraction kit. The annealed oligonucleotides were then ligated into the prepared vector in reaction indicated in table 2.12 overnight at room temperature.

2.10.2 Amplification and purification of plasmids

The following plasmid were used:

- pSLIEW: expression of EGFP and luciferase. (In house (Bomken et al., 2013))
- pLKO5d.SFFV.miR30n: miR30 based for shRNA knockdown (Addgene, cat# 90333)
- pCMVdR8.91: lentiviral packaging plasmid (Life science market, cat#PVT2323)
- psPAX2: lentiviral packaging plasmid, alternative to pCMVdR8.91 (Addgene, cat#12260)
- pMD2.G: VSV-G envelope expressing plasmid (Addgene, cat#90333)

Principle

In order to have sufficient plasmid for lentiviral generation, plasmids were amplified in bacteria and purified using Qiagen Endo-free maxi kit.

Reagents and equipment

- LB agar plates
- LB broth
- QIAfilter cartridge
- Qiagen tip

- Endo free maxi kit buffers: P1, P2, P3, ER, QBT

Procedure

Plasmids were transformed into bacteria and streaked onto LB-agar plates containing the appropriate antibiotic for the plasmid. A colony was selected and grown in LB-broth containing antibiotic, bacteria were harvested during the logarithmic phase of growth. Bacteria were pelleted at 6000g for 15minutes at 4°C. The bacterial pellet was re-suspended in buffer P1. P2 was added mixed by inversion and incubated for 5 minutes in order to lyse the bacteria. The lysis was neutralised by addition of buffer P3. The lysate was filtered with a QIAfilter cartridge. The filtered lysate was treated with buffer ER on ice for 30minutes to remove endotoxins. The Qiagen tip was equilibrated with buffer QBT. The lysate was applied to the column, followed by two washes with buffer QC. Plasmid was eluted from the column with buffer QN and precipitated with isopropanol. The DNA was pelleted by centrifugation at 15,000g for 30 minutes at 4°C. The pellet was washed with 70% ethanol and pelleted 15,000g for 15 minutes at 4°C. The ethanol was removed and the pellet air dried. The pellet was re-suspended in endotoxin free buffer TE. Concentration and purity were determined by Nanodrop.

2.10.3 Amplification of Brunello library

The Brunello library was acquired from Addgene as a plasmid pool. To maintain high library complexity, amplification requires high transformation efficiency. A total of 400ng of plasmid DNA was mixed with 100µl of STLB4 cells (an electrocompetent *E.coli* with high transformation efficiency). This was divided amongst 4 cuvettes (25µl per cuvette). Cells were electroporated with a MicroPulser, BioRad 1652100 on Ec1 setting (1.8kV). SOC media was then added and the cells transferred into tubes and placed into a shaking incubator for 1 hour at 30°C. Bacteria were then plated onto pre-warmed bioassay plates containing LB-Agar with ampicillin. A 40,000 times dilution plate was prepared to check transformation efficiency. Plates were incubated for 18 hours at 30°C

The number of colonies were counted on the dilution plate to approximate the total colonies produced. Bacteria were scraped from plates for plasmid purification where at least $4x10^6$ colonies were present, to ensure at least roughly 50 colonies per construct in the library.

2.10.4 Seeding of 293T

293T cells were thawed and cultured for between 1 and 2 weeks prior to lentiviral generation. 293T cells were seeded at $1x10^5$/ml into 100mm Corning tissue-culture treated culture dishes, with 10mls per dish, 24 hours prior to transfection.

2.10.5 Calcium phosphate transfection

Principle

A calcium phosphate transfection method was used to introduce plasmids into 293T cells. The 293T cell line is a fast growing, highly transfectable derivative of human embryonic kidney cell line 293. 293T has constitutive expression of SV40 large T antigen that allows for episomal replication of transfected plasmids that have the SV40 origin of replication. Transfection was performed with plasmids containing viral envelope, e.g. VSV-G containing MD2.G, and those containing packaging elements such as Gag, Pol Rev and Tat. The transfected 293T then produced lentivirus that was used to transduce cells.

Reagents and equipment

- Packaging plasmid (pCMVΔR8.91 or psPAX2)
- Envelope plasmid (pMD2.G)
- Transfer plasmid
- 0.5M $CaCl_2$
- 2xHeBS pH 7.00 (0.28M NaCl, 0.05M HEPES and 1.5mM Na_2HPO_4)
- HEPES buffered water (water with 2.5mM HEPES (pH 7.3))

Procedure

15µg of packing plasmid and 15µg of envelope plasmid were mixed with 20µg of transfer plasmid and HEPES buffered water to a total volume of 250µl. 250µl of 0.5M $CaCl_2$ was added to the plasmid mix, and these were mixed by vortexing vigorously. The plasmid-$CaCl_2$ solution was then added dropwise to 500µl of 2xHeBS with continuous mixing throughout. The solution was left at room temperature for 30 minutes in order for precipitates to form. This solution was then applied dropwise to the 100mm plates containing a monolayer of 293T cells. After application of the solution 293T cells were returned to the incubator. The morning following transduction (12-16 hours post transduction) the precipitate containing media was removed from the 293T cells, and was replaced with fresh warmed media.

2.10.6 Lentiviral harvest

72 hours (48 hours for CRISPR virus) post transfection lentiviral containing media was harvested from 100mm plates. Lentiviral containing media was centrifuged at 3000rpm for 15 minutes at 4°C to pellet cells and debris. The supernatant was then passed through a low protein binding PVDF 0.45µm filter to remove any remaining 293T cells. The virus containing media was then either concentrated or stored at -80°C depending on the future experimental requirements.

2.10.7 Lentiviral concentration

When viral titre was insufficient to transduce the required cells, lentivirus was concentrated by ultracentrifugation.

Reagents and Equipment

- Open-top Konical™tubes (Beckman Coulter)
- SW32Ti swinging bucket rotor
- Optima XE 100 ultracentrifuge (Beckman Coulter)
- 70% ethanol
- RPMI-1640 with 10% FBS

Procedure

Konical™ tubes, adapters and SW32Ti swinging bucket rotor tubes were sterilised with 70% ethanol prior to use. 30mls of filtered lentiviral supernatant was transferred to the Konical™ tubes placed along with an adapter into the swinging bucket rotor tube. Tubes were then balanced and placed into the rotor in the Optima XE 100 ultracentrifuge and centrifuged fat 120,000g for 2 hours at 4°C. After centrifugation the supernatant was removed and viral pellet re-suspended by vigorous pipetting in 300-1000µl of RPMI-1640 with 10% FBS. Virus was aliquoted and stored at -80°C until use.

2.10.8 Production of Brunello library virus

Lentivirus was generated by calcium phosphate-based co-transfection of 293T cells as discussed 2.10.5. Transfection was scaled up from 100mm^3 plates to 150mm^3 plates, an increase in surface area of 2.7 times. All reagents and plasmids were increased by a factor of 2.7 per plate. Harvest timing and conditions were also adjusted as detailed in chapter 5.

2.11 Transduction of mammalian cells with lentivirus

Principle

Lentivirus is used to introduce the required sequences for expression of a gene, or knock down or even knock out of a gene of interest. This process is known as transduction. Polybrene is added to increase efficiency of transduction by neutralising the negative charge on the surface of the cells decreasing the repulsion between viral particles and the cell surface. Spinfection is known to increase transduction efficiency of lymphoid cells, and entails the centrifugation of cells and viral particles (O'Doherty et al., 2000).

Reagents and Equipment

- Ultra Centrifuge and rotor
- Polybrene (8mg/ml Hexadimethrine Bromide in water with 0.9%NaCl)
- Parafilm
- 12/24 well plate

Procedure

Where non-concentrated virus was sufficient for transduction, cells were pelleted and re-suspended with viral supernatant. For use of concentrated virus cells were re-suspended in fresh media, before addition of the virus. Polybrene was added at a concentration of 8µg/ml. A small-scale transduction was performed prior to each new experiment to check the viral titre. Cells were aliquoted into wells of a 12 or 24 well plates at a density of $1x10^6$/ml. PBS was added to empty wells surrounding the cells to prevent drying out, plates were sealed with parafilm and placed in a centrifuge spinning at 900g for 50 minutes at 34°C. After centrifugation parafilm was removed from the plates before returning them to the incubator. The following morning approximately 75% of the media was removed from the cells by gently aspirating media from the top of the wells being careful not to dislodge the cells that settled to the bottom of the plate. Fresh media was then added. Cells were then passaged and media changed as required.

2.11.1 Selection of Transduced cells with puromycin

The lentiCRISPRv2 vector contains a gene encoding resistance to antibiotic puromycin, we can therefore use puromycin to select the successfully transduced

cells. In order to select the concentration of puromycin to treat cells with, the puromycin sensitivity of the cell line was determined by cytotoxicity assay, in standard culture condition. The lowest possible concentration leading to death of all the cells was then selected.

2.12 Cytotoxicity assays

To establish response to drugs, cells were seeded in a plate containing the drug or inhibitor at increasing concentrations across the plate of cells. The plate was incubated for a set period of time, at the end of the treatment period, cell number was determined across the plate either by cell counting or by an assay that gives an approximation of cell number such as Resazurin assay or cell counting kit.

2.12.1 Resazurin

Principle

Resazurin is a blue fluorogenic dye that is irreversibly reduced by metabolically active cells to Resorufin, a fluorescent red product (excitation 530-545, emission 585-595) (Prabst et al., 2017). Fluorescence was measured when there was optimal difference between background and control well fluorescence, and prior reaching saturation.

Reagents and equipment

- Resazurin sodium salt (R7017, Sigma)
- FLUOstar Omega plate reader

Procedure

10µl of 10x Resazurin solution (100ug/ml Resazurin in PBS) was added to each well of the plate including a media blank, fluorescence was measured on a plate reader between 2-6 hours after addition of Resazurin (dependent upon cell line).

2.12.2 Cell counting kit

Principle

Cell counting kit 8 (Dojindo) is a water-soluble tetrazolium salt based assay. The pale-yellow coloured solution is reduced by metabolising cells to form an orange coloured formazan dye (Prabst et al., 2017). The production of orange reduced formazan is proportional to viable cell number and is detected by absorbance at 450nm.

Reagents and equipment

- Cell counting kit 8 (Dojindo)
- FLUOstar Omega plate reader

Procedure

10µl of Cell counting kit 8 reagent was added to each well of the plate. Absorbance was recorded at 405nm using a plate reader 2-6 hours after addition of the reagent.

2.12.3 Single agent drug assays

Cells were seeded into a 96 well plate with $3x10^4$ cells per well in 80µl. A dilution series was constructed in an empty 96 well plate with the highest concentration 5 times that required in the final assay. 20µl from the dilution series was then added to the respective well of cells. At least 9 different concentrations of each drug were used in addition to a solvent control and media only control well. Plates were incubated at 37°C and 5% CO_2 for 72 hours. Resazurin or cell counting kit assays were used to determine survival of cells compared to solvent control.

2.12.4 Statistical analysis of drug assays

All drug assays were performed in triplicate, for each experiment fluorescence was normalised to the solvent treated control (100%). GraphPad Prism software (GraphPad Software Inc.) was used to plot dose response curves and determine GI_{50}. The Concentrations were log transformed and a then the log inhibitor versus response from the non-linear regression analysis options was selected.

For ABT-737 experiments, concentrations were log transformed and nonlinear regression used to quantify the fold shift in the curves using inbuilt EC50 shift equation of prism. Where EC50 is half the maximal effect. To test if the EC50s were significantly different the null hypothesis that the ratio of EC50s would be 1 (no shift) was tested.

GI_{50} is defined as concentration giving half the maximal effect. In the case of cytotoxic drugs where dose response is from 100 to 0 % this is equivalent to the lethal concentration 50 (LC50). LC50 is the dose required to kill 50% of the cells.

2.12.5 Assessment of asparagine dependence in HPB-ALL

Principle

To assess the dependence of HPB-ALL growth and survival on exposure to L-asparagine, media containing no L-Asparagine –DMEM was used and different concentrations of L-asparagine applied to cells in a 96 well plate. Cell numbers were determined by Resazurin assay.

Reagents and Equipment

- DMEM
- FBS
- L-glutamine
- L-Asparagine

Procedure

HPB-ALL cells were counted, washed and re-suspended in a DMEM media with 10% FBS and L-glutamine (0.3g/L). Cells were aliquoted into a 96 well plate ($3x10^4$ cells per well) and L-asparagine was titrated across the plate (0.001g/L to 0.05g/L). After incubation for 72 hours Resazurin assay was performed.

2.12.6 Rescue from Asparaginase by Asparagine addition in HPB-ALL

Principle

Asparginase breaks down Asparagine into Aspartic acid and ammonia. Increasing the supply of asparagine should reduce the effect of asparaginase, if the decrease in cell number is due to depletion of available asparagine. HPB-ALL was routinely cultured in RPMI-1640 media which contained 0.05g/L L-asparagine by adding an additional 0.15g/L L-asparagine to the media the total L-asparagine amount was quadrupled.

Reagents and equipment

- RPMI-1640 media with 10% FBS
- L-asparagine (Ridges et al.)
- Asparaginase
- Resazurin
- FLUOstar Omega plate reader

Procedure

HPB-ALL cells were pelleted and re-suspended in RPMI-1640 media with 10% FBS, the cells were then separated into two separate tubes. The first tube of cells was aliquoted into the top half of a 96 well plate at $3x10^4$ cells per well. To the second tube an additional 0.15g/L L-asparagine was added, before cells were plated at $3x10^4$ cells per well to the bottom half of the 96 well plate. Asparaginase was then titrated over both halves of the plate. After 72 hours viability was determined by Resazurin assay. The viability at each Asparaginase concentration was compared between the two conditions.

2.12.7 Confirming mutation in the glucocorticoid receptor gene in HPB-ALL

NR3C1 encodes the glucocorticoid receptor to which Dexamethasone binds. Often cells that show resistance to Dexamethasone have mutations in *NR3C1*. RNA sequencing data from the cancer cell line encyclopaedia (Workman et al.) was examined for mutations in NR3C1 (Barretina et al., 2012a). The data highlighted a heterozygous mutation on chromosome 5 in *NR3C1* at position 142675147. This mutation from adenosine to guanine results in a methionine being replaced by threonine at codon 634 within exon 7 (p.M634T) Primers were designed flanking the

region of interest and used to amplify cDNA from HPB-ALL cells (table 2.7), this was subsequently sent for Sanger sequencing to confirm CCLE data

2.12.8 Response of HPB-ALL to dexamethasone

HPB-ALL cells were treated with 10µM and 100nM Dexamethasone at 0, 1, 2, 4, 6 and 24 hours. Cells were taken for analysis of mRNA (section 2.15). Cells were pelleted, RNA was extracted, cDNA synthesised and transcript levels of the glucocorticoid receptor, *GILZ* and *FKBP5* were assessed by real-time quantitative PCR. Primer sequences are given in table 2.7.

2.12.9 Combination treatment at fixed ratios

Principle

Once individual GI50 values had been determined it was important to look at how the cells responded to the drugs when they were combined. Drugs were combined at fixed ratios with each new drug added sequentially to the previous combination.

Drug	GI50 µg/ml (equiv nM)
dexamethasone	0.0916 (50nM)
daunorubicin (hydrochloride)	0.07 (124nM)
vincristine (sulphate)	0.001 (1.1nM)
asparaginase	0.36mU/ml

Table 2.13 GI50s for HPB-ALL

Procedure

GI50 values for HPB-ALL treated with dexamethasone, daunorubicin, vincristine and asparaginase were determined from single agent drug assays. Drugs were then combined at fixed ratios of 0.25, 0.5, 1, 2 and 4 times the GI50. For each drug pair, the drugs were run singularly and combined on the same plate (figure 2.1).

		Drug 1			Drug 2			Drug 1 & 2			
	4			4			4				
	2			2			2				
	1			1			1				
	0.5			0.5			0.5				
	0.25			0.25			0.25				
	0			0			0				

Figure 2.1 Example of plate layout for drug combination treatment. Drug 1 and drug 2 were added at 0.25, 0.5, 1, 2 and 4 times their respective GI50 values individually (yellow and green) and then combined (grey). Media was added to wells to as a control for background fluorescence (Moore et al.) and the plate was surrounded by PBS (light blue).

Assay	Drug 1	Drug 2
1	dexamethasone	daunorubicin
2	dexamethasone + daunorubicin	vincristine
3	Dexamethasone + daunorubicin + vincristine	asparaginase

Table 2.14 Combination assays

The combination of dexamethasone and daunorubicin was assessed first, before adding vincristine and then asparaginase consecutively, with multiple drugs being treated as a single drug as indicated in table 2.14. Plates were incubated for 72 hours and cell viability measured by Resazurin assay.

2.12.10 Analysis of synergy using Calcusyn

Percentage viability scores (normalised to solvent control wells) were converted to effect scores where an effect of 1.0 is where 0% of cells remain and an effect of 0.3 represents where 70% of cells remain compared to the solvent control. Effects of each drug alone or in combination were input into CalcuSyn software to produce Combination index (CI) values. CI values were recorded at 3 different dose points (IC) 50, 75 and 90.

2.12.11 4 drug matrix assay

Principle

When performing *in vitro* screening, it is important to select concentrations of drugs that apply enough pressure to reduce cell numbers, whilst leaving enough cells to analyse. Ideally all four drugs will contribute towards the chemotherapeutic pressure applied. Given dexamethasone, daunorubicin, vincristine and asparaginase were selected based on their clinical relevance, it was worth noting any selected combination should ideally be in keeping with the ratio of drugs found in patients. A matrix-based assay was selected for its ability to illustrate the effect of raising or lowering one drug with respect to the other drugs within the combination. Dexamethasone, daunorubicin, vincristine and asparaginase were titrated across HPB-ALL cells in a matrix assay. The individual GI50 values for each drug were used to guide effective concentration ranges for each drug. The following ranges were selected: dexamethasone 0-39.25ng/ml (~100nM), Daunorubicin Hydrochloride 0-140ng/ml (~248nM), Vincristine Sulphate 0-2ng/ml (~2nM) and Asparaginase 0-0.72mU/ml. Despite these cells being dexamethasone resistant, a top concentration of 100nM was selected to bring the concentration into a more clinically relevant range.

Reagents and equipment

- Multichannel pipette
- Drugs: dexamethasone (Caymen chemicals), daunorubicin hydrochloride (Caymen chemicals) , vincristine sulphate (Caymen chemicals) and asparaginase (Spectrilla, Medac)
- 96 well assay plates
- Resazurin
- FLUOstar Omega plate reader

Procedure

Dexamethasone, daunorubicin, vincristine and asparaginase were all titrated against each other in a matrix assay. In total 96 well plates were used to cover all possibilities of drug combinations. 3 different concentrations of dexamethasone were used and 4 concentrations for Daunorubicin, Vincristine and Asparaginase. Multiple dilutions were prepared for each drug to give 20x the required concentrations. Cells were seeded in 80µl volume, then each drug added in turn in a 5µl volume each, giving a total final volume of 100µl. Table 2.15 and figure 2.2 illustrate the way in which drugs were applied to the plates.

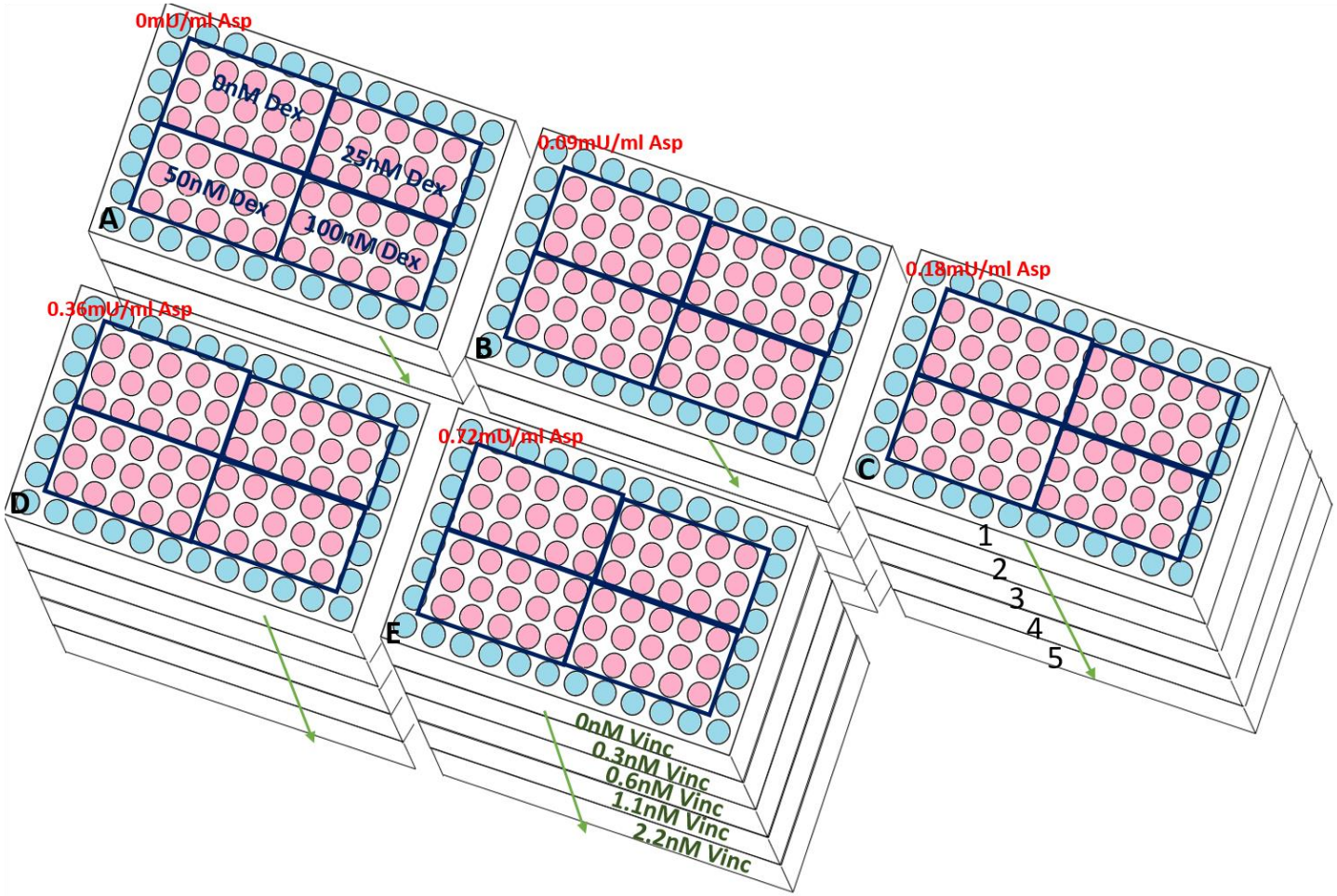

Figure 2.2 Plate layout for drug matrix assay. Shown is 5 stacks of 5 plates. Each plate was divided into quadrants with varying dexamethasone concentrations. Across each quadrant were increasing concentrations of daunorubicin in triplicate. Vincristine was titrated through each stack of plates (plates 1 through 5 had increasing Vincristine) and different asparaginase concentrations were applied to each stack of plates (A through E)

Drug	Conc (nMl)	Location
Dexamethasone	0	Top left each plate
Dexamethasone	25	Top right each plate
Dexamethasone	50	Bottom left each plate
Dexamethasone	100	Bottom right each plate
Daunorubicin	0	Rows 2 and 7 every plate
Daunorubicin	36	Rows 3 and 8 every plate
Daunorubicin	72	Rows 4 and 9 every plate
Daunorubicin	124	Rows 5 and 10 every plate
Daunorubicin	248	Rows 6 and 11 every plate
Vincristine	0	Plates labelled 1 (A-E)
Vincristine	0.3	Plates labelled 2 (A-E)
Vincristine	0.6	Plates labelled 3 (A-E)
Vincristine	1.1	Plates labelled 4 (A-E)
Vincristine	2.2	Plates labelled 5 (A-E)
Asparaginase	0	Plates labelled A (1-5)
Asparaginase	0.09	Plates labelled B (1-5)
Asparaginase	0.18	Plates labelled C (1-5)
Asparaginase	0.36	Plates labelled D (1-5)
Asparaginase	0.72	Plates labelled E (1-5)

Table 2.15 Drug matrix layout and drug concentrations

After 72 hours of incubation with drugs, Resazurin was applied to each plate in turn. Fluorescence was measured with a plate reader 3 hours after addition of Resazurin. The data from each plate was compiled in a spreadsheet. The background fluorescence was subtracted from each well, any anomalous triplicates were removed and then average readings for each condition calculated. Fluorescence

intensity for each condition was compared to a solvent control to give a percentage survival for that condition.

2.12.12 Using combenefit to examine synergy in drug matrix assays

Each position in a drug matrix has a synergy distribution score, calculated by effectiveness of the drug combination in terms of the amount of additional that is obtained is described by the first equation (figure 2.3). The additional effect is calculated by observed effect (E(a,b)) compared to a reference effect for single drugs (R(a,b)). The reference effect is dependent upon the model selected in the case of my work the Loewe model was used (second equation given in figure 2.3). The Reference effect was calculated by the second equation. The data is given by colour coded matrix diagrams with maximal possible score is 100 describing strong synergy are given in blue and where -100 describes strong antagonism in red. To describe the synergy across the whole matrix the sum of synergy and antagonism is used (SUM_SYN_ANT) and this is given by the last equation. This is the sum of synergy and antagonism observed in concentration logarithmic space. The mathematic and models used in combenefit are dare described in more detail in the accompanying publication (Di Veroli et al., 2016).

A Synergistic effect "extra effect"

$$E(a,b) = R(a,b) + S(a,b)$$

B Reference effect Loewe

$$E_A(a_u) = E_B(b_u)$$

$$R_{AB\_Loewe}(a,b) = E(a_u) = E_B(b_u)$$

C

SUM_SYN_ANT

$$\iint_{\boldsymbol{min}(\boldsymbol{a}>0),\boldsymbol{min}(\boldsymbol{b}>0)}^{\boldsymbol{max}(\boldsymbol{a}),\boldsymbol{max}(\boldsymbol{b})} \boldsymbol{S}(\boldsymbol{a},\boldsymbol{b}) \cdot \boldsymbol{dlog}(\boldsymbol{a}) \cdot \boldsymbol{dlog}(\boldsymbol{b})$$

Figure 2.3 Equations used by combenefit software for calculation of synergy. Calculation of synergistic effect of two drugs at conentrations a and b, by subtracting the reference effect R(a,b) from observed effect E(a,b) (A). Reference effect using Loewe model calculations, two doses are found au and bu are identified and for each

dose of (given as a and b) the reference effect is calculated (B). Synergy scores are given for each combination within the matrix, to assess synergy across the whole of the matrix the sum of synergism and antagonism (SUM_SYN_ANT) is used (C).

2.13 Flow Cytometry

2.13.1 Assessing transduction efficiency by flow cytometry

Principle

The plasmid SLIEW contains enhanced green fluorescent protein (EGFP). To identify cells successfully transduced with pSLIEW and expressing EGFP, the presence of EGFP was detected by flow cytometer with a blue laser (488nm).

Reagents and equipment

- Flow cytometer
- FlowJo software

Procedure

Cells were gated by forward and side scatter, doublet discrimination was performed and EGFP detected with the blue laser (488nm). Transduction efficiency was determined using FlowJo software and compared to un-transduced cells.

2.13.2 Detection of human leukaemic cells in murine peripheral blood

Principle

One method of assessing engraftment of leukaemic cells *in vivo* is via peripheral blood monitoring. 50µl of peripheral blood was taken from the mouse tail vein by venepuncture, stained with an antibody cocktail containing antibodies against human CD45 (hCD45) and CD3 (hCD3) and murine CD45 (HPB-ALL is hCD45 and hCD3 positive). These samples were then run on the flow cytometer to determine the percentage (%) of human cells in the peripheral blood.

Reagents and equipment

- BD FACSCanto™ II
- FlowJo software
- Red cell lysis solution (8.3g of NH_4Cl_2, 1g $KHCO_3$ and 0.38g Na_2EDTA in 100ml water)
- PBSA (0.2% bovine serum albumin (BSA) in PBS)
- Antibodies (table 2.3)

Procedure

50µl of murine peripheral blood was transferred into a microfuge tube. Cell surface marker staining was performed by addition of antibodies to murine CD45, human CD45 and human CD3 (using manufacturer recommended test volumes). After a 20-minute incubation red blood cell lysis was performed (section2.13.3). Cells were washed twice with PBSA before adding the viability dye LIVE/DEAD™. Following a 30-minute incubation, cells were washed twice and fixed in 2% Paraformaldehyde (PFA) and stored at 4 degrees until run within 1 week. Samples were run on a BD FACSCanto™ II and analysed with FlowJo software.

2.13.3 Red blood cell lysis

Samples containing large numbers of red blood cells, for instance peripheral blood and some bone marrow samples, underwent red cell lysis prior to analysis by flow cytometry. Red blood cell lysis stock solution (8.3g of NH_4Cl_2, 1g $KHCO_3$ and 0.38g Na_2EDTA in 100ml water) was diluted 1 in 10 in water to prepare the working concentration on the day of use. 1.2mls of red cell lysis solution was added to a 50µl sample. The sample was incubated with regular agitation for 10 minutes to ensure adequate lysis.

2.13.4 Detection of human leukaemic cells in murine tissues

Principle

Leukaemic cells also engraft in tissues in mice, such as bone marrow and spleen. Flow cytometry can be used to assess the percentage of human leukaemic cells in harvested samples. In a similar way to peripheral blood staining, an antibody cocktail containing antibodies against human CD45 and human CD3 and murine CD45 is added to a sample, and this can then be analysed by flow cytometry.

Reagents and equipment

- BD FACSCanto™ II (BD biosciences)
- FlowJo software
- Antibodies (as per table 2.3)

Procedure

Cells were washed, counted and 0.5-2x10^6 cells were re-suspended in 50µl of PBSA. Antibodies as per table 2.3 were incubated for 20 minutes at room temperature protected from light. If performing on freshly harvested samples containing red blood

cells, red blood cell lysis was performed first. The cells were then washed and stained with a viability marker for 20 minutes. When using frozen viable cells this step was omitted, and viability staining was performed at the same time as surface marker staining. Samples were fixed in 2% PFA and stored at 4°C. Samples were run on a BD FACSCanto™ II and analysed with FlowJo software.

2.13.5 Detection of phosphorylated Histone H2A.X in HPB-ALL cells treated with Vincristine, Dexamethasone, Asparaginase and Daunorubicin as a combination *in vivo*

Principle

PhosphoH2AX is a marker of DNA damage (Kuo and Yang, 2008). PhosphoH2AX levels in HPB-ALL cells treated *in vivo* with chemotherapy were compared to those who had received only solvent control. Cells were harvested from murine bone marrow and contained a mix of human HPB-ALL cells and murine cells. Human CD45 targeting antibody with APC fluorophore was used to identify HPB-ALL cells, and an antibody targeting phosphH2AX conjugated with fluorophore PE was used as a measure of DNA damage within these cells. .

Reagents and equipment

- BD Cytofix™ (BD biosciences)
- Phosflow™ Perm Buffer II (BD biosciences)
- BD FACSCanto™ II (BD biosciences)
- huCD45, muCD45, live/dead and phosphoH2AX antibodies (table 2.3)

Procedure

0.5-1x10^6 cells were prepared per tube. Cells were stained in 50µl containing 10µl human CD45 (to identify HPB-ALL cells) and 0.2µl LIVE/DEAD ™ to identify viable cells in PBA. Cells were washed with PBA then fixed for 30 minutes on ice in 250µl of BD Cytofix™. Cells were washed twice with PBA. 300µl of cold Phosflow™ Perm Buffer II was added dropwise during vortex to permeabilise the cells. After a 30 minute incubation on ice, cells were washed with PBA, pelleted and antibody cocktail staining solution containing 2.5µl phosphoH2AX, 1µl mouse serum and 75µl PBA added. Cells were incubated for 45 minutes at room temperature, washed and then run on a BD FACSCanto™ II cytometer.

2.13.6 Competitive assay

Principle

To assess the impact of gene knockdown, cells with targeted shRNA are compared in a competitive assay with cells treated with a non-targeting control shRNA. The targeted shRNA is tagged with a fluorochrome to allow tracking of the knockdown cells. The non-targeting control shRNA is tagged with an alternate fluorochrome for direct comparison. Flow cytometry can be used to detect the relative proportion of fluorochrome conjugated cells over time.

Reagents and equipment

- shBCL-X/ shHECTD2/ shNTC2 in pLKO5d.SFFV.miR30n with GFP
- shNTC in pLKO5d.SFFV.miR30n with RFP657
- ATTUNE NxT flow cytometer
- FlowJo v10.0.8

Procedure

DND41 cells and HPB-ALL cells were re-suspended in lentivirus supernatant (generated as described in 2.10) for shBCl-X, shHECTD2, shNTC2 and shNTC1 in the presence of 8µg/ml polybrene. Cells were spinfected as previously described. Four days post transfection cells were counted and GFP and RFP657 expression was assessed by flow cytometry. RNA samples were taken to assess knockdown efficiency. Cells were combined so that there were even percentages of GFP and RFP657 positive cells. For each cell line the populations listed in table 2.16 were set up. Each flask of cells was then split equally, to one half VXLD was added (dex 50nM, dauno 33nM, vinc 1nM, asp 0.36mU/ml). Figure 2.4 outlines the process. The percentage of GFP and RFP657 cell was assessed every 3-4 days.

Population 1	Population 2
shBCl-X-GFP	shNTC1-RFP657
shHECTD2-GFP	shNTC1-RFP657
shNTC2-GFP	shNTC1-RFP657

Table 2.16 Competitive assays set up for HPB-ALL and DND41

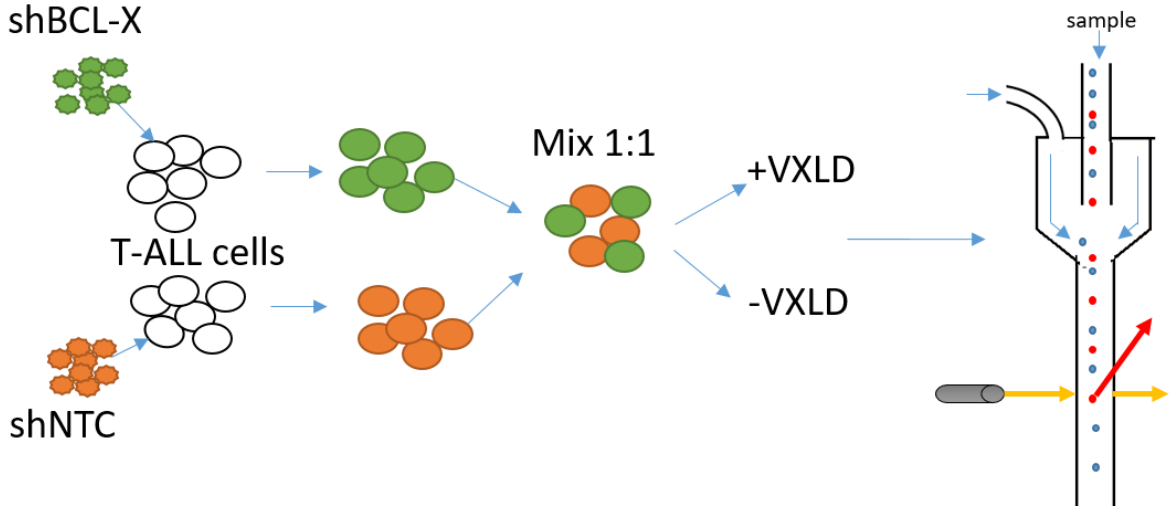

Figure 2.4 Schematic of competitive assay. The T-ALL cell lines were transduced with virus containing shRNAs targeting BCL-X or HECTD2 and GFP. The same cell line was also transduced with virus with non-targeting control (NTC) shRNA with RFP657. Transduction efficiency was assessed by flow cytometry 4 days post transduction. Cells were mixed to give equal percentages of GFP and RFP657 cells. The pooled cells were then halved and to one half VXLD treatment was added. The percentage of GFP and RFP657 was monitored over time by flow cytometry.

2.13.7 Apoptosis

Principle

To assess level of apoptotic cells (for instance with VXLD or ABT-737 treatment) cells were stained with a PE-conjugated Annexin V antibody and LIVE/DEAD viability dye. Annexin V binds to phosphatidylserine (PS) in presence of calcium. PS is normally found on the intracellular part of plasma membrane of healthy cells. During early apoptosis PS translocates to the external leaflet. Combining annexin V with a viability dye such as live/dead aqua in the presence of containing calcium (such as annexin binding buffer) can identify cells with PS on the outer membrane and cells with a permeable membrane.

Reagents and equipment

- Annexin V-PE antibody
- LIVE/DEAD fixable aqua viability dye
- Annexin V binding buffer (Biolegend, 422201)
- ATTUNE NxT flow cytometer
- FlowJo v10.0.8

Procedure

Cells were pelleted and washed twice with PBS. Cells were re-suspended in 1x annexin V binding buffer at a concentration of $1x10^6$/ml. To 100µl of cells in binding buffer 5µl of AnnexinV-PE and 0.5µl LIVE/DEAD fixable aqua was added, before incubation protected from light for 15 minutes at room temperature. 400µl of additional binding buffer was then added prior to running samples through a ATTUNE NxT flow cytometer. Single colour and unstained samples were prepared at the same time to check compensation and gating. Data was analysed with FlowJo.

2.14 Quantification of plasmids, DNA and RNA by nanodrop

The buffer in which the DNA/RNA is dissolved is used to blank the Nanodrop 2000 spectrophotometer. To determine the concentration of DNA/RNA in a sample, 1µl of sample is applied to the nanodrop and the concentration is determined according to the amount of light passing through at 260nm.

2.15 mRNA expression

2.15.1 RNA extraction with RNeasy® Mini kit

Principle

The RNeasy® kit uses silica columns to purify RNA from cells.

Reagents and equipment

- RNeasy® mini column
- Buffer RLT
- RNase free DNase and buffer RDD
- Wash buffers RW1 and RPE
- RNase free water
- 70% ethanol

Procedure

Cells were washed with PBS and pelleted. 350µl of buffer RLT (Qiagen) was added to the cell pellet. The sample was then either extracted immediately or stored at -20°C. The sample was placed into a QIAshredder column and spun at maximum speed for 2 minutes to homogenise the cells. 350µl of 70% ethanol was added to the homogenised lysate. This was all transferred to the RNeasy column. The column was centrifuged at 8000g for 30 seconds and the flow through discarded. The column was washed with 350µl of RW1 buffer and centrifuged 8000g for 30seconds. A DNA digest was performed by applying RNase free DNase (10µl DNase1 in 70µl buffer RDD) to the column and incubated for 15 minutes. The column was washed with 350µl of RW1 and centrifuged at 8000g for 30 seconds. The supernatant was discarded. 500µl of RPE buffer was applied to the column and this was centrifuged at 8000g for 30 seconds and flow through discarded. The column was placed in a fresh tube and spun at full speed for 1 minute to remove residual wash buffer. 30µl of RNase free water was added to the column before spinning at 8000g for 1 min to elute the DNA.

2.15.2 RNA extraction with RNeasy® Micro kit

Principle

If there were a limited number of cells (<3x10^5) the RNeasy® Micro kit was used, instead of the RNeasy® mini kit, since this kit is optimised for smaller cell numbers. It uses a silica membrane column like the RNeasy® mini kit.

Reagents and equipment

- RNeasy® mini column
- Buffer RLT
- RNase free DNase and buffer RDD
- Wash buffers RW1 and RPE
- RNase free water
- 70% ethanol
- 80% ethanol prepared with RNase free water

Procedure

Cells were washed with PBS and pelleted. 350µl of buffer RLT (Qiagen) was added to the cell pellet. The sample was then either extracted or stored at -20°C and extracted later. The sample was placed into a QIAshredder column and spun at maximum speed for 2 minutes to homogenise the cells. 700µl of 70% ethanol was added to the homogenised lysate. This was all transferred to the RNeasy column. The column was centrifuged at 8000g for 30 seconds and the flow through discarded. The column was washed with 350µl of RW1 buffer and centrifuged 8000g for 30seconds. A DNA digest was performed by applying RNase free DNase (10µl DNase1 in 70µl buffer RDD) to the column and incubated for 15 minutes. The column was washed with 350µl of RW1 and centrifuged at 8000g for 30 seconds. The supernatant was discarded. 500µl of RPE buffer was applied to the column and this was centrifuged at 8000g for 30 seconds and flow through discarded. 500µl 80% ethanol was applied to the column, which was centrifuged at 8000g for 30seconds. The column was placed in a fresh tube and spun at full speed for 5 minutes to remove residual ethanol. 9µl of RNase free water was added to the column, this was incubated for 5 minutes before spinning at 8000g for 1 min to elute the DNA.

2.15.3 cDNA synthesis

Principle

RevertAid H Minus First Strand cDNA synthesis kit (Thermo Fisher Scientific) was used to produce cDNA from mRNA. The kit uses a reverse transcriptase enzyme lacking RNase H activity to reduce RNA degradation and RiboLock RNase inhibitors which protect the RNA from RNases.

Reagents and equipment

Reagent	Volume (µl)
RNA (500-1000ng)	
Random hexamer (100µM)	1
RNase free water	11-RNA volume

Table 2.17 cDNA synthesis step 1 reagents

Reagent	Volume per reaction (µl)
5x Reaction Buffer (250 mM Tris-HCl (pH 8.3), 250 mM KCl, 20 mM MgCl2, 50 mM DTT)	4
dNTP (10mM)	2
RiboLock inhibitor (20 units/µl)	1
RevertAid H Minus M-MulV Reverse Transcriptase (200 units/µl)	1

Table 2.18 master mix components (step 2 cDNA synthesis)

Procedure

500 to 1000ng of RNA was added to a PCR tube, with 1µl of Random hexamer primers and RNase free water to give a total volume of 12µl. The reaction mix was placed into a Thermo cycler PCR machine. Samples are heated to 70°C for 5 minutes and then cooled to 4°C. Samples were then removed from the PCR machine. Master Mix consisting of (reaction buffer, dNTPs, RiboLock inhibitor and Reverse Transcriptase) was added to each sample (8µl/sample). The samples were put back into the PCR machine for the following settings: 25°C for 10 minutes, 42°C for 60 minutes and 70°C for 10 minutes, samples were then kept at 4°C until removed from the PCR machine. 100µl of RNase free water was added and the cDNA stored at -20°C until use.

2.1.6 Quantitative Real Time polymerase chain reaction (qRT-PCR)

Principle

To determine changes in gene expression in cells after drug treatment, quantitative real time PCR was performed. Primers were designed for genes of interest, PCR was performed and the levels of PCR product were measured by use of SYBR® Green that intercalates with double stranded DNA. The fluorescence from SYBR Green was proportional to DNA content, allowing quantitative measurement of PCR products.

Reagents and Equipment

- SYBR Green (Platinum® SYBR® Green qPCR SuperMix-UDG with ROX, 2X, Invitrogen)
- RT-PCR primers
- ViiA Real-Time PCR System (Applied Biosystems)

- 384 well PCR plates
- MicroAmp® Optical Adhesive Film (Applied Biosystems)

Procedure

For each gene a mix was prepared containing SYBR Green (5µl), 10µM primer mix of forward and reverse primers (0.3µl per well) and nuclease free water (2.7µl per well). 8µl of the mix was pipetted into each of the required wells in a 384 well PCR plate before 2µl of cDNA was added. Each sample was run in triplicate. The plate was sealed with a MicroAmp® film and centrifuged to ensure all liquid was within the wells. The plate was run on the ViiA Real-Time PCR System with the conditions shown in figure 2.5.

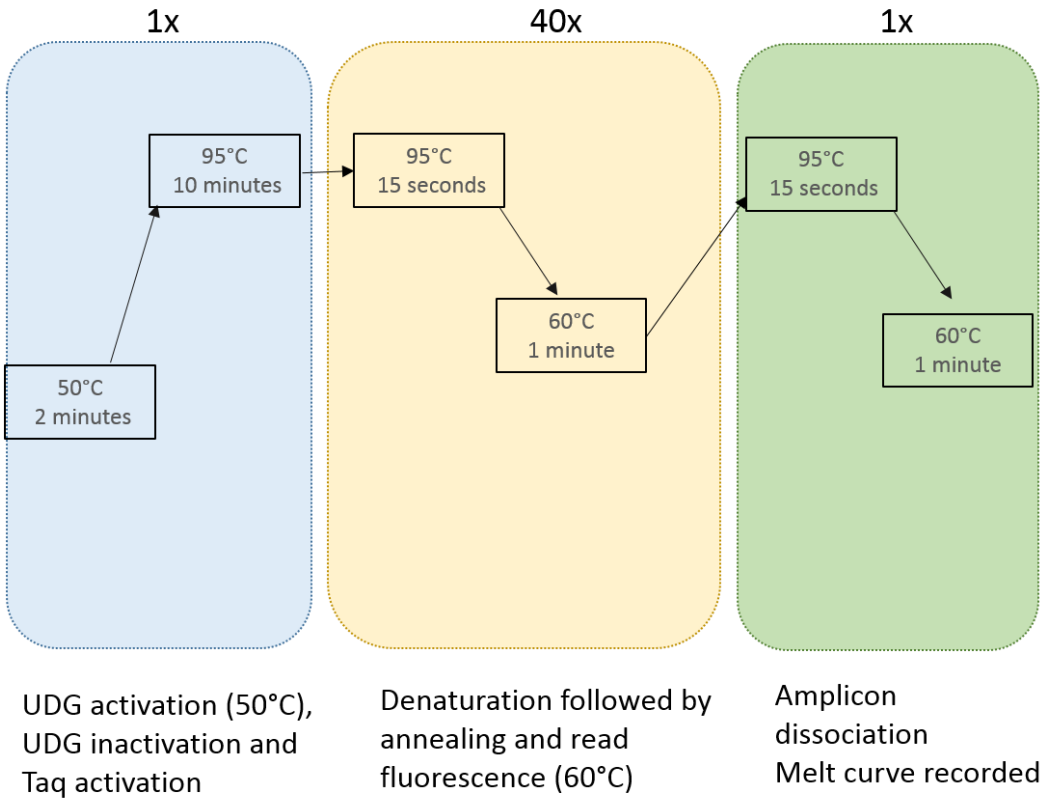

Figure.2.5 Real-time quantitative PCR conditions.

2.16 Statistics for expression changes

Data from triplicate experiments were input into GraphPad Prism for *in vitro* dexamethasone treated cells, a one way annova with repeated measures and then Holm Sidak's multiple comparisons test was used to assess if changes in expression were significant at each time point compared to the starting 0 hour time point.

For *in vivo* samples a single time point was used. Data from 3 control mice and data from 3 VXLD mice were treated as independent replicates. GraphPad prism was used to perform an unpaired t-test.

2.17 Agarose gel electrophoresis

The appropriate weight of ultrapure agarose is dissolved in 50ml of 1xTAE buffer, and 0.01% GelRed is added and set in gel setting apparatus. Gels are placed in a BioRad tank containing 1xTAE buffer. Samples are mixed with 5xloading buffer before being loaded into the gel alongside a molecular weight marker. Gels are run at up to 100 Volts until there is sufficient separation. Gels are imaged using either a GelDoc (BioRad) or G:BOX (Syngene).

2.18 Mouse lines

2.18.1 NSG (NOD.Cg-PrkdcscidIlrgtm1Wjl/SzJ)

Severely immunocompromised these mice have no mature B, T or NK cells, and have defective dendritic cells and macrophages. They can successfully engraft a wide range of cancers and better engrafts cancer stem cells than NOD scid or nude mice (Adams et al., 2017, Shultz et al., 2005, Ishikawa et al., 2005).

2.18.2 RAG2 (Rag2-/- gamma c-/-)

Rag 2 and gamma common chain homozygous mutant mice with a BALB/c background from in house colony (Traggiai et al., 2004).Mice lack B ,T and NK cells.

All *in vivo* work was carried out under the personal licence ICDB9C2D0 with project licence PPL60/4222, except for the pharmacokinetic additional time points that were carried out under project licence PPL70/8769. Mice were bred in house.

2.18.3 Animal husbandry

Mice were housed in a specific pathogen free (SPF) environment in individually ventilated cages (IVC). Mice were weighed and checked for signs of ill health weekly after injection with leukaemic cells (intra-femoral injection), and daily during drug

treatment. In accordance with the home office licence, mice were killed if they lost >20% of their heaviest previous weight or lost >15% maintained for 3 days, or had tumours exceeding 15mm. Mice were monitored for other signs of ill health, including piloerection, hunched position, paleness of ears and tails, porphyrin staining of nose/eyes, abdominal breathing, unusual gait and loss of muscle tone. Mice were killed by cervical dislocation, a schedule 1 listed method for humane killing of laboratory animals. Ear notching was used to distinguish mice within a single cage.

2.19 **Intra-femoral injection**

Principle

Leukaemia arises within the bone marrow, the bone marrow microenvironment forms the niche that contributes to survival and propagation of leukaemia (Duarte et al., 2018). When introducing leukaemic cells to mice, they are implanted into their natural nice in the bone marrow of the femur via intra-femoral injection.

Reagents/Equipment

- Category II laminar flow hood
- Anaesthetic rig with induction box and small animal face mask
- Isoflurane
- Carprofen (Rimadyl small animal solution for injection, Zoetis)
- 29 Gauge needles (BD microfine U-100 insulin needles, BD biosciences)
- Skin disinfectant (Hydrex Derma Pink spray)

Procedure

The procedure was carried out in a category II laminar flood hood to provide a sterile environment. Mice were placed in an induction box with 5% Isoflurane, and then moved to a face mask with ~3% Isoflurane to maintain a surgical depth of anaesthesia. Analgesic Carprofen was given at 5mg/kg by sub-cutaneous injection at the start of the procedure. The injection site was prepared by shaving of the fur and application of skin disinfectant. The leg was flexed and held as a 29 Gauge needle was used to drill into the femur. The sample was then injected in a 20-30µl volume using a fresh needle. Mice were removed from anaesthetic and placed in their home cage for monitoring as they recovered.

2.20 **Administration of substances by injection**

Administration of drugs and other substances was performed by 3 routes of injection: subcutaneous, intra-peritoneal or intra-venous. Dosing was performed in accordance with home office licence requirements and guidelines set out in guidelines for the welfare and use of animals in cancer research (Workman et al., 2010).

2.20.1 Subcutaneous injection

A subcutaneous injection was used to administer the analgesic Carprofen prior to intra-femoral injection. The injection was performed with mice already anesthetised. The skin around the scruff was tented and 25 Gauge needle inserted at a parallel angel to the mouse, and 5mg/kg Carprofen was injected under the skin.

2.20.2 Intra-peritoneal injection

Intra-peritoneal injection was used to give drugs during VXLD dosing and to administer luciferin for IVIS procedure. The mouse was restrained by tightly grasping the scruff in the hand. The other hand was used to insert a 29-gauge insulin needle into the lower left/lower right quadrant of the abdomen at a 45 degree angle to the mouse. During dosing alternate side of the peritoneum were injected.

2.20.3 Intra-venous injection

Daunorubicin was given by intravenous injection. Daunorubicin was administered by injection into a lateral tail vein using a 29-gauge insulin needle by a competent member of staff.

2.21 *In vivo* imaging

Principle

Cells transduced with a vector containing luciferin, for instance pSLIEW, can be visualised using an *in vivo* imaging system. Mice are injected with the substrate luciferin and where the cells containing the luciferase gene are present, a light signal is produced which is detected by the camera within the imaging system.

Reagents and Equipment

- D-luciferin potassium salt powder (Intrace Medical SA)
- DPBS
- IVIS spectrum (Caliper life sciences)
- Living image ® (Caliper life sciences)

Procedure

Anaesthetic equipment and the IVIS machine were cleaned and prepared for imaging. Luciferin aliquots (30mg/ml D-luciferin potassium salt in DPBS) were removed from the -20°C freezer and allowed to come to room temperature protected from light. Mice were injected via intra-peritoneal route with 150mg/kg Luciferin. Mice were put in an induction chamber with 5% Isoflurane and then transferred to the heated stage of the IVIS spectrum with the face within a nose cone providing maintenance of anaesthesia (2.5-3% Isoflurane). Mice were imaged ventrally, and sometimes additionally dorsally and on each side. Images were analysed with Living Image software.

2.22 Peripheral blood collection

Peripheral blood samples can be taken from mice in order to assess drug levels in the plasma or to detect human leukaemic cells as a measure of engraftment.

2.22.1 Blood sampling by venepuncture of tail vein

Small volumes of blood (less than 10% of the circulating blood volume) can be taken from mice for analysis. Mice are placed within a restraining device before making a small puncture in one of the lateral tail veins with a scalpel blade. A Microvette® with a lithium-heparin coating (Sarstedt) is used to draw up approximately 50µl of blood.

2.22.2 Blood collection by terminal cardiac puncture

When large volumes of blood were required (>10% circulating blood volume), blood was taken under terminal anaesthesia by cardiac puncture. Heparin solution (Multiparin, CP Pharmaceuticals) was used to coat the syringe and collection tube to prevent clotting. Mice were placed into an induction box with 5% isoflurane and then transferred to a face mask. After confirming surgical depth of anaesthesia, a needle was inserted into the heart and 1ml with blood slowly withdrawn. The blood was placed in a tube. Mice were killed whilst still under anaesthetic by cervical dislocation.

2.23 VXLD toxicity testing

Principle

The use of any agent in an *in vivo* setting requires consideration of tolerability as well as efficacy. Giving 4 drugs in combination, it was particularly pertinent that we established a tolerable and efficacious dosing regimen before proceeding with a large-scale screen. These 4 drugs have already been used as a combination in NOD/SCID mice in a published study, albeit with issues of toxicity associated with Daunorubicin (Samuels et al., 2014a). Since the use of these 4 drugs isn't documented in the $Rag2^{-/-}\gamma c^{-/-}$ RG mice, or used in our facility in other strains, it was important to check the toxicity of the published regimen in our mice and with our specific licence constraints. We initiated toxicity testing in 2 male and 2 female mice with the same dexamethasone, vincristine and asparaginase doses published and a lower daunorubicin (2.5mg/kg reduced to 0.45mg/kg).

Reagents/Equipment

Drugs at concentrations and routes listed in table 2.5. Dexamethasone was used initially at 5mg/kg then lowered to 2.5mg/kg.

Procedure

Mice were given drugs by the routes, doses and frequencies given in table 2.5. All 4 drugs were given on Monday and then Dexamethasone and Asparaginase also given Tues-Friday. Mice were dosed with all 4 drugs on the first day of treatment starting with an intravenous (IV) dose into the lateral tail vein of Daunorubicin, followed by a dose of Vincristine via the intra-peritoneal (IP) route, they were then given dexamethasone by IP, and lastly Asparaginase IP. The following four days mice received Dexamethasone by IP and then Asparaginase by IP.Mice were carefully monitored and their weights recorded daily. If weight loss reached 10%, dosing was suspended and continued once weight was regained. Adjustments to doses and frequencies were made as required. In addition to weight monitoring, mice were observed for changes in appearance and behaviour. Mice were monitored for 1 hour after administration of each drug to check for adverse effects. VXLD dosing efficacy studies

2.24 **VXLD efficacy testing**

Principle

Once a tolerable dosing regimen was established, further dosing was performed to test the efficacy of the dosing and further adjustments were made to the starting time of dosing and frequency of dosing blocks.

Reagents and equipment

Drug formulations, concentration, doses and routes as given in table 2.5. Dexamethasone was given at 2.5mg/kg.

Procedure

HPB-ALL cells transduced with pSLIEW were injected into mice. The engraftment was confirmed by IVIS procedure. Mice were then each assigned a number and using a random number generator, 3 were assigned to receive control injections, the remaining 6 received treatment. The first block of treatment was given from days 11 through to 15, a second block of treatment was then given from day 25 to day 29. Drugs were given at doses indicated in table 2..5, that had previous been established during toxicity testing. IVIS was performed weekly to monitor changes in leukaemic

burden. Additionally, samples were harvested (section 2.18.9), RNA was extracted for analysis of mRNA with primers specific for human genes (table 2.16). Viable cells were frozen to be used for flow cytometry analysis of leukaemic burden and phosphoH2AX levels.

2.24.1 Analysis of bioluminescent imaging data

Living image software was used to obtain total flux measurements for each mouse after imaging. Total flux is a measure of the radiance (photons per second) over a region of interest- in this case the whole mouse was used.

Total flux measurements were calculated for each mouse at every imaging time point. GraphPad Prism was used to perform 2-way annova (with repeated measures) to assess if there was a significant difference in total flux between control and treated mice.

2.24.2 Analysis of event free survival

Mice were weighed and monitored for signs of leukaemia. When a mouse reached a predefined study endpoint (weight loss >15%, abnormal gait, abdominal breathing or reduced body temperature) they were killed, and this was recorded as an event. A survival curve was generated with the GraphPad Prism software. Significant differences between groups and hazard ratio were reported by Log Rank method.

2.24.3 Analysis of murine bone marrow engraftment

Flow cytometry was used (as previously described in 2.13.4). Data was analysed using the FlowJo software to determine the percentage of human cells within each sample. Differences in engraftment between treated and control samples were analysed in GraphPad Prism using an unpaired t-test.

2.25 Harvesting leukaemic cells from mouse spleen

Principle

Splenomegaly is common feature of acute lymphoblastic leukaemia, where leukaemic cells collect within the spleen causing increased spleen size and weight. Often xenograft models of T-ALL show splenomegaly due to engraftment of leukaemic cells. Leukaemic cells can easily be harvested from the spleen for analysis or for use as patient derived xenograft cells.

Reagents and Equipment

- Skin disinfectant (Hydrex Derma Pink spray)
- Scissors and forceps
- Falcon cell strainer 40µm Nylon
- syringe

Procedure

Mice were humanely killed at the end of the study. A skin disinfectant was applied to the mouse before cutting the skin and peeling back the fur. The peritoneal wall was cut and the spleen extracted from the mouse using scissors and forceps. The spleen was weighed and then homogenised with the end of sterile syringe. The cells are were then mixed with PBS and passed through a 40µm Nylon cell strainer to give a single cell suspension.

2.26 Harvesting leukaemic cells from bone marrow (flushing method)

Principle

Leukaemic cells often reside in the bone marrow. Cells can be extracted from murine bone marrow in addition to spleen, or as an alternative to splenic samples when the leukaemia does not infiltrate the spleen.

Reagents and Equipment

- 29 Gauge needles (BD microfine U-100 insulin needles, BD biosciences)
- PBS
- Skin disinfectant (Hydrex Derma Pink spray)
- Scissors and forceps

Procedure

Mice were humanely killed at the end of the study. A skin disinfectant was applied to the mouse before cutting the skin and peeling back the fur. Muscle was trimmed from the hind limbs. The hind limbs were then removed by cutting at the hip joint. The femurs were separated by breaking the kneecap backwards and then dissecting the ligaments. The ends of the femur were removed leaving just the diaphysis (central part of the bone). A needle and syringe filled with PBS was then inserted into the bone and used to flush out the bone marrow.

2.27 **Harvesting of mouse bone marrow (crushing method)**

Principle

A flushing technique of bone marrow extraction only uses the centres of the long bones, a lot of bone marrow is lost during the flushing procedure from the ends of the bones, as well as from flat bones such as the cristae. An alternative is to crush the bones to release the bone marrow, which can be performed on any bone. Bone marrow was extracted by this method from any of the sites highlighted in figure 2.6.

Reagents and Equipment

- Falcon cell strainer 40µm Nylon
- Pestle and mortar
- 29 Gauge needles (BD microfine U-100 insulin needles, BD biosciences)
- PBS
- Skin disinfectant (Hydrex Derma Pink spray)
- Scissors and forceps
- Trypan blue
- Methylene blue

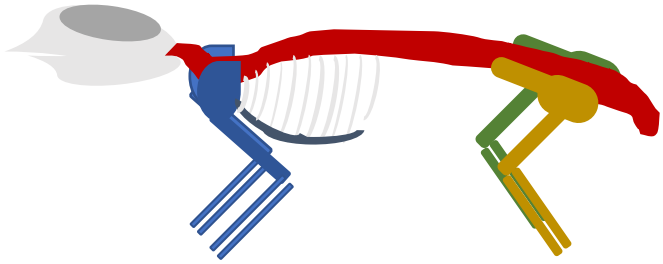

A - injected hind limb

B - contralateral hind limb

C - forelimbs and sternum

D - spine

E- calvaria

Figure 2.6 Diagram of mouse skeleton. The different bones from which cells were harvested are highlighted.

Procedure

Mice were killed by cervical dislocation. The body was sprayed with skin disinfectant, prior to the removal of skin and fur. Muscle was then dissected away from the limbs, and the limbs detached from the body using scissors and forceps. The limbs were separated into individual bones which were then cleaned with tissue. To remove the sternum, the rib cage was exposed and straight cuts are made through the ribs either side of the sternum to release it. To harvest cells from the spine, the spine was cut at the base of the tail and at the neck. The muscle was cut away from the vertebrae, before passing a needle down the spinal column to remove the spinal cord. The vertebrae were then separated and cleaned. Cleaned bones were placed into a mortar with a small amount of PBS and were crushed with a pestle to release the cells from the bone marrow. The PBS containing the cells released from the bones was passed through a 40µm sieve to remove clumps and large bone fragments. If separate bone marrow compartments were required bones were crushed and filtered separately, otherwise bones were pooled prior to crushing. To harvest cells from the calvaria, scissors were inserted into the opening at the base of the skull and then up and round the outside of the calvaira so that the calvaria lifted away from the rest of the skull. The inside surface of the calvaria containing the leukaemic cells was washed in PBS to lift of the cells. The PBS containing cells was then filtered through a 40µm sieve. Cells were washed with PBS and counted with both trypan blue to assess viability and methylene blue (to exclude red cells).

2.28 Pharmacokinetic study

2.28.1 Timetable and collection of samples

Principle

Once a tolerable and efficacious drug regimen had been established, we wanted to determine whether the levels of drug we were using was within a clinically applicable range. In keeping with the principle of the 3Rs, we reduced the number of mice in the pharmacokinetic study to a minimum (Prescott and Lidster, 2017). We chose to only assess the pharmacokinetics of the drugs as used in the combination and chose time points based around already published data (Szymanska et al., 2012b).

Reagents and equipment

- Drugs as per table 2.5
- Anaesthetic rig and isoflurane
- Mouse re-strainer
- Heparin
- Microvette®
- Biofuge 15 Centrifuge (Heraeus)

Procedure

A total of 7 groups of mice (3 mice per group) were used to collect plasma for pharmacokinetic analysis (figure 2.7 and table 2.19). Except for group 1, all mice contributed 2 time points; one sample was taken by tail venepuncture and the other by cardiac puncture (section 2.18.4). The collected blood was centrifuged in a Biofuge 15 at 14000rpm, for 5 minutes to separate the cells and plasma. Plasma was then transferred to a fresh centrifuge tube and stored at -20°C (or -80 °C for asparaginase quantification) until analysis.

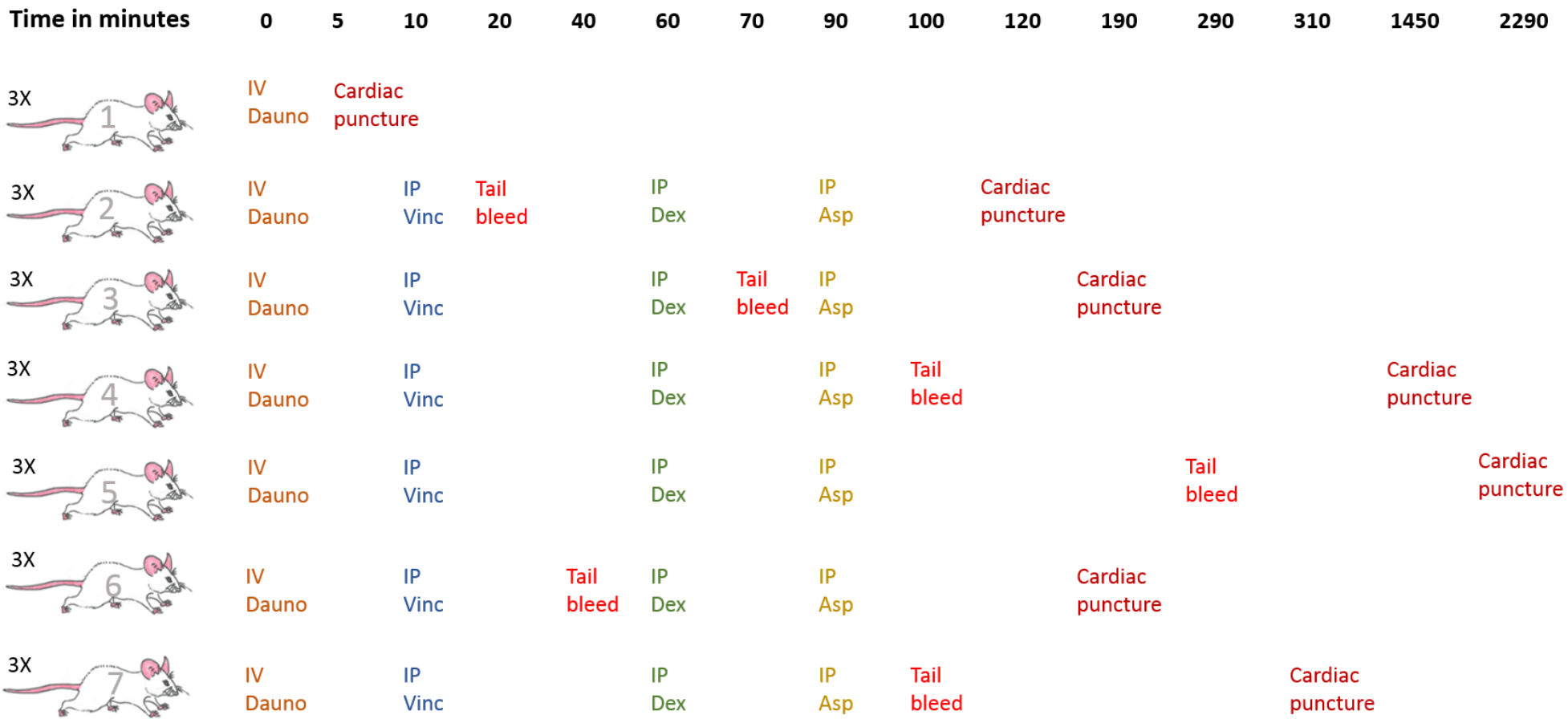

Figure 2.7 Outline of pharmacokinetic study. The groups of mice, relative dosing time for administration of drugs, and timings and method of blood collection.

Drug	Time point 1	Time point 2	Time point 3	Time point 4	Time point 5	Time point 6	Time point 7

Daunorubicin	5	20	40	70	100	120	190
Vincristine	90	110	180				
Dexamethasone	10	40	60	130	230	400	1390
Asparaginase	10	100	220	1360	2490		

Table 2.19 Pharmacokinetic time points. Summary of time points taken for each of the 4 drugs during pharmacokinetic testing

2.28.2 Asparaginase activity assay

Principle

Asparaginase is an enzyme and it is the active enzyme that is effective against leukaemia through its depletion of asparagine. Enzyme activity is measured in units with 1 milliunit of asparaginase being the amount of enzyme that catalyses the formation of 1 mmol of aspartate per minute at 25°C. To determine the levels of active asparaginase within the plasma of mice treated with asparaginase, asparaginase activity was measured with an asparaginase activity assay kit. The active asparaginase in the sample generates aspartate from asparagine. The aspartate is converted using a coupled enzymatic reaction to a colourimetric product which is proportional to the amount of aspartate generated. The colourimetric product is detectable at 570nm using a plate reader. Multiple readings are taken over time, the readings from samples are compared to an aspartate standard curve to calculate the aspartate generated over time.

Reagents and equipment

- Asparaginase activity assay kit (Sigma-aldrich)
- FLUOstar Omega plate reader

Reagent	Volume (µl per sample/standard)
Asparaginase assay buffer	40
Substrate mix	4
Aspartate enzyme mix	2
Conversion mix	2
Flourescent Peroxidase Substrate	2

Table 2.20 Asparaginase activity assay reaction mix composition

Procedure

Kit components were thawed on ice, reconstituted where needed, aliquoted for use and stored at -20°C and only thawed just prior to use. Plasma samples were removed from the -80°C freezer and thawed on ice. Dilutions of plasma were made in assay buffer. Several dilutions were made for each sample to ensure the result would be within the linear range of the assay. 50µl of assay buffer was added to each well. Aspartate standards were prepared to give 0, 2, 4, 6, 8 and 10nmol/well. Dilutions of samples were then added to the wells. Each sample and standard were performed in duplicate. A reaction mix was prepared for the samples and standards as shown in table 2.20. For the sample “blank”, a reaction mix was prepared as in table 2.20 with the aspartate enzyme mix omitted. 50µl of reaction mix was added to each well, the plate was placed on a rocker for mixing before transferring to the FLUOstar Omega plate reader with incubation set at 25°C. The plate was regularly mixed by shaking. Readings were taken at 570nm every 3-5 minutes for 1 hour. The penultimate reading prior to the sample exceeding the linear range of the standards was taken as the final time point. The flowing calculation was used to determine asparaginase activity

$$\text{Activity (milliunit/ml)} = (B*\text{Dilution factor})/ ((T_{final}-T_{initial})*V)$$

Where “B” is the amount in nmol of aspartate generated between $T_{Initial}$ and T_{Final}, “$T_{Initial}$” is the time of the first reading in minutes, “T_{Final}” is the time in minutes of the final time point and “V” is the sample volume in mL added to the well.

2.28.3 Determination of plasma concentration of dexamethasone, daunorubicin and vincristine by LC-MS

Principle

Drugs are precipitated from plasma, dried out then re-suspended in a mobile phase so they can be loaded onto a liquid chromatography machine. In liquid chromatography there are two phases the mobile and stationary phase, sample is injected into the mobile phase which permeates through the stationary phase packed within a column. Analytes are separated depending on their chemical affinity with the mobile and stationary phase. An interface transfers separated components to the mass cytometry ion source. Mass cytometry measures the mass to charge ratio of ions. Each drug has a specific mass cytometry signature. The more of a compound that exists the greater the area of peak produced by chromatography. By running samples alongside a standard curve, the concentration of compounds can be determined.

Reagents and equipment

- Shimadzu LC-MS 8060 triple quadrupole mass spectrometer
- Drying machine with nitrogen gas
- Borosilicate tubes
- Acetonitrile

Procedure

Prepare serial dilution of drugs in plasma for standard curve of 1000ng/ml, 500ng/ml, 100ng/ml, 50ng/ml and 10ng/ml. To 20µl of sample (or standard) 380µl of acetonitrile was added (for vincristine 200µl plasma and 3800µl acetonitrile). Once precipitated samples were centrifuged for 3 minutes at maximum speed in a benchtop centrifuge. 350µl of supernatant was removed. To remove remaining supernatant samples were placed in a drying machine at 40°C for 40-45 minutes. The samples were then re-suspended in 150µl of a 60:40 water: acetonitrile. Dexamethasone samples were diluted 1 in 10. 5µl and 20µl were then loaded onto the LC-MS.

2.29 Extraction of Genomic DNA from screening samples

After the bulk of the screening had finished, harvested samples required processing in order to prepare for sequencing. The first stage of which requires extraction of genomic DNA from the samples.

2.29.1 Selection of kit and procedure

Genomic DNA was extracted from frozen cell pellets using the Qiagen Blood Maxi/Qiagen Blood Midi kits. 10ml of PBS was used to re-suspend the thawed cell pellet. *In vitro* samples were clean and were simply re-suspended in PBS and processed according to normal processing instructions for blood samples. All *in vitro* samples and pooled mouse bone marrow samples were extracted with QIAamp maxi columns, the *in vitro* samples via the method below and the mouse samples with the amendments stated in the following section. Bone marrow compartments harvested individually had lower cell numbers and were extracted with QIAamp midi columns or multiple QIAamp midi columns depending on cell number.

2.29.2 Genomic DNA extraction of in vitro samples

Frozen cell pellets were thawed and re-suspended in 10mls of PBS. 500ul Qiagen protease was added and mixed. 12ml of buffer AL was added and mixed by inversion and then vigorous shaking. Samples were then placed in a water bath set to 70°C for at least 10 minutes. 10mls of 100% ethanol was then added and mixed by vigorous shaking. Half of the solution was then applied to the QIAamp column and centrifuged at 1850g for 3 minutes in centrifuge and the filtrate was discarded, this was repeated with the remaining solution. The column was washed with 5ml buffer AW1 and centrifuged at 4500g for 1minute. 5mls of AW2 was then applied and centrifuged at 4500g for 15minutes. The QIAamp column was transferred to a clean 50ml tube, genomic DNA was eluted by application of 1ml Buffer AE onto the column, 5 minutes incubated then centrifuged at 4500g for 2 minutes. A further 1ml of buffer was then applied to the column, incubated for 5 minutes and centrifuged to elute at 4500g for 5 minutes. Approximately 1.8mls of eluted DNA was recovered.

In vitro screening samples extracted by the above method gave good yields of genomic DNA, however some samples taken from mice were giving poor yields which seemed to be caused by inefficient lysis.

2.29.3 Genomic extraction from *in vivo* samples

Samples collected from the *in vivo* arm contained multiple cell types and murine blood and these sample did not adequately lyse with the standard reagents and protocol. The protocol was therefore amended to include a more thorough lysis, with Qiagen tissue lysis buffer ATL. Since buffer ATL is not compatible with Qiagen protease, proteinase K was used in its place.

2.29.4 Genomic extraction of individual *in vivo* bone marrow compartments

The QIAamp blood midi kit was used with individually harvested bone marrow compartments using a maximum cell number of $2x10^7$ cells per column. If multiple columns were required, reagents were increased accordingly and the sample split across the correct number of columns. Samples were re-suspended in a small volume of less than 500µl of PBS. 2 ml of buffer ATL was added with 150µl of Proteinase K (Qiagen). This was incubated at 56°C for 2-4 hours to ensure adequate lysis. Regular vortexing was performed during incubation. 2 ml of buffer AL was then added and mixed by inversion. This was followed by addition and mixing of 1mls of 100% ethanol. The lysate was applied to the columns and centrifuged at 1850g for 3 minutes. The filtrate was discarded, and this process repeated until all lysate had been applied to the column. 2mls of buffer AW1 were applied to the QIAamp midi column, it was centrifuged at 4500g for 1 minute. 2mls of AW2 buffer were added to the column which was centrifuged at 4500g for 15minutes. The column was moved to a clean tube. Buffer AE was applied to the column and incubated for 5 minutes before centrifugation at 4500g for 2minutes, this process was repeated with further buffer AE (or the same buffer AE). Buffer AE volumes were selected based on cell numbers - higher cell numbers were treated with greater buffer AE volumes up to a total of 600µl, with a minimum of 150µl (passed through the column twice).

2.30 Bioinformatics analysis of screening results

Post sequencing, data was passed to Sirintra Nakjang from the bioinformatics support unit in the form of FASTQ files, separated into files according to the unique barcodes, for analysis. The general outline of data analysis is summarised by figure 2.8. For details relating to choice in analysis pipeline refer to chapter 6.2

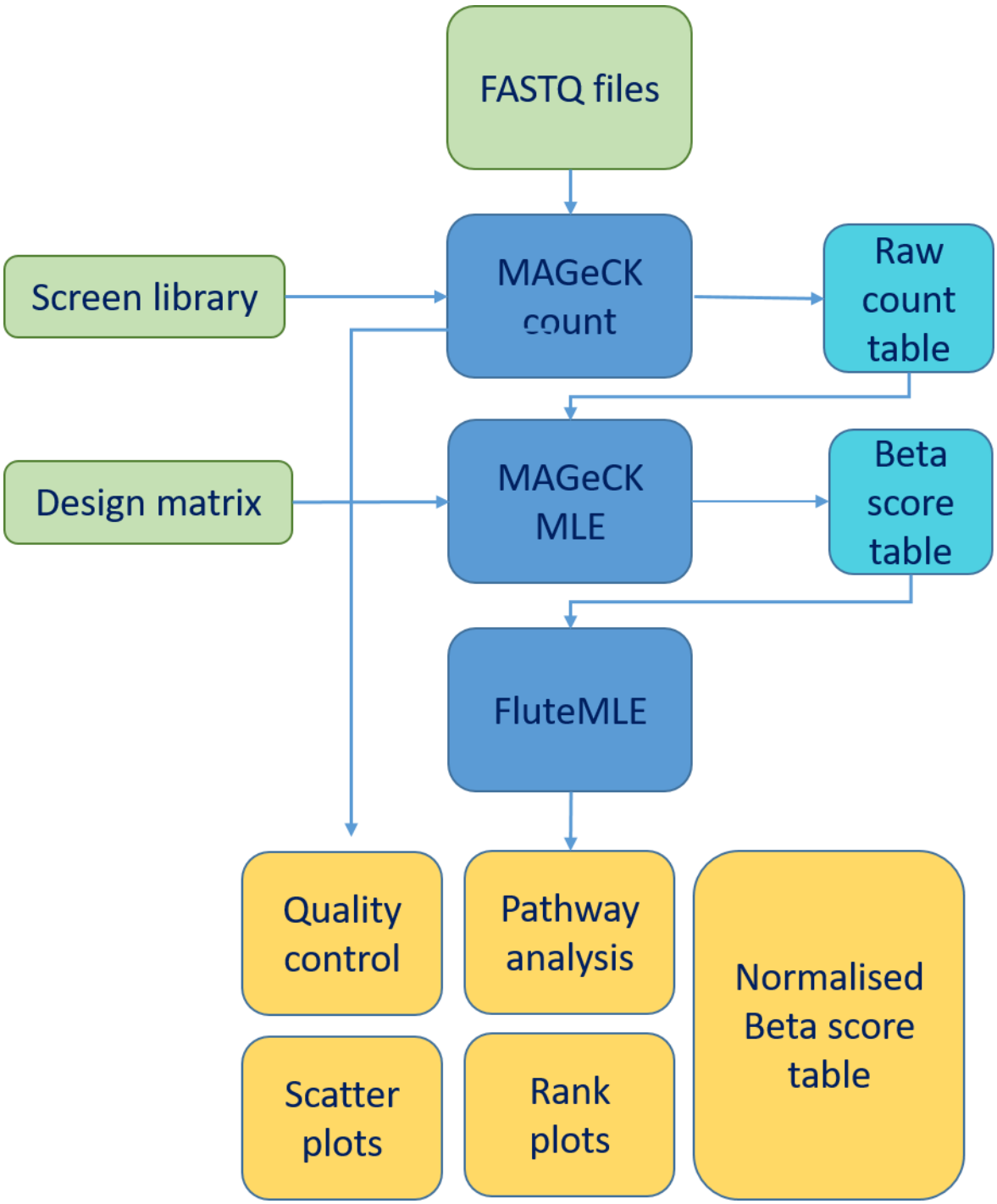

Figure 2.8 Bioinformatics Pipeline. MAGeCK and MAGeCKFlute were used to process data. Input files are shown in green, aqua highlights output files that are fed back into the pipeline and final output files are shown in orange. A raw read count table for each guide RNA was produced fromFATSQ files using the MAGeCK pipeline. The read count table was used for MAGeCK-Maximum likelihood estimation (Kosztyu et al.) analysis, raw reads counts are used to compute a single Beta score (a measure of change) for each gene between baseline and samples. Beta scores were normalised to account for differences in cell cycle between treated and control settings as part of MAGeCKFlute. MAGeCKFlute allowed for visualisation of differential enriched and depleted beta scores between control and treated settings. Normalised beta scores were also used for further analysis

FASTQ files from the sequencing run, and Brunello library files were used to generate count tables using the count function of MAGeCK. The trimming and sgRNA length are automatically determined. No mismatches are allowed during aligning.

MAGeCK-MLE analysis was then performed using read count tables and design matrix file which indicates which samples was affected by each condition.

A cell cycle normalisation method based on essential genes was developed as part of the MAGeCKFlute pipeline. Beta scores were normalised according to essential genes to generate normalised beta scores.

Normalised beta scores were used to perform various analyses, including differential hit analysis upon treatment and functional pathway analysis within MAGeCKFlute.

Comparing beta scores allowed identification of guides differentially altered with VXLD treatment compared to control conditions. This was visualised in several ways:

- Rank plots- differences in normalised beta score between control and VXLD treated are calculated, ranked and plotted with RankView function
- Scatterplot- produced using ScatterView function. Control beta scores are plotted against treated beta scores. A cut of is made around normal distribution of 2 standard deviations
- Nine square scatterplot- a scatter plot of control normalised beta scores against treated beta scores. Cut-offs of 1 and -1 are used for both x and y axis to define placement of 9 square grid to divide guides into categories based on control and treated beta scores. The SquareView function is used to plot this.

Lists were generated for in vitro screening where guides differentially enriched under drug treatment (greater than 2 standard deviations from mean as identified and visualised on scatterplot) and guides differentially depleted under drug treatment.

This process was repeated for *in vivo* screening and hits compared and displayed as venn diagrams. The differentially enriched and depleted lists were used to look at functional interactions with STRING and pathways with WEB-based GEne SeT AnaLysis Toolkit (WebGestalt).

Chapter 3. Cell line selection for screening and assessment of cell line sensitivity to chemotherapeutics

3.1 Introduction to chapter

When performing screening one can choose to perform the same screen across a panel of different samples or to select a representative sample. Selection of a representative sample can reduce time and cost but can increase the validation required. For this work a representative sample will be used. Imperative to the success of the screen was rumination on the most appropriate choice of the cell line to be used. This give us the first aim of this chapter:

- Identify a cell line suitable for screening

It was important to select a cell line that best represented a typical T-ALL in terms of its genetic profile. Additionally, the practicalities of potential candidate cell lines, such as transduction potential, *in vivo* engraftment, and ploidy required consideration. Lastly, but crucially, the responsiveness of potential cell lines to the chemotherapeutics to be used during the screening as individual agents and then in combination was required, in order to allow the second aim of this chapter.

- Select an appropriate concentration of vincristine, dexamethasone, asparaginase and daunorubicin to use for *in vitro* screening

3.2 Genetic profiles of T-ALL cell lines

CRISPR knockout screens rely upon the cleavage of a gene target site specified by a 20-nucleotide single guide RNA (sgRNA) sequence (Mali et al., 2013, Jinek et al., 2012). Double stranded break (DSB) are generated by cutting of target sequence by Cas9 , repair of the newly generated double stranded breaks often results in creation of insertions or deletions (indels) which can lead to mutations that impact on transcription and translation (Mali et al., 2013).

3.2.1 Ploidy

Repair of breaks does not necessarily result in mutations that lead to loss of gene function. Polyploid cell lines with increased gene copy number would potentially suffer from an increased likelihood of incomplete knockout, which could mask potential phenotypes of interest. Thus, the preference was for cells to be used with diploid karyotype for this type of screening. It was pertinent that any selected cell lines re-capitulated the genetics found in patients with T-ALL.

3.2.2 Chromosomal rearrangements

The ectopic expression of transcription factors due to chromosome rearrangements are common in T-ALL and each transcription factor lesion defines the molecular genetic subgroup of T-ALL. The most commonly affected transcription factors are *TAL1*, *TLX1*, *TLX3*, *HOXA*, *NKX2-1*, *NKX2-2*, *MYB* and *LMO1* genes, with *LMO1* deregulation normally occurring alongside *TAL1* or *LYL1* overexpression (Figure 3.1). The Catalogue of Somatic Mutations in Cancer (COSMIC) hosted by the Wellcome Sanger Institute contains a vast array of information relating to somatic mutations in cancer, including mutations found in cell lines (Harsha et al., 2018). The Deutsche Sammlung von Mikroorganismen und Zelkulturen (DSMZ) biological resource centre holds many human cell lines including T-ALLs and provides information regarding karyotype, chromosomal translocations and common mutations found within the cell lines (Leibniz-Institut). The Broad Institute Cancer Cell Line Encyclopaedia (Workman et al.) database holds information on a variety of somatic mutations found within different cancer types and within cancer cell lines (cell lines project) (Barretina et al., 2012b). The DSMZ Guide to Leukaemia-Lymphoma cell lines contains further information on many leukaemic and lymphoblastic cell lines (Drexler et al., 2005). Information for T-ALL cell lines was collated from the literature, COSMIC, DSMZ and CCLE regarding the karyotype and translocations and is summarised in Table 3.1, and the presence of common T-ALL somatic mutations is summarised in Table 3.2.

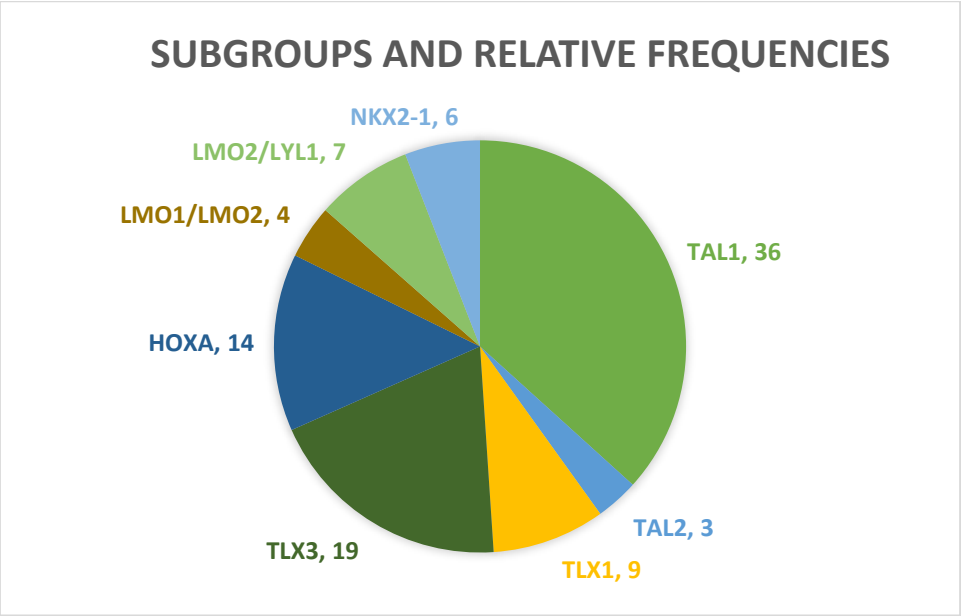

Figure 3.1 Transcription factor aberrations in T-ALL. T-ALL can be grouped according to altered expression of transcription factors due to chromosomal rearrangements. Shown are the most common translocations and their relative percentages in childhood T-ALL (Liu et al., 2017)

cell line	karyotype	translocations
HSB2	pseudodiploid (4% ploidy)	t(1;7)(p34;q34) *LCK-TCRB*
KARPAS-45	hypotetraploid (8% ploidy)	t(X;11)(q13;q23) *MLL-MLLT7/AFX* fusion
RPMI-8402	hypotetraploid	t(11;14)(p15;q11) *LMO1/TTG1-TRAD* and *STIL-TAL1*
CCRF-CEM	near-tetraploid	t(5;14)(q35.1;q32.2) *NKX2-5-BCL11B* and *SIL-TAL1*
JURKAT	hypotetraploid (7.8% ploidy)	
CUTLL1	hyperdiploid	t(7;9)(q34;q34) *TRB-NOTCH1*
MOLT4	hypertetraploid	
CTV-1	near tetraploid (9% polyploidy)	t(1;7)(p34.2;q34) *TAL1-TRBx2* , t(12;16)(q24.32;q11)x2
HPB-ALL	pseudodiploid (8% ploidy)	t(5;14)(q35;q32.2) *TLX3-BCL11B*
PEER	pseudodiploid (7% ploidy)	t(5;14)(q35.1;q32.2) *NKX2-5-BCL11B,* and *NUP214-ABL1*
KOPT-K1	hypertetraploid	t(11;14)(p13;q11) *LMO2-TRD*
ALL-SIL	hypertetraploid	t(10;14)(q24;q11) *TLX1/HOX11-TRAD* and *NUP214-ABL1*
SUP-T1	hypotetraploid (1.8% polyploidy)	t(7;9)(q34;q34.3) *TRB-NOTCH1/TAN1*
LOUCY	hypodiploid (16% ploidy)	t(16;20), *SET-NUP214*
DND41	near-tetraploid (12% polyploidy)	t(5;14)(q35;q32.2) *TLX3-BCL11B*
MOLT16	near diploid	t(8;14)(q24;q11*) MYC-TRAD, SIL-TAL1,* t(3;11)(p21;p13)
P12/ ICHIKAWA	hypotetraploid (1.6% ploidy)	
PF-382	near-diploid	
DU.528	diploid	t(1;14)(p33;q11) *TAL1/SCL-TRD*

Table 3.1 Karyotype and translocations in T-ALL cell lines. ***Information regarding karyotype and translocations in common T-ALL cell lines was collated from literature searches, DSMZ , Guide to Leukaemia*-**Lymphoma cell lines , CCLE and COSMIC. (Barretina et al., 2012b, Drexler et al., 2005, Harsha et al., 2018, Palomero et al., 2006)

Upon examination of the karyotypes of 19 T-ALL cell lines, 10 cell lines had a proportion of cells with additional ploidy, indicating potential heterogeneity. 11 were either hypo or near tetraploid, and 8 were near/hypo/pseudodiploid. Diploidy was preferable over tetraploidy in this case due to the additional gene copies in tetraploid lines which increases the chance of incomplete knockout. The cell lines showed a mix of translocations in which the genes *TAL1*, *TLX1*, *LMO2*, *NKX2-5* appear commonly rearranged within T-ALL patients. Of the (near) diploid cell lines, HSB2 had an unusual *LCK* translocation so was ruled out. Whilst most T-ALL patients have aberrant NOTCH signalling due to mutations, translocations of NOTCH1 –like that observed in CUTLL1 are relatively rare. HPB-ALL, PEER, LOUCY, MOLT16 and DU5.28 had close to diploid karyotypes and translocations commonly observed in T-ALL patients.

3.2.3 Common mutations

In addition to transcription factor translocations, there are several other common abnormalities observed in T-ALL, including inactivation of *PTEN*, and deletion of *CDKN2A* (Downing et al., 2012, Girardi et al., 2017, Neumann et al., 2015), activation of IL7 receptor pathway components (Ribeiro et al., 2013), activating mutations of *NRAS* and *NOTCH1* (or inactivation of NOTCH1 negative regulator *FBXW7*), The most common mutations affecting over 50% of cases are *NOTCH1* and *CDKN2A* abnormalities (Genescà et al., 2018, Weng et al., 2004b). A table of mutations was compiled for each of the T-ALL cell lines in our collection, with information collated from COSMIC, CCLE and literature searches (Table 3.2).

Cell line	NOTCH/ FBXW7	CDKN2A	IL7R	NRAS	PTEN	P53	Others of note
HSB2	NOTCH	yes		yes		no	CDKN2B, RB1
KARPAS-45	both		yes	no	yes		NF1
RPMI-8402	FBXW7	yes	no	no	yes		CDKN2B, NF1, MYBdup
CCRF-CEM	FBXW7	yes	no	no	no	yes	NF1 KRAS, MYB dup
JURKAT	FBXW7	yes	no	no	yes	yes	AKT, LCK, TAL1, CDKN2B
CUTLL1	NOTCH translocation					yes	
MOLT4	NOTCH (multiple)	yes	no	yes	yes	yes	
CTV-1	both					yes	LCK, FLT3, NF1
HPB-ALL	NOTCH	yes			no	yes	
PEER	NOTCH	yes				yes	
KOPT-K1	NOTCH	yes					CREBP
ALL-SIL	NOTCH	yes	no	no	no		RB1
SUP-T1	no	yes	no	no	no	yes	CDKN2B
LOUCY	no		no	no	no	yes	
DND41	NOTCH	yes	yes	yes	yes	yes	CDKN2B
MOLT16	no	yes	no	no	yes	yes	CDKN2B
P12 /ICHIKAWA	FBXW7	yes	no	yes	no	yes	CDKN2B, MYB dup
PF-382	no		no	yes	yes		NF1
DU.528	FBXW7						

Table 3.2 Status of common T-ALL mutations in a panel of T-ALL cell lines. Information regarding mutation status of T-ALL cell lines was collated from a variety of sources including the CCLE and COSMIC databases (Barretina et al., 2012b, Drexler et al., 2005, Harsha et al., 2018, O'Neil et al., 2007, Zuurbier et al., 2012)

Of the diploid cell lines with common translocations, 2 of the 5 cell lines (LOUCY and MOLT16) did not possess known activating mutations in NOTCH signalling (through NOTCH1 activation or inactivation of the negative regulator FBXW7) representing the most commonly mutated pathway in T-ALL. DU.528, although classified as a T-ALL cell line, is derived from a patient who underwent a switch from a T- lymphoblastic to a promyelocytic phenotype during treatment: this unique feature may complicate findings from screening with chemotherapeutics.

3.2.4 Summary of cell line selection

PEER and HPB-ALL are both of pseudodiploid karyotype and harbour common translocations; PEER has two translocations namely *NKX2-5-BCL11B* and *NUP214-ABL1*. HPB-ALL has a translocation involving TLX3. Both PEER and HPB-ALL possess *NOTCH1* mutations and *P16INK4A* deletions, which are the most prevalent mutations in T-ALL. HPB-ALL are simple to culture and will grow in RPMI-10%+FBS medium, whist PEER are considerably more difficult, grow in RPMI-20% FBS and in our experience transduce poorly. All things considered, based on mutational status, translocations and karyotype, HPB-ALL was the best choice for further study.

3.3 Dose response of T-ALL cell lines to chemotherapeutics as single agents

Given the desire to conduct screening under a chemotherapeutic pressure recapitulating clinical conditions, it was essential to establish the sensitivity of potential candidate cell lines to the selected agents. Firstly, the 4 selected drugs dexamethasone, daunorubicin, vincristine and asparaginase were applied as single agents to assess their effective range in a panel of T-ALL cell lines. Each cell line was plated, and each of the 4 drugs titrated across the cells. After 72 hours of incubation, a resazurin assay was used to assess cell viability. At each concentration viability was calculated compared to a solvent control and plotted in Prism (GraphPad) (Figure 3.2), a non-linear regression curve was fitted, and used to determine effective GI50 values and are summarised in table 3.3. The GI50 values refer to the concentration at which half of the maximal effect was achieved.

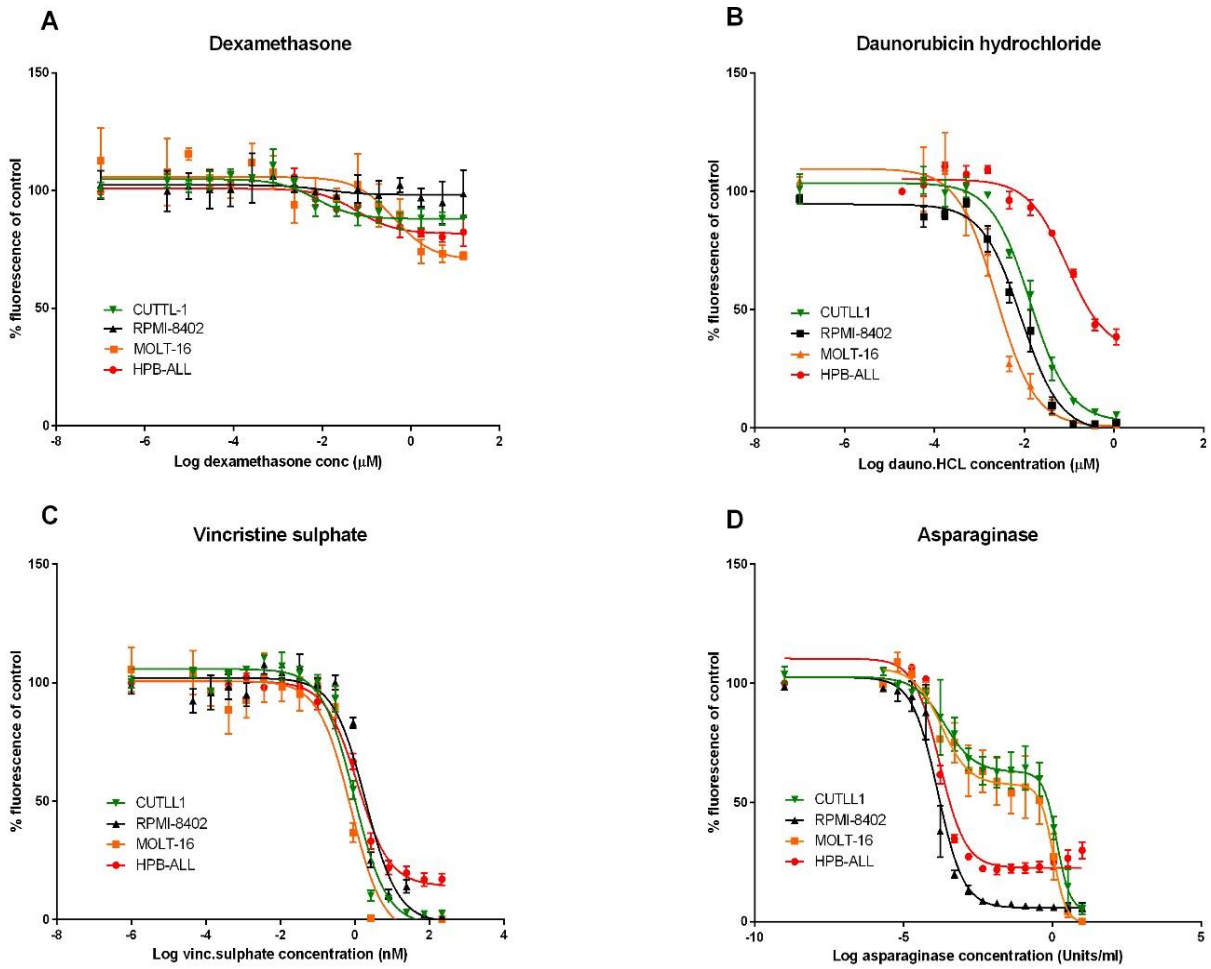

Figure 3.2 In vitro single agent drug responses. Drug response of T-ALL cell lines CUTLL1, RPMI-8402, MOLT-16 and HPB-ALL to dexamethasone (a), daunorubicin hydrochloride (b), vincristine sulphate (c) and asparaginase (d) as single agents. Survival was assessed at 72 hours by resazurin assay and calculated relative to an untreated control well as shown on the y-axis. The drug concentration range used is shown on the x-axis (log concentration). Error bars represent standard error of the mean of three independent experiments

.

CUTLL1, RPMI-8402, MOLT-16 and HPB-AL all showed little change in viability in response to dexamethasone, even at the highest concentration of 10 µM. A range of responses were observed for daunorubicin with the most sensitive being MOLT-16 and the least sensitive being HPB-ALL. All 4 cell lines responded similarly to vincristine with a GI50 of around 1nM. HPB-ALL and RPMI-8402 showed a typical dose response after exposure to asparaginase, whereas CUTTL-1 and MOLT-16 did not show a typical dose response, but appeared biphasic. A biphasic dose response was fitted using prism in this case. Calculated GI50 values and effect correspond to the first phase.

Drug	Dexamethasone			Daunorubicin			Vincristine			Asparaginase		
Cell line	GI50 μM	95% CI GI50	effect at GI50	GI50 μM	95% CI GI50	effect at GI50	GI50 nM	95% CI GI50	effect at GI50	GI50 U/ml	95% CI GI50	effect at GI50
CUTLL1	resistant	N/A	N/A	0.013	0.01 to 0.02	0.46	0.938	0.7 to 1.3	0.48	0.0002	0.00008 to 0.0007	0.17
RPMI-8402	resistant	N/A	N/A	0.009	0.007 to 0.01	0.54	1.888	1.3 to 2.8	0.49	0.0001	0.0001 to 0.0002	0.45
MOLT-16	0.5	0.09 to 2.0	0.20	0.002	0.001 to 0.004	0.43	0.788	0.5 to 1.2	0.53	0.0002	0.00008 to 0.0004	0.18
HPB-ALL	resistant	N/A	N/A	0.012	0.06 to 0.1	0.35	1.161	0.9 to 1.5	0.43	0.0002	0.0001 to 0.0002	0.43
DU.528	resistant	N/A	N/A	0.004	0.003 to 0.006	0.49	0.549	0.3 to 1.0	0.51	N/A	N/A	N/A
SUP-T1	0.04	0.01 to 0.2	0.20	0.004	0.02 to 0.05	0.41	N/A	N/A	N/A	N/A	N/A	N/A
ALL-SIL	0.05	0.02 to 0.1	0.21	N/A	N/A	N/A	N/A	N/A	N/A	N/A	N/A	N/A
KOPT-K1	0.01	0.008 to 0.02	0.23	N/A	N/A	N/A	N/A	N/A	N/A	N/A	N/A	N/A

Table 3.3 Single agent GI50 values for T-ALL cell lines. T-ALL cell lines were treated with either dexamethasone, daunorubicin, vincristine or asparaginase for 72 hours. Survival after drug exposure was determined by resazurin assay compared with solvent control. GI50 values and effect sizes were determined from dose response curves using Prism software, where the GI50 was greater than 10μM cells were considered to be resistant

The candidate cell line HPB-ALL had GI_{50} values of 124nM, 1nM and 0.00036U/ml for daunorubicin, vincristine and asparaginase respectively. HPB-ALL was resistant to dexamethasone (GI50 greater than 10μM), as were MOLT-16 and CUTLL-1. Half of the tested T-ALL cell lines were resistant to dexamethasone, and those who did respond had very small effect size. After looking at response to single agents by resazurin assay, I moved on to look further into two of the 4 drugs asparaginase and dexamethasone; the former due to issues with its by-product ammonia and the latter due to resistance in the candidate cell line HPB-ALL.

3.4 Investigation of asparagine dependence in HPB-ALL

Asparaginase breaks down L-asparagine into aspartic acid and ammonia, depriving the cells of asparagine, but additionally creating ammonia, which in an *in vitro* setting accumulates within the media. Ammonia can be a source of toxicity to cells. Thus, to investigate if the sensitivity of HPB-ALL to asparaginase was due to asparagine depletion and not ammonia toxicity, additional experiments were performed.

HPB-ALL is routinely cultured in RPMI-1640 media containing 0.05g/L asparagine. The effect of adding additional asparagine (0.15g/L) to standard media, on the sensitivity of HPB-ALL to asparaginase was assessed (figure 3.3).

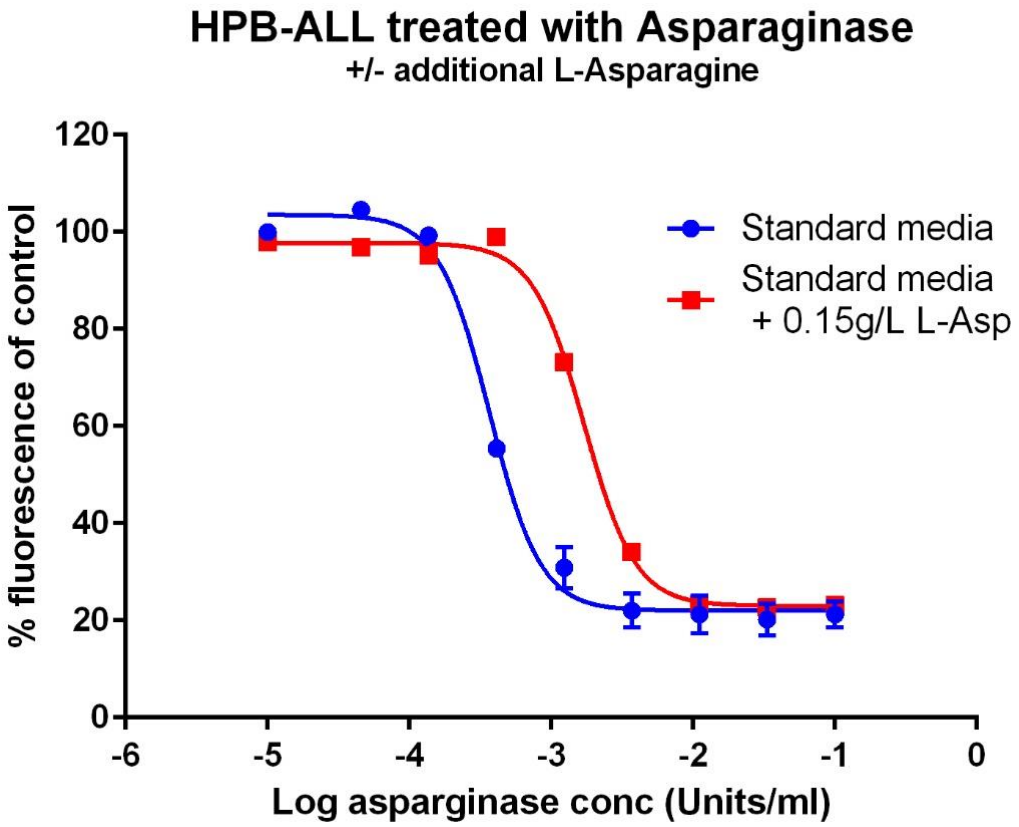

Figure 3.3 Treatment of HPB-ALL with asparaginase with and without the addition of asparagine. Asparaginase was titrated across HPB-ALL cells cultured in standard media (blue) and with addition of an extra 0.15g/L l-asparagine (L-Asp) in the culture media (red) for 72 hours. Survival was determined by Resazurin assay and is normalised to a solvent control. Error bars represent standard error fo the mean of 2 independent experiments.

I observed a shift in the dose response curve to asparaginase in HPB-ALL upon the addition of asparagine. A greater enzyme concentration is required to achieve the same effect on cell number at higher asparagine levels. To examine the dependence of HPB-ALL survival and proliferation on asparagine. HPB-ALL cells were grown in a media without asparagine (DMEM), and asparagine was titrated across the cells in a 3-fold dilution. Cell numbers were assessed after 72 hours by resazurin assay and normalised to a standard media asparagine concentration of 0.05 g/L (figure 3.4).

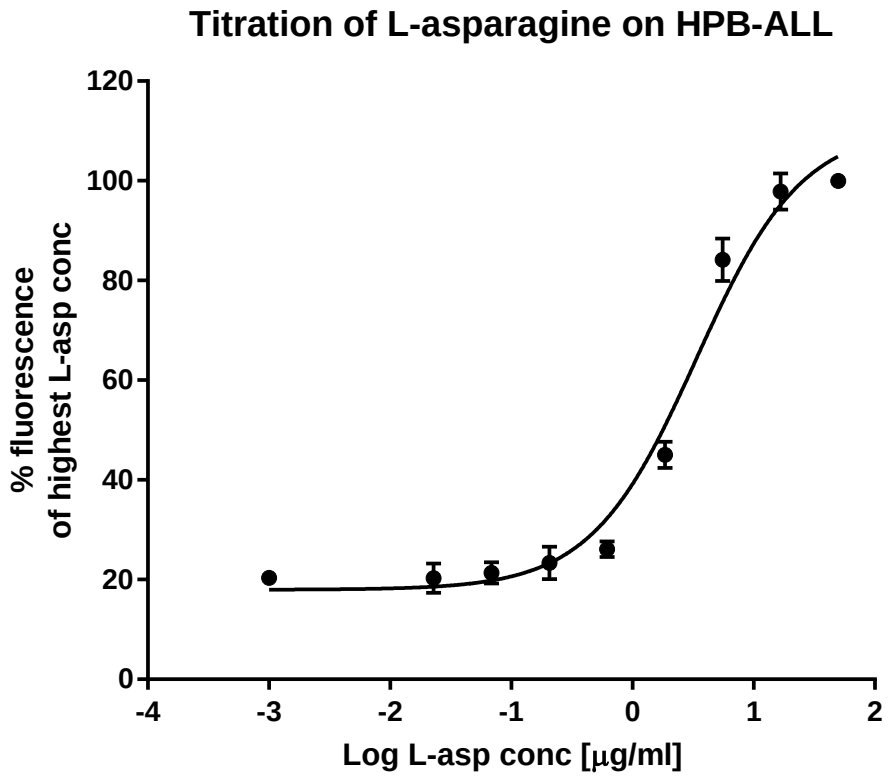

Figure 3.4 Survival of HPB-ALL cells in varying concentrations of asparagine. HPB-ALL cells were seeded in a media without asparagine. Asparagine was then applied to cells in a concentration ranging from 0 to the concentration found in standard conditions- 0.05g/L. Cells were cultured for 72 hours and resazurin assay used to determine survival relative to standard asparagine concentration 0.05g/L. Error bars represent standard deviation of technical replicates.

A concentration dependent effect of asparagine concentration on cell numbers was observed. This suggests a dependence on asparagine for growth and/or survival of HPB-ALL. Taken together the dose dependant response of HPB-ALL to asparagine and the decreased effect of asparaginase enzyme on HPB-ALL cultured with additional asparagine, I conclude that at least in part the reduced viability of HPB-ALL cells upon asparaginase treatment was due to depletion of asparagine from the culture medium. After absolving concerns about asparaginase it was then important to assess the use of dexamethasone.

3.5 Dexamethasone response in HPB-ALL

HPB-ALL, like many other tested T-ALL cell lines, showed limited change in total metabolising cells in response to dexamethasone, as demonstrated by resazurin assay results. This poses the question regarding the purpose of including dexamethasone as part of the chemotherapy regimen for screening. Dexamethasone is taken up by cells via the glucocorticoid receptor (GR). If uptake is impaired by

mutations in GR then this may explain lack of effect on cell viability. It is also important to bear in mind a resazurin assay provides no information on any other phenotypic changes within HPB-ALL, for instance in cell signalling that can occur in response to drug treatment. Dexamethasone could be entering HPB-ALL causing changes in cell signalling, which may also affect how the cells respond to other chemotherapeutics, in which case its inclusion in the chemotherapeutic pressure would be warranted.

3.5.1 Heterozygous NR3C1 mutation in HPB-ALL

The *nuclear receptor subfamily 3 group C member 1* (*NR3C1*) gene encodes the glucocorticoid receptor protein, which when bound to a glucocorticoid such as dexamethasone translocates to the nucleus and conducts a plethora of transcriptional activities. (Mutations in *NR3C1* are often associated with resistance to steroids such as dexamethasone and have been shown to be associated with an inferior outcome in ALL. (Bray and Cotton, 2003, Moorman AV, 2015). Mutations in *NR3C1* should be detectable from publicly available sequencing data The CCLE database holds RNA sequencing and whole exome sequencing data for HPB-ALL (Barretina et al., 2012b), and lists mutations reported within the cell line. Within the mutation list for HPB-ALL is a heterozygous missense mutation on chromosome 5 in *NR3C1* at position 142675147 (NCBI build number: 37). This mutation from adenosine to guanine results in a methionine being replaced by threonine at codon 634 within exon 7 (p.M634T). This mutation is predicted to be damaging by the programme SIFT (score: 0.02). I designed primers to amplify exon 7 in cDNA from HPB-ALL cells. The PCR products were subsequently sent for Sanger sequencing which confirmed the CCLE data (figure 3.5).

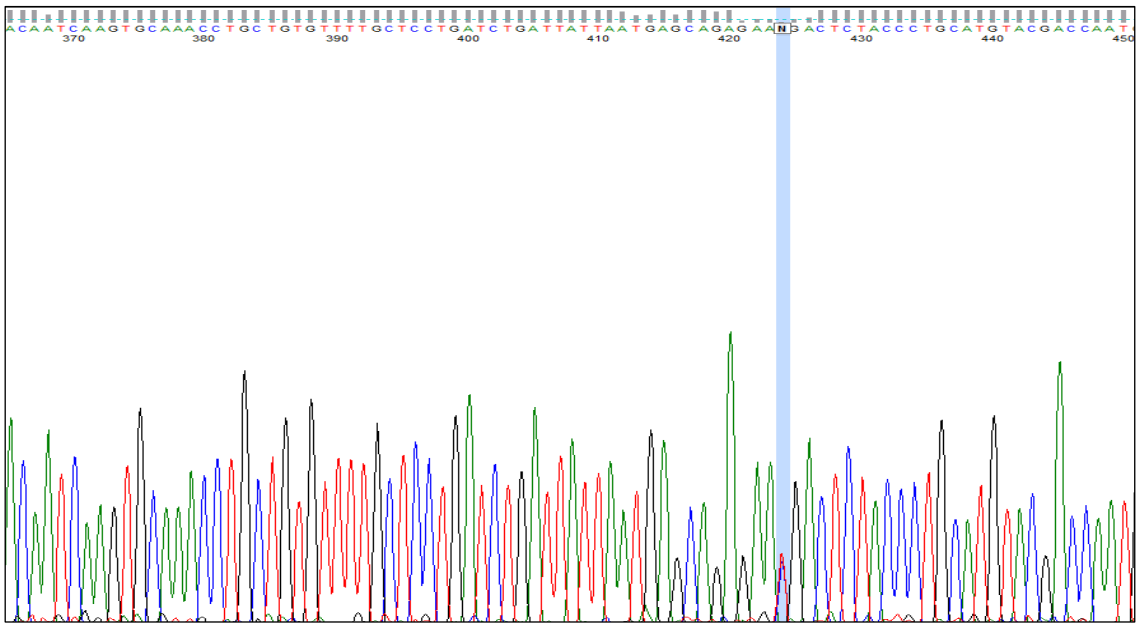

Figure 3.5 Electropherogram of mRNA of the glucocorticoid receptor in HPB-ALL. RNA was extracted from HPB-ALL cells, cDNA was synthesised. Primers flanking the region carrying the mutation reported by CCLE were used to amplify the region of interest. The PCR product was purified and sent for Sanger sequencing. Highlighted is the base of interest.

The Sanger sequencing matched the recorded sequences for the wild type glucocorticoid receptor transcript apart from the single highlighted base. There is a 50:50 mix of Thymine and Cytosine at this location, with Thymine representing the wild type allele and Cytosine the mutated allele, which is concordant with the CCLE data. These findings are concordant with that published by CCLE (Barretina et al., 2012b). Although the impact of such a mutation is unknown, it is within the ligand binding domain and so may explain the lack of sensitivity to dexamethasone. Given the mutation is heterozygous, the action of glucocorticoids may not be fully impaired.

3.5.2 Detection of dexamethasone response genes after dexamethasone treatment in HPB-ALL

Given the apparent resistance of HPB-ALL to dexamethasone at least in terms of cytotoxicity, it was important to determine if the application of dexamethasone affected HPB-ALL on a molecular level. There are several genes known to be upregulated in response to dexamethasone treatment. These include Glucocorticoid Induced Leucine Zipper factor (*GILZ*) and FK506 Binding Protein 5 (*FKBP5*) (Goossens and Van Vlierberghe, 2016, Ayroldi and Riccardi, 2009, Pratt and Toft, 1997). The mRNA levels of the *GR*, *GILZ* and *FKBP5* were assessed by quantitative RT-PCR at several time points following treatment with dexamethasone.

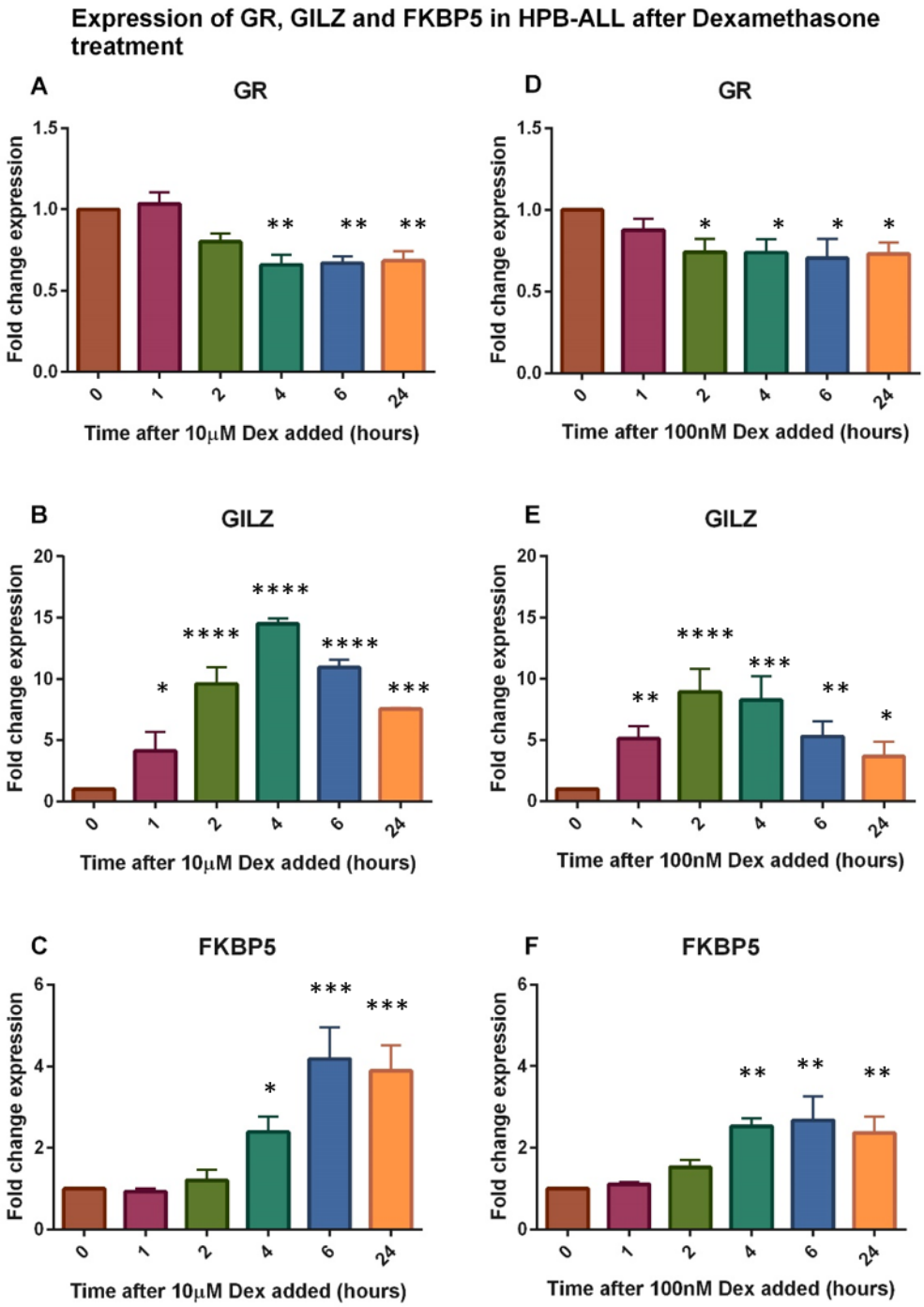

Figure 3.6 Relative expression of Glucocorticoid receptor (GR) and dexamethasone response genes GILZ and FKBP5 in HPB-ALL treated with 10μM and 100nM dexamethasone over time. HPB-ALL were treated with either 10μM (A-C) or 100nM (D-F) dexamethasone and samples of cells were taken at 0, 1, 2, 4, 6 and 24 hours. RNA was extracted from cells and cDNA synthesised. Fold change was calculated using delta delta Ct method using GAPDH as the housekeeping control. Error bars represent standard error of the mean of 3 independent experiments. Astericks indicate significant difference from 0 hours with * $p < 0.05$, ** $p < 0.01$ and *** $p < 0.001$, **** $p < 0.0001$. (One way annova, repeated measures, Holm Sidak's multiple comparisons test)

The expression of the glucocorticoid receptor decreases with increasing time post dexamethasone exposure, with the reduction being significant under both tested dexamethasone concentrations at 4, 6 and 24 hours (figure3.6). This decrease in *GR* expression could represent the autoregulation of receptor expression. *GILZ* expression is increased after dexamethasone addition, peaking at 2-4 hours post dexamethasone exposure. The greatest increase is observed at 4 hours after addition of 10µM dexamethasone where *GILZ* is increased by nearly 15 fold. *FKBP5* is also increased with treatment of both 10µM and 100nM dexamethasone, although the increase is less marked than for *GILZ,* and peaks later between 4-6 hours post dexamethasone treatment.

The significant upregulation of dexamethasone response genes subsequent to dexamethasone treatment indicates dexamethasone does indeed enter the cells and impacts transcriptional activity in HPB-ALL, which may also impact upon the action of other drugs when used in combination.

3.5.3 Synergism of dexamethasone and daunorubicin in HPB-ALL

To look at the impact of dexamethasone in combination with other chemotherapeutics, dexamethasone was combined with daunorubicin in HPB-ALL. Dexamethasone and daunorubicin were combined at fixed ratios (see section 3.6) and effect determined by relative fluorescence compared to a solvent control with resazurin at 72 hours. CalcuSyn was used to assess the effect of the combination relative to single agents. CalcuSyn uses the Chou-Talalay's Combination Index Theorem, additivity between two drug has a combination index of 1(Chou and Talalay, 1983). Combination indices exceeding 1 suggest an antagonistic effect, and values less than one synergism between 2 drugs (Chou and Talalay, 1983). Table 3.4 shows the combination index (CI) 3 different dose points for HPB-ALL.

Dose	LC50	LC75	LC90
Reported CI value	0.5	0.8	1.1

Table 3.4 Combination index (CI) values for dexamethasone and daunorubicin

At the LC50 (Dose where 50% of cells effected) the combination index value for dexamethasone and daunorubicin was 0.5 indicating synergism. A value of 0.8 at LC_{75} also indicated weak synergism. At LC_{90} the CI values was 1.1, here the effect of

daunorubcin alone was so great that we did not observe much additional effect by addition of another drug. Overall, this suggests dexamethasone and daunorubicin at lower concentrations are weakly synergistic in HPB-ALL.

Despite the resistance of HPB-ALL to dexamethasone as a single agent, it was still incorporated into the drug regimen on the basis of its important role in T-ALL therapy, the synergistic effect when used with in combination with daunorubicin, and the increase in expression of dexamethasone response genes indicating an effect at a molecular level. Since in the final combination there will be a total of 4 drugs it was next important to consider how all the drugs act when combined.

3.6 **Combination treatment of HPB-ALL at fixed ratios**

After assessment of dexamethasone, daunorubicin, vincristine and asparginase as single agents, the effect of the drugs as combinations was determined in HPB-ALL. Drugs were assessed at fractions of their GI50 values (for dexamethasone 10μM was used as a surrogate GI50 value since HPB-ALL is dexamethasone resistant). Dexamethasone was combined with daunorubicin. Subsequently dexamethasone and daunorubicin were treated as a single drug and were combined with vincristine. The three drugs were then combined with asparaginase. Dose response curves are shown in figure 3.7.

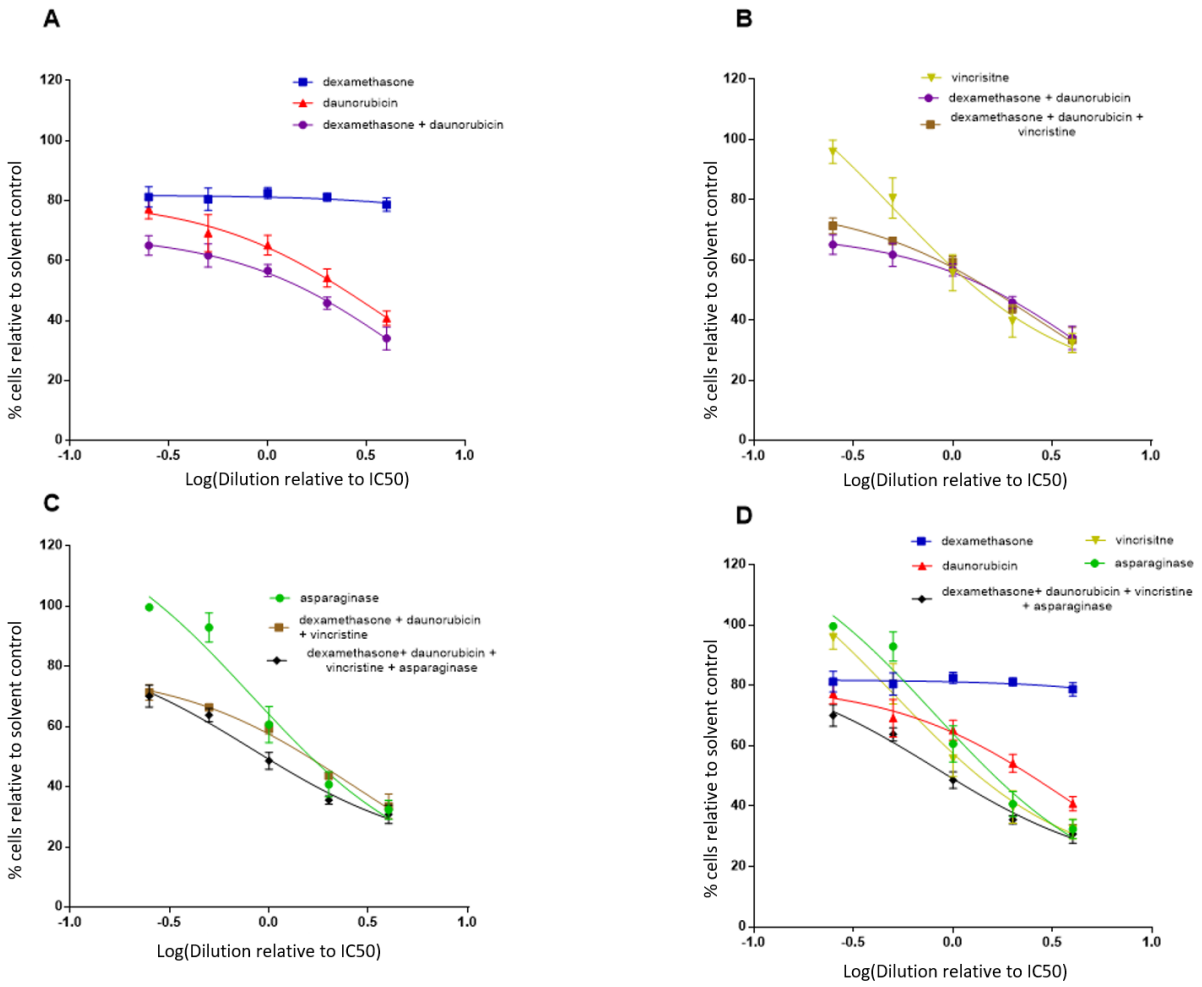

Figure 3.7 Percentage of HPB-ALL cells after 72 hours of treatment with combinations of dexamethasone, daunorubicin, vincristine and asparaginase at fixed ratios. Concentrations are given on a logarithmic scale relative to calculated GI50 values, where O is 124nM, 1nM, 0.00036U/ml and 10µM for daunorubicin, vincristine, asparaginase and dexamethasone respectively (note a surrogate GI50 value of 10µM was used for dexamethasone since GI50 exceeded 10 µM). The following combinations were assessed: dexamethasone and daunorubicin (a), dexamethasone and daunorubicin combined as one drug with the addition of vincristine (b) and dexamethasone, daunorubicin and vincristine combined as one drug and the addition of asparaginase (c). All 4 drugs as single agents and all 4 drugs combined is also shown (d).

In 3.7D it is evident the effect of all 4 drugs combined is greater than any single drug used alone. In 7A there is limited effect of dexamethasone, whereas daunorubicin decreases survival of HPB-ALL as its concentration is increased and combining the two drugs seems to further decrease cell viability (synergy). In 7B vincristine has less effect than dexamethasone and daunorubicin combination at ratios less than the GI50, but has a bigger impact on survival at ratios greater than the GI50. In 7B the combination curve lies between the two single drug curves indicating there may be some antagonism occurring. 7C shows the inclusion of asparaginase increases the effect again. To assess if any synergism or antagonism was present, CalcuSyn software was used to calculate the combination index (CI) values, the results of which can be seen in table 3.5. CI values close to 1 indicate an additive effect, as values increase antagonism is indicated and as values decrease it is indicative of synergistic effects.

Drug 1	Drug 2	CI at LC 50	CI at LC 75	CI at LC90
dexamethasone	daunorubicin	0.5	0.8	1.1
dexamethasone + daunorubicin	vincristine	1.9	3.0	7.3
dexamethasone + daunorubicin + vincristine	asparaginase	0.8	0.7	0.8

Table 3.5 Combination indices for drug combinations in HPB-ALL. Drugs were applied at fixed ratios to each other for 72 hours. Resazurin assays were used to measure effect on cell viability compared to a solvent control. Effects of each drug alone or in combination were input into CalcuSyn software to produce CI values. Where greater than 2 drugs were used, multiple drugs were combined and applied as a single drug. CI values were recorded at 3 different effective dose points (ED) 50, 75 and 90, where the effect of the drugs is 50%, 75% and 90% of the maximum effect respectively.

The combination of dexamethasone and daunorubicin was discussed in the previous section. The addition of vincristine to the dexamethasone daunorubicin double combination was antagonistic at all calculated dose points. Adding asparaginase to the triple drug (dexamethasone + daunorubicin + vincristine) gave CI values just below 1 (0.8, 0.7 and 0.8) indicating an additive or weakly synergistic effect.

Combining drugs at fixed ratios allowed the assessment of synergism and gave us insight into the effect on overall survival when they were combined. The fixed ratio approach did not however, consider the ratios at which these drugs are found clinically, nor did it allow for assessment of the impact on changing the concentration of a single drug within the combination. Therefore, I assessed the effect of combining these 4 drugs in a 4D style drug matrix assay, where all drugs were titrated against each other.

3.7 **Drug Matrix assay in HPB-ALL**

Dexamethasone, daunorubicin, vincristine and asparaginase were titrated across HPB-ALL cells in a matrix assay. A matrix-based assay was selected for its ability to illustrate the effect of raising or lowering one drug with respect to the other drugs within the combination. We aimed to select concentrations of drugs that gave the required effect on cell numbers, and that were most in keeping with the ratio of drugs found in patient protocols. The individual GI50 values for each drug were used to guide effective concentration ranges for each drug, the maximum concentration used was twice the GI50. One exception was dexamethasone. As HPB-ALL cells were resistant, a maximum value of 100nM was selected to keep the concentration within a clinically relevant range. The concentrations used are listed in table 3.6.

Drug	Concentration 1	Concentration 2	Concentration 3	Concentration 4	Concentration 5
Dexamethasone	0nM	25nM	50nM	100nM	N/A
Daunorubicin	0nM	36nM	72nM	124nM	248nM
Vincristine	0nM	0.3nM	0.6nM	1.1nM	2.2nM
Asparaginase	0mU/ml	0.09mU/ml	0.18mU/ml	0.36mU/ml	0.72mU/ml

Table 3.6 Drug concentrations used in matrix assay

3.7.1 Drug matrix full results

Cells were plated and drugs applied and incubated for 3 days. Resazurin was used to determine cell viability compared to a solvent treated control. The matrix was performed 3 times and then averages calculated (after removal of any outliers). The results from the matrix assays are shown in figure 3.8.

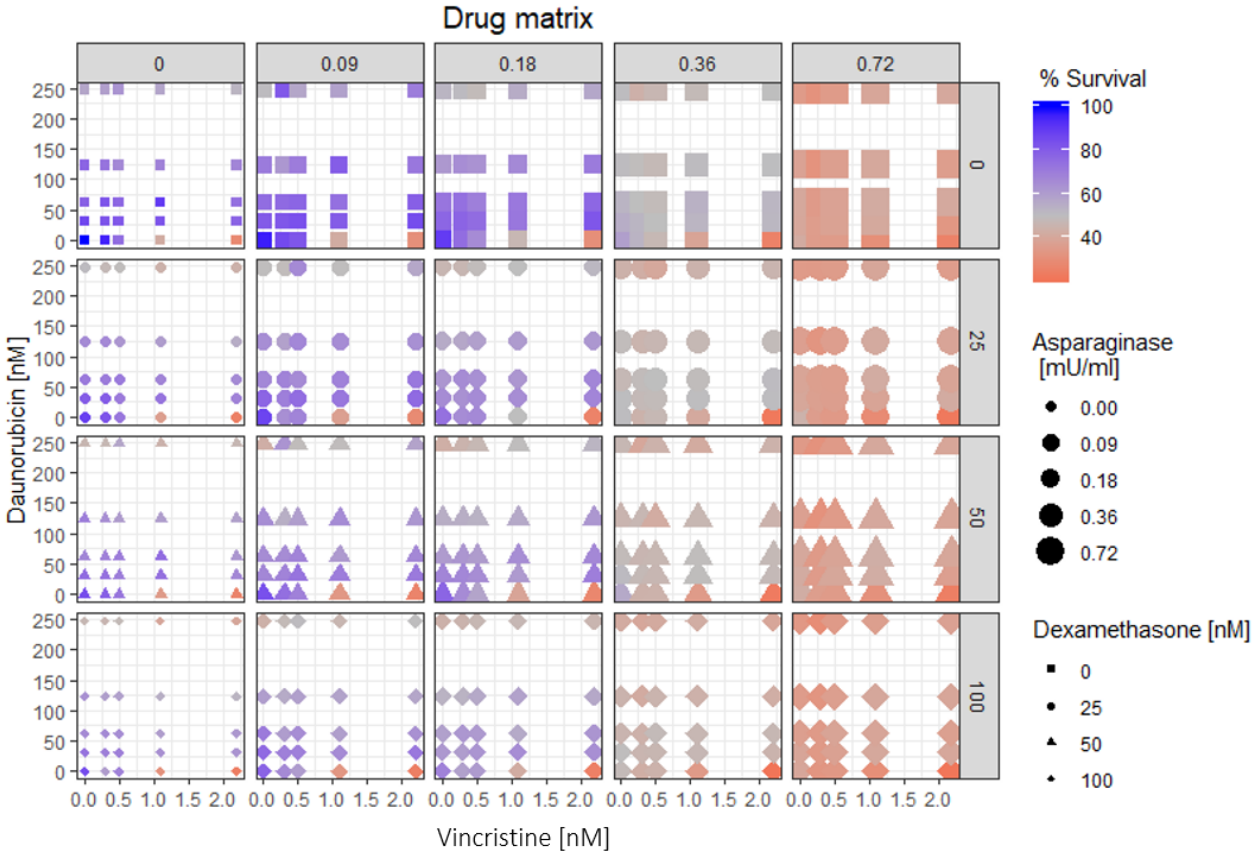

Figure 3.8 Results of Drug matrix for HPB-ALL. Dexamethasone, daunorubicin, vincristine and asparaginase were titrated in matrix base system over HPB-ALL cells. Effect was determined by resazurin assay after 3 days. Each point represents the average of 3 independent experiments. The following facetted plot was created with R studio. Each individual graph shows vincristine concentration on the x axis and daunorubicin on the y axis. The colour bar indicates the relative survival, such that each point is coloured according to the relative survival at that drug concentration compared to a solvent control. As you move from left to right through the plots asparaginase concentration is increased, also represented by increasing point size. Moving top to bottom through the plots is increasing dexamethasone concentration, which is also reflected in the change of the shape of the point.**Assessment of synergy and antagonism in HPB-ALL**

Within the drug matrix a zero concentration for each drug was present, this meant that the effect of each drug could be observed individually and in combination with just 1 other drug at a time. This process was performed for all possible combinations of the 4 drugs (a total of 6 times). This data was tabulated before using a platform for investigating drug combinations called Combenefit to assess synergy using the Loewe model (Di Veroli et al., 2016). Loewe was selected over Bliss independence, since Bliss independence assumes independent action and since dexamethasone is known to have pleiotropic effects and daunorubicin having many debated mechanisms of action an assumption of independence was not appropriate. A

synergy score is given for each point in the drug matrix combination (figure 3.9). The synergy score is a measure of the additional effect given by the two drugs compared to a reference effect, where positive scores indicate synergy and negative scores antagonism. An overall measure of the synergy across the matrix is described by the sum of synergy and antagonism (detailed explanation in methods section). This is the sum of synergy and antagonism observed in concentration logarithmic space and is described by the equation given in figure 3.9G

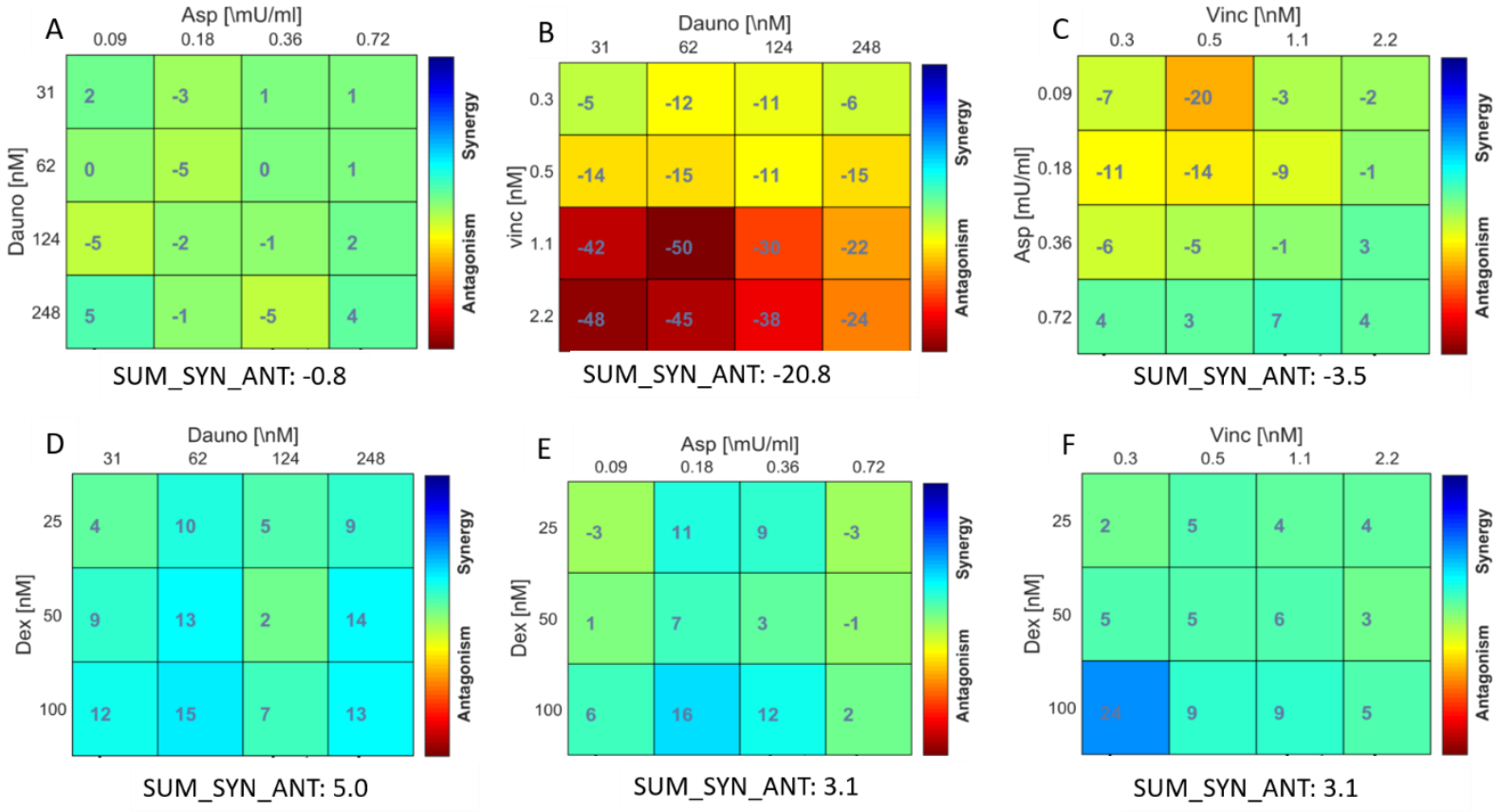

Figure 3.9 Synergy in drug matrix data. Drug matrix data was used to determine effect of each possible pair of drugs within the matrix.Combenefit was used to assess synergy for each pair with the Loewe model. A- asparaginase and daunorubicin, B- vincristine and daunorubicin, C- asparaginase and vincristine, D-dexamethasone and daunorubicin, E- dexamethasone and asparaginase and F- dexamethasone and vincristine. The sum of synergy and antagonism (SUM_SYN_ANT) across each matrix is given underneath.

For Figure 3.9A most values lie close to zero suggesting no additional effect of the drugs – or additive only effect of asparaginase and daunorubicin, this is confirmed by the calculation of sum of synergy and antagonism score of -0.8, a score so close to zero indicates no additional effect of the combination. In figure 3.9B there are areas of strong antagonism illustrated by the strong red colouring and highly negative synergy effect scores (approaching -50) between vincristine and daunorubicin. Figure 3.9C shows mild antagonism at lower concentrations moving through additivity at higher concentrations of vincristine and asparaginase. Figure 3.9D dexamethasone and daunorubicin, in line with previous data, are synergistic. Figure 3.9E shows predominantly synergy between dexamethasone and asparaginase. In 3.9F dexamethasone and vincristine show predominantly additivity but with synergy at the lowest concentrations of vincristine and highest concentrations of dexamethasone. This data highlights the complexity of combining multiple drugs, with each drug pair acting differently from another. Predicting the effect of altering a single drug in the combination on the overall effect is not easy, reinforcing the requirement to perform the matrix assay to achieve the desired combined effect.

3.7.3 Selection of in vitro screening concentrations

The matrix data was then used to identify combinations of the drugs that give an overall survival of around 50% which was my ideal effect for screening, since this will be a substantial enough effect to observe changes in enrichment and depletion of sgRNAs but without too harsh a selection that only a minority of sgRNAs survive. A subset of the matrix data was selected to include only data where the final survival was between 45 and 55% and combinations where any of the 4 drugs had a concentration of 0 were removed. The subset data was then plotted in a 3D scatter diagram (figure 3.10) using R studio plot3D. This gave a substantial number of potential drug combinations; to narrow this down and select the most appropriate combination, I looked for a ratio of the drugs that would most reflect the clinical setting.

I compared the drug assay concentrations with plasma serum maximum concentration (C_{max}) levels of each drug achieved in patients. Asparaginase levels seen in patients were far higher than those required *in vitro*. Due to differences with in asparaginase concentrations clinically and *in vitro*, I considered only the ratio of dexamethasone, daunorubicin and vincristine to each other to select a combination for screening, recapitulating clinically achieved concentrations of 254nM for

dexamethasone , 190nM for daunorubicin and 4nM vincristine as sumamrised in table 3.7 (Moore et al., 2011b, Hempel et al., 2010b, Liston and Davis, 2017, Jackson et al., 2016a). The black line through figure 3.10 from a concentration of zero of each of the drugs through to their clincal C_{max}, any where along this line through 3D space represents constant ratios of these drugs to one another.

Drug	**Clinical C_{max}**	***In vitro* concentrations**
Dexamethasone	254nM	50nM
Daunorubicin	190nM	33nM
Vincristine	4nM	1nM
Asparaginase	3U/ml	0.00036U/ml

Table 3.7 Plasma C_{max} values for drugs clinically and concentrations selected for in vitro use

The orange square with a black outline on figure 3.10 indicates my selected combination of 50nM dexamethasone , 31nM daunorubicin , 1.1nM vincristine and 0.18mU/ml asparaginase, which gave a survival of 52% of HPB-ALL.

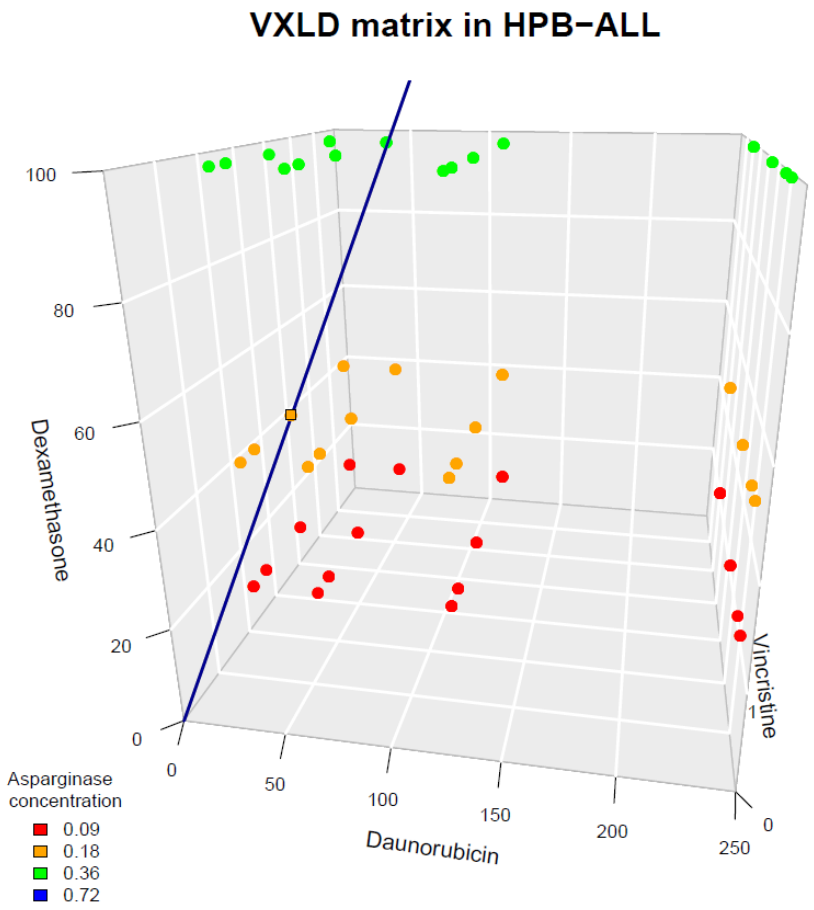

Figure 3.10 3D scatter plot of a subset of HPB-ALL drug matrix data that gave a survival between 45 and 55%. The x- axis shows daunorubicin concentration, the y -axis dexamethasone and the z-axis vincristine. The different colours show the differing asparaginase concentrations. A line is plotted from 0,0,0 through to the plasma C_{max} concentrations of dexamethasone, daunorubicin and vincristine. A concentration lying on the line was selected and is indicated by a black square.

3.8 Chapter discussion

The chapter specific aims outlined in the introduction of the chapter were to:

- Identify a cell line suitable for screening
- Select a appropriate concentrations of vincristine, dexamethasone, asaparaginase and daunorubicin to use for *in vitro* screening

These aims were achieved by assessing factors such as genetic background and ploidy to select a cell line that best represented a typical T-ALL in terms of its genetic profile. To select doses of chemotherapeutics, the dose response was first assessed as single agents and then in combination.

3.8.1 Cell line selection

A panel of T-ALL cell lines were assessed for their suitability for CRSIPR screening based on karyotype and mutational status. HPB-ALL was highlighted to be the preferential candidate for screening. It has pseudodiploid karyotype, which was preferable over the tetraploid cell lines which have double the copies of most genes. HPB-ALL has a TLX3 translocation which is found within 19% of T-ALL patients and a mutational profile similar to a typical T-ALL patient with mutations in NOTCH pathway and *CDKN2A* deletion, and *TP53* mutation.

3.8.2 Response of T-ALL cell lines to the 4 induction chemotherapeutics

A number of T-ALL cell lines were assessed for sensitivity to the 4-key chemotherapeutics in T-ALL induction therapy, namely dexamethasone, daunorubicin, vincristine and asparaginase. Most tested cell lines were resistant to dexamethasone, which is perhaps not surprising as most cell lines are derived from refractory or relapsed T-ALL patients. In patients with primary ALL, median *in vitro* GI50 for dexamethasone was 0.67µg/ml compared to in relapsed ALL which had a median GI50 of greater than 6µg/ml (Styczynski et al., 2007b). Despite HPB-ALL being dexamethasone resistant, dexamethasone does display synergism with daunorubicin in HPB-ALL, and additionally induction of dexamethasone response genes after dexamethasone treatment was observed. All tested T-ALL were sensitive to vincristine in a nano-molar range. The sensitivity to vincristine was high compared to primary ALL as a whole according to data from Styczynski et al where primary ALLs had a median lethal dose 50 (LD_{50})-concentration required to kill 50% of the cells of 1.24µg/ml (1.3µM), but the low nM sensitivity I observed is in keeping with GI50s obtained for other T-ALL cell lines (Anderson et al., 2014). Daunorubicin GI50s

were in keeping with the literature for both T-ALL cell lines and primary ALL cells, (Styczynski et al., 2007b, Silveira et al., 2015). *In vitro* GI50s for asparaginase were in the milliunit range, which is far lower than a clinically relevant level and highlighted a potential discrepancy between *in vitro* screening conditions. Some of the disparity can be explained by the differences in asparagine availability, in an *in vitro* setting there is a finite amount of asparagine, that is removed by the action of asparaginase, *in vivo* asparagine can be provided from other cells within the niche and this has been reported to be the case in AML (Kaspers, 2019) . HPB-ALL and RPMI-8402 were particularly sensitive to asparaginase treatment which is consistent with the literature (Silveira et al., 2015, Serravalle et al., 2016). This sensitivity can be explained by its low expression of asparagine synthetase compared to other T-ALL cell lines such as CCRF-CEM (Serravalle et al., 2016).

3.8.3 Selection of in vitro drug combinations

After assessing dexamethasone, daunorubicin, vincristine and asparaginase as single agents, I examined the effect of combining these drugs. Despite all 4 drugs being used for many years, there is very little literature on how these drugs interact together in terms of synergy or antagonism. I observed synergism between dexamethasone and daunorubicin, and an antagonism between vincristine and daunorubicin. Vincristine and daunorubicin cross resistance has been reported in many cell lines and appears to result from commonalities in method of uptake into the cells, and in the exclusion of the drugs via the multidrug resistance protein (Skovsgaard, 1978, Rappa et al., 1997) perhaps shared uptake routes contribute to the less than additive effect I observed between daunorubicin and vincristine. This is an area warranting further investigation, it would be important to establish if this antagonism is present in other cell lines and patient samples, as this could have implications for dose scheduling clinically. I used a matrix-based assay which allowed for the selection of combinations resulting in an overall desired effect, instead of having to consider all the drug interactions in turn.

Given the desire to perform negative screening and identify sgRNAs that become depleted under drug treatment, a less harsh drug treatment was required. Published screens that investigate synthetic lethality with drug treatment use sub-lethal doses of drugs for instance IC_{20} or IC_{25} as opposed to screens purely focusing on enrichment where a much harsher treatment can be used (Wang et al., 2019, Whitehurst et al., 2007). Since I wished to identify an effect of the 4 drugs combined,

I allowed for a higher level of overall effect of 50%. An effect of 50% should provide enough pressure to observe enrichment of guides whilst preserving the majority of sgRNA constructs to analyse depletion.

Multiple drug combinations resulted in the desired effect on HPB-ALL cells. I selected the combination of drugs for the screen based on patient plasma C_{max} concentrations. There were several limitations to selecting the final combination in this manner. Firstly, as previously noted, asparaginase clinical C_{max} concentrations were far higher than the GI50 for HPB-ALL *in vitro* so asparaginase was not considered when selecting drug ratios. Secondly, plasma C_{max} alone is a poor measure of the amount of drug reaching the cancer cells or how long the drug lasts (Meibohm and Derendorf, 1997). Total drug exposure is more relevant than plasma C_{max} in end response (Paci et al., 2014). When performing such screening in future one might want to consider using a measure of total drug exposure in patients to select *in vitro* concentrations to better reflect the clinical setting.

3.8.4 Chapter summary

Through considering genetics, ploidy, transduction potential an appropriate cell line was selected for screening. By assess single agent dose responses of T-ALL cells lines, calculation of GI50s then performing combination studies suitable drug concentrations were selected for screening. The chapter aims were met as described by the following:

- HPB-ALL was identified as the cell line that best fit my requirements for screening with a pseudodiploid karyotype, patient relevant genetics (TLX3 translocation, NOTCH pathway mutation and CDKN2A/B deletion).
- A matrix assay identified the following drug concentration for in vitro screening with HPB-ALL: 50nM dexamethasone , 31nM daunorubicin , 1.1nM vincristine and 0.18mU/ml asparaginase.

Chapter 4. Establishment of *in vivo* VXLD treatment protocol

4.1 Introduction to chapter

Patients with T-cell acute lymphoblastic leukaemia receive a 4 drug induction regimen encompassing vincristine, dexamethasone, asparaginase and daunorubicin referred to here as VXLD. As described earlier response to induction treatment is predictive of outcome and therefore resistance to this 4 drug combination is of significant interest. One of the objectives of the project, and the focus of this chapter, was to:

- Develop an *in vivo* combination drug regimen akin to that received by T-ALL patients

Ultimately this *in vivo* combination regimen could be used with a CRISPR screen to identify candidate genes for resistance alongside an *in vitro* screen with a drug regimen outlined in the preceding chapter. To obtain the most comparable results of *in vitro* and *in vivo* screening, screening should be performed in parallel within the same T-ALL cell line. For *in vivo* studies, it was essential that the selected cell line engrafts in immunocompromised mice, and that engraftment could be monitored to observe effects of drug treatment. It was imperative that any drug treatment regimen would be well tolerated to prevent any unnecessary loss of mice due to adverse effects. Additionally, it was important that enough cells survive treatment, to be analysed upon culmination of screening. Lastly, it was important to determine the levels of each drug achieved in the mice to ensure they were typical of levels found in patients undergoing therapy. In order to successfully achieve the primary objective, a number of other objectives needed to be met:

- Engraft mice with T-ALL cell line and successfully monitor disease
- Create dosing regimen that is tolerated in mice
- Check regimen is effectively reducing leukaemia
- Assess plasma levels of drug received by mice

4.2 Selection of immunocompromised mouse strain

The T-ALL cell line for *in vivo* screening needed to xenograft in immunocompromised mice (since the cells will be cleared by the immune system in immune competent mice). There are many different immunocompromised mouse strains. The NOD/Scid

IL2Rγ null (NSG) mice are the most immunocompromised and are used for haematopoietic stem cell engraftment. Routinely, NSG mice are used to engraft T-ALL samples, however NSG mice have a SCID mutation. The SCID mutation leads to deficient DNA repair, and therefore damage caused by DNA damaging agents cannot be repaired leading to increased toxicity (Fulop and Phillips, 1990). Since the drug regimen would include DNA damaging anthracycline daunorubicin, the NSG mice were not ideal. A less immunocompromised strain *Rag2*$^{-/-}$γc$^{-/-}$ can also be used to engraft haematopoietic cells, and unlike NSG these do not possess a SCID mutation. The *Rag2*$^{-/-}$*γc*$^{-/-}$ mice were therefore selected over the NSG mice due to the inclusion of daunorubicin in the drug regimen.

4.3 Introduction of T-ALL cells into Rag2-/-γc-/-

T-ALL cells were introduced into mice via intra-femoral injection, this placed the cells directly into the bone marrow microenvironment. A limited number of cells could be injected into a single mouse, due to the limited space at site of injection. Previous experiments have shown 1-2 million cells can be injected per mouse. The Brunello library was used for CRISPR screening and is comprised of 76,441 unique guides. To ensure we maintained good library representation a coverage of 400 times was used, equating to 30,576,400 or approximately 31x10^6 cells. As it was not possible to inject this number of cells into a single mouse. 2x10^6 cells was used per mouse and during screening multiple mice were injected to cover the complete sgRNA library.

4.4 Measurement of engraftment

The route of injection used produced systemic disease; whilst this better models disease in patients, it cannot be measured reliably by external observations (unlike for subcutaneous tumour models where tumour size is measurable with callipers). An alternative method for tracking disease progression was required. In this study, two different methods of measuring leukaemic burden were used; firstly *in vivo* bioluminescent imaging and secondly flow cytometry detection of blasts in the peripheral blood.

4.4.1 Measuring engraftment of HPB-ALL by IVIS

An *in vivo* imaging system can be used to reveal the localisation of leukaemic cells within a mouse by the capture of bioluminescence (BLI) or fluorescence signals (Sato et al., 2004). Cells can be engineered to express luciferase via introduction of a plasmid containing the firefly luciferase gene such as the SLIEW plasmid (pSLIEW),

which also contains a green fluorescent protein (GFP) (Bomken et al., 2013). Luciferase produces a bioluminescent signal in the presence of the substrate luciferin, and the emitted light signal can be captured using a sensitive camera.

HPB-ALL cells were transduced with pSLIEW. Successful transduction was confirmed by positive GFP expression by flow cytometry. HPB-ALL^{Luc+} was injected into 3 Rag2$^{-/-}$γc$^{-/-}$. Mice were injected with D-luciferin, anesthetised and imaged using an IVIS (Xenogen , Caliper) at weekly intervals. The acquired images provided information on both localisation and intensity of the bioluminescent signal, and that correlates to the location and number of cells respectively. Images acquired at week 4 are shown in figures 4.1A and 4.1B.

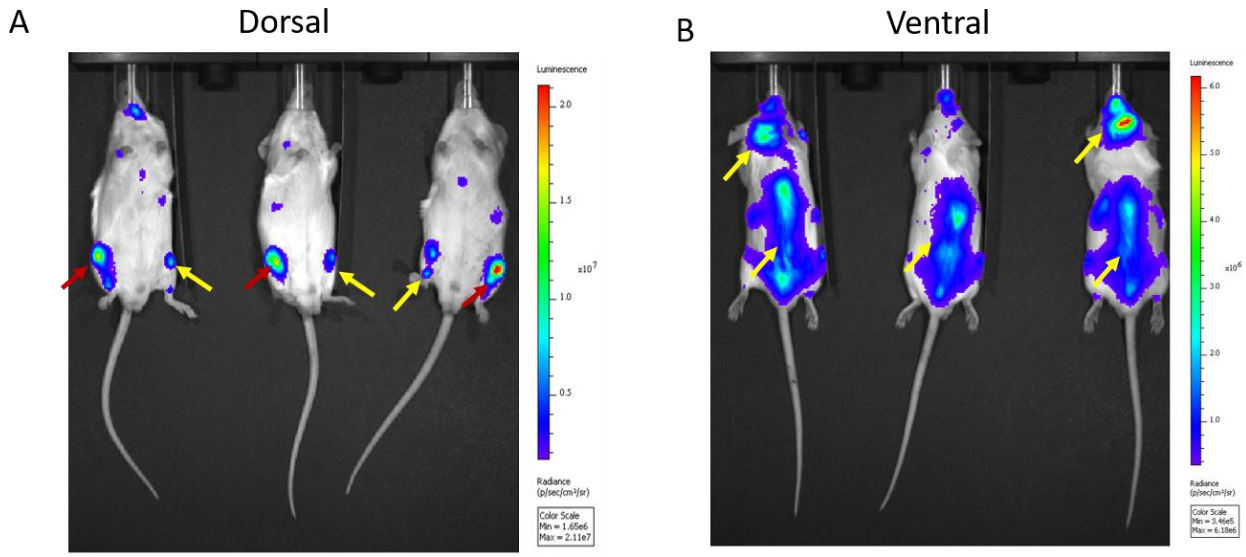

Figure 4.1 Bioluminescent IVIS imaging (BLI) of mice injected with HPB-ALL^{Luc+} Scale bars represent the light intensity. A) Dorsal view of mice. Red arrows indicate cells in the injected femur. Yellow arrows indicate areas to which cells have spread. B) Ventral view of mice. On this scale it is possible to see that signal present through-out the mice.

The total flux (total light emitted throughout the whole of the mouse) from BLI increased each week. The signal localisation also changed, initially detectable only in the injected femur, signal appeared in the contralateral femur and then throughout the mouse (figure 4.1A). Imaging of the ventral side of the mice (figure 4.1B) showed presence of leukaemic cells in the spine and head of the mice as indicated by the yellow arrows. Drawbacks of using BLI were administration of general anaesthesia, and the use of specialist equipment, therefore alternative methods of monitoring leukemic burden were considered.

4.4.2 Detection of HPB-ALL in peripheral blood by flow cytometry

An alternate method of assessing engraftment is the detection of leukaemic cells in the peripheral blood referred to as peripheral blood monitoring. This technique, unlike BLI , does not require a general anaesthetic and does not require luciferase to be expressed by T-ALL cells. This technique is described in 2.13.4. Peripheral blood samples were taken weekly from mice engrafted with HPB-ALL for a total of 4 weeks. The resulting data is summarised in figure 4.2.

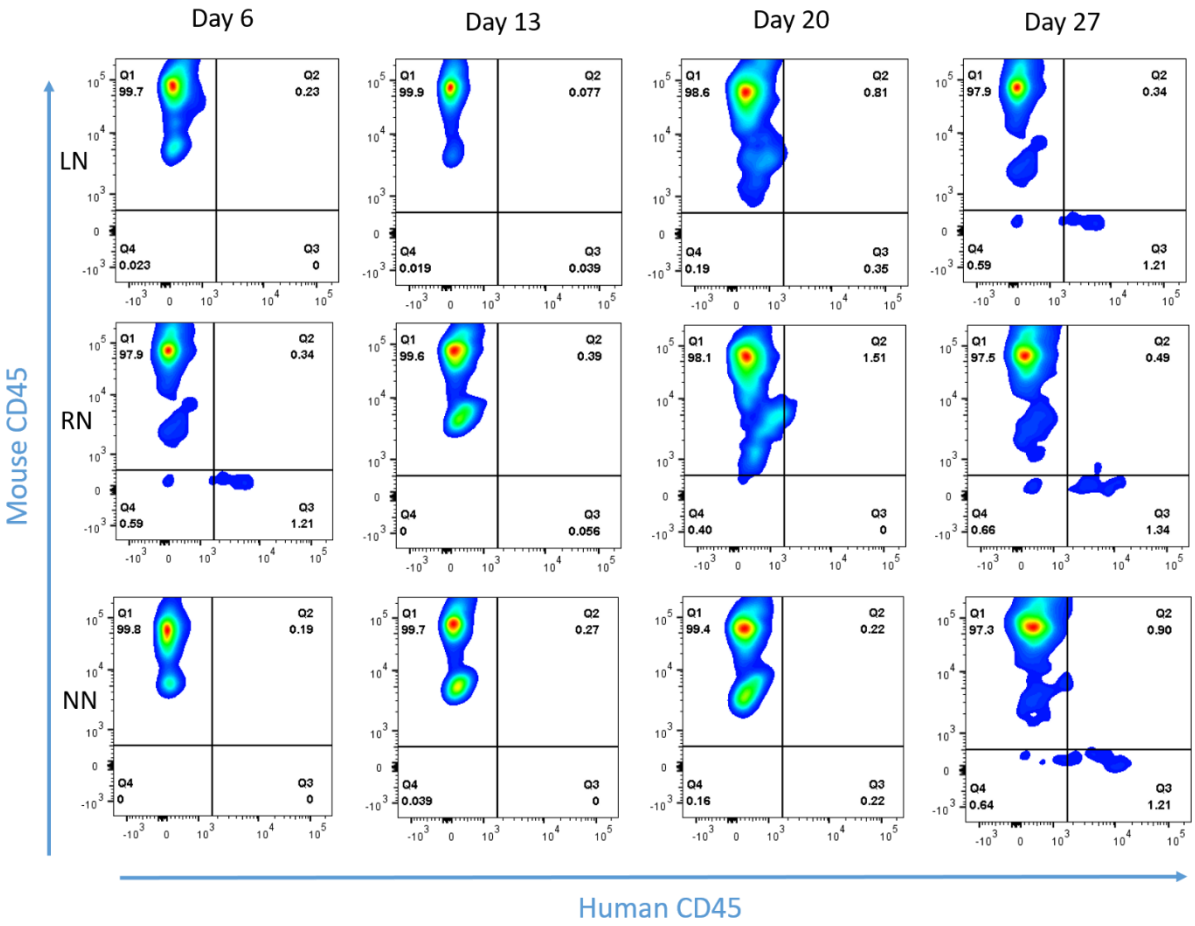

Figure 4.2 Flow cytometry analysis of peripheral blood samples taken from 3 mice (LN, RN and NN) injected with HPB-ALL cells over time. Peripheral blood monitoring at days 6, 13, 20 and 27 post intra-femoral injection of HPB-ALL cells. Human CD45 staining is shown against murine CD45 on viable gated single cells, Q3 represents the human cell population.

Peripheral blood staining showed an increase in the percentage of circulating human cells (Q3) from 0 through to 1% over the 4-week period. When populations of cells are small, it can be hard to distinguish a true positive result from any background and requires collection and analysis of a larger total number of events. For a population appearing as 1% of total events, 10^6 events are required, for accurate detection. For a population around 0.1% of the total population, 10^7 events are required (at a coefficient of variation (CV) of 1%) (Allan and Keeney, 2010) . Since only small volumes of blood can be taken weekly it is challenging to acquire 10^7 events. HPB-ALL engrafted mice did not consistently show greater than 1% human cells in the peripheral blood until 4 weeks post intrafemoral injection. By this time mice already have some signs of ill health due to leukaemia and had to be killed going into week 5 in accordance with humane endpoints for the study (inactive, piloerection of coat, pale).

To allow for direct comparison the two techniques for which data was given were performed in parallel. The matched timepoints are shown for the two techniques in figure 4.3.

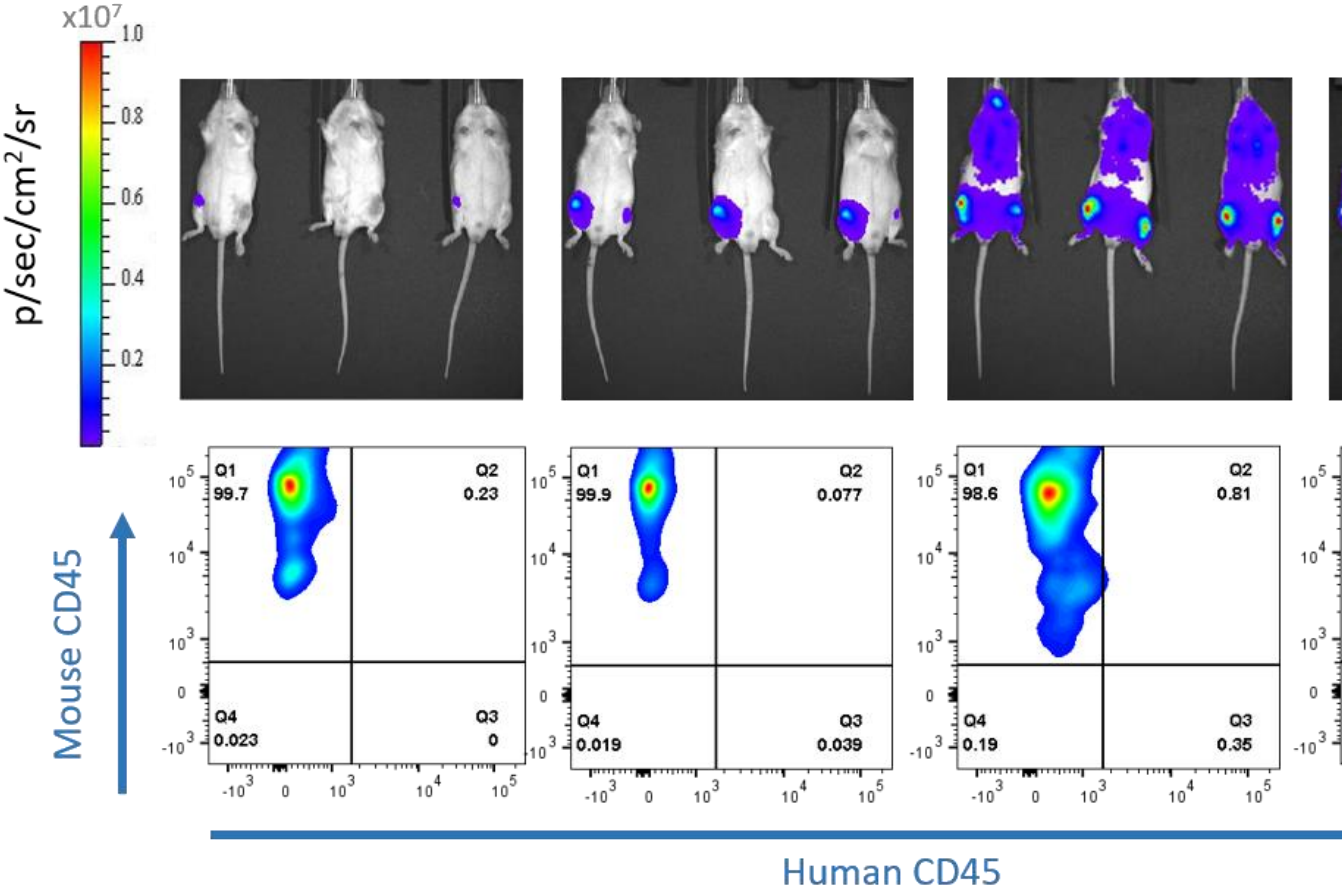

Figure 4.3 BLI and peripheral blood monitoring. BLI (top panel) with colour scale by photons/second/square centimetres/ steradian (p/sec/cm^2/sr). Representative peripheral blood monitoring (PB) from one of the three mice (bottom panel) at weekly intervals. For peripheral blood monitoring, mouse CD45 is shown in the vertical direction and human CD45 in the horizontal.

Both IVIS and human CD45 signals (from peripheral blood) increased over time, however signal from the IVIS was visible at a much earlier stage. The percentage of human cells in peripheral blood was very low reaching less than 2% at the last time point of 4 weeks - which was only days prior to the onset of ill-health.

Given the low frequency of leukaemic cells detected by peripheral blood monitoring from 1 to 3 weeks post implantation, peripheral blood monitoring was not considered an optimal method of tracking engraftment in this case. Similar low peripheral blood blast levels have been observed in the ALL cell line preB-697 and some fast growing ALL PDX samples (Dormon, 2017). BLI was selected to monitor leukaemic burden under drug treatment as it allows earlier detection of leukaemic cells and provides additional information regarding the distribution pattern of cells.

4.4.3 Confirmation of the presence of HPB-ALL cells in murine bone marrow by flow cytometry

At the end of the screening process, leukaemic cells need to be harvested from all of the mice for analysis of guide representation. In order to confirm and determine which compartment these cells should be extracted from, the percentage of human cells present in different murine tissues was analysed by flow cytometry 4 weeks post injection. BLI indicated predominantly bone marrow engraftment of the HPB-ALL cells, therefore bone marrow was harvested from the hind limbs of the mice. Although the spleens of HPB-ALL engrafted mice were not significantly increased in weight (average 0.1g compared to average normal weight 0.04g), leukaemic cells are commonly found in spleens of T-ALL patients, therefore samples were taken to assess the presence of human CD45 positive cells by flow cytometry.

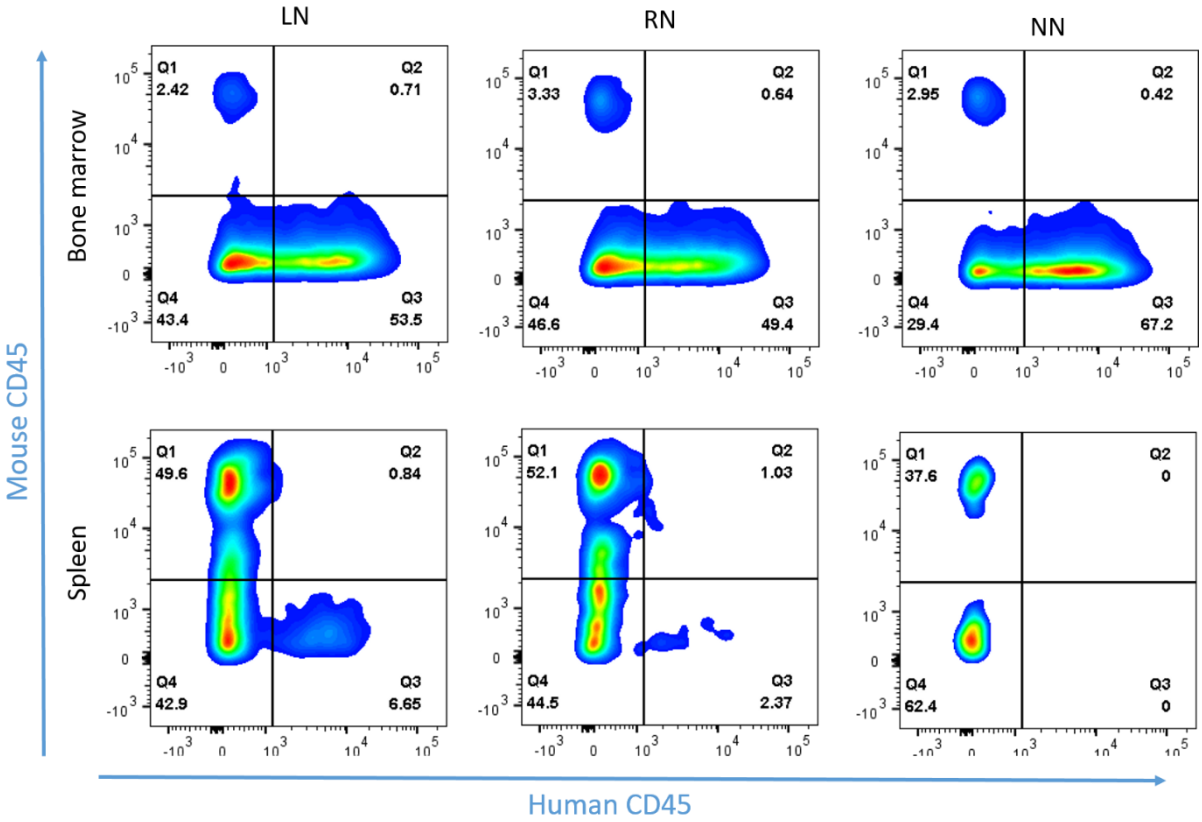

Figure 4.4 Flow cytometry analysis of spleen and bone marrow cells harvested from mice injected with HPB-ALL. Approximately 1 million cells from bone marrow and spleen of 3 different mice (LN, RN and NN) were stained with an antibody cocktail containing fluorophore conjugated antibodies to human CD45, Mouse CD45 and human CD3, along with a viability dye. Human CD45 staining is shown against murine CD45 on viable gated single cells on the plots above.

Flow cytometry analysis shown in figure 4.4 identified a clear population of human CD45 positive cells in the bone marrow of all 3 mice, and in the spleens of 2 . The percentage of human CD45 cells in the bone marrow was around 50% whereas in the spleen engraftment varied between 0 – 6%. This finding was consistent with BLI and peripheral blood monitoring, with lower levels of leukaemic cells in the blood stream that are taken up by the spleen, and high levels residing within the bone marrow.

Once it was confirmed that HPB-ALL engraft in the Rag2$^{-/-}$γc$^{-/-}$ mice, there was a method to monitor the disease burden during treatment via BLI, and tissue engraftment, design of a drug treatment regimen commenced.

4.5 VXLD toxicity testing

The use of any agents in an *in vivo* setting requires considerations of tolerability to prevent unnecessary loss of study numbers, to ensure adherence to limits set within the Home Office Project licence, and to maintain the principle of the 3Rs (Reduction, replacement, refinement)(Burden et al., 2015). Given our aim to use 4 drugs in combination, it was particularly pertinent to determine a tolerable and efficacious dosing regimen before proceeding with a large-scale screen.

A dosing regimen encompassing all the drugs in the VXLD combination had previously been published using NOD/SCID mice albeit with some toxicity issues (Samuels et al., 2014b). In the published study 4 drugs were used in one single treatment block, and then daunorubicin was omitted from later blocks due to poor tolerability. The combination of these 4 drugs had not previously been used within our facility or on *Rag2*$^{-/-}$γc$^{-/-}$ RG mice. The published VXLD regimen provided a starting point for the selection of doses. We initiated toxicity testing in a pilot study at the doses given summarised in table 4.1 (and explained in detail in the methods section) in two female and two male *Rag2*$^{-/-}$γc$^{-/-}$ mice.

Drugs given	Dose and route	Number of times given per treatment block
Daunorubicin	0.45mg/kg IV	1
Vincristine	0.15mg/kg IP	1
Dexamethasone	5mg/kg IP	5
Asparaginase	1000U/kg IP	5

Table 4.1 Initial *in vivo* VXLD doses. Doses, routes and frequency of each of the 4 drugs used in the first block of VXLD treatment during toxicity testing. Daunorubicin was given by intravenous injection (IV) the remaining drugs were given by intra-peritoneal injection (IP). Doses were given relative to body weight.

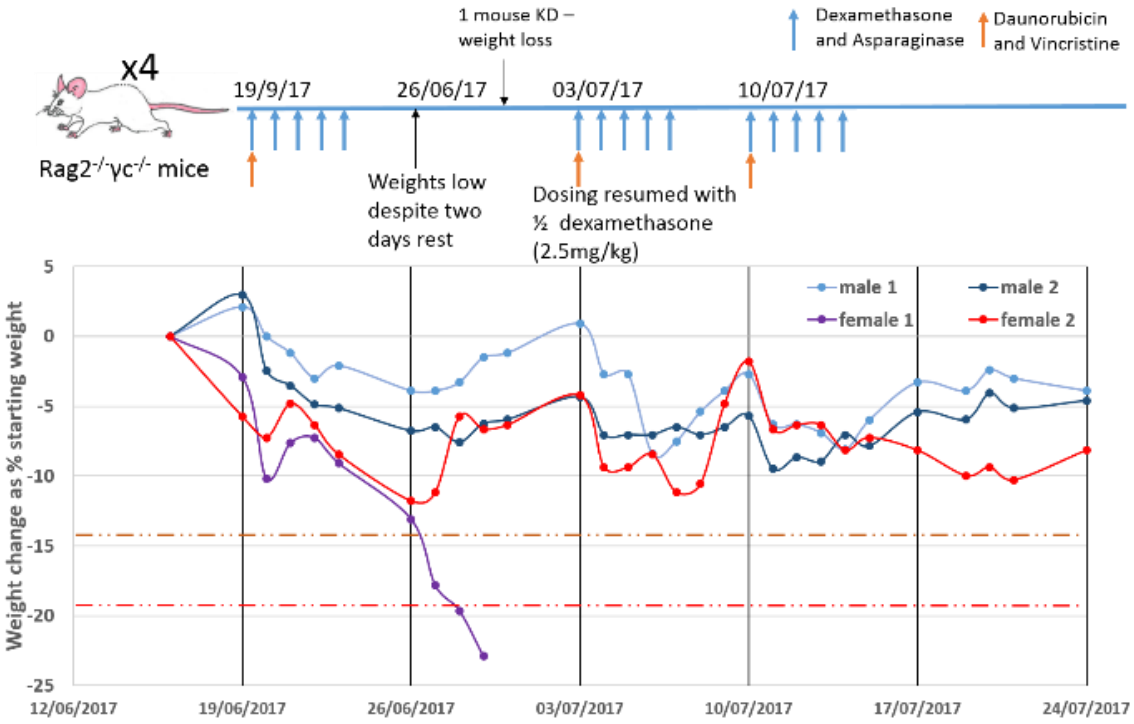

Figure 4.5 Weight monitoring of 4 *Rag2-/-γc-/-* mice during toxicity testing of 4 drug induction regimen. Upper schematic- representation of the pilot VXLD dosing schedule. Lower schematic- weight change of the mice within the pilot study. Each coloured line represents the weight change as a % of the start weight. The dashed lines indicate key weight changes for the project licence with the brown dashed line indicating a 15% weight loss (where dosing should be suspended) and the red dashed line indicating a loss of 20% of original start weight (where the animal must be killed). Drugs were initially given at doses, routes and frequencies shown in table 4.1, with all 4 drugs being given on Monday (as indicated by both blue and orange arrows) and then dexamethasone and asparaginase also being given Tues-Fri (as indicated by the blue arrows). Mice were dosed Monday through Friday as indicated by arrows. Doses for the first block are given in table 4.1. The dose of dexamethasone was halved after the first dosing block due to excessive weight loss as indicated. The subsequent doses are summarised in table 4.2.

Mice were weighed daily during dosing and otherwise every 2-3 days. Dosing was initiated with the schedule summarised in table 4.1 on a Monday and ending the following Friday. It was anticipated that 2 days free of dosing would allow for regaining of weight in the mice in preparation for a second week of dosing, however both females exhibited further weight loss after 2 days (figure 4.5). Neither male had returned to their original pre-dosing weight. Dosing plans were suspended for the following week to allow mice to regain weight. During this time one of the female mice had to be culled due to excessive weight loss. The remaining toxicity testing was performed in the remaining 3 mice. Given the weight loss seen in all mice the dosing required amendment to improve tolerability.

From previous experience in the research group similar weight loss and failure to regain weight was observed with dexamethasone treatment. Additionally, pharmacokinetic studies showed that doses lower than the 5mg/kg still achieved plasma concentrations comparable to those found in patients (Matheson et al., 2019)

Drugs given	Dose and route	Number of times given per treatment block
Daunorubicin	0.45mg/kg IV	1
Vincristine	0.15mg/kg IP	1
Dexamethasone	2.5mg/kg IP	5
Asparaginase	1000U/kg IP	5

Table 4.2 *In vivo* VXLD doses. Doses, routes and frequency of the 4 drugs used in second and third blocks of VXLD treatment in toxicity testing and subsequent VXLD dosing

Therefore, the dexamethasone concentration was reduced by half to 2.5mg/kg (table 4.2), whilst doses of other drugs remained the same. After lowering the dexamethasone dose to 2.5mg/kg, all mice tolerated 5 days of treatment and had regained enough weight with 2 days free of dosing to tolerate a second week of treatment. Monitoring the weights and mouse wellbeing continued after dosing was complete to determine any latent effects. These were not observed. The toxicity testing was initially performed in healthy mice. Next, toxicity and efficacy of VXLD was assessed in leukaemic mice.

4.6 Measuring leukaemic burden by IVIS signal over time

Upon establishment of an adapted dosing protocol that was tolerated, leukaemic mice were treated to assess efficacy of treatment. To assess the ability of the VXLD combination to reduce HPB-ALL proliferation and/or survival *in vivo*, 9 $Rag2^{-/-}\gamma c^{-/-}$ mice were injected with HPB-ALL^{Luc+} cells. One -week post cell injection, BLI was performed to determine engraftment. 9 mice were assigned to treatment n=6 (to account for individual variation to treatment) or vehicle n=3. Mice were given two blocks of VXLD chemotherapy each lasting 5 days each, separated by a week (from day 11 through 15 and day 25 through 29). Mice were imaged weekly by IVIS.

Figure 4.6 displays the weekly bioluminescent (BL) images of VXLD treated and control mice. In general BL signal increased over time (moving from blue through to red) and signal area also increased. In the first BL image at week 1 (day 7), the signal is low and restricted to the injected femur; there is a similar pattern between treated and control arms prior to commencement of treatment. At week 2 (day 14 and day 4 of 5 of the first block of VXLD treatment), differences were observed in localisation of signal between the treated and control groups. In control mice signal was present in both the injected hind leg and contralateral leg, whereas in the controls the signal was limited to the injected femur. During week 3 (when the treated mice were not receiving VXLD therapy), the signal spread to the contralateral femurs. During week 4 a second block of VXLD therapy was applied. During this week signal continued to increase in the treated mice but to a lesser extent than in the controls. At week 4 the control mice displayed signal throughout the whole body. The difference in total flux between treated and control mice at week is apparent in figure 4.7 which displays total flux over time. The non-linear fit demonstrated the overall trend in increasing total flux for control and VXLD treated groups however the difference between the two groups was not significant (2-way anova repeated measures).

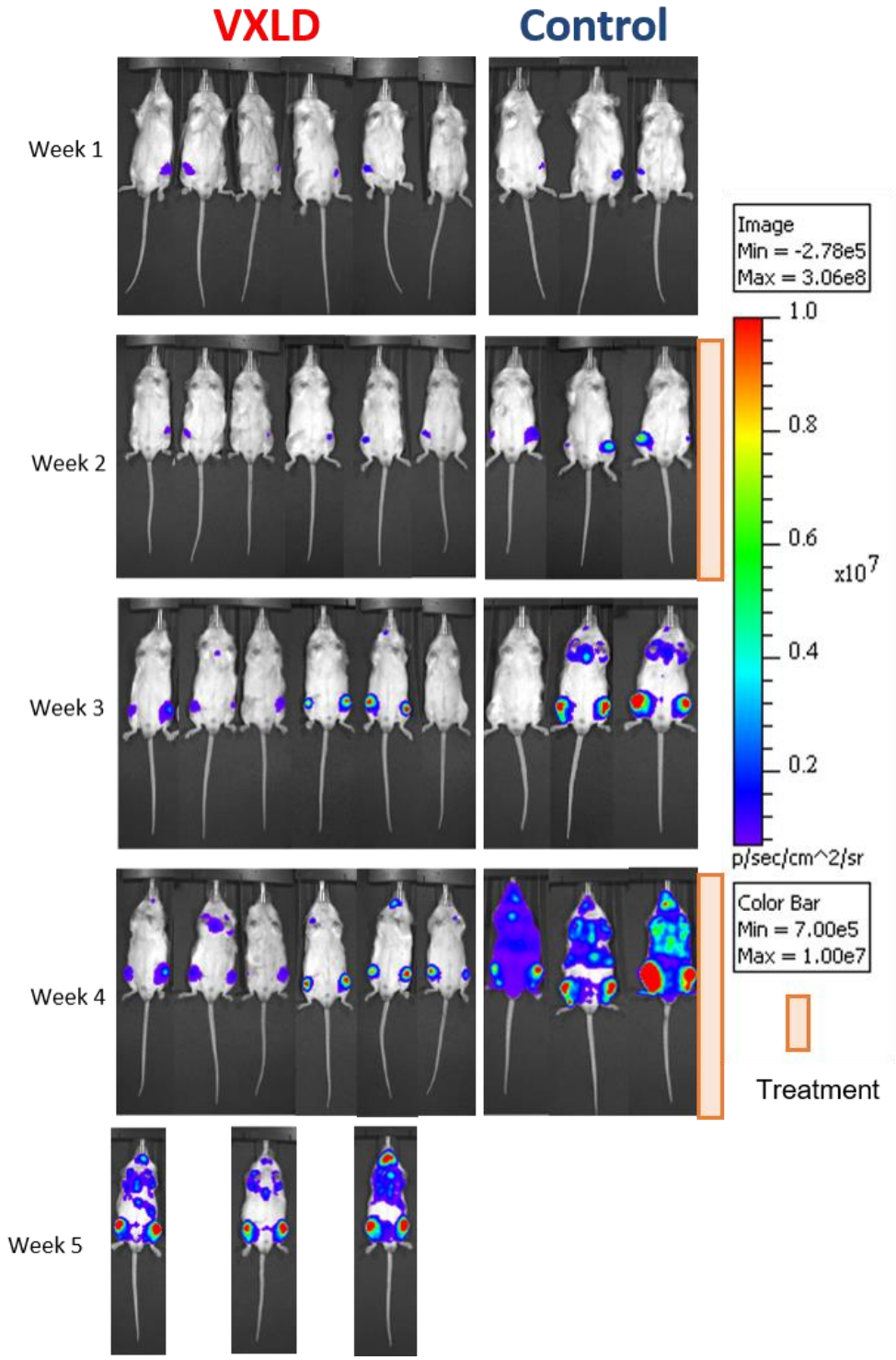

Figure 4.6 Bioluminescent images of each mouse each week. Treated mice are shown on the left (n=6) and control mice are shown on the left (n=3). BLI was performed on days 7, 14, 21, 28 and 35 corresponding to weeks 1,2,3,4 and 5 respectively. Dosing was performed from days 11-16 and 25-29. Weeks 2 and weeks 54 images were taken whilst mice on treatment. Only 3 mice are shown for week 5 treatment arm as 3 mice were culled at week 4 for pharmacodynamics studies. All images are shown on the same scale for comparison. Signal intensity is shown on a scale from blue through to red with increasing intensity

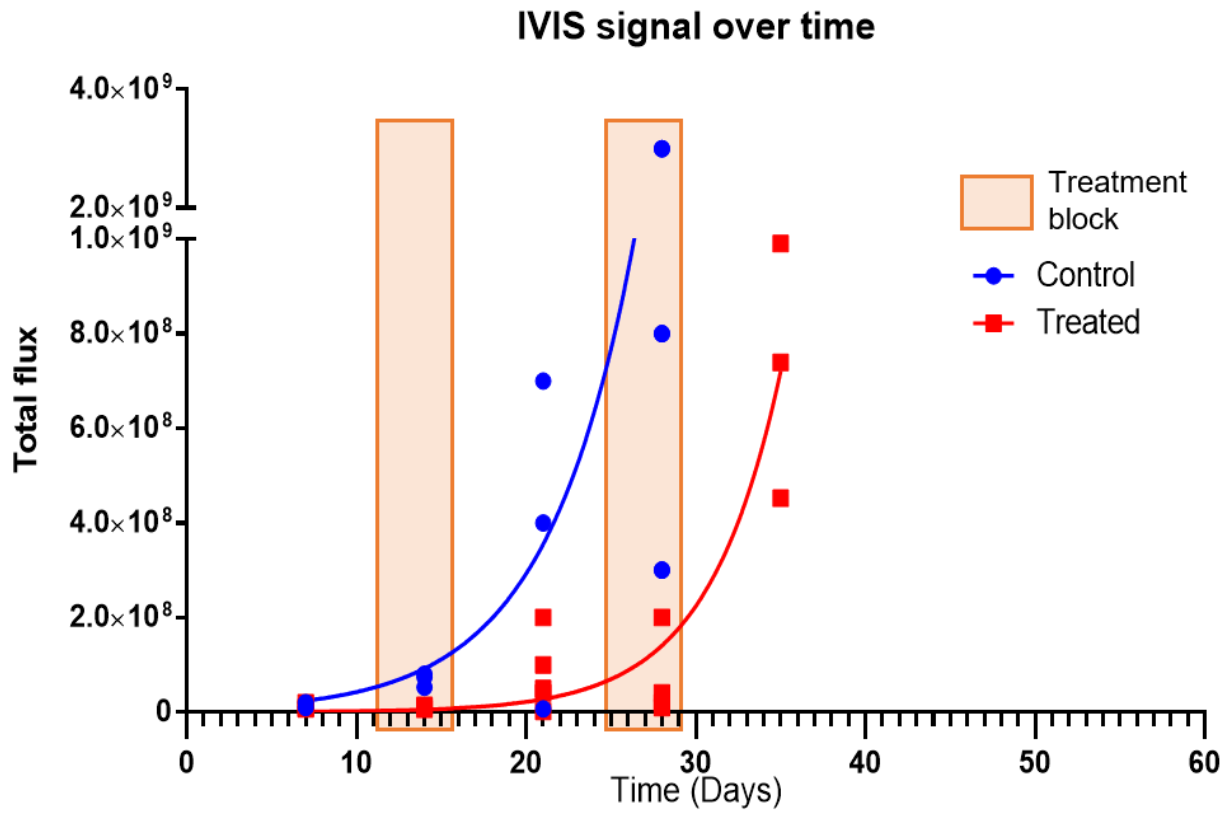

Figure 4.7 Total flux of treated and control mice over time. HPB-ALL cells were injected on day 0. Time in days is given on the x-axis and total flux (photons per second) is given on the y axis. Orange boxes represent treatment blocks. Each point represents a single mouse at the imaging time points; VXLD treated mice (n=3) are shown in red and control mice (n=3) in blue. Red and blue lines indicate trend of the group. There is an additional set of points for the treated group since they survived longer. There is no significant difference between the two groups (two-way anova, repeated measures)

In addition to BLI, event free survival was recorded for treated (n=3) and non-treated (n=3) mice. Mice were monitored until they reached predefined clinical endpoints (weight loss ≤15% from highest previous weight, abnormal gait, abdominal breathing). They were humanely killed by a schedule 1 method and the date of death recorded, the injection date was subtracted from this date to give time until event (figure 4.8).

Despite the lack of significant difference in total flux measured by IVIS between control and treated mice, there was a significant difference in survival with a p value of 0.02 (Log-Rank test). Two control mice were killed on the same day (day 31) and the remaining mouse the following day. All treated mice reached endpoint at the same time as one another on day 39, an average of 7.7 days longer than the

controls. The non-treated mice survived for a median of 32 days whereas the treated mice survived a median of 39 days, an increase in survival of 7 days. To ensure enough pressure was applied to HPB-ALL cells during screening, it was important to establish a significant reduction in BLI which corresponds to cell number. To improve on the increased survival time and achieve a significant difference by BLI with VXLD treatment, the experiment was repeated with intensified dosing.

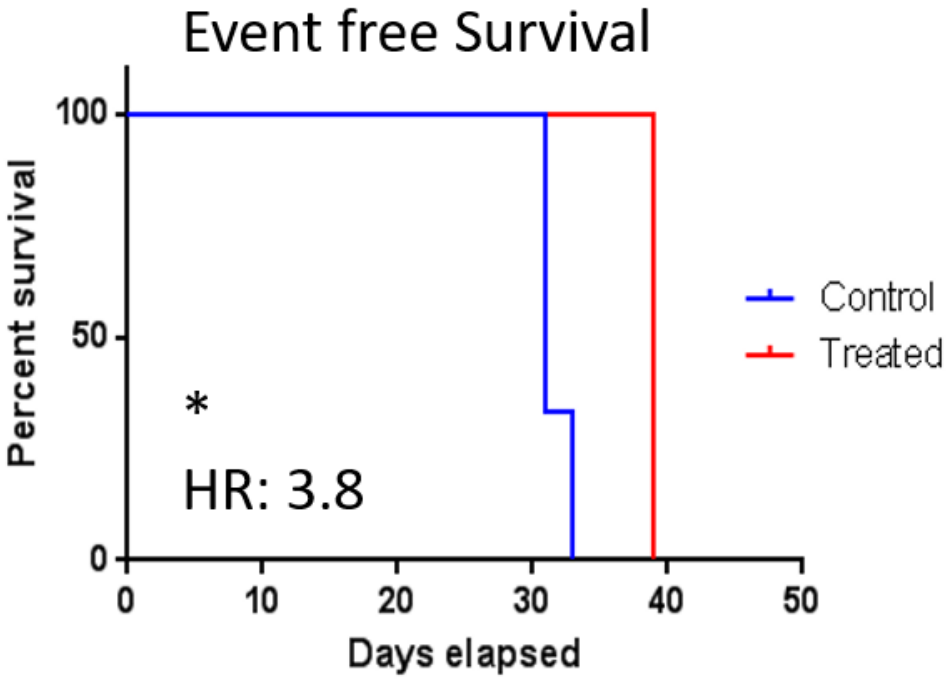

Figure 4.8 Event free survival of HPB-ALL engrafted mice treated with 2 blocks of VXLD chemotherapy. Mice injected with HPB-ALL were randomised to receive VXLD treatment n=3 or vehicle control n=3. VXLD treated mice began treatment 8 days after injection and received a total of 2 blocks of treatment. Mice were weighed and monitored for signs of leukaemia in addition to weekly IVIS imaging. Once mice reached pre-defined end points, they were killed and their date of death recorded. This was used to calculate the number of days since injections and the number of days recorded as event free survival. (* indicates significant difference between groups by Log Rank test with $p<0.05$ and HR indicates the hazard ratio of vehicle:treated by the log rank method).

4.7 Increasing the effect of VXLD chemotherapy on HPB-ALL engrafted mice

To achieve a significant effect in reduction of HPB-ALL *in vivo*, the dosing schedule was intensified. Six mice were injected with HPB-ALL^{Luc+} and randomised to receive treatment or vehicle control (3+3). In the previous study, dosing started at day 11 after cell injection to allows cells to become established prior to onset of treatment, in attempt to increase the amount of treatment given, in the following study the first block of VXLD dosing was initiated 4 days after injection of the cells, the second block was then given from day 11 through 15 and lastly a block was included from 24-29 days post injection, giving a total of 3 blocks of VXLD therapy. BLI was performed 1-2 times a week to monitor the progression of leukaemia in the mice. For each imaging day, the total flux for each mouse was measured and plotted against time (figure 4.9).

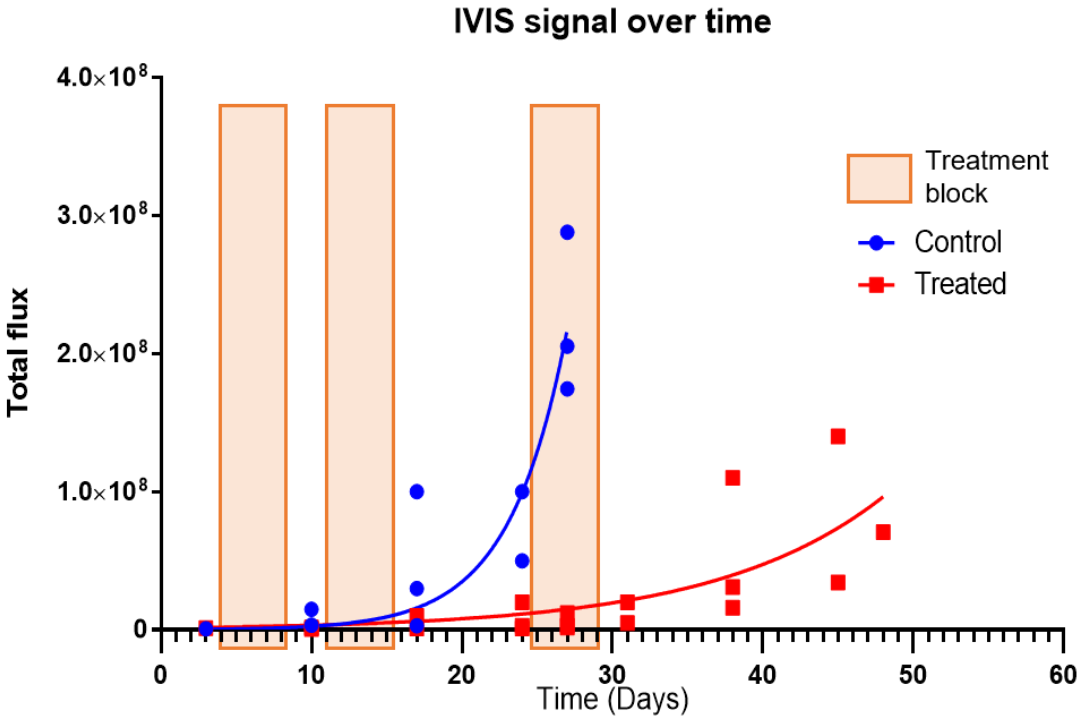

Figure 4.9 Total flux as calculated by BLI over time from intra-femoral injection of cells, for control and VXLD treated mice. Time in days is given on the x-axis and total flux (photons per second) is given on the y axis. Orange boxes indicate where treatment was applied. Lines indicate the trend of the control (blue line) and VXLD (red line) over time. A significant difference in IVIS signal between treated and untreated was observed ($p < 0.05$; 2-way anova, repeated measures)

The total flux signal increased more rapidly in the control mice compared to the VXLD treated mice ($p<0.05$, 2 way anova repeated measures). Event free survival was also recorded for the treated and non-treated mice. Once mice reached predefined clinical endpoints, they were humanely killed by a schedule 1 method and their date of death recorded, the injection date was subtracted from this date to give time until event (figure 4.10).

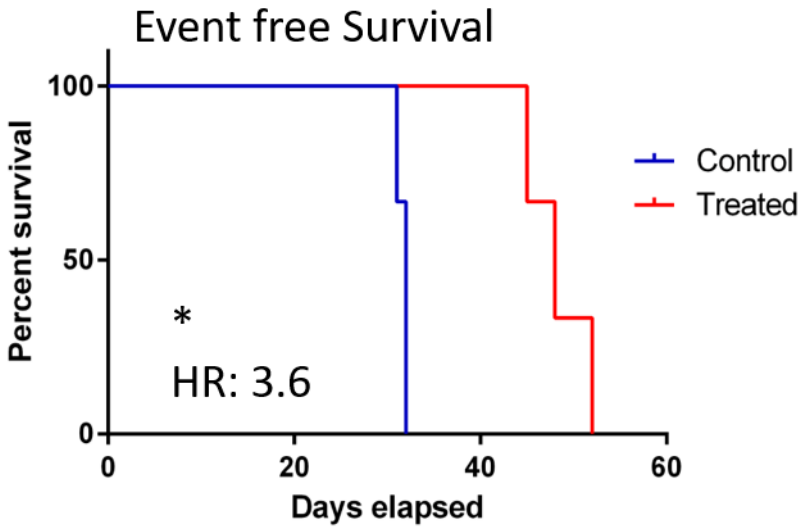

Figure 4.10 Event free survival of HPB-ALL engrafted mice treated with 3 blocks of VXLD chemotherapy. Mice injected with HPB-ALL were randomised to receive VXLD treatment n=3 or vehicle control n=3. Mice were weighed and monitored for signs of leukaemia. Once mice reached pre-defined end points (weight loss <15%, abnormal gait, reduced body temperature, abdominal breathing), they were killed and their date of death recorded as an event, this was used to calculate the number of days since injections and the number of days recorded as event free survival.(* indicates significant difference between groups by Log Rank test with $p<0.05$ and HR indicates the hazard ratio of vehicle/treated by the log rank method).

The treatment significantly prolonged event free survival ($p=0.03$, Log Rank test). Median event free survival was increased from 32 days to 48 days. Disease progression was successfully monitored over time using BLI in HPB-ALL injected mice. A VXLD treatment was established that was tolerable and significantly reduced total flux and increased event free survival. To further validate the effect of VXLD on HPB-ALL, *in vivo* samples harvested from treated and non-treated mice were analysed.

4.8 Response of HPB-ALL cells to *in vivo* treatment with VXLD

Mice were treated with 2 blocks of VXLD chemotherapy or vehicle control injections and were killed on the last day of the second block of therapy. Bone marrow samples were harvested from both treated and control mice and were analysed as previously by flow cytometry. Additionally, RNA was also extracted from the cells to assess mRNA expression of the *glucocorticoid receptor* and *FKBP5*, markers which are commonly altered by treatment with dexamethasone. The amount of DNA damage within the leukaemic cells harvested from treated mice was assessed by flow cytometry using phosphorylated histone 2 as a marker of DNA damage.

4.9 Flow cytometry analysis of percentage blasts in murine bone marrow with and without VXLD treatment

1 million harvested cells from each mouse were stained for viability, murine CD45, human CD45 and human CD3. Flow cytometry was used to detect the presence of human leukaemic cells within harvested bone marrow samples in mice that had undergone VXLD chemotherapy and in controls. For method details refer to 2.13.3.

A significant reduction was observed in the percentage of human CD45 positively stained cells from total bone marrow samples from VXLD treated mice ($p=0.0046$, unpaired t-test), reducing from an average of 63.8% to 24.8% (figure 4.11). This was in line with the reduction in bioluminescent signal and confirmed that the VXLD dosing was indeed reducing leukaemic burden in the bone marrow. The reduction in percentage of human cells may even underestimate the effectiveness of the drugs, since VXLD treatment is likely to have also impacted the murine cells within the bone marrow.

The reduction in leukaemic infiltration in the bone marrow could be attributed to any of the drugs used within the VXLD regimen. Given the effect of dexamethasone was detectable by measuring dexamethasone response gene upregulation *in vitro*, the impact of dexamethasone treatment on cells *in vivo* was analysed.

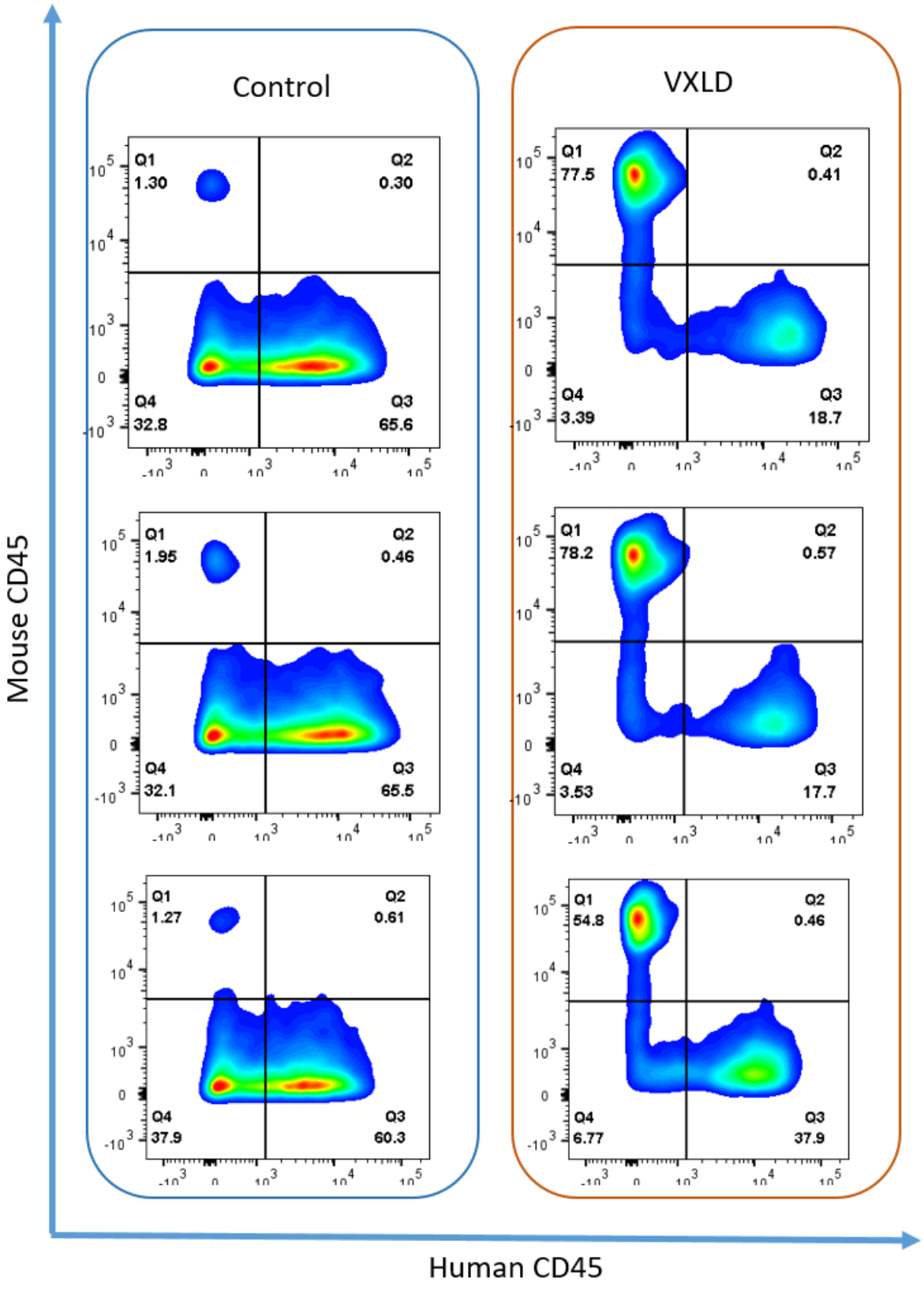

Figure 4.11 Analysis of percentage human leukaemic cells within murine bone marrow of 6 mice. 3 mice had previously received 2 blocks of VXLD treatment (right) and 3 received only vehicle injections (left). Mice were killed 4 weeks post intra-femoral injection of HPB-ALL cells. Human CD45 is shown on the horizontal axis and murine CD45 is shown on the y-axis.

4.9.1 Expression of glucocorticoid response genes in HPB-ALL treated *in vivo* with VXLD

In vitro treatment of HPB-ALL with dexamethasone had limited effect on cell survival or proliferation but caused upregulation of dexamethasone response genes. To determine if HPB-ALL cells treated *in vivo* displayed changes in dexamethasone response gene expression, RNA was extracted from bone marrow harvested from 6 HPB-ALL engrafted mice; 3 that had received VXLD treatment and 3 controls. The extracted RNA was used to synthesise cDNA and quantitative PCR used to assess expression of glucocorticoid receptor mRNA and dexamethasone response gene FKBP5 (figure 4.12). Primers were designed to amplify only human sequences to ensure the measured expression was from the HPB-ALL and not murine cells.

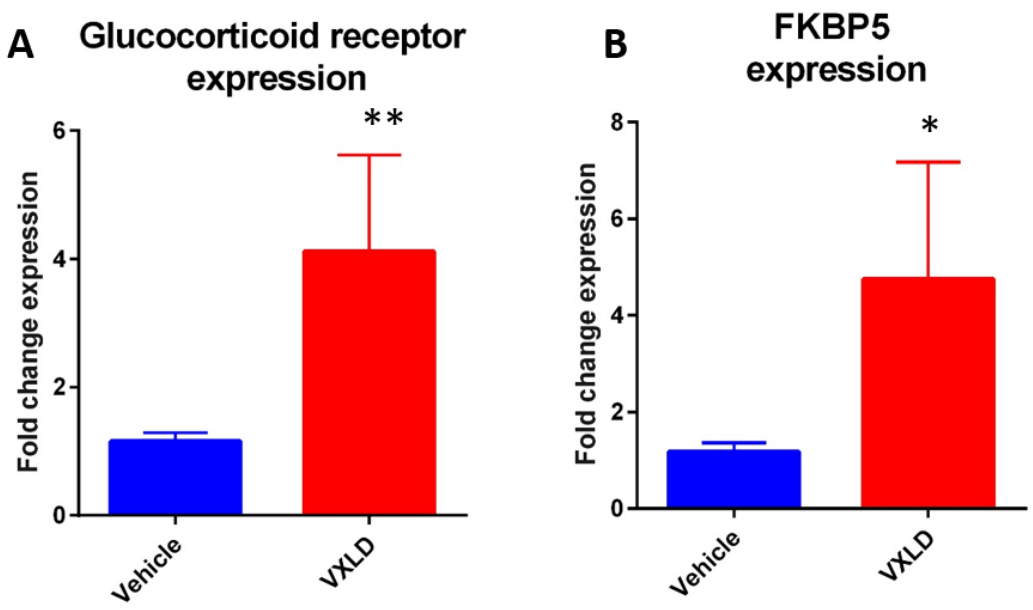

Figure 4.12 mRNA expression of glucorticoid receptor and response gene FKBP5. Glucocorticoid receptor mRNA expression (A) and FKBP5 expression (B) in HPB-ALL cells harvested from the bone marrow of mice treated with VXLD chemotherapy. Expression was normalised to housekeeping gene GAPDH and shown relative to expression in HPB-ALL cells from mice receiving only vehicle control. * indicates p value <0.05 ** indicates p value < 0.01 (unpaired t-test)

HPB-ALL cells harvested from the bone marrow of mice treated with vehicle or with VXLD chemotherapy showed a difference in mRNA expression of the glucocorticoid receptor. *In vivo* VXLD treatment caused a significant increase in mRNA expression of the receptor, this could be attributed to the positive regulation of the glucocorticoid receptor pathway by dexamethasone described previously in leukaemic T-cells

(Ramdas et al., 1999). FK506 binding protein 51 (FKPB5) is a co-chaperone found in complex with heat shock protein 90 (HSP90) and steroid receptors (Scharf et al., 2011). The mRNA expression of *FKPB5* was assessed in HPB-ALL extracted from VXLD treated and vehicle control mice. There was a significant increase in *FKBP5* expression in the VXLD treated cells when expression is normalised to housekeeper *GAPDH*. There were variations in GAPDH levels between control and treated mice, which may reflect the differences in purity of samples as they were derived from mixed human and mouse populations but may also be due to a change in *GAPDH* expression under treatment. This may have resulted in an overestimation of the increase in *FKBP5* and *GR* expression, additional analysis with alternate housekeeping genes could help clarify this. The apparent increase in glucocorticoid receptor and *FKBP5* expression indicates dexamethasone is reaching the HPB-ALL cells *in vivo* and is able to influence steroid receptor signalling pathways.

4.9.2 Changes in DNA damage marker phosphoH2AX in HPB-ALL treated *in vivo* with VXLD chemotherapy

Treatment with daunorubicin causes DNA damage which results in the phosphorylation at Serine 139 (Ser139) on histone H2AX (Sharma et al., 2012). *In vitro* treatment of HPB-ALL cells with daunorubicin leads to an increase in the levels of phosphorylated H2AX (figure 4.13). If daunorubicin reaches HPB-ALL cells *in vivo*, an increase in levels of phosphorylation of Ser139 on H2AX is expected.

Bone marrow from HPB-ALL engrafted mice that received either vehicle or VXLD chemotherapy was examined. The level of phosphoH2AX in HPB-ALL were assessed by flow cytometry by first gating human CD45 positive cells and secondly evaluating the intensity of fluorophore conjugated antibody staining related to phosphH2AX expression.

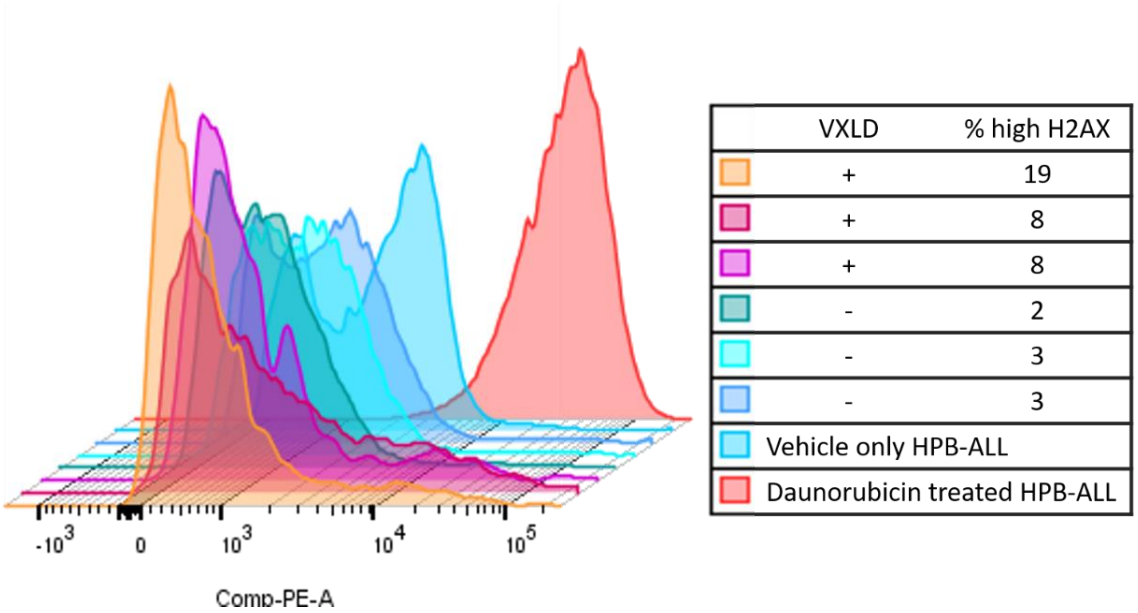

Figure 4.13 Phosphorylated histone H2AX expression on HPB-ALL cells . Bone marrow from mice receiving vehicle n=3 or VXLD chemotherapy n=3 was stained for human CD45 and phosphorylated histone 2. The expression of phosphorylated H2AX is shown for the single gated CD45 positive HPB-ALL cells. HPB-ALL cells treated with high dose daunorubicin in vitro and HPB-ALL cells receiving vehicle in vitro are shown as controls. HPB-ALL cells treated in vitro with daunorubicin show high levels of phosphoH2AX, whereas cells treated with vehicle alone show only moderate levels of phosphoH2AX. The in vitro Daunorubicin treated cells were used to set the gating for high phosphoH2AX levels. The table on the right summarises each sample and the percentage of cells with high levels of phosphorylated H2AX. There was no significant difference in phosphoH2AX levels in VXLD treated and control mice (unpaired t-test*).*

Figure 4.13 shows *in vitro* treatment of HPB-ALL cells with daunorubicin lead to an increase in the levels of phosphorylated H2AX, compared to cells treated with vehicle only. There were still cells stained positively for phophoH2AX in the untreated cell samples, but the staining was less intense. The positivity in untreated cells could be due to the involvement of phosphH2AX in DNA replication, or genomic instability (MacPhail et al., 2003). In HPB-ALL cells harvested from mice, neither treated nor untreated cells should high levels of staining for phosphorylated H2AX but the percentage of cells was marginally higher in mice receiving VXLD treatment at an average 12% of cells staining positive for phophoH2AX compared to 3% in control mice, which was a non-significant change by t-test (p=0.07). The lack of cells *in vivo* achieving the same high levels of phosphoH2AX as seen *in vitro* could be due to the time point at which the samples were analysed. The last dose of Daunorubicin was received 5 days prior to taking *in vivo* samples, whereas *in vitro* samples were analysed after 24 hours. Given the presence of phosphoH2AX in control samples and without cell cycle information, it is not possible to draw definitive conclusions.

No further pharmacodynamics *in vivo* were pursued. However, pharmacokinetic profiles of the four drugs in the *in vivo* model were considered.

4.10 **Pharmacokinetic study**

In order to determine pharmacokinetic profiles of each of the drugs in the *in vivo* model peripheral blood samples were obtained after treatment of non-leukemic (naïve) mice at varying time points with all 4 drugs in combination (figure 4.14 A-D). Plasma was used to assess asparaginase activity (via a colorimetric assay) and the concentration of dexamethasone, daunorubicin and vincristine was assessed by liquid chromatography-mass cytometry (LC-MS). The extraction, processing and analysis of plasma samples for dexamethasone, daunorubicin and vincristine were kindly performed by Mankaran Singh and Philip Berry (NICR clinical pharmacology group).

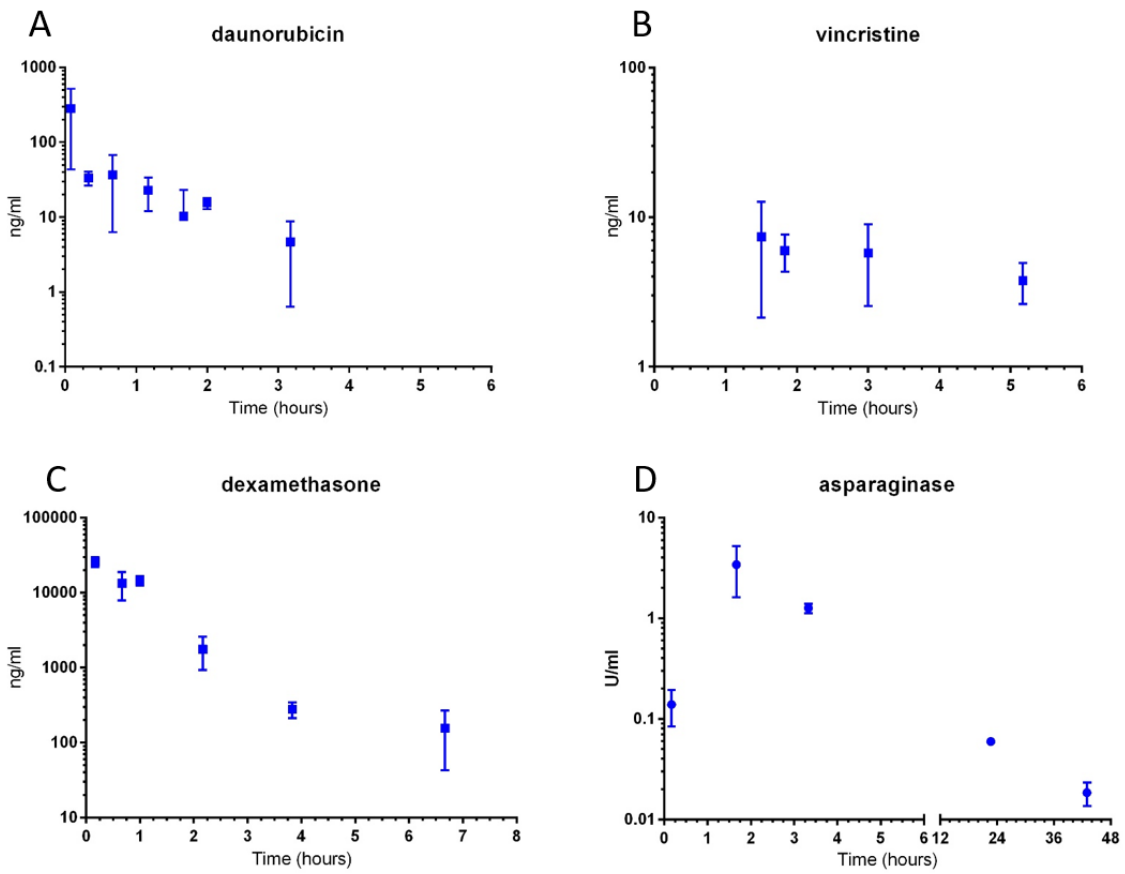

Figure 4.14 Plasma levels of drugs. Concentration of chemotherapeutics daunorubicin (a), vincristine (b), and dexamethasone(c) and activity level of asparaginase (d) in the plasma of mice treated with VXLD chemotherapy. Each time point is derived from 3-6 mice, error bars represent standard deviation.

There were 7 evaluable time points for daunorubicin. The maximum recorded concentration was at the first 5 minute time point and was a mean of 281ng/ml. Vincristine had only 4 evaluable time points, with the first at 90 minutes after intra-peritoneal injection, the mean recorded at 90 minutes was 7.4ng/ml and the average concentration declined over time to 3.8ng/ml at 310 minutes (5.2 hours). Dexamethasone concentrations were measured at 6 different time points. The highest median dexamethasone concentration was 25933ng/ml, 10 minutes post dosing (IP). Dexamethasone levels reduced rapidly but were still detectable after 6.7 hours with a mean concentration of 155ng/ml. Asparaginase activity was highest at 100 minutes with a median activity of 3.4U/ml. Asparaginase activity levels had reduced below 0.1U/ml by 23 hours (mean 0.06U/ml).

4.11 Chapter discussion

4.11.1 Effectiveness of VXLD treatment regimen *in vivo*

Intra-femoral injection of HPB-ALL leads to very rapid leukaemia engraftment in *Rag2*$^{-/-}\gamma c^{-/-}$ mice with predominant bone marrow engraftment and survival of 32 days. Optimised VXLD treatment was able to significantly increase survival to 48 days. Weight-loss was seen in mice undergoing treatment but was within the limits stipulated by the home office project licence.

Enough HPB-ALL cells could be extracted from murine bone marrow for analysis of sgRNA representation at the end of screening. *In vitro* multiple screening time points could be taken whereas *in vivo* cells could be harvested at a single point in time. The maximum screening length is largely determined by the time from injection to development of leukaemia. Since mice succumb to disease in less than 5 weeks and the number of cell doublings occurring *in vivo* is unknown, screening will be terminated just prior to mice becoming unwell to ensure the maximum possible number of cell doublings has occurred. Mice were harvested at day 27/28 for control and at day 37/38 for treated mice, or earlier if mice became unwell. We estimate that this will provide adequate cell doublings to show changes in sgRNA abundance, but there is a possibility that too many doublings have occurred and highly proliferative sgRNAs might predominate and obscure other hits.

4.11.2 Representation and library coverage for *in vivo* screening

In addition to lack of control of cell doublings, we have limited control over the number of cells that can be input into the screen. Injection of the T-ALL cells into the femur of the Rag2-/-γc-/- mice, whilst putting them directly in the bone marrow niche it restricts the number of cells that can be injected. Only 2 million cells were injected per mouse, with 76,441 unique guides at recommended 400 times coverage, means 30,576,400 cells were required in total (Doench et al., 2016). It is not possible to inject such a high number into a single mouse. The 2 million cells only allow for a 26 times coverage per mouse. Injecting multiple mice per screening arm allows us an increase in cells injected and increases the likelihood of full library coverage when mouse samples are combined.

The low complexity in each mouse may be further confounded by the number of leukemic cells that can engraft from the total number injected, and this information is an unknown factor (Patel et al., 2014). Clonality within samples can lead to variations in engraftment ability, although this is reduced by using a cell line compared to clonality in patient derived xenografts (Clappier et al., 2011, Poglio et al., 2016).

In addition to the uncertainty in the number of cells able to engraft, it is unknown if all cells that engraft demonstrate the same engraftment pattern. We have shown HPB-ALL engrafts within murine bone marrow compartments, however we do not know if all cells can equally engraft in all compartments. Two separate groups have published work on the clonality of ALL cells within the murine bone marrow (Belderbos et al., 2017, Elder et al., 2017). Individual barcoding of ALL cells revealed that different bones within a single mouse housed differently barcoded cells. We harvested total murine bone marrow from all limbs, sternum, calvaria and spine in order to have the best representation. For the majority of the mice, cells were pooled from different bones but for a small number of mice (5 treated and 5 not treated) individual bone marrow compartments were harvested and kept separate for DNA extraction and PCR, and barcoded individually, to allow for compartmental based analysis.

4.11.3 The benefits and limitations of the choice of *in vivo* model

Despite the unknowns and added complexity of performing *in vivo* screening, there are potential benefit of this approach. Performing the screen *in vivo* allows for exploration of niche specific targets, and it is possible that some drugs act specifically

upon the niche-leukaemia interaction. Culturing cells independent of a niche in standard *in vitro* screening closes doors on a whole manner of therapeutic options (Tasian et al., 2018). The bone marrow microenvironment is complex and constructed of many cell types and is not easily replicated outside of an *in vivo* model (Asada et al., 2017). The benefit of a xenograft model means the leukaemia itself has relevant human genetics in a niche environment. Although one must bear in mind a human niche and a mouse niche are not synonymous.

There are many critical differences between mice and humans, several of which relate to haematopoiesis and bone marrow microenvironment (Mestas and Hughes, 2004). Firstly, there are differences in how blood cells are being produced with blood cell production in the spleens of mice continuing into adulthood whereas this only occurs *in utero* in humans. Secondly, chemokines differ between mice and humans, many of which may be relevant to how the leukemic cells interact with other cells (Zlotnik and Yoshie, 2000, Olson and Ley, 2002). In future, use of humanised mouse models may further improve this model.

In addition to the cells being within a murine environment, it is also an immunocompromised environment, to allow the leukaemia to engraft. The immune system is very important in the development of cancer – in fact it is a hallmark of cancer (Hanahan and Weinberg, 2011). An immunocompromised model restricts our ability to assess the impact of immune system on the leukaemia. Use of a cell line that grows independently of a niche is also a consideration: we many not achieve the same niche interactions in this model as when using niche dependant cells such as PDX. Despite this, whilst cell lines can survive independent of niche, it does not mean that the niche will not offer additional growth or proliferative advantage particularly under a treatment setting.

T-ALL cells were injected into mice via an intra-femoral route. This was to put the all the cells into direct contact with bone marrow stromal cells. The role of the stroma for the support of T-ALL is well established. Stromal derived cells are regularly used for the *ex vivo* culture of patient and patient derived xenograft T-ALL cells (Hawkins et al., 2016, Holmes and Zuniga-Pflucker, 2009). The introduction of T-ALL cells via an intravenous route is also common practice for T-ALL engraftment. Whilst intra-femoral injections places all the cells within proximity to one another, less control is achieved with intravenous injection, there is a chance of losing more cells (and therefore library representation) if the cells do not end up in a supportive niche. An

intravenous injection however is far less invasive than intra-femoral injection and can accommodate a larger number of cells. Examining latency, spread of disease and the number of leukemic initiating cells could help determine the most optimum route of introducing T-ALL cells for screening.

4.11.4 Relationship between *in vivo* drug concentrations and clinical levels

Despite a low dose of daunorubicin being administered to the mice (0.45mg/kg) the resultant peak plasma concentration of 281ng/ml is within a clinically applicable range if anything at the higher end with a typical patient C_{max} of 100ng/ml (Hempel et al., 2010a). Table 4.3 summarises the relationship between in vitro doses, *in vivo* C_{max} and clinical C_{max}. Pharmacokinetic of daunorubicin usually show a rapid decrease in plasma concentration followed by a slower elimination phase, which we also observe in our data.

Drug	In vitro	*In vivo* C_{max}	Clinical C_{max}
Dexamethasone	50nM	6600nM	254nM
Daunorubicin	33nM	500nM	190nM
Vincristine	1nM	10nM	4nM
Asparaginase	0.00036U/ml	3.4U/ml	3U/ml

Table 4.3 Comparison of in vitro drug doses, C_{max} levels reached *in vivo* and clinical C concentrations for dexamethasone, daunorubicin, vincristine and asparaginase.

Vincristine plasma levels are in agreement with the plasma levels published in PLoS One in 2012 by Szymanska *et al*. reported C_{max} for vincristine in combination was 8.7ng/ml at 30 minutes, our first time point was later than this at 90 minutes with a concentration of 7.4ng/ml this appears to be in agreement with their data at similar time points (Szymanska et al., 2012a). They record an area under the curve of 1.75mg/L*min which falls lower than the median reported in humans but still lies

within a range recorded in ALL patients (Szymanska et al., 2012a, Moore et al., 2011a, Lonnerholm et al., 2008).

For asparaginase Szymanska *et a*l. reported a maximum activity of 8.9U/ml at 1.9 hours, here a maximum mean activity of 3.4U/ml at the closest time point of 1.7 hours was determined. The asparaginase was depleted to 0.06U/ml within less than 24 hours, this falls just below the minimum desired trough level of 0.1U/ml (Rizzari et al., 2000). Asparaginase concentrations were slightly lower than anticipated at each time point when comparing to previous publications, however given that the pharmacokinetics of different asparaginase preparations have been shown to be greatly variable: this is perhaps not so surprising (Asselin et al., 1993, Boos et al., 1996).

Dexamethasone dosing was lowered from the 5mg/kg used by Szymanska *et al* and Samuels *et al* to 2.5mg/kg. Dexamethasone was detected at very high concentration in mouse plasma at 25933ng/ml at peak. This is far higher than a clinical C_{max} of standard arm patients in UKALL2011 (average 78.6ng/ml) and higher than that seen in Szymanska *et al* (Jackson, 2017)).

The dexamethasone concentration however was in line with data obtained in our facility at comparable time points (Matheson et al., 2019, Dormon, 2017). Comparable studies using dexamethasone in mice (including Szymanska et al) did not include use of daunorubicin in their pharmacokinetic study, with both drugs being metabolised by cytochrome P450 enzymes in the liver, their co-administration could result in different dexamethasone kinetics. Dexamethasone can activate pregnane X Receptor which can induce CYP3A family expression (which are important for its metabolism), the ability of dexamethasone to activate the receptor is different between mice and humans and this may relate to differing pharmacokinetics (Scheer et al., 2010).

The plasma levels analysed in this study just touch the surface in terms of pharmacokinetics and allow us a snapshot at exposure of drug we achieve. A greater number of time points per drug would allow us to better analyse the kinetics of each drug, their total exposure and clearance. It would be beneficial to look further into the dexamethasone kinetics in the VXLD regimen and to see how this compares to the clinical dose and if conditions can be altered to better reflect a clinical setting. Many factors can impact drug kinetics including order of drug administration, the

formulation and the mouse genetic background and the gender of the mice. This is something that should be carefully considered when repeating drug studies particularly in multidrug combinations.

In its current form the dosing regimen leads to weight loss in the realm of 10 to 15%, and a 15% weight-loss calls for the suspension of dosing. The dexamethasone concentration was initially used at a very high dose compared to that found in patients. There may be scope to further reduce the dexamethasone dose. Ideally, we would like to have the possibility for adding additional drugs to the VXLD block, but additional drugs may bring additional toxicity and make the regimen intolerable.

4.11.5 Chapter summary

In this chapter the preparations made for the *in vivo* screen, are optimised and discussed.

- HPB-ALL cells injected intra-femorally produced a systemic disease which can be monitored by *in vivo* imaging
- A tolerated VXLD dosing regimen was established (5 day treatment blocks of dexamethasone IP 2.5mg/kg daily, asparaginase IP 1000U/kg daily, daunorubicin IV 0.45mg/kg once per block, vincristine IP 0.15mg/kg once per block)
- Dosing was optimised to reduce leukaemic burden which will ensure a selective pressure is applied to cells during screening. 3 blocks of treatment starting on days 4,11 and 25 post injection of cells significantly decreased bioluminescence and increased event free survival

Combined with the *in vitro* data from the previous chapter, including cell line selection and *in vitro* drug dosing, the CRISPR screen could be planned.

Chapter 5. CRISPR screen method optimisation

5.1 Introduction to chapter

The intended genome wide CRISPR screen required many different processes, many of which necessitated adaptations and creations of protocols. The Brunello library (a genome wide CRISPR library (selected due to its optimised guide design)) was purchased from Addgene. This pooled plasmid library required amplification before being used to generate lentivirus. The generation of lentivirus and the transduction of T-ALL cells with the as aforementioned lentivirus required optimisation. Once introduced to T-ALL cells, the screening could then take place using conditions outlined in chapters 3 and 4. Ultimately the number of each guide present within each sample was to be determined by next generation sequencing. Prior to sequencing extraction of genomic DNA from the harvested cells was required. A PCR step could then be used to amplify the guide containing region (an ultimately tiny quantity of the total DNA of each cell), from pooled cells in a representative way. After cleaning and quantification of PCR products, samples could be pooled and sequenced. The aim of this chapter was:

- Create a streamlined screening process from introduction of library into cells to sending material for next generation sequencing

This can be broken into smaller specific requirements:

- Optimise lentivirus introduction of library into T-ALL cells
- Check method of amplification of guide containing region
- Optimise clean-up of PCR products

5.2 Transduction of T-ALL cell lines with CRISPR lentivirus

The screen required many transduced cells, to ensure high coverage of the 76,441 sgRNA containing library. Ideally, coverage should be in the region of 400 times per guide meaning a requirement of a minimum number of 31 million library containing cells (assuming one guide per cell). This is to ensure each sgRNA is well represented. A transduction efficiency of around 30% would be ideal to obtain approximately 1 integration per cell. Higher transduction efficiencies may lead to multiple integrations, whereas lower transduction efficiencies mean a far greater number of cells would need to be prepared to obtain enough transduced cells for the screening. Standard transduction procedures were designed for production of virus from different vectors some with much higher titres and where only a small total

amount of lentivirus was required. Protocols required optimisation for the larger scale of the genome wide CRISPR screen.

5.2.1 Optimisation of transduction process with GFP containing vector

Initially the in-house protocol was used for transduction of T-ALL cell lines, as this had worked successfully for transduction with other vectors. To summarise the protocol, it required counting cells, pelleting and re-suspending them in fresh RPMI-8402 10% FBS media at a density of $2x10^6$/ml. A stock of 8mg/ml polybrene was then added to re-suspended cells in a 1 to 1000 dilution to give a final concentration of 8µg/ml polybrene. Cells were aliquoted into 48 well plates with 500µl added to each well. Lentivirus was thawed and added to the wells. The plate was then sealed with parafilm and spinfection performed. Spinfection involved centrifugation at 900g for 50minutes at 34°C. Parafilm seals were then removed from the plates and placed in standard incubation overnight. The following morning as much media as possible was removed from the plate whilst being careful not to disturb the cells, fresh media was then added and cells transferred to a 24 well plate, and culture continued as per standard cell culture.

To determine if transduction efficacies could be increased by adjusting the conditions above. The cell seeding density, use of polybrene and seeding medium were considered. A lentiviral expression vector that contained the green fluorescent protein GFP, was used so that the transduction efficiency was easily quantifiable using flow cytometry.

5.2.1.1 Seeding density

Alternative protocols for transduction of lymphocytes included seeding cells at lower densities ranging from $0.5x10^6$/ml to $1.0x10^6$/ml. Transduction efficiency was compared at the following densities: $2x10^6$/ml, $1x10^6$/ml and $0.5x10^6$/ml. Transduction efficiencies were comparable between $0.5x10^6$/ml to $1.0x10^6$/ml. A seeding density of $1.0x10^6$/ml would allow a greater number of cells to be transduced per well and reduce the total virus volumes needed compared to 0.5 $x10^6$/ml. $2x10^6$/ml gave consistently less transduction than $1.0x10^6$/ml, an example of which is shown in figure 5.2 .Moving forward a seeding density of $1.0x10^6$/ml was selected.

5.2.1.2 Polybrene

Polybrene is a cationic polymer added to cells to help aid transduction efficiency by neutralising the repulsion of negatively charged virus particles and cell surface.

However, polybrene can be toxic to some cells, and may not aid the transduction efficiency. Omitting polybrene from transduction of HPB-ALL cells lowered the transduction efficiency (figure 5.1), so use of polybrene was retained in future transduction protocols.

5.2.1.3 Media

The initial transduction protocol requires re-suspension of cells in fresh media. This removes cells from media containing cytokines they have produced and can stress some cells. The media removed from cells may be depleted in nutrients but contains many cytokines. When pelleting cells, this media was removed from cells but then retained. Fresh media was then mixed in ratio of 1 to 1 with previous conditioned media before re-suspending cells in an appropriate volume prior to transduction. Some cell lines seemed to benefit from the use of conditioned medium, whereas the transduction efficiencies of HPB-ALL remained mostly unaffected by the change in media (figure 5.1).

5.2.1.4 Summary of optimisation of transduction of HPB-ALL using GFP vector

The biggest improvement in transduction efficiency of HPB-ALL came from reducing the seeding density from $2x10^6$/ml to $1x10^6$/ml. The transduction protocol was amended to reduce cell density to $1x10^6$/ml. Polybrene addition improved HPB-ALL transduction efficiency so its inclusion in transduction would be useful to helping achieve optimum transduction levels.

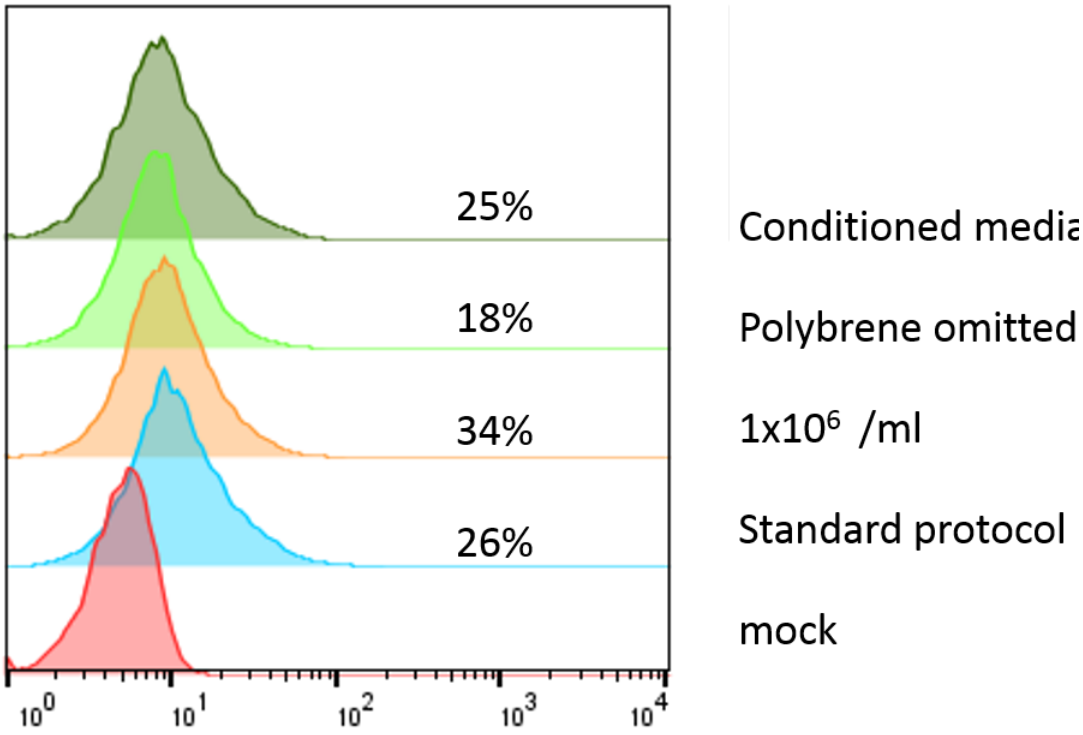

Figure 5.1 Transduction efficiency of HPB-ALL with SLIEW plasmid. Cells were transduced by spinfection with SLIEW virus (HPB-ALL 5ul/well, with 8ug/ml polybrene (except where indicated). Cells were counted and re-suspended at either 1 million per ml or 2 million per ml in media. For the conditioned media, cells were re-suspended in a mixture of fresh and current media at a 1 to 1 ratio, prior to addition to virus and spinfection. Mock transduced cells were re-suspended in fresh media at 1 million per ml with 8ug/ml polybrene and were also subject to spinfection but without virus addition. Graphs show GFP signal (x axis) versus cell count (y axis). GFP positivity was gated on mock transduced cells.

5.2.2 Optimisation of transduction with lentiv2 CRISPR vector

Previous optimisations were performed with fluorophore containing vectors due to the ease of measuring transduction efficiency via flow cytometry, however the backbone of the vector could affect viral titre and transduction of cells. To optimise the transduction efficiency in this context without depleting the stock of the library, a plasmid was selected with the same backbone as the Brunello library (lentiv2), with a non-targeting control sgRNA, which I will refer to as lentiv2-NTC. Since the lentiv2 vector does not contain a fluorophore, transduction could not be assessed simply through flow cytometry. The puromycin resistance gene contained within the vector for positive selection of transduced cells was used instead to assess transduction by selection of cells and cell counting described in detail in section 5.5.

5.2.2.1 Transduction efficiency with lentiv2-NTC

Virus was prepared from lentiv2-NTC, concentrated and stored at -80°C until use. HPB-ALL cells were counted, re-suspended at $1x10^6$/ml, polybrene was added to a final concentration of 8µg/ml and plated into 24 or 48 well plates for transduction. Lentiv2-NTC virus was titrated across HPB-ALL cells and then spinfection was performed. 3-4 days after transduction, cells were placed under puromycin selection, including mock transduced cells. Transduction efficiency was determined by cell counts under puromycin selection as described in 5.3. Table 5.1 shows a summary of some of the results.

Virus volume (µl)	Final concentration (relative to viral supernatant)	Percentage transduction		
		Replicate 1	Replicate 2	Average
1	0.6	15	4	9.5
5	3	8	12	10
10	6	30	25	27.5
25	15	22	8	15
50	30	20	36	28
Supernatant	1	3	1	2

Table 5.1. Percentage transduction of HPB-ALL cells with lentiv2-NTC virus. Virus volume refers to the volume of virus added to each 500ul of plated cell suspension. Final concentration is the final concentration of virus in the well compared to re-suspended cells in virus supernatant with 1 being the same concentration as viral supernatant.

Transduction efficiencies varied between batches of virus. Up to 10µl of virus in a 500µl well increased transduction efficiency to an average of 27.5%, higher virus volumes did not improve transduction efficacy further. A transduction efficiency of around 30% would be ideal for genome wide screening as it would reduce the starting number of cells to transduce, make puromycin selection easier and avoid such high transduction that cells would risk multiple integrations. The only drawback of this method was the requirement of large amounts of concentrated lentivirus. Lentivirus is concentrated by ultracentrifugation in a process taking in excess of 2hours with only 120mls of virus being able to fit in the ultracentrifuge at any one time. Additionally, ultracentrifugation can damage virons reducing the overall active viral titre.

5.2.2.2 Concentration of lentivirus and lentiviral viral supernatant

Whilst cells could be transduced with concentrated Brunello virus, the screen itself would require vast amounts of virus, which whilst feasible was not particularly practical. An alternative to using concentrated lentivirus is to use lentiviral supernatant. Whilst transduction efficiencies with non-concentrated virus may be substantially lower than that achieved with concentrated virus, if enough transduction

could be achieved so that cells can be positively selected it could help save both time and money, by removing the additional concentration step. Initially transduction efficiency with non-concentrated virus was low at only 2% on average. Steps were taken to improve viral titre to increase transduction with lentiviral supernatant.

5.2.3 Optimisations of lentiviral production

The morning following transfection, 293T cells were placed in DMEM media with 10% FBS. The media supernatant was then harvested between 72 and 96 hours post transfection to allow sufficient generation of lentivirus (which is released into the media). Although this can mean a higher concentration of lentivirus is achieved compared to multiple harvests , there is a smaller total volume of lentiviral supernatant and virons produced within the first 24-48 hours are at 37°C for an extended period of time. Lentivirus is not stable at 37°C and loss of activity can be seen by prolonged incubation at 37°C. The transfected 293T cells also require adequate nutrients to produce lentivirus which is provided by the addition of fresh media. Without media change 293T face the risk of nutrient deprivation.

Several amendments were made with the view to improve overall viral titre. The FBS content in the harvest media was increased to 30%, as extra protein helps stabilise viral particles. To prevent loss of virus activity due to prolonged incubation at 37°C, lentivirus was harvested at 48 hours post transfection. To increase total viral yield from a single transfection, a double harvest was introduced. After the 48-hour harvest, fresh media was added to the 293T and an additional harvest performed at 72 hours post transfection. The two harvests were then checked for ability to transduce cells. When both harvests produced significant transduction, they were pooled to increase the total amount of virus available.

5.2.4 Summary of transduction with lentiv2-NTC virus

Using the optimised transduction conditions and the amendments made to the lentiviral harvesting transduction efficiencies in HPB-ALL varied from 10 to 40% with non-concentrated lentiv2-NTC virus. We proceeded to use the optimised protocol to generate Brunello viral supernatant without concentration and checked transduction efficiencies achieved with aliquots of each harvest and batch.

5.3 Assessment of Transduction efficiency with a lentiv2 vector

5.3.1 Methods of assessing transduction efficiency with lentiv2

5.3.1.1 Cell counting

Since the plasmid contains the gene for resistance to antibiotic puromycin, transduced cells can be selected for by exposing cells to puromycin, such that only cells that have been successfully transduced will survive. By performing cell counts by trypan blue exclusion assay, it is possible to determine the percentage of surviving cells which is relational to the percentage transduction using the equation in figure 5.2

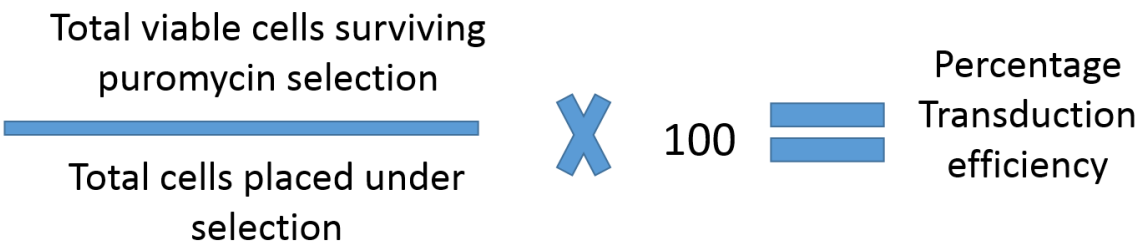

Figure 5.2 Equation for calculation of transduction efficiency. Transduced and mock transduced cells were counted and placed under puromycin selection. Once there were no viable cells in the mock transduced well remaining, the transduced cells were counted using trypan blue exclusion assay. The equation was then used to calculate the percentage of cells that had survived puromycin selection, which acts as a surrogate measure of transduction efficiency.

5.3.1.2 Cas9 expression with RT-PCR

In addition to the cell counting method to estimate transduction efficiency, expression levels of a vector component can be measured. Since expression of Cas9 is essential for gene knockout with CRISPR, expression of Cas9 would help give confidence that cells have been transduced effectively. Positively transduced cells should express Cas9 whereas non transduced cells will not, we can therefore gauge the success of transduction by Cas9 expression relative to a housekeeping control such as GAPDH using quantitative PCR.

Prior to the large-scale transduction of HPB-ALL with Brunello virus for screening, a small quantity of the Brunello virus was applied to HPB-ALL and these cells were examined for successful transduction by selection with puromycin, cell counting and by examining Cas9 expression by PCR. Cells exposed to Brunello virus and wild type cells were counted and pelleted. RNA was extracted, cDNA synthesised, and qRT-

PCR used to measure Cas9 expression relative to GAPDH by delta delta Ct method (as in 2.15.4).

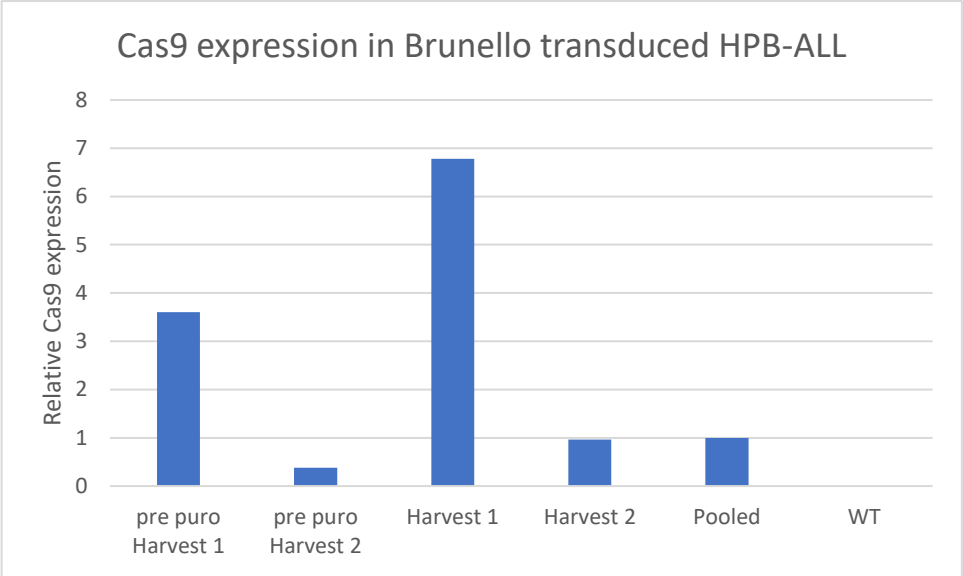

Figure 5.3.*Cas9 expression* in Brunello transduced HPB-ALLVirus harvested at 48 hours (Harvest 1) and 72 hours (Harvest 2) post 293T transfection, was used to transduce HPB-ALL cells. Cas9 mRNA expression was determined by qRT-PCR. Cas9 expression was determined both pre puromycin selection and during puromycin selection of cells. GAPDH was used as a housekeeping gene and Cas9 expression was normalised toCas9 expression achieved with virus pooled from harvest 1 and 2.

HPB-ALL cells showed increased expression of Cas9 compared to wild type cells 3 days after transduction with Brunello virus (figure 5.3). HPB-ALL transduced with either harvests caused expression of Cas9 within the cell pool. Once cells were placed under puromycin selection, there was an increase in expression of Cas9 which could be due to the loss of non-transduced cells from the cell pool. The Cas9 expression results were concordant with cell counts showing transduction with both virus harvests and a greater transduction with the earlier harvest. Despite higher transduction efficiencies with earlier harvest of lentivirus, pooling both harvests still gave adequate transduction levels (cells still survive puromycin selection and express Cas9). Real-time PCR can be used as alternative or in addition to cell counting to estimate transduction efficiency with lentiv2 vectors such as Brunello library. For the screen itself a combination of the two methods was used to have greater assurance of successful transduction. Two lentivirus harvests were [performed and then pooled for screening.

5.3.1.3 Detection of Cas9 expression by flow cytometry

An attempt was made to establish a flow cytometry-based assay to detect the expression of Cas9 in Brunello transduced cells. An antibody against Cas9 with Alexa Fluor 488 conjugate (Cell signalling technologies, 34963) was used at a range of dilutions from 1:50-1:200 , and although it was possible to see a shift increase in median fluorescence intensity between wild type and positively transduced cells, there was insufficient resolution of the populations to determine percentage transduction. This technique was not pursued further as it was outside the remit of the project, but there is potential to optimise a flow cytometry-based assay to measure transduction with this library.

5.3.2 Assessment of DNA concentration, quality and integrity

DNA was extracted as described in section 2.29. A Nanodrop 1000 spectrophotometer (Thermo) was used to measure the quantity of DNA in each sample. 1µl of buffer AE was used to blank the nanodrop, 1µl of the sample was applied to the pedestal, DNA concentration was measured using the DNA-50 setting for dsDNA and recorded. 260/280 and 260/230 values were also recorded. Deviations from optimal ratios (~1.8 for 260/280 and 1.8-2.2 for 260/230) indicated an impure sample.

Assessment of integrity of extracted DNA was made using agarose gel electrophoresis as described in section 2.16. An example of which is given in figure 5.4. In figure 5.4 most of the extracted DNA was retained at the top of the gel with minimal smearing indicating the extracted DNA remained in high molecular weight fragments with limited degradation.

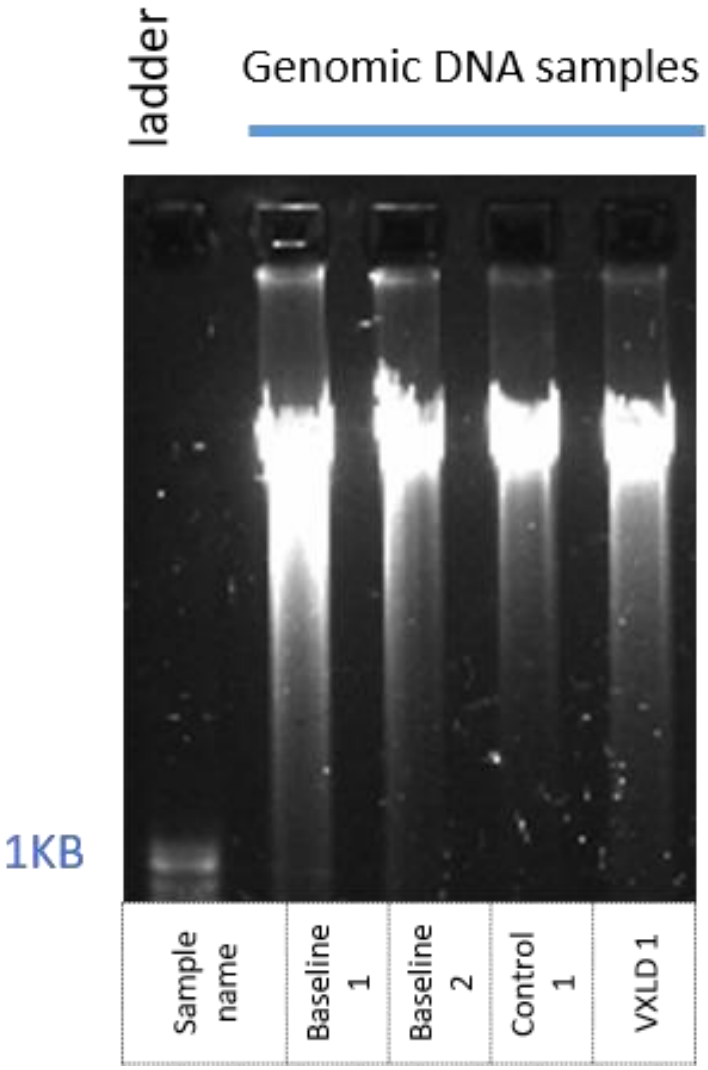

Figure 5.4 Image of genomic DNA samples run on a 2% Agarose gel. Lane 1 contains a marker indicating 1KB and the following 4 lanes contain in vitro samples from the CRISPR screen extracted with a DNA Blood Maxi kit.

5.4 Optimisation of PCR amplification of guide containing region

Once genomic DNA has been extracted, a PCR step can be used in order to amplify the guide containing region, since this is a relatively small amount of DNA within the total cell genomic content. In order to ensure the sgRNAs from each harvested cell are amplified, all the harvested DNA had to be input into a PCR. This meant a large number of PCR reactions must be performed per sample in order to maintain library coverage The Broad Institute provide protocols for PCR amplification of sgRNAs, shRNAs and ORFs for Illumina sequencing. The protocol for sgRNA amplification from lentiv2 is shown in figure 5.5.

Reagent	Details	Volume per reaction
reaction buffer	Takara ex taq 10x	10µl
dNTP		8µl
P5 100µM	Mix of 8 p5 primers with varying stagger	0.5µl
P7 primer 5µM	Individually barcoded for each sample	10µl
polymerase	Takara ExTaq	1.5µl
genomic DNA	up to 50µl and up to 10µg	-
water	Molecular biology grade	Adjust final volume to 100ul

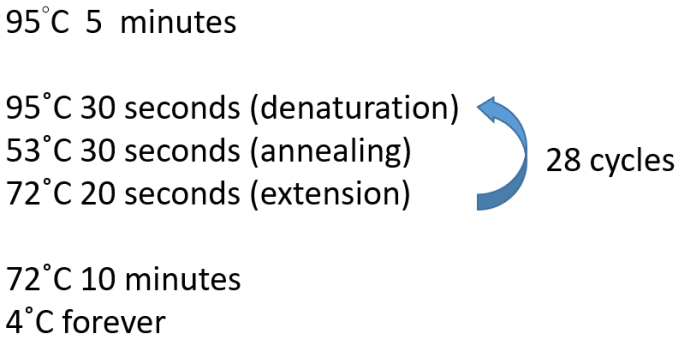

Figure 5.5 Broad insitute protcol for amplifcation of sgRNAs for Illumina sequencing

The protocol allows for high input of genomic DNA which will decrease the overall number of PCR reactions that need to be performed. The primer sequences provided with the protocol also allow for the simultaneous addition of adaptor and barcoding in the single PCR step. To ensure the protocol works well for my samples, the suggested primer sequences were ordered, and several tests performed prior to amplification of screen samples.

5.4.1 Method and Primer design

For each sample a primer pair is used, a p5 forward primer contains a flow cell attachment for Illumina sequencing, Illumina sequencing primer region, stagger – this is random nucleotides added to create diversity during sequencing and lastly the vector binding site. The p7 reverse primer also contains a flow cell attachment. Each P7 primer contains a unique 8 nucleotide barcode sequences used to distinguish each sample when they are pooled, Illumina sequencing primer and vector binding region. This is summarised in figure 5.6.

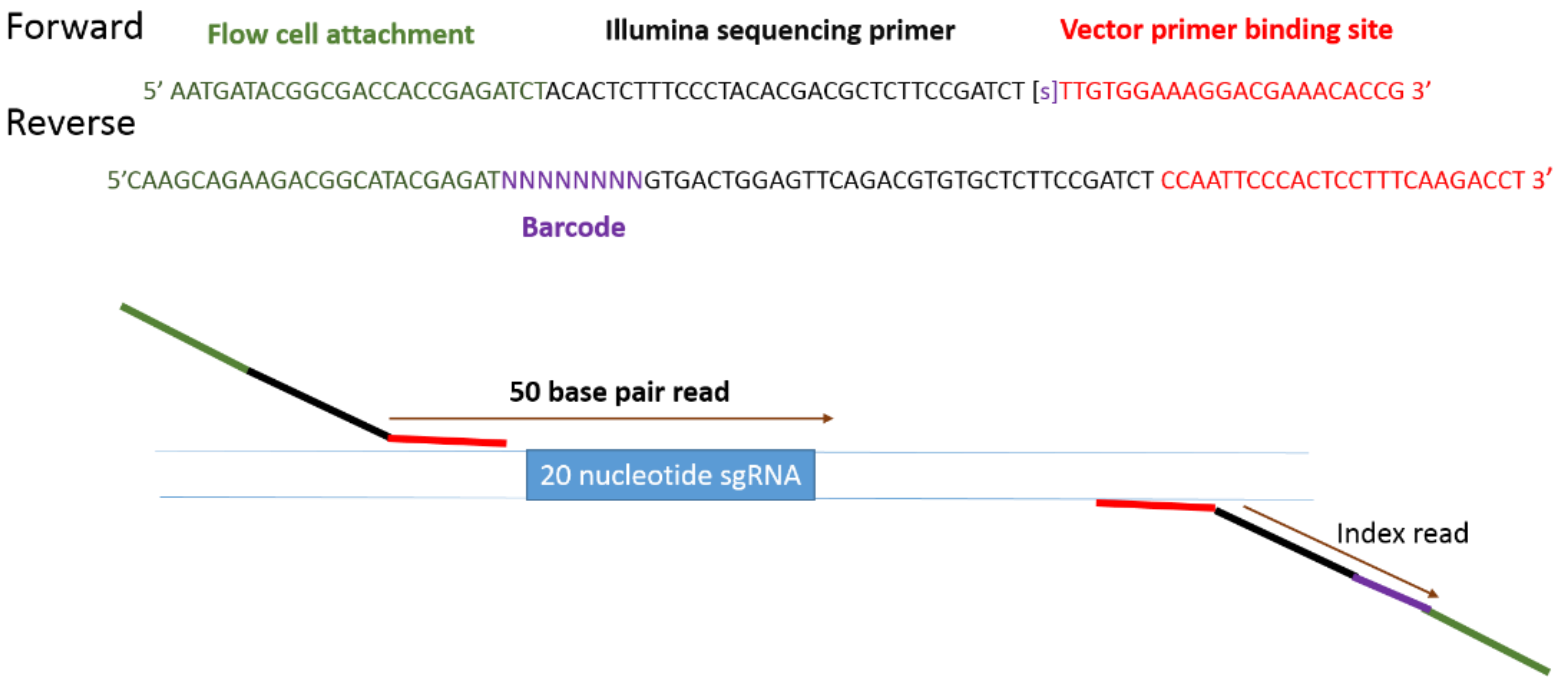

Figure 5.6 Primer design for amplification of guides. Both forward and reverse primers contain Illumina sequencing primer regions, flow cell attachments and regions complementary to the vector, the forward binding just upstream of the 20 nucleotide sgRNA and reverse binding on the complimentary side flanking the sgRNA region. 8 forward primers with varying amounts of stagger ([s]) were ordered and pooled together to add diversity to sequencing. The reverse primer has an 8-nucleotide barcode region, each sample was assigned its own barcoded reverse primer. Sequencing can be performed by a single ended 50 base pair long read as indicated above, an indexing read will allow correct assignment of the read to each sample.

This primer design was favourable as it allowed single step PCR, a short-read length and allowed for a vast number of unique barcodes to label all the samples uniquely so that they can be pooled for sequencing.

5.4.2 Detection of amplicons by agarose gel electrophoresis

To check for primer specificity, PCR products were run on an agarose gel, and any bands compared to a DNA ladder to determine if the size corresponded to that of the expected amplicon. DNA from HPB-ALL containing a lentiv2 vector was used as the genomic input to test PCR reactions. One reaction was performed according to the Broad protocol and a further 2 were performed using an alternative taq polymerase and associated buffers - KOD. For the KOD enzyme, the PCR was performed at two different annealing temperatures; the recommended based on primers and a lower one, closer to the Broad protocol. Afterwards PCR samples were taken and equivalent volumes loaded onto an agarose gel (figure 5.7). The expected amplicon size was approximately 290 base pairs.

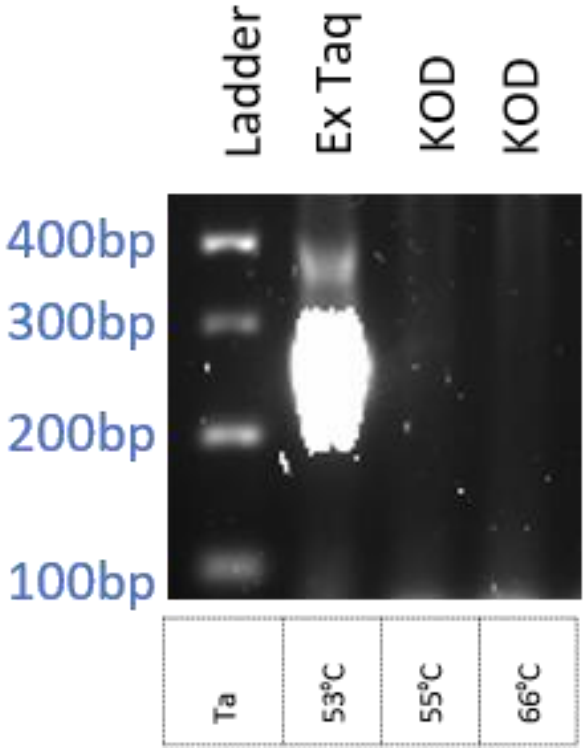

Figure 5.7 Amplification of guide containing regions. Genomic DNA containing the Brunello library was amplified by PCR using Ex Taq® polymerase or KOD enzyme (for two different annealing temperatures Ta), PCR products were run out on a 1% Agarose gel along with a 100bp Sigma ladder. There was a band present at around 375bp in the Ex Taq polymerase, a very faint band in the KOD enzyme reaction with 55°C Ta and no bands present in the final KOD sample.

Given the presence of an amplicon of the correct size using the Broad protocol and Ex taq® polymerase, and lack of clear amplicon in alternatives when used as per manufacturers' protocol, the decision was made to continue with the Broad protocol and Ex taq polymerase. Since it seemed there was a potential non-specific secondary band appearing, several controls were tested to rule out non-specific amplification from genomic DNA.

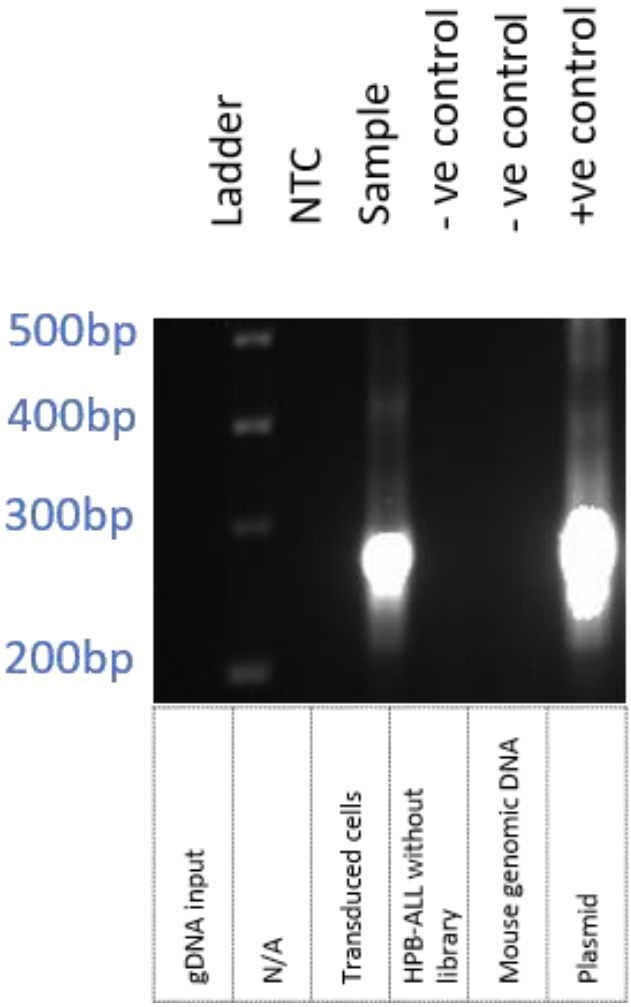

Figure 5.8 PCR controls. From left to right: genomic DNA input, DNA ladder, non template control (NTC), HPB-ALL transdcued with a lentiv2 vector, wild type HPB-ALL, human genomic DNA, mouse genomic DNA and Brunello plasmid DNA.

To check for non-specific amplification, PCR reactions were performed using wild type HPB-ALL genomic DNA and mouse genomic DNA; since neither contain the lentiv2 vector any amplicons present could be attributed to non-specific amplification. HPB-ALL cells transduced with lentiv2 vector and Brunello plasmid DNA were amplified using the same PCVR mix and act as positive controls for the PCR. 700ng were used in each reaction except for plasmid DNA where 5ng was used (figure 5.8).

There was clear amplification in both positive controls, and no amplification in any of the negative controls, ruling out non-specific amplification from genomic DNA.

5.4.3 Selection of PCR conditions

Once confirmed that PCR was generating amplicons of the predicted size in samples and the absence of any amplification in controls, the PCR conditions were adjusted to investigate whether PCR efficiency or specificity could be improved. Increasing annealing temperatures could help increase primer specificity, and it was considered that this adjustment might reduce the formation of the secondary band. Several different cycles of the same PCR reactions were also performed to ensure the PCR had not become saturated. Lastly, each of the barcoded reverse primers were checked individually to ensure each primers was giving the same level of amplification and not producing any unspecific bands.

5.4.3.1 Annealing temperature

Increasing annealing temperatures can increase the specificity of the primer binding. Three equal PCR reactions were prepared and run on the same protocol as before altering only the annealing temperature. After the PCR had finished, 4µl of PCR product was mixed with 1µl of loading dye and loaded onto a 1% agarose gel. The gel was run until the 100bp ladder was well separated and the gel was imaged, shown in figure 5.9. Increasing the annealing temperature decreased the amount of PCR product, whilst the ratio of amplicon to additional 400bp product was relatively unchanged. Moving forward the original annealing temperature of 53°C was maintained.

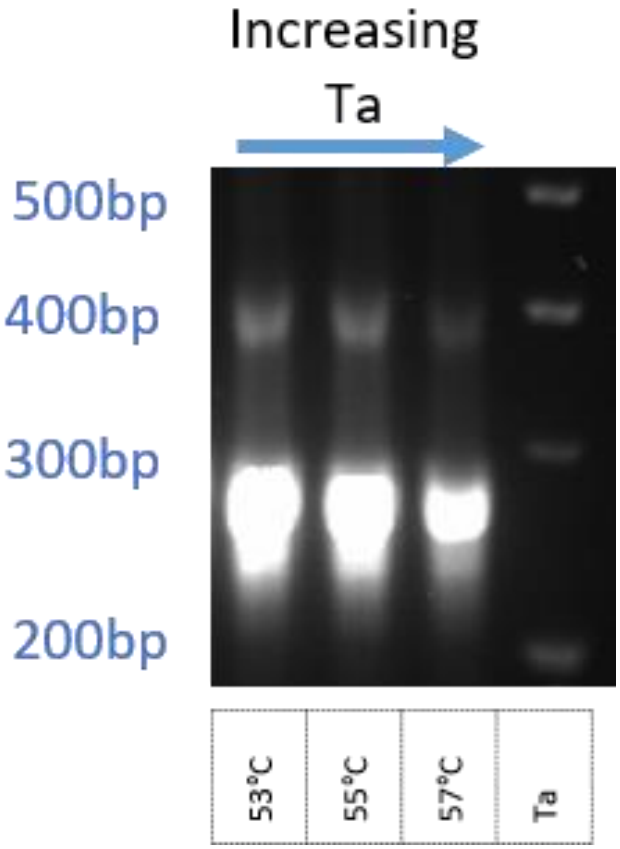

Figure 5.9 PCR reactions with increasing annealing temperatures. Identical PCR mixes were made and ran on the same protocol for PCR with the exception of the annealing temperature. In the far left was the PCR product from using the initial annealing temperature of 53°C. In the second lane the annealing temperature was increased by 2°C to 55° and lastly a further 2°C increase to 57°C. Marked in blue are the size of the 100bp ladder markers in the last lane. The expected amplicon size was 285 base pairs. There was also an additional band present at ~400 bp.

5.4.3.2 Cycles

A PCR master mix was prepared, and genomic DNA added (either 5µg or 10µg), the PCR was then run for differing cycle numbers 20, 23, 25 or 28 (figure 5.10). The least amount of amplicon was produced using 5µg DNA and 20 cycles of PCR, the highest was with 10µg DNA and 28 cycles. There was amplification with both 5µg and 10µg genomic input. There were more intense bands observed with higher genomic input which is most easily seen with the lower cycles. With increasing cycles there was increasing amount of amplicon, which was expected as long as the PCR was not saturated. To ensure high concentrations of amplicon the higher cycle number of 28 was selected.

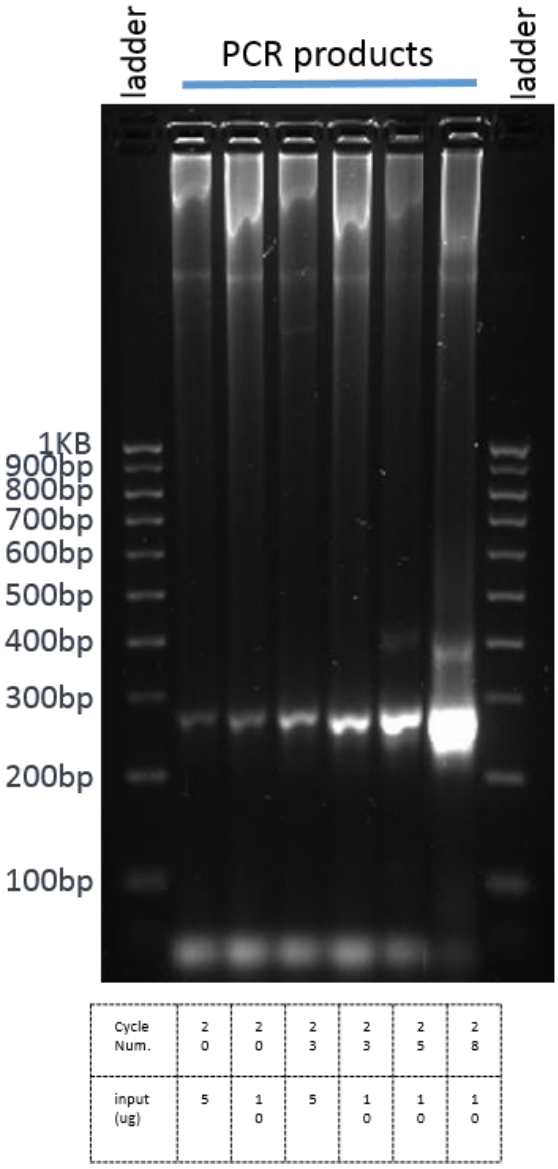

Figure 5.10 PCR products with increasing cycles of PCR. A PCR master mix was prepared from either 5 or 10µg genomic DNA. Reactions were placed in a thermocycler for 20, 23, 25 or 28 cycles of PCR. Products are visualised on a 1% agarose gel.

5.4.3.3 Barcode testing

Each barcoded PCR primer was tested individually in a PCR using conditions specified in 5.8. P7 primers were tested in batches of 8 to 12. A master mix was prepared of PCR components excluding p7, this was distributed into PCR tubes. Genomic DNA was added, and all PCR tubes placed in the thermocycler. PCR products were then run side by side on an agarose gel (figure 5.12). The gel was checked for relative amplicon generation and for presence of additional bands.

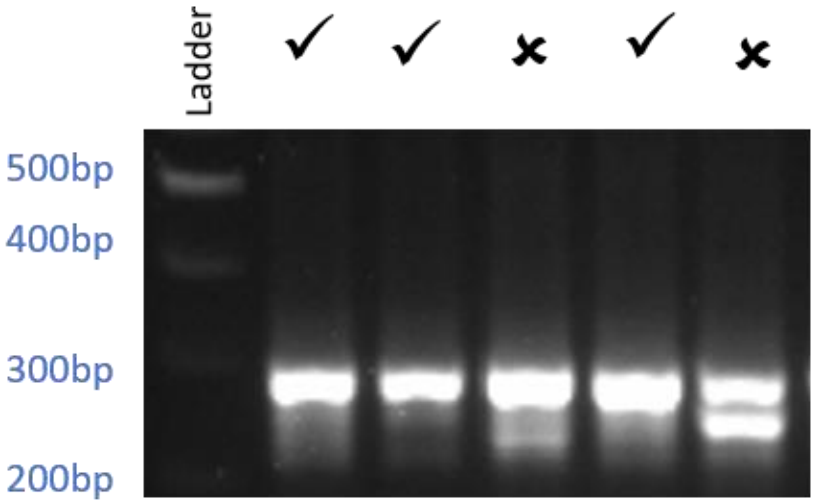

Figure 5.11 Examples of issues with specific P7 barcoded primers. PCR was performed with the same PCR mix except for the P7 primer which was unique to each PCR reaction. The agarose gel image shows amplicons from 5 different p7 primers next to a 100bp ladder (far left).

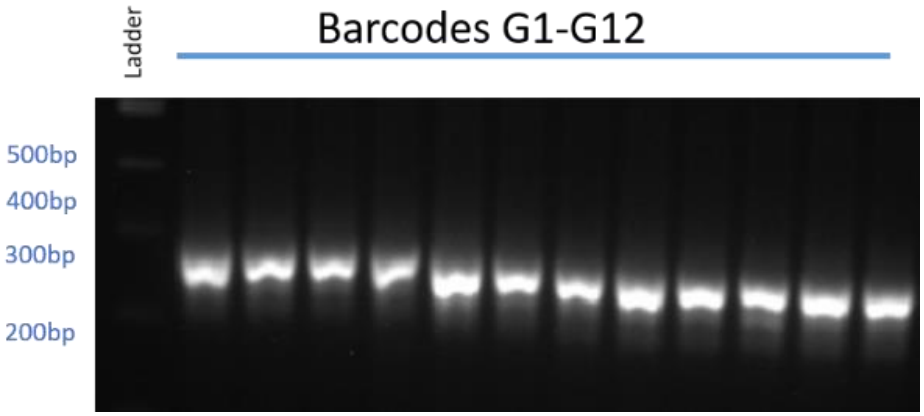

Figure 5.12 PCR amplifcation using P7 primer set G. The same PCR reaction was performed for each of the 12 P7 primers of set G . PCR prodcuts from each indivdual P7 primer are visualised ona 1% agarose gel.

Examples of issues with specific P7 barcoded primers include presence of additional bands as seen in figure 5.11. Whilst 3 primers produced very similar amplicons, 2 did not. The middle PCR appears to have extra smearing underneath the amplicon and potentially a small additional band. The reaction on the right shows an example of a poor barcode primer; here there were two bands of equal size - one the size of the amplicon and one below. This could be due to unspecific amplification or primer degradation. Were poor amplification occurred or additional bands were present the p7 primers were omitted from use on screening samples. This process was carried out on all 96 primers, the results of p7 primers G1 through G12 are shown in figure 5.12.

5.5 Final PCR conditions for amplification of guide containing region

Reconstitution of primers and preparation of PCR reaction mixes was performed inside a PCR hood. Ultraviolet light was used to prepare the hood and equipment. Surfaces and tubes were wiped down with DNase Away prior to use. A reaction mix was prepared according to table 5.2 using Ex taq® polymerase, dNTPs and buffer from Takara.

Reagent	Volume per reaction
10X reaction buffer	10µl
dNTP 2.5mM	8µl
P5 primer mix 100µM	0.5µl
P7 primer 5µM	10µl
Ex Taq 5U/µl	1.5µl

Table 5.2.PCR reaction mix components

Enough reactions were prepared to allow amplification of 400µg of genomic DNA (or the total available genomic DNA if less than 400µg). Reaction mixes were aliquoted into PCR tube strips EasyStrip™ (Thermofischer) in a cool block. Up to 10µg (in up to a 50µl volume) of genomic DNA was added to each PCR tube. PCR grade water was then added to a total volume of 100µl. PCR tubes were placed in a thermocycler set with conditions as in figure 5.13.

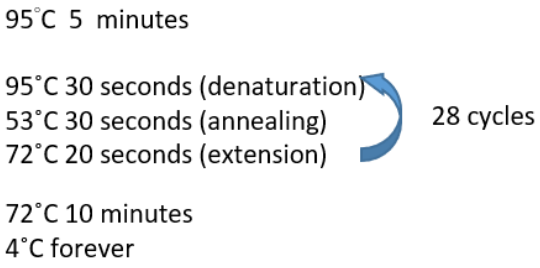

Figure 5.13 Thermocycler settings for PCR amplification of guides for Brunello library screen

PCR products were removed from the PCR machine. To check amplification efficiency, 3-4 randomly selected samples were taken and mixed with loading dye before running on an agarose gel, to check for presence of an amplicon (figure 5.14).

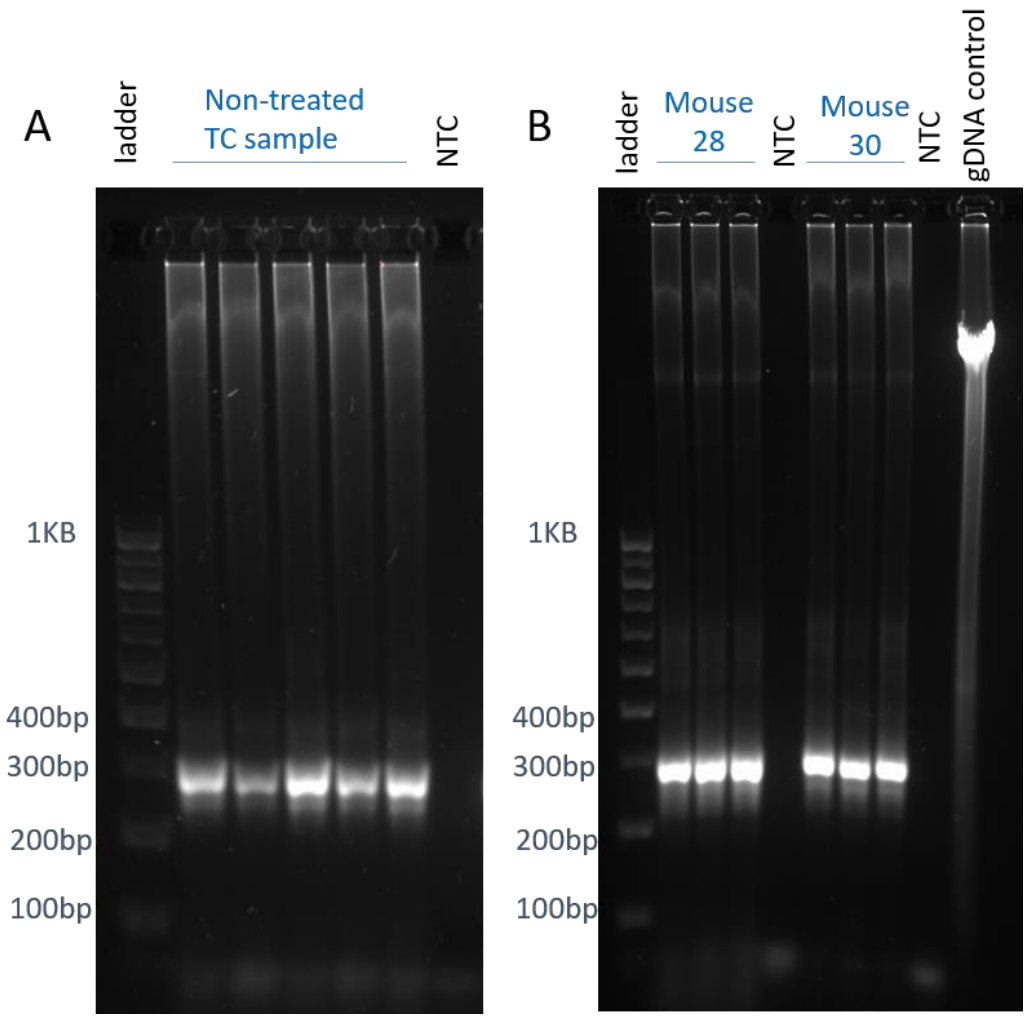

Figure 5.14 Amplification of library samples prior to sequencing. Genomic DNA was distributed over multiple PCR tubes so that in total 400ug of genomic DNA or all the total genomic DNA available whichever was smaller. Prior to pooling PCR products, PCR products for several tubes were checked on an agarose gel for presence of amplicon. (A)An example of the amplification from an in vitro sample. (B) Amplification of two different *in vivo* samples. A 100 bp ladder (Sigma, P1473) is shown in the first lane of each gel. No template controls (NTC) and a genomic DNA control (gDNA) were also run alongside samples

Once successful amplification was confirmed, PCR products from each sample were pooled and stored at -20°C until PCR clean-up. If there were any issues with the PCR, amplification was repeated where material was available, or in the case of 4 samples 3 from pooled mice and 1 from a single compartment (22T , 29T, 26T and 15D) genomic DNA was removed from failed PCR reactions by use of QIAquick PCR Purification kit, before being diluted and the PCR repeated.

5.6 Optimisation of PCR clean up

5.6.1 Purification method introduction

Bead-based purification was selected, since this is much more efficient with large sample numbers and far less susceptible to contamination during the clean-up process compared to gel extraction. Agencourt AMPure XP beads (Beckman coulter) utilise a solid phase reversible immobilisation technology to purify amplicons. The beads bind fragments greater than 100bp and above and remove the majority of primer dimers.

5.6.2 Size selection using AMPure beads

AMPure beads contain PEG and NaCl; by adjusting the ratio of beads to PCR product, the concentration of PEG and NaCl can be altered. With lower concentrations of PEG and NaCl, the larger fragments will bind, whereas smaller fragments bind with increased bead to PCR product ratios. By adjusting the ratio of beads to PCR product, different sized products can be selected. Initially a 1 to 1 ratio of beads to PCR product was tested.

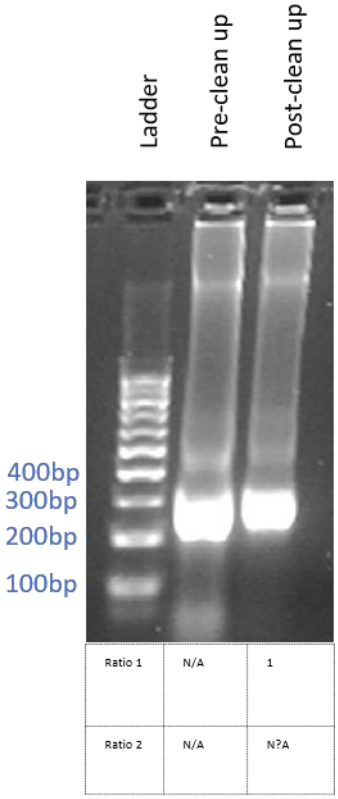

Figure 5.15 PCR clean up with AMPure beads. A 1:1 PCR product to bead ratio was used. The cleaned and non cleaned PCR products visualised on a 1% gel

A 1 to 1 ratio did not give 100% recovery but did successfully remove most adapter dimers (figure 5.15). In order to increase the recovery of amplicon, the bead to PCR product ratio was increased. A PCR reaction was divided into 3 tubes; one was cleaned with AMPure beads at a 1 to 1 ratio of PCR product to beads, another at a 1 to 1.6 and the last a 1 to 1.8 (figure 5.16).

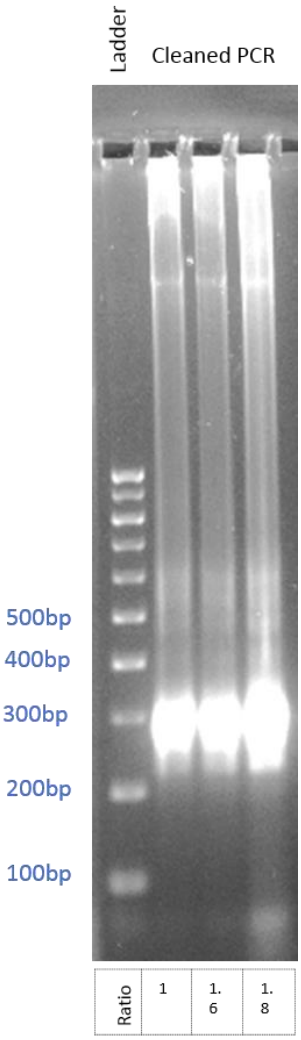

Figure 5.16 PCR products after clean up with differing ratios of AMPure beads. Single step PCR clean up with increasing bead to PCR product ratios from a 1:1 then a 1:1.6 and lastly a 1:1.8. Post clean-up products were run on a 1% agarose gel for visualisation.

As anticipated, the highest ratio of beads provided the largest recovery but inefficiently removed primer dimers. Recovery of amplicon was not greatly improved by increasing the bead ratio from 1 to 1.6. Genomic DNA was still readily detectable in cleaned PCR samples by the smeared pattern in the region of high molecular weight DNA.

Multiple step clean-ups could also be used to remove excess high molecular weight DNA. A 2 step clean up can be used to first reduce the presence of genomic DNA, prior to binding an elution of amplicon. PCR product is mixed with a lower ratio of beads first to remove larger fragments and then the supernatant is removed and mixed with further beads to purify the amplicons. This process is described in figure 5.17. Since some samples contained high amounts of genomic DNA, this process should help produce more pure amplicons. The same PCR product was subjected to a single step clean at a 1:1 ratio, a single step PCR clean up at a 1:1.6 ratio, or a 2 step PCR of 1:0.65 followed by 1:1 and a 2 step PCR of ratio 1:0.5 followed by 1:1 (figure 5.18).

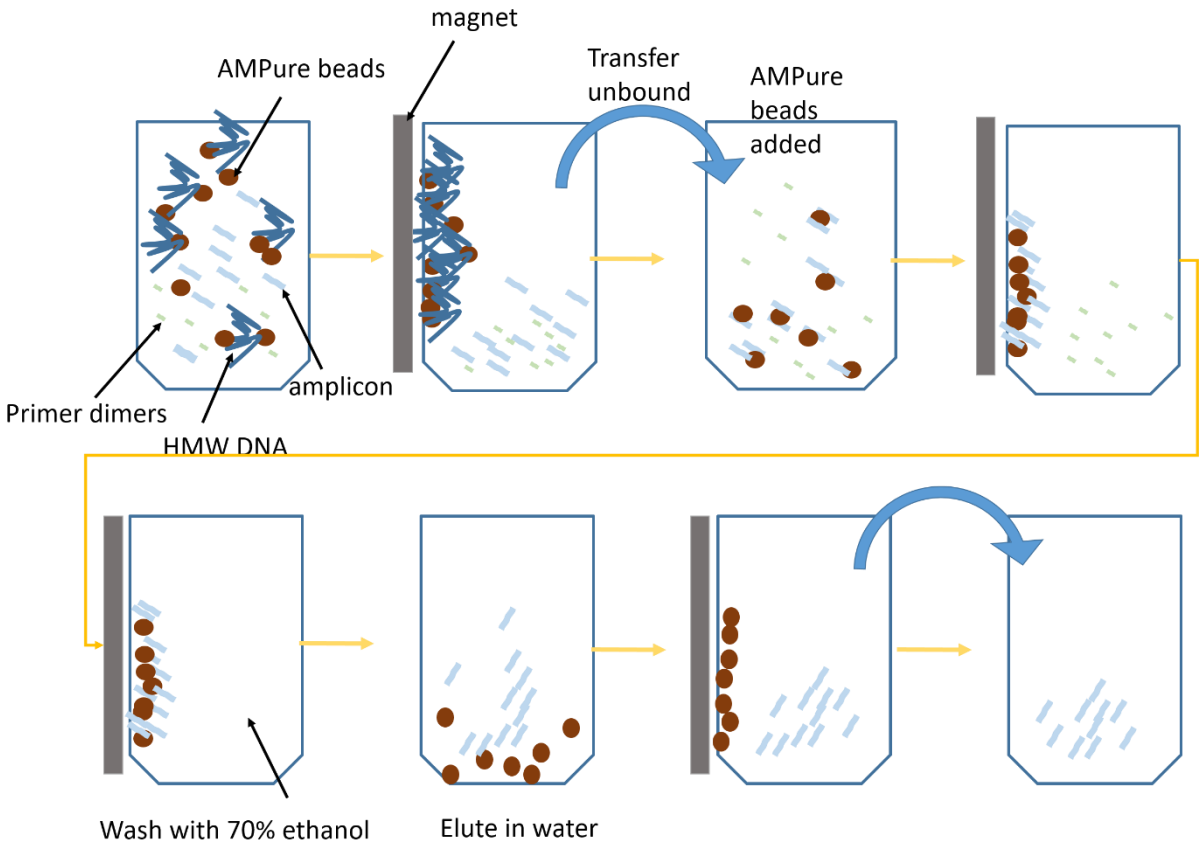

Figure 5.17 Dual step PCR clean up with AMPure beads. A lower ratio of AMPure beads were mixed with PCR product. The beads bind the high molecular weight DNA. A magnet is used to draw the beads (and bound DNA) to the side. The supernatant contusing PCR amplicons is transferred to a new tube. A greater ratio of AMPure beads are then mixed with the PCR products. The amplicons bind to the beads. A magnet is used to draw beads (and amplicons) to one side. The supernatant containing primers is removed. The beads are washed with 70% ethanol. The tube is removed from the magnet and amplicons eluted into water. A magnet is again used to draw beads to the side. The supernatant containing eluted amplicons is moved to a clean tube for storage.

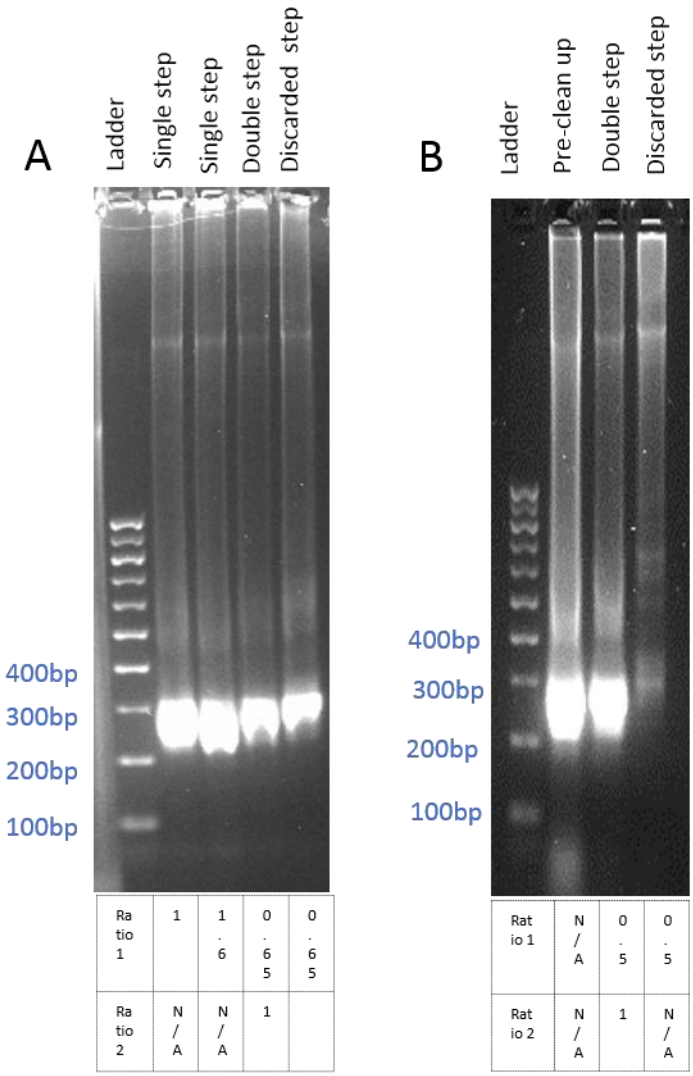

Figure 5.18 PCR products after different methods of AMPure bead based clean up. Single step PCR clean with a 1:1 and 1:1.6 ratio of PCR product to beads, and a 2-step clean up at ratios of 1:0.6 and 1:1 and discarded first step from 2-step clean up (a), compared to original PCR product, a 2 step clean up at 1:0.5 and then 1:1 and the first discarded step from this (b)

The single step PCRs were consistent with that seen in figure 5. 16.The 2-step clean up reduced the amount of high molecular weight genomic DNA. The 2-step clean up with a first ratio of 0.65:1 drastically reduced the yield as shown by a smaller amount amplicon and is confirmed by the presence of amplicon in the fraction to be discarded. Conversely the 2-step PCR starting with a 0.5:1 ratio reduced the yield of amplicon minimally and still removed genomic DNA. A 2 step PCR clean up using a 0.5:1 ratio followed by a 1:1 ratio was selected.

5.6.3 Post clean-up assessment of purity and concertation of samples

After PCR product had been purified, it was important to check primer dimer had been successfully removed and there were not large amounts of HMW DNA present, as these could adversely affect the sequencing process. In the first instance agarose gel electrophoresis was used, once confident with the results on the gel a bioanalyzer machine was used.

5.6.3.1 Agarose gel electrophoresis

As a first port of call, each sample was checked using agarose gel electrophoresis, as previously described. In figure 5.19 cleaned PCR products of 10 different samples are run on a 1% agarose gel. Amplicons are present in all samples, although the quantity of amplicon does vary per sample. There are some additional bands present above the amplicon for some samples and some high molecular weight DNA. These samples were further analysed by a more sensitive method using a Bioanalyzer.

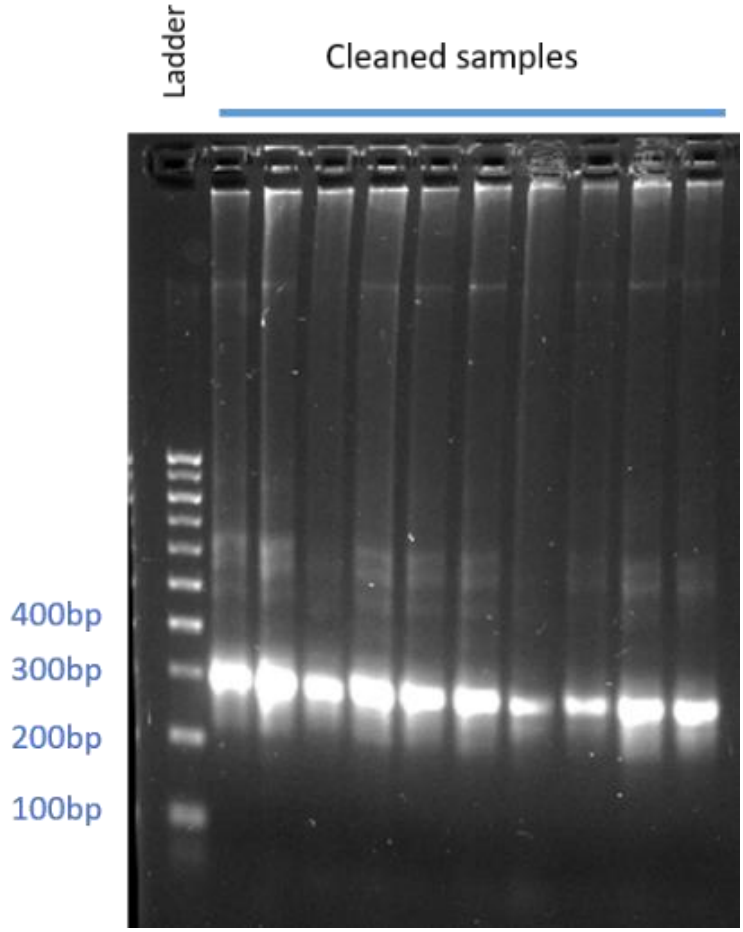

Figure 5.19 Example of 10 samples post clean up. PCR products from every sample underwent a 2-step PCR clean up. 4ul of the clean PCR product was mixed with 1µl of 5x loading buffer and run on a 1% Agarose gel with a 100bp Sigma ladder. Images of gels were checked for presence of amplicon, absence of primer dimer and low amounts of HMW products.

5.6.3.2 *Bioanalyzer method*

A DNA 1000 kit and Bioanalyzer (Aiglent) were used to assess the purity of PCR samples. A gel-dye mix is prepared by adding 25µl of dye concentrate to gel matrix, vortexing and filtering using a spin filter step (2240g for 15minutes). A chip is placed on a chip priming station. 9.0µl of gel-dye matrix is added to the marked well (indicated in figure 5.19). The gel-matrix is then put under pressure using the priming station. Further gel-dye matrix is added to other marked wells. 5µl of DNA marker is added to each sample well and the ladder well. 1µl of ladder is added to the ladder well. 1µl of sample is added to each sample well, with up to 12 samples being run on a single chip. The chip is placed in a vortex for 60seconds at 2400rpm. After cleaning the electrodes of the Bioanalyzer, the chip is inserted into the Bioanalyzer, the correct assay selected, and the run initiated. For each sample run a trace is produced, an example of which is given in figure 5.20.

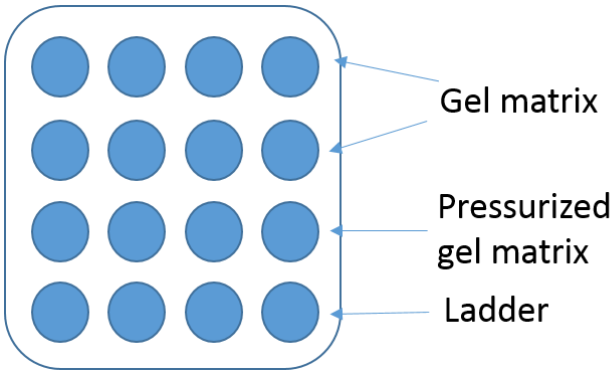

Figure 5.20 Bioanalyzer chip layout. Marked are the wells where gel matrix and DNA ladder are added. The remaining wells contain sample and DNA marker.

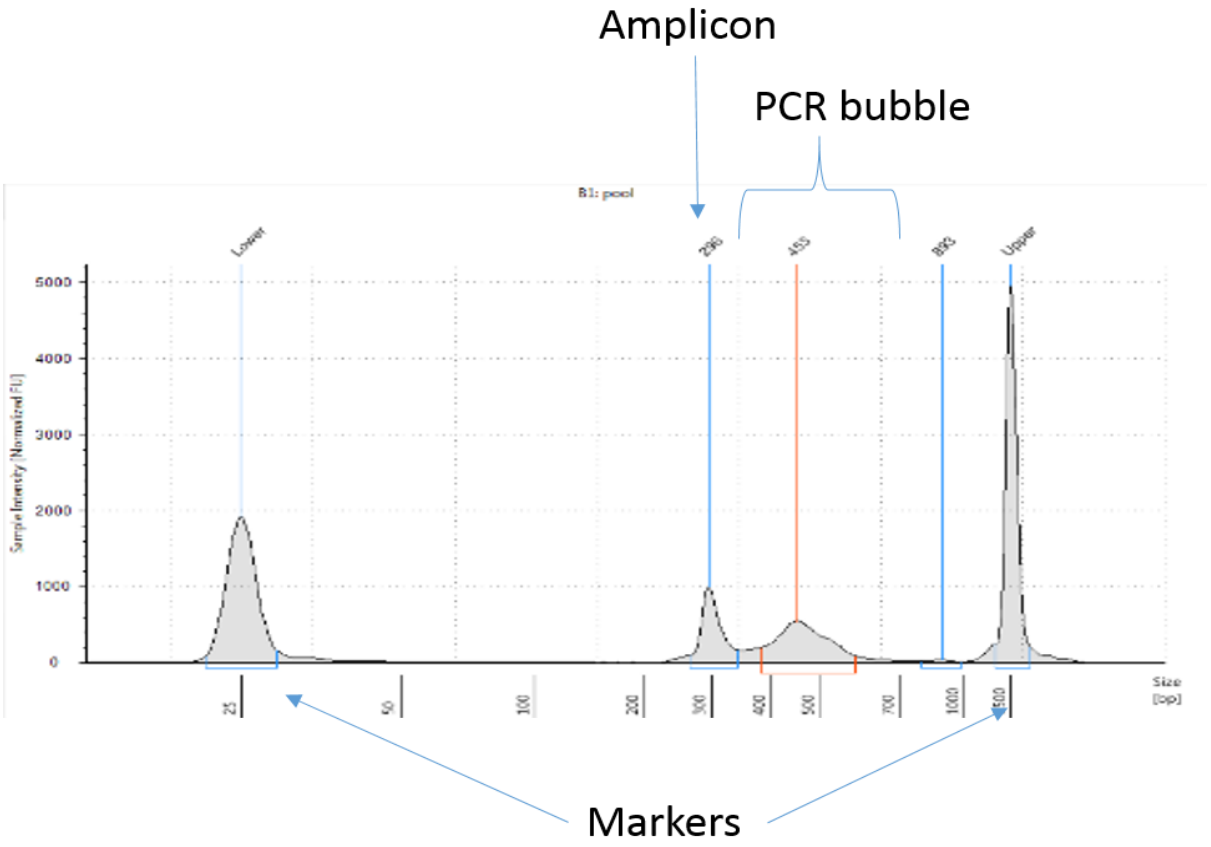

Figure 5.21 Bioanazlyer trace of pooled samples. Marked are where the upper and lower bioanalyzer marker peaks are located, along with the amplicon peak and additional peak which is believed to be PCR bubble

There is a clear peak at the predicted amplicon size, however the secondary band that is sometimes visible in some samples by agarose gel electrophoresis was far more prominent when viewed by Bioanalyzer trace (figure 5.21). Since this peak is not observed in any control run on agarose gel or Bioanalyzer, I suspect this to be associated with amplification of the correct region. Given the slower movement through the gel giving a predicted size much larger than the amplicon, is consistent with this fragment being PCR bubble. A PCR bubble is generated when two non-complementary fragments anneal at the ends where there are complementary adapters. Due to differences in the sequences in the middle, these do not anneal and sections bugle out, creating a bubble effect of partly single stranded and partly double stranded DNA. Since the Illumina sequencing process separates annealed fragments into single strands, this should not adversely affect the sequencing process.

1.1.1.1 Sanger sequencing of amplicons

To confirm the amplicon produced at ~290 base pairs indeed contained guide containing region from lentiv2 vector amplification, Sanger sequencing of the amplicon was performed. Additionally, sequencing was performed on the additional band ~400bp that is sometimes visible to ascertain if this is lentiv2 amplicon retarded by being part of a PCR bubble or some form of unspecific amplification. A PCR reaction to amplify the guide containing region was performed as previously described. The PCR products were run on a 2% gel. The amplicon containing band was cut from the gel and the region of around 400 base pairs where a faint additional band was present was also excised. DNA was extracted from both using the Monarch gel purification kit. Both samples were sent for Sanger sequencing using a primer targeting the same sequence as the P7 primer.

Figure 5.22 Sanger sequencing of PCR generated amplicons Amplicons were extracted from a gel at approximately 290 base pairs and 400base pairs. Electropherogram of two PCR products excised at 190bp and 400bp from an agarose gel, after PCR amplification of Brunello library containing HPB-ALL cells. Sanger sequencing was performed using a primer against the reverse priming site. The schematic above indicates the regions expected in an amplicon with the segment in green representing what is visible in the elctropherogram.

Sanger sequencing (figure 5.22) confirms both bands to contain sequences consistent with amplification of lentiv2 vector and suggest that the additional 400bp peak is indeed PCR bubble not unspecific amplification.

5.7 **Final PCR clean up method**

PCR reactions were pooled and mixed. 300µl of PCR product was taken for each sample (note for individually barcoded bone marrow compartments this was reduced but the ratios were maintained). The 300µl of PCR product was mixed with 150µl of AMPure beads. After a 5-minute incubation the tube was transferred to a magnet. After 5 minutes the solution was transferred to a fresh tube leaving behind the beads with HMW DNA attached. 300µl of beads were then added to the transferred PCR product. After 5 minutes incubation, the tube was placed in a magnet for 5 minutes. The solution containing primer dimers was discarded, the beads were then washed twice with 70% ethanol. The tube was removed from the magnet. 100µl of water was added to the beads to elute the amplicons. The tube was then placed back on the magnet to bind the beads. The eluted amplicons were then transferred to a fresh tube leaving the beads behind. For samples with low amounts of PCR product, volumes were lowered accordingly. Where amplicon yield was low, elution volume was reduced.

5.7.1.1 Assessment of concentration using Qubit® 3.0 fluorometer

A Qubit® dsDNA high sensitivity kit was used with a Qubit® 3.0 fluorometer. The assay is highly selective for double stranded DNA. Assay reagent is prepared by diluting Qubit® HS reagent 1 in 200 in Qubit® working solution. 199µl of assay reagent is mixed with 1µl of cleaned PCR product in a thin walled clear 0.5ml PCR tube. After brief vortex, samples were incubated for 2minutes. The fluorometer was calibrated using standards prepared at the same time as samples (10µl of each standard in 190µl of assay reagent) and then each sample is measured in turn. I recorded the original concentrations of each PCR product. If samples were outside the linear range, they were diluted, and the assay repeated.

5.8 **Performing the screen with optimised methods**

The screen itself can be broadly broken into two categories, the running of the screen including everything from introduction of the library through to harvest of cells, and then the processing of samples. The later stage representing DNA extraction, PCR amplification, PCR clean-up and sequencing.

5.8.1 Transduction, selection, culture and harvest of cells

This section focuses on the stages between transduction up until harvest of samples. Figure 5.23 summarises from transduction of HPB-ALL cells through to separation of cells into screening arms. It describes the steps until the setup of 4 arms of screening at Day 0 from transduction of HPB-ALL with the Brunello library 16 days prior.

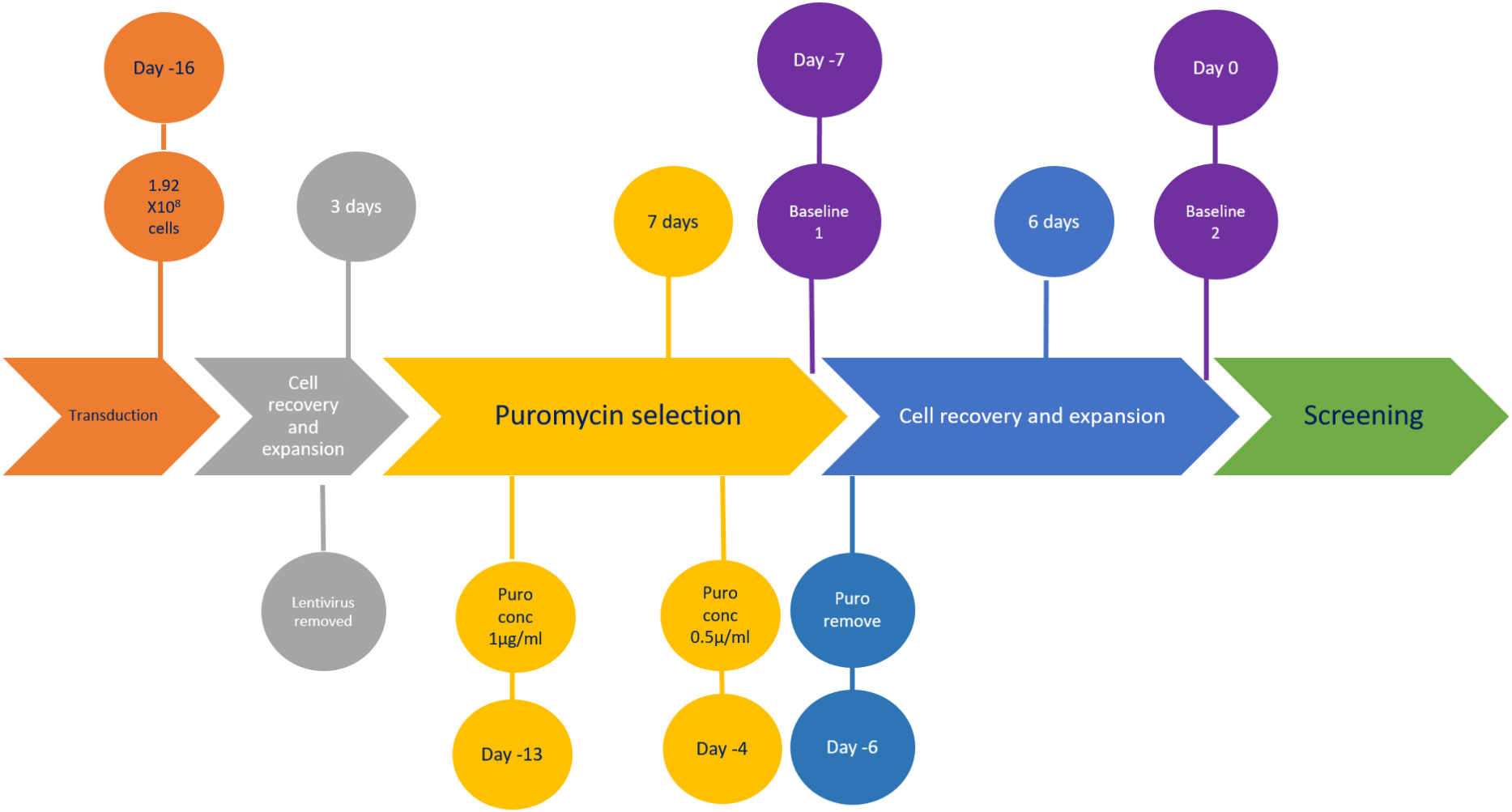

Figure 5.23 Timeline overview from transduction of cells up until separation into 4 different arms. At day 0. 16 days prior to the setup of screening arms, HPB-ALL cells were transduced with Brunello virus, cells were left to recover from transduction before being placed under puromycin selection for 7 days. Cells were then given a period of recovery and expansion to get adequate numbers of healthy cells to commence screening.

5.8.1.1 Transduction

Brunello virus containing tubes from both harvests (48h and 72h) were removed from -80°C storage, thawed and mixed so that the virus would be the same in each tube. Flasks of HPB-ALL cells were pooled and counted, 8 tubes each containing 24 million cells were centrifuged at 350g for 5 minutes to pellet the cells. Media was removed from the cells and each cell pellet was re-suspended in 24 ml of Brunello virus, so that the cells were at a density of $1x10^6$/ml. 24µl of 8mg/ml polybrene was added to each tube to a final concentration of 8µg/ml. Cells suspended in lentivirus were then distributed into 24 well plates (1ml per well). Plates were sealed with parafilm before placing them in a centrifuge for spinfection. The spinfection conditions were 900g for 50minutes at 34°C. After spinfection, parafilm was removed from the plates before placing them into the incubator overnight. The following morning 700µl of virus and polybrene containing media was removed from each well being careful not to disturb the cells. Cells were transferred to a 12 well plate and 1.5ml of fresh RPMI-10%FBS was added.

5.8.1.2 Puromycin selection

HPB-ALL cells transduced with Brunello library were selected with 1ug/ml of puromycin. During puromycin selection transduction efficiency was confirmed by cell counting and visual inspection under the microscope (figure 5.6) and further qualified by mRNA expression of Cas9.

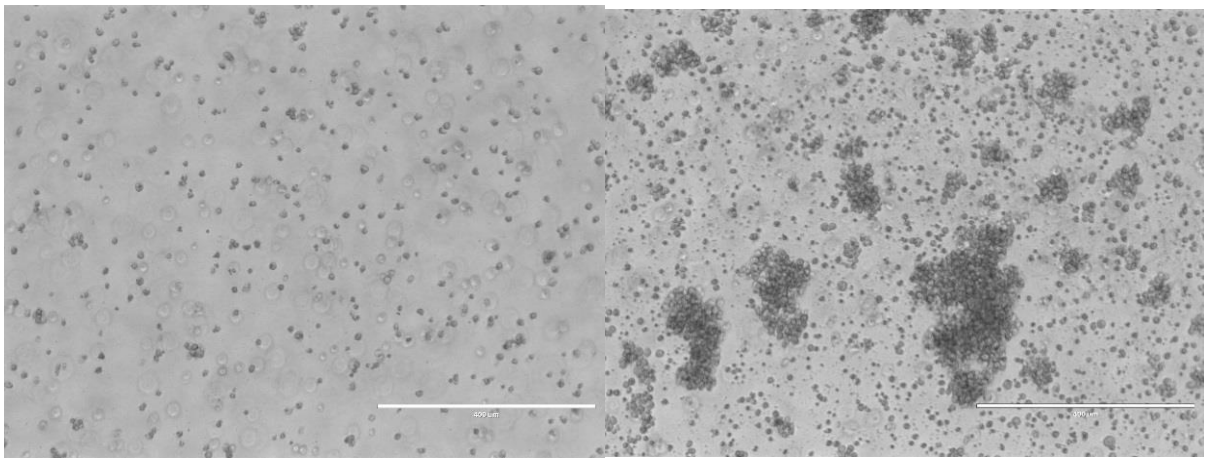

Figure 5.24 Image of puromycin treated HPB-ALL cells.HPB-ALL transduced Brunello library (right) and mock transduced (left) treated with puromycin for 6 days. Imaged with a 10x objective lens.

The transduced HPB-ALL possess resistance to puromycin. Examining the cells in the puromycin containing media under the microscope, it was possible to see a difference in cell viability and number between HPB-ALL cells with Brunello virus compared to mock transduced cells (figure 5.24). There were far more clumps of evenly shaped rounded cells in the right-hand side picture showing Brunello transduced, compared to a few cells of varying shapes and sizes in the left-hand side mock transduced cells. This difference was consistent with trypan blue counting, which gave a transduction efficiency of 53 %.

5.8.1.3 Harvest of baseline samples

Two baseline samples were harvested; the first during puromycin selection on day -7, so that the representation of the library going into the screen was known and a second prior to the separation of transduced cells into the arms for screening on day 0, so that we could account for any *in vitro* changes occurring prior to *in vivo* screening taking place. Cells were mixed and counted. 35 million cells were washed twice with PBS and frozen as a cell pellet until genomic DNA extraction.

5.8.1.4 In vitro screening

Cell counts were performed every 2-3 days, cells were maintained at a density of $0.5x10^6$cells/ml to 1.5 $x10^6$/ml, with media replenished as necessary. Drug treated cells were counted and seeded at a density of $1x10^6$/ml. A combination of dexamethasone, vincristine, daunorubicin and asparaginase was applied to drug treated arm for 72 hours at a time in the concentrations as follows: dex 50nM, dauno

33nM, vinc 1nM , asp 0.36mU/ml (as determined by work outlined in Chapter 3). After 72 hours cells were pelleted, washed with PBS and re-suspended in fresh media to remove the drugs. Cells were grown without drugs for 7-9 days to allow recovery before addition of the drug combination at the same concentrations as listed previously. This drug pulsing was performed throughout. Proliferation of the cells during *in vitro* screening is shown against time in figure 5.25

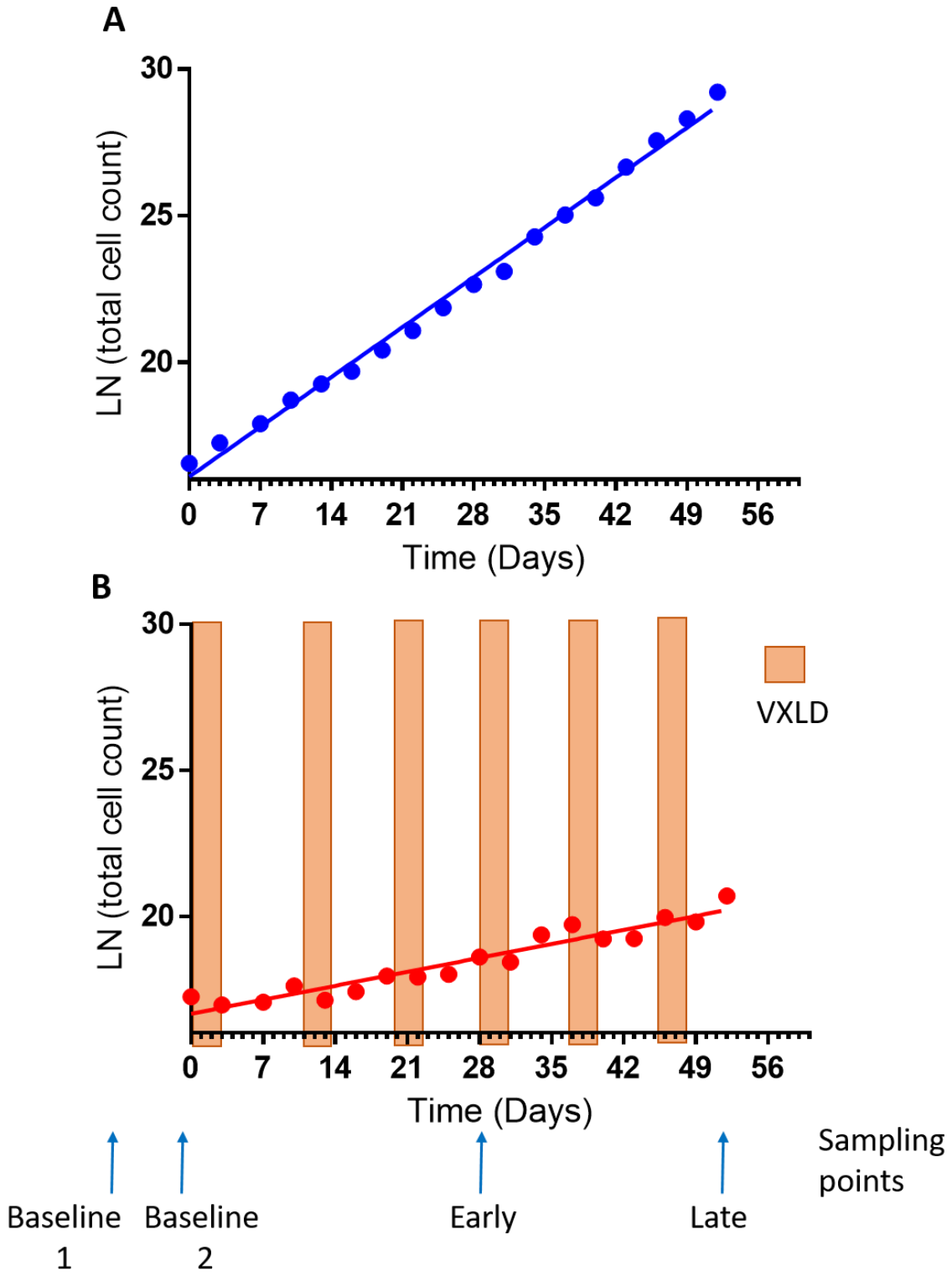

Figure 5.25 Proliferation of HPB-ALL during screening. Proliferation curves for in vitro screening control conditions (a) and VXLD treated conditions (b) Orange bars indicate when cells were exposed to VXLD. Blue arrows indicate sampling points for baseline samples (baseline 1 -during selection of transduced cells and 2 at the start of screening) and the two points at which in vitro samples were harvested (early and late)

Two time points were taken for each *in vitro* arm; an early time point at day 28 and a later time point at day 52 equivalent to 9 and 18 cell doublings in the control arm respectively. At each time point cells were pooled and counted. 35 million viable cells were washed twice in PBS and pelleted. Cell pellets were stored at -20°C until genomic DNA extraction.

5.8.1.5 In vivo screening

HPB-ALL-Brunello cells were counted, washed and re-suspended in media prior to injection into mice. 2 million cells were injected in a 30µl volume per mouse via intra-femoral route (refer to 2.19 for detailed method). In total 30 mice were injected. Mice ears were notched to identify each mouse.

Mice were examined and weighed at least 5 times weekly, to ensure weight loss did not exceed 15% of initial starting weight for more than 3 days or reach 20%, which would require humane killing. Mice were monitored for signs of leukaemic engraftment previously observed with this cell line including paleness of ears, hind limb weakness, change in gait, piloerection and growth of leg tumours. Mice displaying clinical endpoints as defined by the project licence protocol were humanely killed by schedule 1 methods.

Cages of mice were randomised to receive either VXLD treatment or vehicle control injections. Cages were not mixed for VXLD and control since drugs can be present within excrement that may be consumed by other mice. Mice received a total of 3 blocks of 5 days treatment. The first block was initiated 3 days post injection. The second block followed 2 days after the first, and the final block was given 9 days after the second. This treatment regimen was established previously in chapter 4.

As established in chapter 4, HPB-ALL cells predominantly engraft within the bone marrow of mice. It has previously been reported that ALL cells can engraft clonally within different bone marrow compartments (Belderbos *et al*.., 2017) .Therefore in 10 mice (5 treated , 5 non treated) individual bone marrow compartments (shown in figure 5.26) were harvested and stored separately so they could be barcoded differently during PCR and analysed separately to see if any differences in target enrichment between compartments could be identified. Table 5.3 shows the summary of the *in vivo* harvested samples.

Cage	mouse	Vxld y/n	Injected leg	Days from IF injection	ID	Sample
185	LN	N	R	28	1	T
185	RN	N	R	28	2	T
185	BN	N	R	27	3	A-E, spleen
185	NN	N	R	28	4	T
2606	LN	N	L	27	5	A-E
2606	RN	N	R	27	6	T
2606	BN	N	R	27	7	A-E
2606	NN	N	R	27	8	T, tumour
4486	LN	N	R	28	9	T
4486	RN	N	R	27	10	A-E, tumour
4486	NN	N	L	28	11	T
1469	LN	N	L	28	12	T
1469	RN	N	L	28	13	T
1469	NN	N	L	28	14	T
13396	LN	N	L	27	15	A-E
13478	LN	Y	R	42	16	T
13478	RN	Y	R	39	17	A-E, spleen
13478	NN	y	R	45	18	A-E
3033	LN	Y	R	45	19	A-E, spleen
3033	RN	Y	R	42	20	T
3033	BN	Y	R	43	21	A-E, spleen
3033	NN	Y	R	45	22	T
3269	LN	Y	R	41	23	T
3269	RN	Y	L	39	24	T
3269	BN	Y	R	41	25	A-E, spleen
3269	NN	Y	R	45	26	T
3269	2LN	Y	R	39	27	T
2250	LN	Y	L	45	28	T
2250	RN	Y	L	45	29	T
2250	NN	Y	R	45	30	T

Table 5.3. Mouse harvest details. Harvest details from all mice used for *in vivo* screening, indicating the cage code and mouse ear notches (left notch LN, right notch RN, both notch-BN and no notches NN)) which leg was injected left(l) or right (r) the number of days between injection of cells and harvest, and what samples were collected (T – total bone marrow , A-E individual compartments, spleen and tumours where present) .

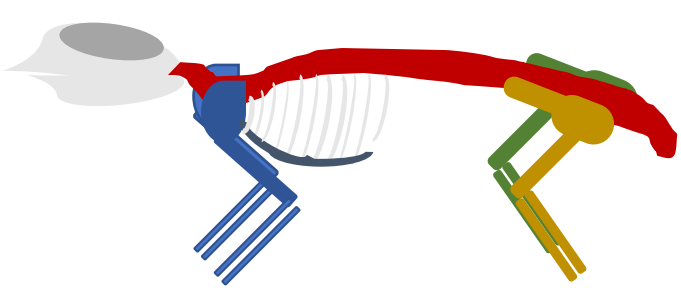

A injected hind limb

B contralateral hind limb

C forelimbs and sternum

D spine

E calvaria

Figure 5.26 Bone marrow harvest locations for mice from Brunello screening. Bone marrow was harvested from 5 different locations, the injected hind limb (A), the contralateral hind limb (B) , the forelimbs and sternum (C), the spine (D) and the calvaria (E). Bone marrow samples from each of these 5 compartments were pooled for 20 mice and stored separately for the remaining 10.

5.8.2 Genomic DNA extraction, PCR amplification, PCR-clean up and sequencing of screen samples

After the bulk of the screening had finished, harvested samples required processing in order to prepare for sequencing. The first stage of which requires extraction of genomic DNA from the samples. The *in vitro* samples provided an average of approximately 450ng of DNA. The *in vivo* samples were far more variable (table 5.3), this could be attributed to differences in engraftment in the mice and also the differing quality and purity of harvested samples. DNA extraction provide adequate clean DNA in all except 5 mouse samples 15D, 4T, 26T and 27T. Some samples had lower than expected DNA quantity (based on harvested cell numbers) and these are highlighted in yellow in the table 5.4.

ID	elute volume	concentration (ng/ul)	total DNA (ug)	1.7 < 260/280 < 2.0
1T	1800	573.9	1033.02	y
2T	1800	529.3	952.74	y
3A	350	276.4	96.74	y
3B	350	404.5	141.575	y
3C	260	138.9	36.114	y
3D	180	74.4	13.392	y
3E	700	368.8	258.16	y
4T	2200	69.8	153.56	n
5A	350	328.2	114.87	y
5B	300	189.2	56.76	y
5C	250	184.8	46.2	y
5D	190	178.2	33.858	y
5E	750	348.5	261.375	y
6T	1800	155.3	279.54	y
7A	350	192.8	67.48	y
7B	350	264.3	92.505	y
7C	260	57.3	14.898	y
7D	180	841.1	151.398	y
7E	700	177	123.9	y
8T	1800	544.1	979.38	y
9T	1800	108.3	194.94	y
10A	350	123.5	43.225	y
10B	300	251.4	75.42	y
10C	270	163.7	44.199	y
10D	190	159.7	30.343	y
10E	700	393.5	275.45	y
11T	1800	167.5	301.5	Y
12T	1800	337.3	607.14	Y
13T	2200	98.5	216.7	y
14T	1800	92.9	167.22	y
15A	700	351.9	246.33	y
15B	700	239	167.3	y
15C	700	216	151.2	y
15D	350	17.9	6.265	y
15E	700	187.8	131.46	y
16T	2400	295.8	709.92	y
17A	350	336.1	117.635	y

17B	350	332.5	116.375	y
17C	270	410.6	110.862	y
17D	180	109.7	19.746	y
17E	700	737.1	515.97	y
18A	700	295.9	207.13	y
18B	350	331.1	115.885	y
18C	270	216.7	58.509	y
18D	190	56.7	10.773	n
18E	1400	455.2	637.28	y
19A	750	86.7	65.025	y
19B	750	253.8	190.35	y
19C	270	205.9	55.593	y
19D	270	101.2	27.324	y
19E	350	321.7	112.595	y
20T	1800	289.8	521.64	y
21A	190	333.1	63.289	y
21B	190	271.5	51.585	y
21C	190	104.5	19.855	y
21D	190	114.9	21.831	y
21E	190	238.2	45.258	y
22T	1800	168.2	302.76	y
23T	2200	60.1	132.22	y
24T	1800	152.7	274.86	y
25A	350	220	77	y
25B	370	171.2	63.344	y
25C	370	79.3	29.341	y
25D	190	51.2	9.728	y
25E	700	318	222.6	y
26T	2200	81.4	179.08	n
27T	800	17.6	14.08	n
28T	1800	282.1	507.78	y
29T	1800	213.2	383.76	y
30T	1800	315.9	568.62	y

Table 5.4. Summary of mouse samples extracted from *in vivo* CRISPR screening mice. Mice are labelled 1 through 30 with 1 through 15 receiving no chemotherapy and 16-30 received VXLD. T= total pooled bone marrow was collected. A-E indicate specific bone marrow compartments. Elute volume, concentration (as determined by nanodrop) and total DNA quantity is indicated. IF 260/280 values did not lie between 1.7 and 2.0 this is also indicated y=yes lies within range n= not within range. Very low concentrations and poor DNA quality are indicated by red shading, lower than expected DNA quantities are indicated by yellow.

Samples were amplified by single step PCR using the protocol described earlier. For total pooled bone marrow, a total of 400µg of genomic DNA or all available DNA (whichever higher) were input into PCR reactions, with a maximum of 10µg per reaction. For compartments A, B, C, D and E: 70, 70, 60, 30 and 170µg were used respectively (giving a total of 400µg), different quantities per compartment reflect relative compartment size and cell numbers obtained (Shaposhnikov, 1979).

5.8.2.1 Mixing of samples

Individually barcoded samples were diluted to a concentration of 50nM based on concentration obtained from Qubit® data. In the first instance, amplicons from tissue culture samples and mice where all bone marrow was pooled were sequenced as listed in table 5.5 below. Two mouse samples failed to amplify, and these were omitted. In total 2 baseline samples, 4 in vitro samples (2 treated, 2 untreated), 9 untreated mouse samples and 9 treated mouse samples were sent for sequencing alongside two additional samples for another project. All samples were combined in even ratios. Samples were sent to the Genomics core facility at Newcastle University. Note that individual bone marrow compartment samples were sent in a separate batch and are not discussed in the results chapters for this thesis.

Sample	Details	Barcoded primer code	barcode associated with primer
Baseline 1	first baseline	A1	TTGAACCG
Baseline 2	second baseline	A2	AATCCAGC
control1	untreated timepoint 1	A3	CCGAGTTA
vxld1	VXLD timepoint 1	A4	AACTGTTA
control2	untreated timepoint 2	A6	TTCTCAGC
vxld2	VXLD timepoint 2	A7	CCTCCAAT
1T	Mouse sample	A9	GGTCACCG
2T	Mouse sample	B1	AATCCAAT
6T	Mouse sample	B2	CCGAGTAT
8T	Mouse sample	B3	TTCTCATA
11T	Mouse sample	B4	AACTGTGC
12T	Mouse sample	B5	AATCCACG
9T	Mouse sample	A10	CCTCTGTA
13T	Mouse sample	F7	GGCTTGGC
14T	Mouse sample	F8	GGAGGTGC
16T	VXLD mouse sample	B6	TTCTACTA
20T	VXLD mouse sample	B7	AATCGTGC
22T	VXLD mouse sample	B8	GGCTACCG
24T	VXLD mouse sample	B9	AAGAACTA
28T	VXLD mouse sample	A11	TTGACAAT
30T	VXLD mouse sample	A12	AAGACATA
29T	VXLD mouse sample	B10	AACTTGTA
23T	VXLD mouse sample	F9	CCAGGTGC
26T	VXLD mouse sample	F10	GGTCTGGC

Table 5.5 Sequencing pool summary. Each sample was added to the pool in even quantities. Each sample had genomic DNA extracted, PCR was used to amplify guide containing regions for sequencing, and each sample was given a unique barcode sequence by use of barcoded primers. PCR products were then cleaned, and the DNA concentration measured. Even quantities of each sample were then mixed prior to sending for sequencing.

5.8.2.2 Sequencing details

Sequencing was performed by Jonathon Coxhead and colleagues at the Genomics Core Facility (Centre for Life, Newcastle upon Tyne). The sequencing quality and barcode distribution was checked by running a single MiSeq lane; this confirmed sequencing quality and barcode distribution to be good. Higher depth sequencing was then performed. Pooled samples were loaded onto 2 NextSeq flow cells each with 400 million 50 base pair single ended reads.

5.9 **Bioinformatics pipeline for results analysis**

The Model-based Analysis of Genome-wide CRISPR/Cas9 Knockout (MAGeCK) tool and the newly published (March 2019) MAGeCKFlute - an additional tool in CRISPR analysis – were applied. MAGeCK has an algorithm designed to identify positively and negatively selected sgRNAs. The process is described in materials and methods section 2.30.

5.10 Chapter discussion

This chapter has summarised the CRISPR screening specific methods, their development and how they were employed in the final screen.

5.10.1 Introduction of library to cells via lentivirus

The Brunello library was successful introduced into the T-ALL cell line HPB-ALL, this was confirmed by survival of cells with puromycin selection and by real time PCR quantification of Cas9 expression. Transduction efficiency was 53% which was higher than anticipated by prior optimisation work. Although the transduction efficiency exceeded the 30% to ensure single guide integration per cell, it was decided this was unlikely to adversely affect the screen, given the large number of cells transduced, high coverage and multiple guides per gene a small number of multiple integrations should not adversely affect the screen.

5.10.2 Preparation of material for sequencing

An extraction processes using the Qiagen blood maxi columns was adapted for extraction of DNA from large quantities of cells harvested from murine bone marrow. This process was employed to successfully harvest material from 28 mice and 6 *in vitro* samples. A PCR protocol available through the GPP web portal maintained by the Broad Institute was validated for use in amplification of my samples. Alterations to the PCR conditions did not improve the amplicon production, and the protocol was followed, which allowed for amplification of 10µg of DNA in a single reaction and addition of required adapters for Illumina sequencing all in a single step PCR. Amplification was successful in 70 out of 74 samples, with 4 samples requiring repetition of the PCR.

5.11 Chapter summary

This chapter describes the final stages but critical parts of the CRISPR screen.

All the specific requirements outlined in the introduction were met:

- Lentivirus generation and introduction into T-ALL cells was optimised
- A Broad Institute protocol was tested and adapted for the amplification of the guide containing region and barcode samples
- A 2-step bead-based strategy was devised to clean-up of PCR products

These steps ensured a successfully process from introduction of library into HPB-ALL through to the final sequencing samples.

Chapter 6. Screen results

6.1 Introduction

The aim of this chapter was:

- Identify genes that confer sensitivity or resistance to VXLD chemotherapy.

Prior to using the generated screening data to identify genes associated with treatment it was important to check that the data generated from screening was of good quality with good library coverage.

After checking the coverage and distribution of guides present in screening samples data was processed using a bioinformatics pipeline- MAGeCKFlute. MAGeCKFlute was designed to identify differential effect of two screening conditions, in the case of this project it was used to identify guides which were differentially enriched or differentially depleted in VXLD treated arms compared to the control arms. First a single score (beta score) was generated using a maximum likelihood estimate (MLE) analysis of the score from the count of each individual guide compared to the baseline (figure 6.1). Then beta scores between treatment conditions were compared to identify genes with guides that were enriched preferentially by VXLD treatment, and genes with guides that are differentially depleted (figure 6.2). Note the Beta score gives a gene level score based on how the 4 guides change, where negative beta scores reflects where guides are lost (depleted) compared to the baseline, and positive scores where guides are increased (enriched) compared to baseline. For simplicity I will use enrichment and depletion of guides -this refers to the gene level beta score. Genes with differentially enriched and differentially depleted guides were identified from both *in vitro* and *in vivo* screens. Overlap between guides identified through *in vitro* screening and *in vivo* screening was then analysed. Figure 6.3 Summarises the different data obtained and presented along with the relevant chapter section.

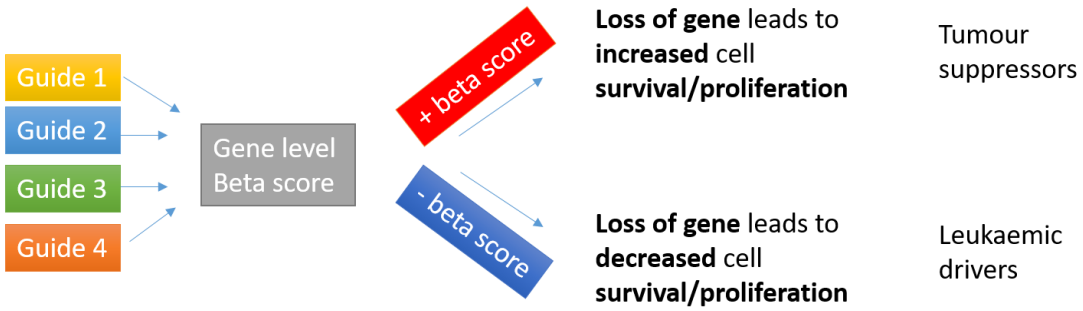

Figure 6.1 Relationship between guides, beta scores and the effect on cells. MAGEcK-MLE can be used to generate a single beta score from the different guides targeting a gene. The beta score is a measure of change from the baseline, where positive beta scores represent overall increase in guides during treatment. Positive beta scores indicate the number of cells with the guides are increased compared to the baseline, this means that knockout of this gene is providing a benefit to the cells. Genes with a tumour suppressive effect will fall into this category. Negative beta scores indicate the number of cells with these guides are reduced compared to the baseline, this means that knockout of this gene has a negative impact on the cells- including genes that function as leukaemic drivers.

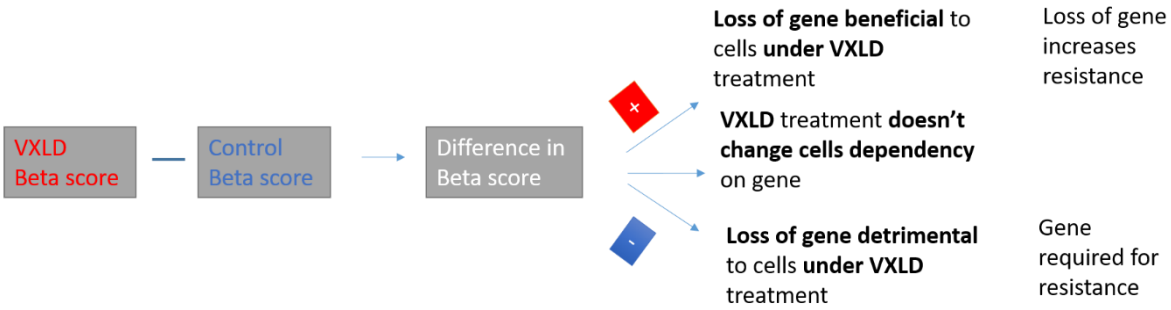

Figure 6.2 Explanation of differential enrichment/depletion After obtaining beta scores for each screening arm, these can be compared to see how guide presentation changes with VXLD treatment. Where beta scores are higher under VXLD treatment it indicates that loss of the gene is beneficial to cells surviving drug treatment. Where treated and control arm beta scores are similar there is no change to the cell's dependency on that gene when under treatment, benefit or detrimental effects of gene loss in this case are not related to treatment. Where the beta score is lower with VXLD treatment compared to control it is indicative of the gene being required for resistance to therapy, and therefore when this gene is knocked out cells do not survive, leading to less guides present after screening.

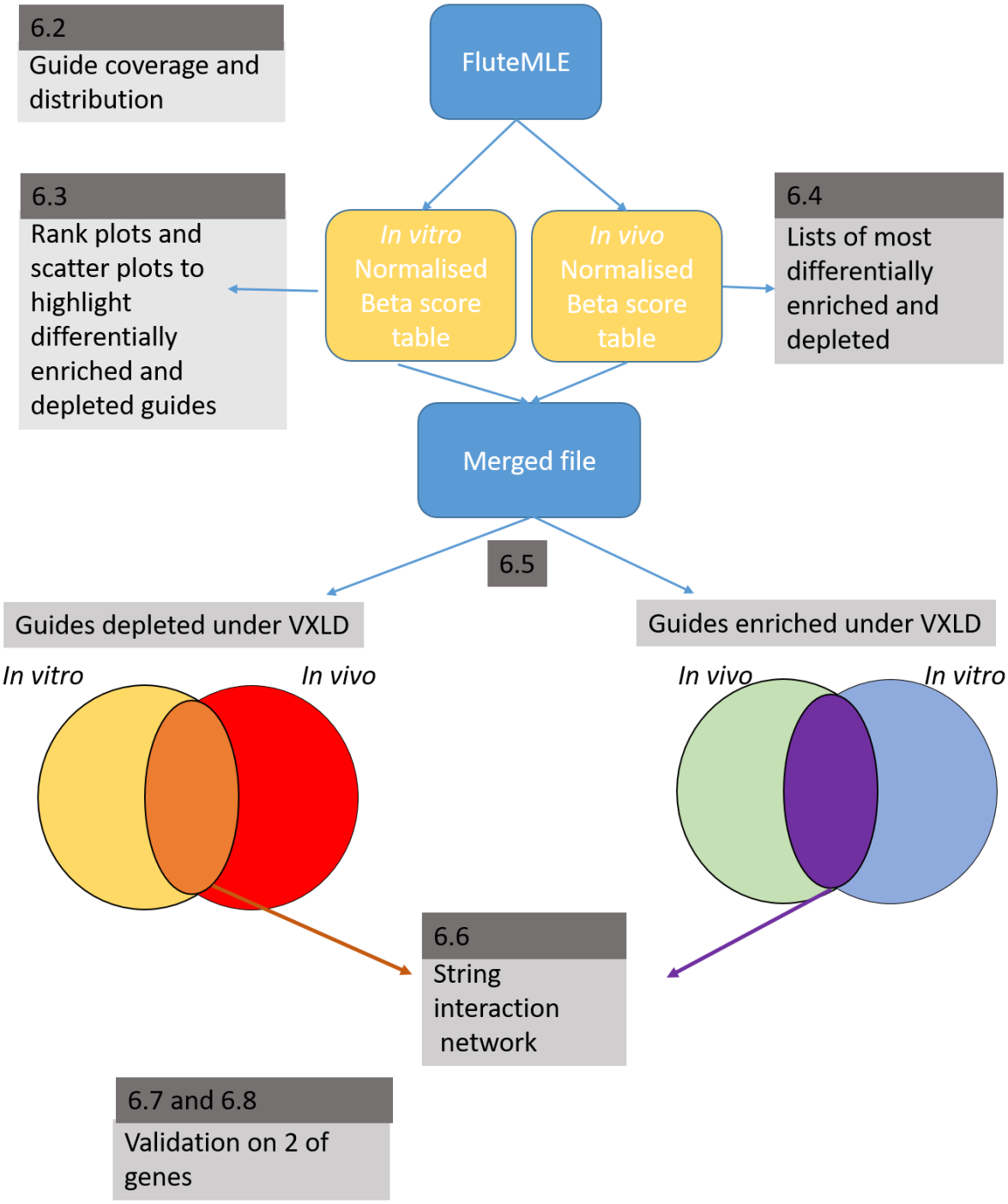

Figure 6.3 **Screen results chapter summary.** After read counts are generated the data is checked for guide distribution and coverage (presented in chapter 6.2) prior to downstream analysis. Results from differential enrichment and depletion analysis for *in vitro* screening are given in chapter 6.3 and for *in vivo* screening in chapter 6.4. These lists were then compared for overlap between in vitro and in vivo with results shown in 6.5. Further analysis was then performed hits identified both in vitro and in vivo (chapter 6.6) and lastly two targets found depleted in both *in vitro* and *in vivo* screening are taken for validation in chapters 6.7 and 6.8.

6.2 Quality control and processing of screening data

6.2.1 Guide coverage

Read count tables were interrogated to establish the total number of guides present in each sample and the average read count per guide to gauge library coverage (figure 6.4 and 6.6).

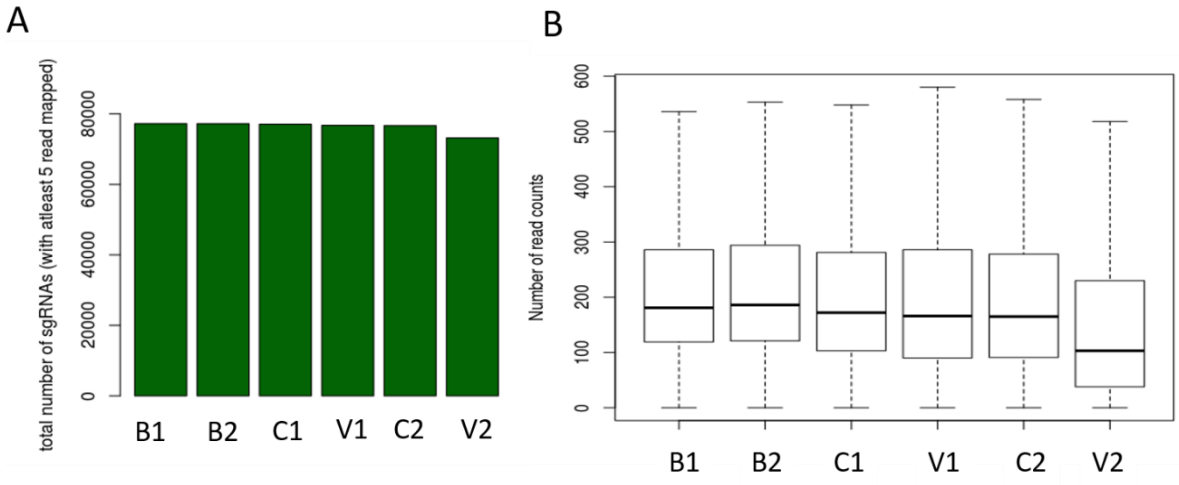

Figure 6.4 Quality control for in vitro samples. Number of guides with at least 5 reads mapped for each in vitro sample (a) and boxplot of read counts for each in vitro sample (b). Baseline samples (B1 and B2), control screening samples for both first time point (C1) and second later time point (C2) are shown alongside VXLD treated samples (V1 and V2)

The first baseline had the highest number of guides (read count >= 5) at 77,237 representing 99.7% of the total library. The lowest number of guides was seen in the latest VXLD treated time point at 73,191 which still represent 94.5% of the total library. The median read count per guide was around 200 for all *in vitro* samples except for the later VXLD treated cells which was slightly lower.

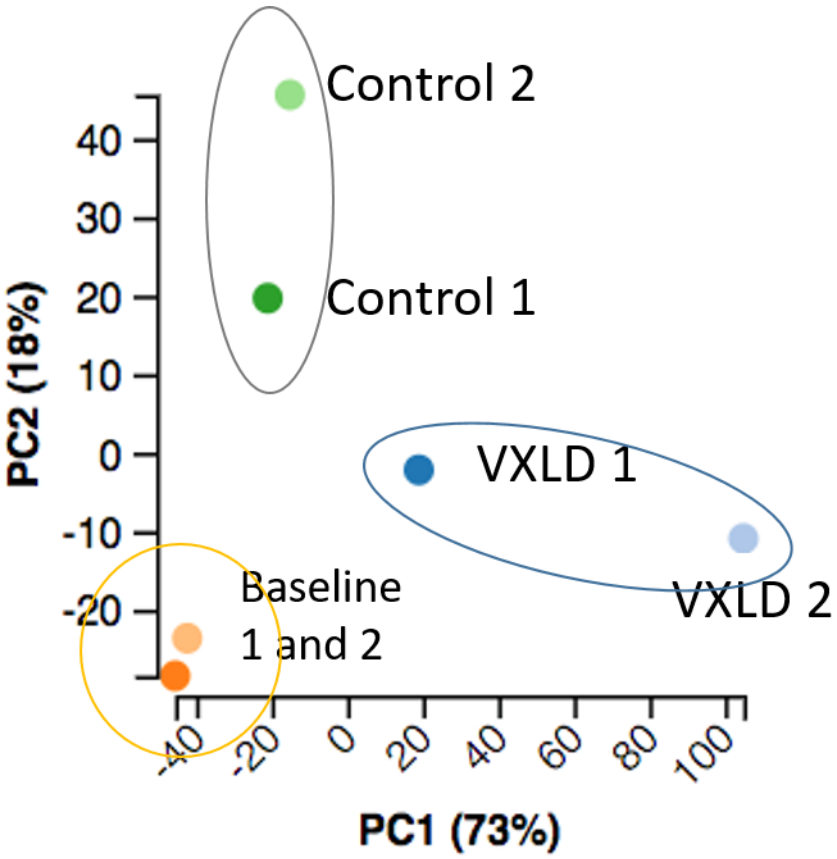

Figure 6.5 Principal component analysis of in vitro screening samples. Baseline samples are indicated in orange, control samples in green and VXLD treated in blue, where VXLD1 refers to earlier VXLD treated time point and VXLD2 the later

Principal component analysis (figure 6.5) shows the baselines group closely together and they were therefore combined for enrichment and depletion analysis in MAGEcKFlute. The 2 VXLD treated time points were combined, as were the 2 control time points. MLE analysis was also performed on samples without combination of VXLD treated and control time points in order to visualise the change in abundance of genes over time.

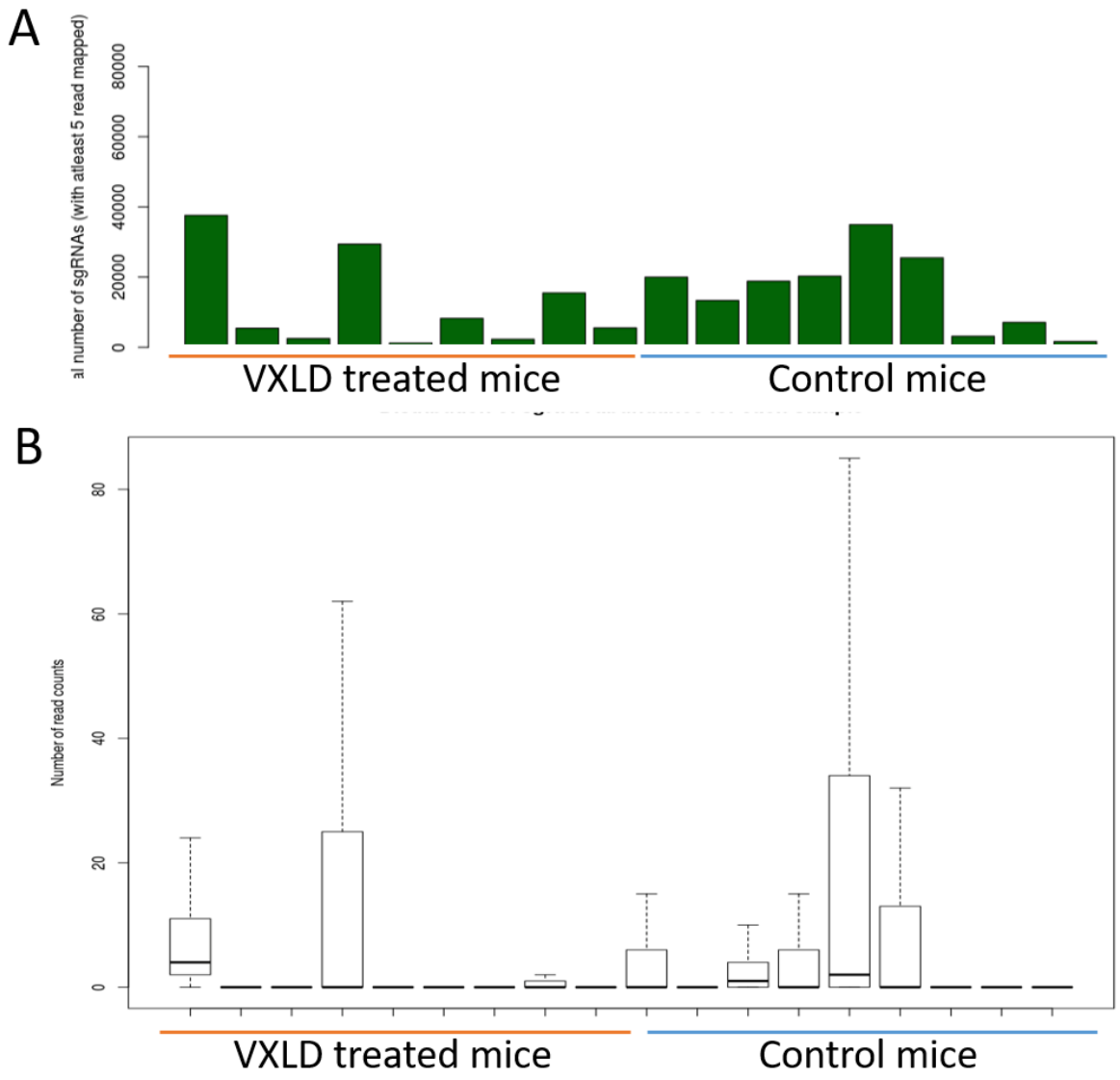

Figure 6.6 Quality control for each individual mouse from *in vivo* screen. The number of guides with greater than or equal to 5 reads are shown for each individual mouse for both VXLD treated mice n=9 and control mice n=9 (a). Boxplots are also given showing the distribution of reads per guide for each mouse (b).

The total guide number and read count distributions were vary variable between different mice (figure 6.6). The total guides within each mouse were far lower than found *in vitro* samples. The smallest number of guides identified in a single mouse was 1201 and the maximum was 37595. The distribution of these guides was uneven with many reads taken up by a relatively small number of guides, lead to low median reads per guide. To increase the coverage of guides the 9 treated mice were pooled as were the 9 non-treated control mice. Guides with greater than 5 reads were then determined again and read count distribution checked.

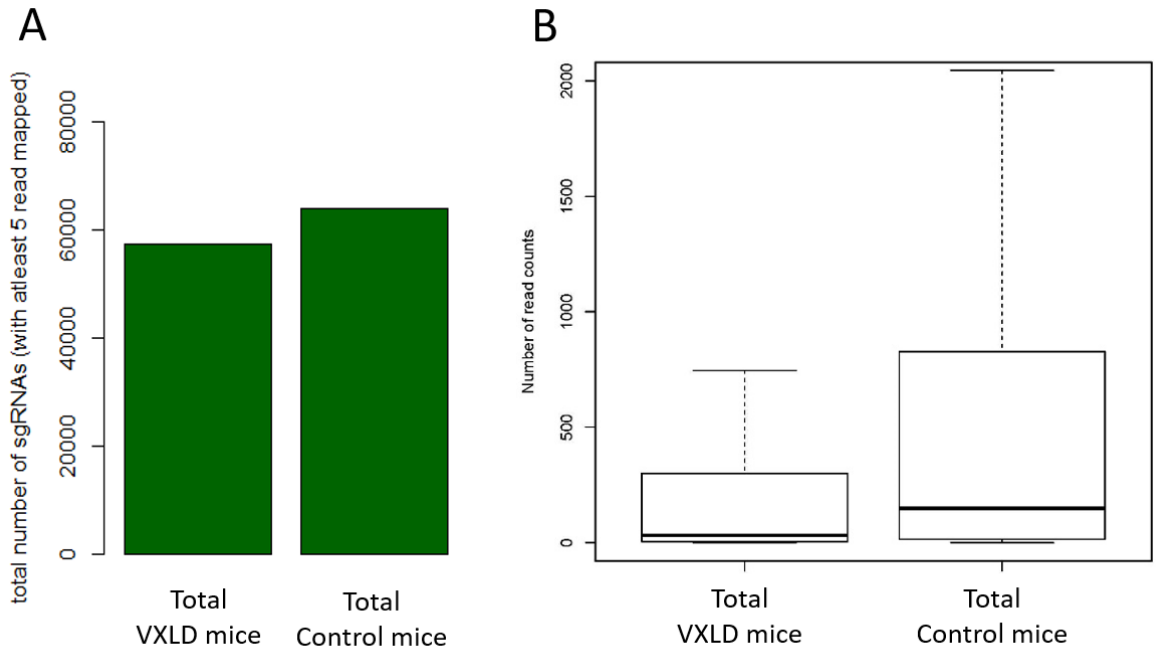

Figure 6.7 Quality control for pooled *in vivo* samples. The number of guides with greater than or equal to 5 reads are shown for the pooled 9 VXLD treated mice and pooled 9 control mice n=9 (a). Boxplots are also given showing the distribution of reads per guide for each group (b).

Pooling the mouse samples gave much greater library coverage with over 60,000 guides (63,985) present in the non-treated mice and just under 60,000 guides (57,286) for the VXLD treated (figure 6.7). The total guides in the library was 77,441 so at 60,000, 77% of the library was present in the pooled *in vivo* samples. Read count distributions were more variable *in vivo* compared to *in vivo* with more guides with extremely high read counts. Despite this median guide read counts was 32.4 for VXLD treated mice and 148.3 for control mice.

6.2.2 Bioinformatics analysis

This section describes the reasoning and background behind the bioinformatics tools used for data analysis -for overview of the general pipeline refer to method section 2.30.

The MAGeCK toolkit has been specifically designed for the analysis of CRISPR screening data. It has been shown to outperform over computational models for analysis of this type of data and is commonly used for CRISPR screen analysis (Li et al., 2014). The maximum likelihood estimation (MLE) function of MAGeCK uses a maximum likelihood estimation (statistical method of estimating probability distribution parameters) for identification of hits and uses raw counts of sgRNAs to produce a single beta score and p value for each gene. Due to low sgRNA representation per mouse, calculation of beta scores on a mouse level was not reliable. Counts from the 9 treated mice were pooled and counts the 9 control mice were pooled, prior to MLE analysis. Two samples were sequenced for each condition (baseline, control and treatment) since these were sufficiently similar to each other they were used in the place of true replicates for MLE analysis.

Beta scores are a measure of change (like fold change expression in RNAseq analysis), where change in relative abundance of sgRNAs is determined in each sample relative to a baseline. A positive beta score means guides targeting the gene are positively selected, implying loss of the gene under screening conditions. Negative beta score means guides targeting the gene are negatively selected or lost, implying the gene is required under screening conditions.

After generation of beta scores, normalisation was performed to correct for the different doubling times found between control and treated conditions which can lead to bias in hit identification (selection will appear stronger in more rapidly proliferating

cell). The MAGeCKFlute pipeline has a normalisation step based on a list of 350 highly essential genes, which are assumed to be equally negatively selected between the two conditions despite differences in proliferation rate.

Normalised beta scores from VXLD treated and control arms can then be compared to identify differentially enriched and differentially depleted guides, these are displayed as rank plots, scatterplots and nine-square scatterplots. Lists were formed of guides identified as differentially enriched and guides differentially depleted for both *in vitro* and *in vivo* screening. These lists were analysed further by looking at common hits, common pathways and interactions.

6.3 Differentially enriched and depleted guides with VXLD chemotherapy *in vitro*

FluteMLE was used to identify guides with significantly different beta score between treated and control conditions. Firstly, this analysis was performed on *in vitro* data. In figure 6.8 each gene is plotted based on its beta score for the control arm (x-axis) and the beta score from the treated arm (y axis). Rank plots were also generated and offered an alternative way to visualise the data (figure 6.9).

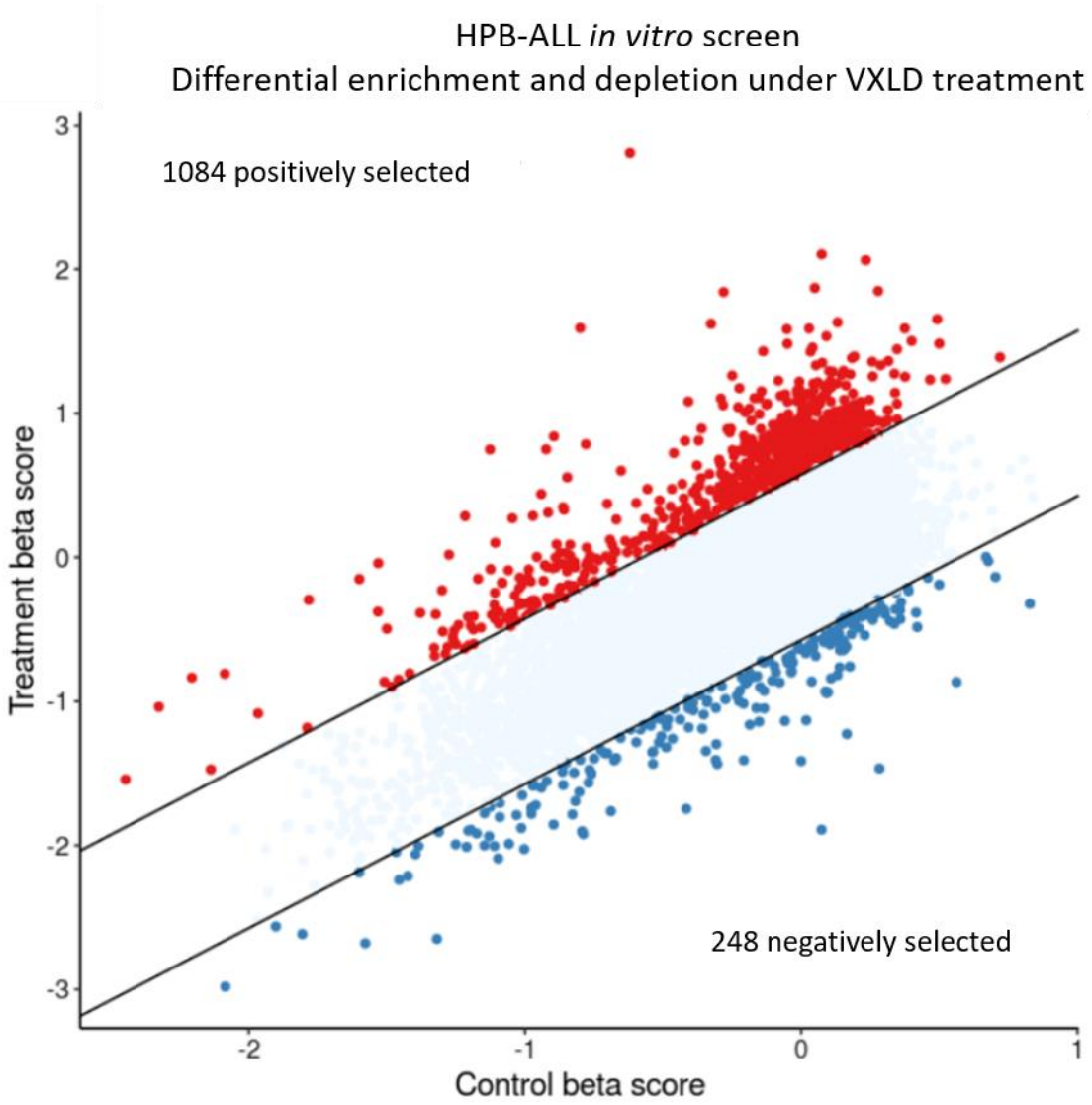

Figure 6.8 Scatter plot of *in vitro* differentially ernciched and depleted guides (at gene level). Scatter plot of Control beta score (x-axis) against treated beta score (y-axis) for each gene. Red points indicate genes where the beta score is higher under VXLD treatment. Blue points indicate genes where the beta score is decreased with VXLD treatment.

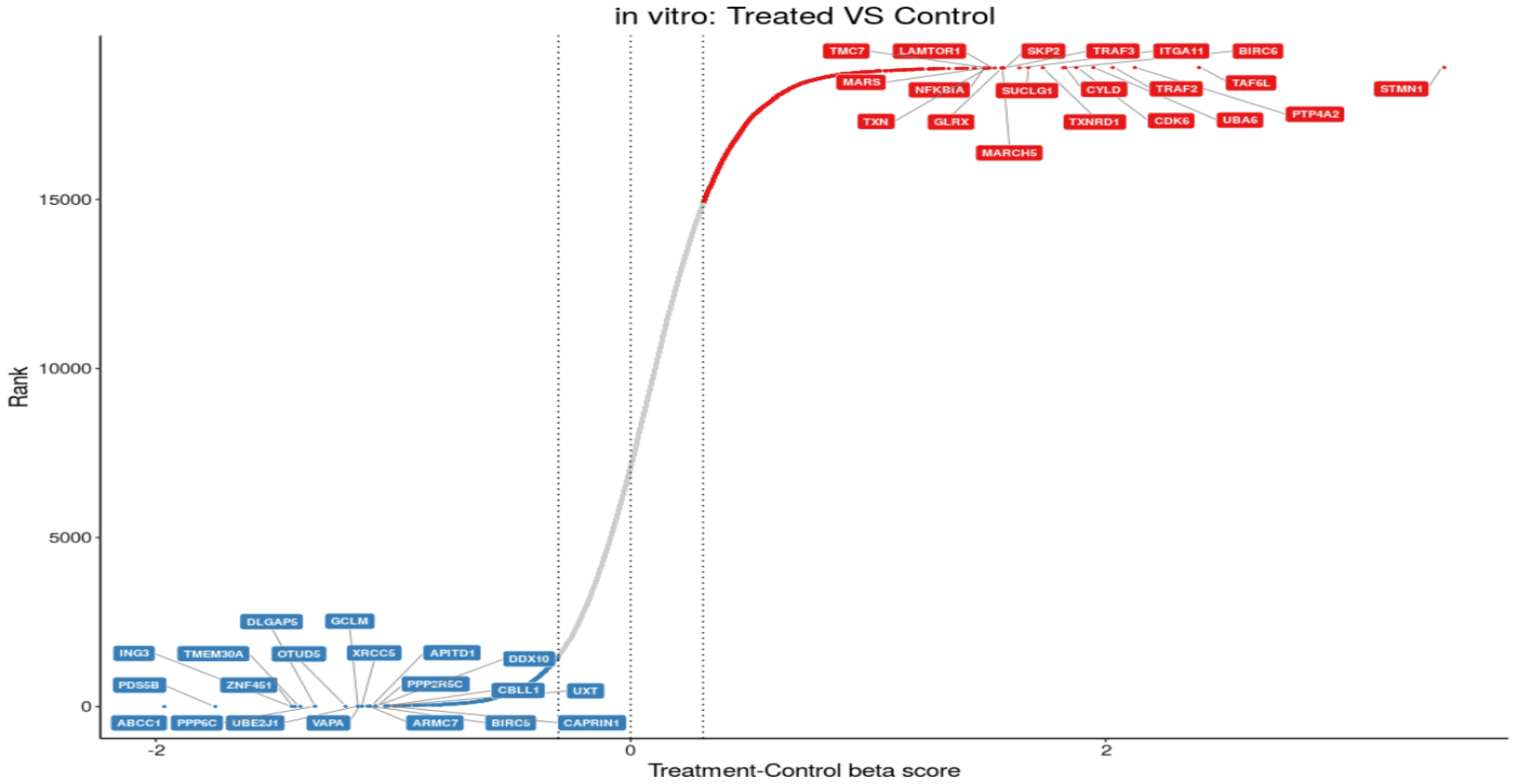

Figure 6.9 Rank plot of *in vitro* differentially enriched and depleted guides (at gene level). Rank plot of 20 most differentially enriched (red) and 20 most differentially depleted (blue) guides under VXLD treatment *in vitro.*

Among the top 20 differentially enriched guides are members of nuclear factor kappa-light-chain-enhancer of activated B cells (NF-κB) signalling: TNF receptor-associated factor 2 (*TRAF2*), TNF receptor-associated factor 3 (*TRAF3*) and NFKB Inhibitor Alpha (*NFKBIA*). The most differentially *in vitro* depleted guides were for ATP binding cassette subfamily C member 1 (*ABCC1)* also known as Multidrug Resistance-Associated Protein 1. A ubiquitously expressed transporter of organic anions it is associated with resistance to various chemotherapeutic including anthracyclines, and vincristine (Munoz et al., 2007).

Genes were also grouped according to how the guide beta scores differ between the control and under VXLD treatment. Beta scores are plotted in a scatter graphs and 4 groups were identified (figure 6.10). The first group (orange) guides were unchanged under control conditions and are enriched in VXLD treatment. The second group (purple) comprised genes with unchanged guides under control conditions and depleted guides in treatment. The genes depleted in control but unchanged in treatment form a third group (coloured green).

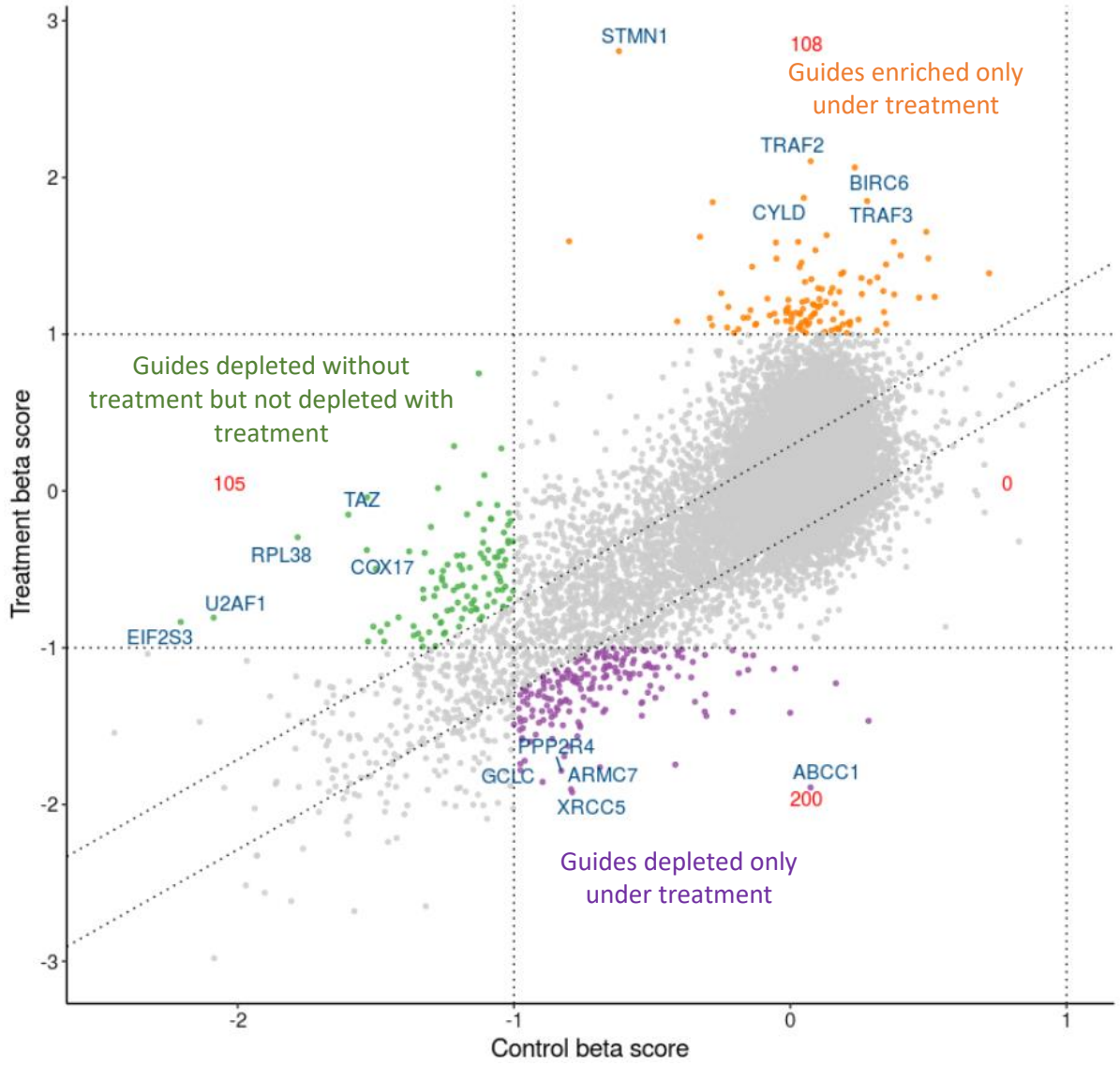

Figure 6.10 Scatter plot of Control and Treated arm beta scores. Scatter plot of in vitro control (x-axis) versus treated beta score (y-axis). Genes are grouped according to treated and control beta scores in quadrants dictated by beta scores between -1 and 1, greater than 1 or less than -1. Green group1: negative beta score in control arm, but neutral score under treatment this group contains 105. Orange group 2, neutral beta score in control arm but positive beta score under VXLD, here there are 108. Blue group 3: 0 in this group where enriched under control conditions and unchanged under treatment. Purple group 4: Unchanged beta scores in control conditions but negative beta score under treatment. Guides not part of these 4 groups are shown in grey. The top 5 genes in each group are labelled.

The first group of guides (coloured orange) represent genes that when lost conferred resistance to VXLD treatment (they are required for response to VXLD). One hundred and eight genes from *in vitro* screening fell within this group one of these is the Cylindromatosis genes (*CYLD*). *CYLD* removes ubiquitin chains from lysine 63. CYLD is repressed by the NOTCH1 target gene HES1 which is responsible for sustaining IKK activation in T-ALL (D'Altri et al., 2011, Espinosa et al., 2010). The NOTCH1-HES1-CYLD-NF-κB pathway is important for leukemic survival and it has been suggested as a targetable pathway (D'Altri et al., 2011, Espinosa et al., 2010). *CYLD* is discussed further in 6.12.1.

Purple indicates genes that were required for resistance to VXLD treatment (guides depleted under treatment). *ABCC1* described earlier is known to provide resistance to chemotherapy. Also included in this group was X-ray repair cross-complementing protein 5 (*XRCC5*) required for DNA double strand break repair. After analysing the *in vitro* data, the same analysis was used to identify differential changed genes under VXLD treatment in *vivo*.

6.4 VXLD treatment *in vivo* identifies guides that are more positively and more negatively selected than without treatment

The genes associated with drug sensitivity and resistance *in vivo* were determined in a similar manner to *in vitro*. Beta scores (measure of change of guides from baseline) was plotted on a scatter diagram (figure 6.11) according to control beta score (x-axis) and treated beta score (y-axis). There were 736 positively selected genes and 358 negatively selected genes. The top 20 differentially enriched and depleted guides (at level of the gene) are given in table 6.1. Data is also shown on a 9 square scatter graph (6.12).

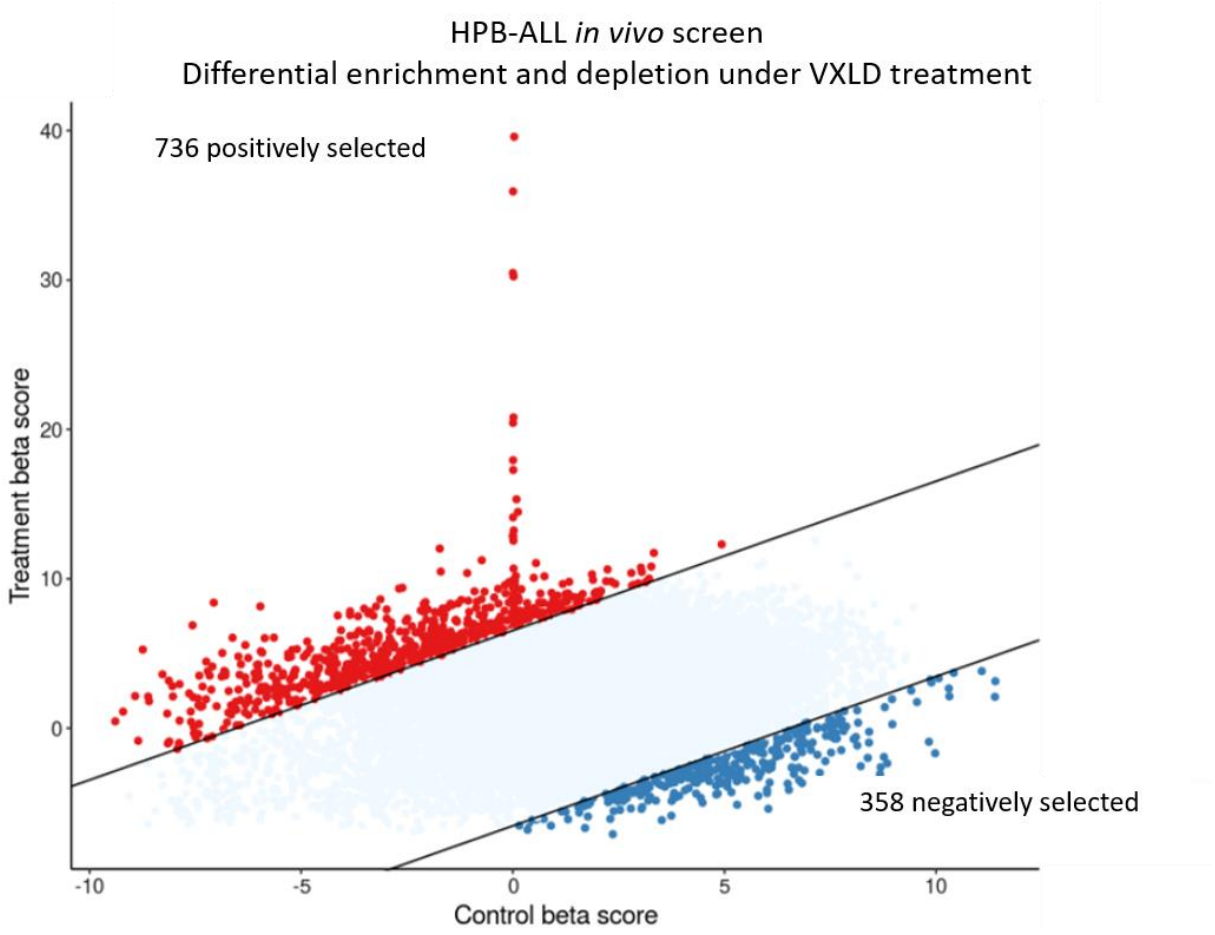

Figure 6.11 Scatter plot of *in vivo* differentially enriched and depleted guides (at gene level) Scatter plot of gene control beta score on x-axis against treated beta score on y-axis. Genes which were negatively selected under VXLD treatment compared to control conditions are shown by blue points. Guides with a higher beta score with VXLD treatment compared to control are shown by red points.

Guides Enriched	Guides depleted
HACD1	TRAPPC8
DUSP4	PKD1L2
ARF3	PPIL1
BTRC	TEX29
MTERF2	SYNGR3
HMGCLL1	BCAS1
SERPINB5	CDCA5
LMOD2	SAP30
ADGRF4	NPIPB5
RS1	SUMF2
NPIPA7	CBLN4
PDF	SLC25A25
USP17L17	OR8D1
DDX25	GABBR2
HSD17B12	PUS10
PRRC1	BABAM1
TESK1	NKX6.1
IDH2	MAGEL2
ATP13A3	IGFBP4
KCNT1	ENG

Table 6.1 Most differential enriched and differential depleted guides from *in vivo* screening. . Top 20 most differentially enriched guides (gene level beta score) under VXLD treatment *in vivo* and the top 20 most differentially depleted guides (gene level beta score) under VXLD treatment *in vivo*.

The most differentially enriched was 3-Hydroxyacyl-CoA Dehydratase 1 (*HADC1*) which is involved in very long chain fatty acid (VLCFA) production (Ikeda et al., 2008). On figure 6.12 *HADC1* is 1 of 426 genes with beta score in group 2 with a control beta score around 0, whereas the treated beta score is greater than 30. Other components in VLCFA production such as ELOVL Fatty Acid Elongase 1 (*ELOVL1*) or Ceramide synthase 2 (*CERS2*) have been implicated in sensitivity to chemotherapeutics (Sassa et al., 2012).

Dual specificity protein phosphatase 4 (*DUSP4*) was the second most enriched differentially enriched gene, and similar appears in group 2 with a beta score in the control arm close to 0 but high beta score under treatment. *DUSP4* negatively regulates the mitogen activated protein kinases (MAPK) pathway. DUSP4 appears to have contrasting roles in different cancers, with reduced DUSP4 helping drive basal-like breast cancer, lung cancer, colorectal cancer and diffuse large B-cell lymphoma, and increased DUSP4 being associated with chemo-resistance and poorer prognosis in gastric cancer and invasive ductal carcinoma (Balko et al., 2013, Chitale et al., 2009, Saigusa et al., 2013, Schmid et al., 2015, Kang et al., 2017, Kim et al., 2015).

Trafficking protein particle complex subunit 8 (*TRAPPC8*) was the most significantly differential depleted with VXLD treatment. Knockdown of TRAPPC8 was shown to lead to defects in autophagy by other authors (Imai et al., 2016).

The 9 square grouped scatter graph (figure 6.12) highlights different genes to the most enriched list. One gene with a negative beta score with VXLD treatment but not a negative beta sore in the control arm was RNA binding protein 14 (*RBM14*), which has been shown to have a role in repair of double stranded breaks (Jang et al., 2020). Deficient double strand break repair can make cells more susceptible to anthracyclines like daunorubicin (Saffi et al., 2010).

After identifying differentially enriched and depleted genes under VXLD treatment *in vivo*, the identified genes were compared to genes identified through *in vitro* screening to be differential enriched or depleted with VXLD.

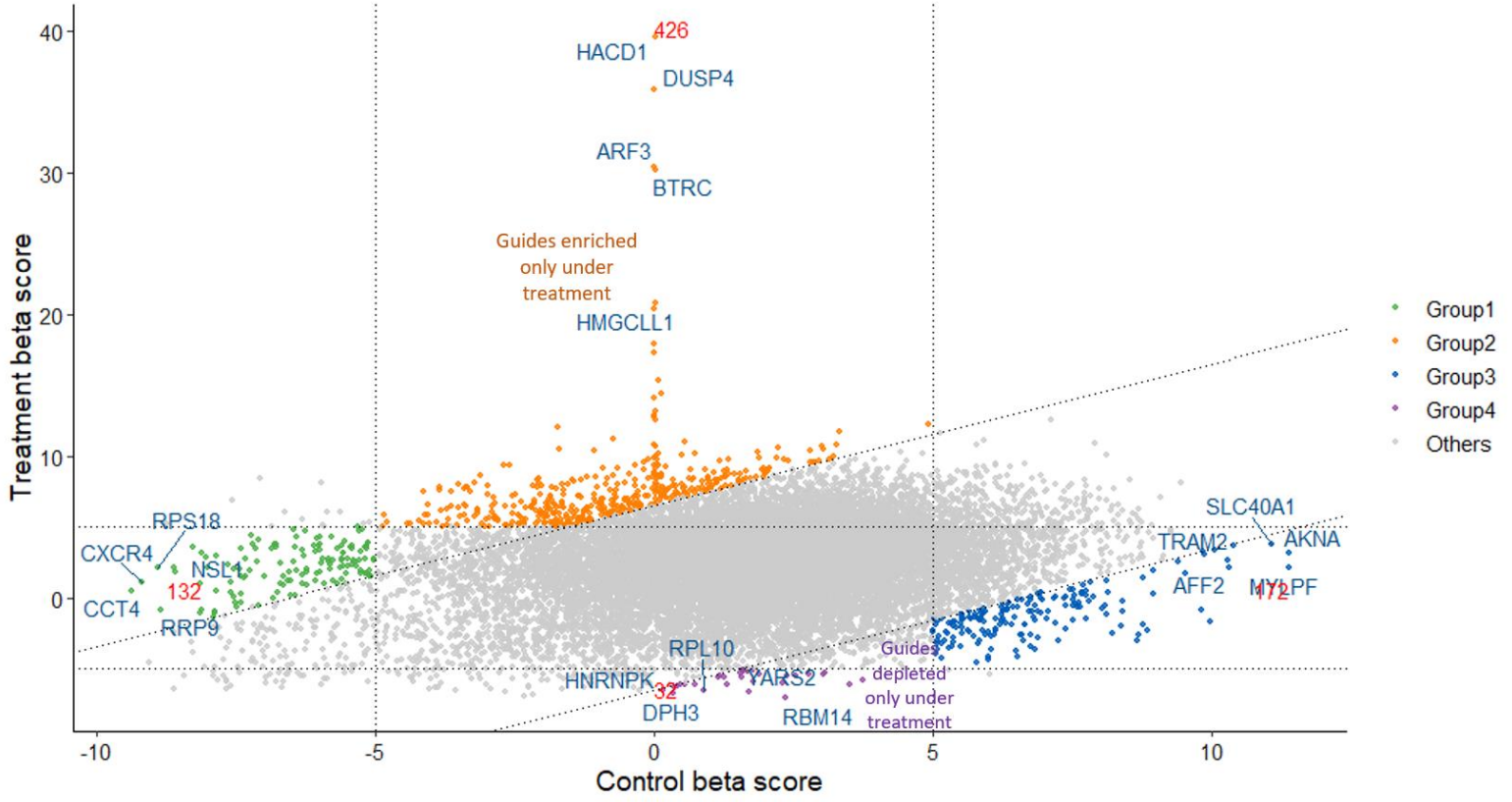

Figure 6.12 Scatter plot of Control and Treated arm beta scores. Scatter plot of in vitro control (x-axis) versus treated beta score (y-axis). Guides are grouped according to treated and control beta scores in quadrants dictated by beta scores between -5 and 5, greater than 5 or less than -5. Green group 1: negative beta score in control arm, but neutral score under treatment this group contains 105. Orange group 2, neutral beta score in control arm but positive beta score under VXLD, here there are 108. Blue group 3: 0 in this group where enriched under control conditions and unchanged under treatment. Purple group 4: Unchanged beta scores in control conditions but negative beta score under treatment. The top 5 in each group are labelled. Guides not falling in any group are coloured grey.

6.5 Differential enriched and depleted genes with VXLD chemotherapy both *in vitro* and *in vivo*

R studio was used to compare lists differentially enriched and depleted guides from *in vitro* screening and differential enriched and depleted in *in vitro* screening (figures 6.13 and 6.14). Six guides (gene level beta score-) were found to be differentially depleted with VXLD treatment both *in vitro* and *in vivo,* these are listed in appendix A. Forty-seven genes were found to be commonly enriched in VXLD treatment (listed in appendix A).

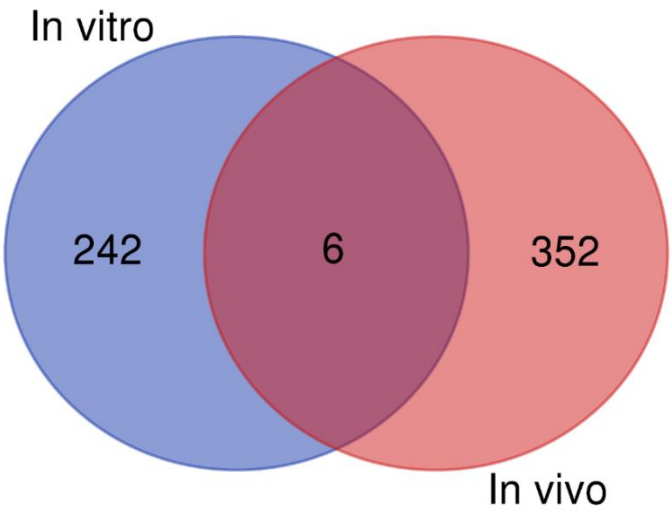

Figure 6.13 Differentially depleted guides under VXLD treatment compared to control. Guides depleted (gene level beta score) *in vitro* screening are in the blue circle, and the guides depleted (gene level beta score) *in vivo* the red circle, intersection of the two circles represent those in common.

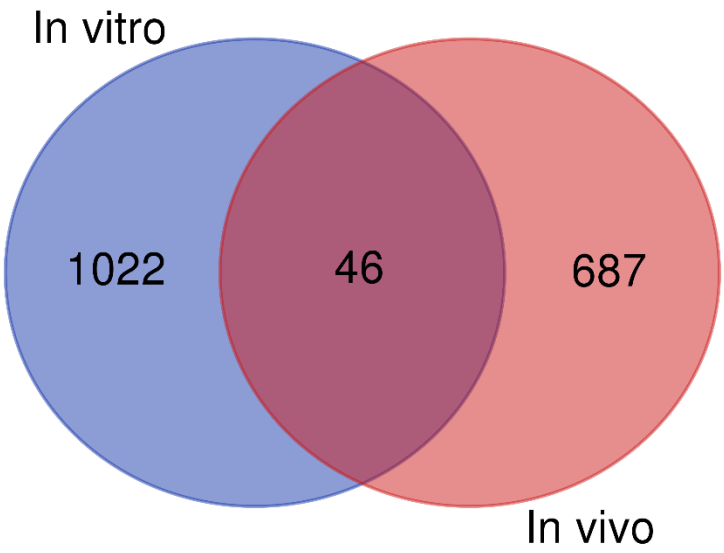

Figure 6.14 differentially enriched guides under VXLD treatment compared to control. Guides enriched (gene level beta score) *in vitro* screening are in the blue circle, and the guides enriched (gene level beta score) *in vivo* the red circle, intersection of the two circles represent those in common. .

There were several hundred guides (gene level beta scores) identified as depleted with VXLD treatment in both *in vitro* and *in vivo* screening but only 6 were shared (listed in appendix A). Loss of different genes within the same pathway could have led to the same phenotypic effect. Gene lists comprised of the depleted guides from the *in vitro* and *in vivo* screen was used in pathway analysis using WebGestalt (figure 6.15).

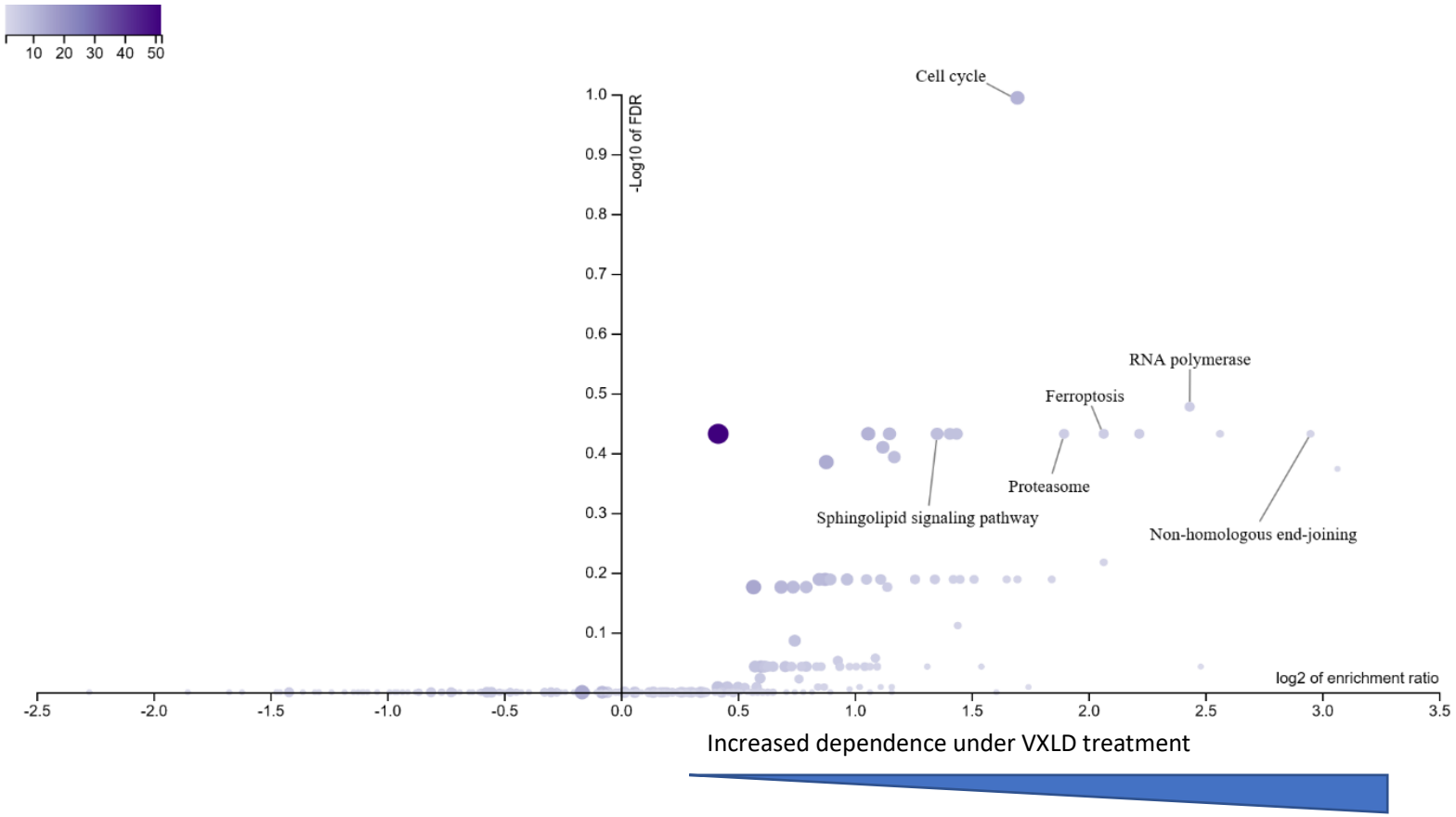

Figure 6.15 Pathway analysis of genes where guides are differential depleted under VXLD treatment *in vitro* or *in vivo.* Genes that were identified as differential depleted *in vitro* or *in vivo* were input as a gene list into WebGestalt. An over representation analysis was performed using the Kegg database. The Log2 of the enrichment score is plotted against the negative log ten of the false discovery rate (FDR). The colour scale indicates the number of genes mapped to the pathway. The top ten pathways are labelled. Since the gene list comprised guides that were differentially depleted under VXLD treatment, the most enriched pathways indicate where there is increased dependence on these pathways under VXLD treatmen

Cell cycle had the lowest false discovery rate in pathway analysis at 0.1. Twelve genes were associated with cell cycle (enrichment ratio 3.2). Another pathway enriched in the data was the proteasome (FDR 0.4, Enrichment ratio 3.7). The proteasome was of interest since this pathway was targetable with proteasome inhibitors and these have been under investigation in combination with VXLD chemotherapy (Messinger et al., 2012). One of the 6 overlapping depleted genes HECT Domain E3 Ubiquitin Protein Ligase 2 (HECTD2) is an E3 ubiquitin ligase, ubiquitination targets proteins for proteasome mediated degradation (Yamaguchi et al., 2012).

6.6 Guides differentially enriched/depleted both *in vitro* and *in vivo*

The genes where guides were differentially changed under VXLD treatment both *in vitro* and *in vivo* (enriched- 47 and depleted- 6) were analysed for interaction using STRING (figure 6.16).

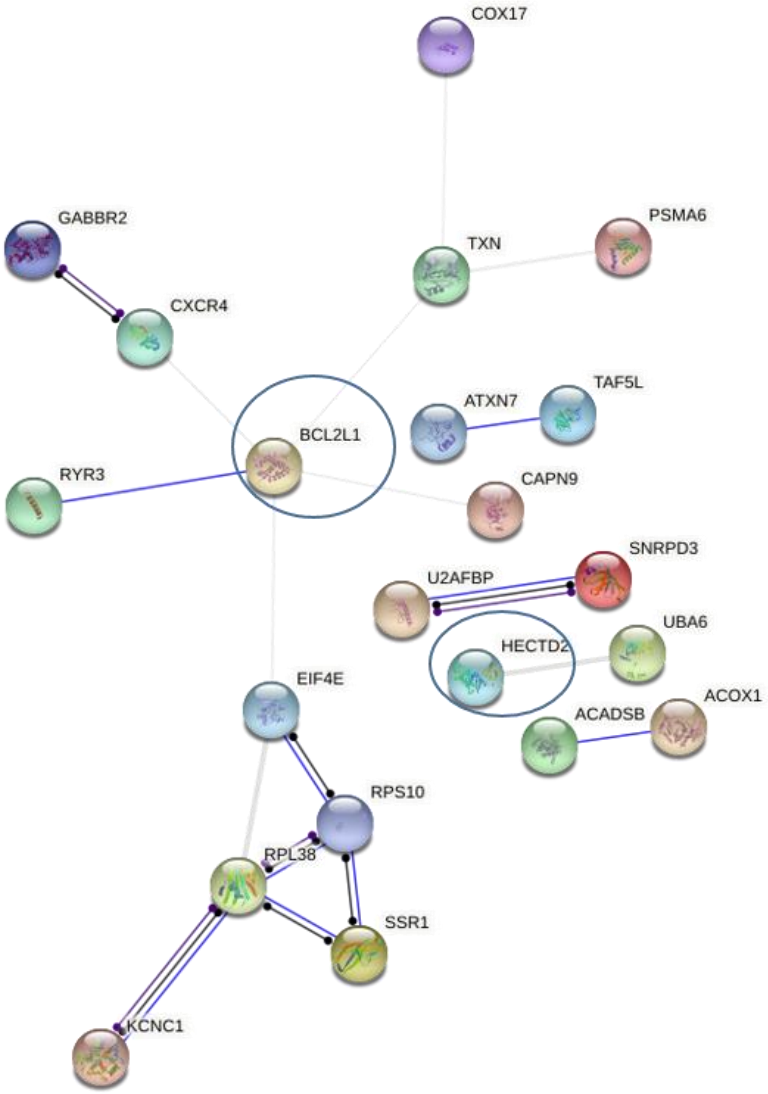

Figure 6.16 String interaction of genes with differentially enriched and depleted guides under VXLD treatment. Genes that were common between *in vitro* and *in vivo* differentially enriched/depleted guides under VXLD treatment where input as a gene list into STRING. For clarity only interacting genes are shown. Line colour indicates the type of interaction blue –binding, black-reaction, purple-catalysis.

The STRING interaction network showed 21 interacting genes. Highlighted are 2 of the 6 genes that had depleted guides (gene level) under treatment that were shared between *in vitro* and *in vivo* conditions. Bcl-2-like 1 (BCL2L1) had many predicted interactions within the differential genes. BCL2L1 encodes BCL-X which is a key player in regulation of apoptosis. Bcl-2-like 1 *(BCL2L1)* was selected for further validation for 3 main reasons:

- Identified in both *in vitro* and *in vivo* screening
- Known role in apoptosis (see 6.7.2)
- Can be inhibited pharmacologically

6.7 The importance of BCL-X in resistance to VXLD chemotherapy in TLX3 T-ALL

6.7.1 Introduction

BCL2L1 was selected for further validation after screening. In the interest of time validation was performed using HPB-ALL (in which the screen was performed) and another T-ALL cell line- DND41. HPB-ALL has a TLX3 background, as does DND41. The dependence of TLX3 cells lines on BCL-XL was assessed prior to considering validation in a wider genetic background, in *ex vivo* xenograft cells or in mouse models. The first step in validation was to assess the change in expression of BCL2L1 at the mRNA level with VXLD drug treatment (6.7.2), this was followed by pharmacological inhibition (6.7.3) and finally knockdown experiments with shRNA (6.7.4).

6.7.2 BCL2L1 background information

Bcl-2-like 1 (BCL2L1) encodes apoptotic regulator BCL-X. BCL-X is a BCL2 family member. BCL2 family members are regulators of apoptosis via regulation of mitochondrial membrane permeability and activation of caspases (Chao and Korsmeyer, 1998). BCL2 family members are recognised by their shared alpha helical domains known as Bcl2 homology domains (BH) domains, and family members have differing numbers up to 4 BH domains labelled 1 through 4 from C to N terminus (Chao and Korsmeyer, 1998). BH4 is important to ant-apoptotic functions and is less conserved in pro-apoptotic family members. Conversely BH3 is important to pro apoptotic functions.

BCL-X is alternatively spliced to a shorter pro-apoptotic isoform *BCL-X*$_S$ or a longer anti-apoptotic form *BCL-X*$_L$. Exons 2 and 3 are coding exons. There are two known isoforms of the noncoding exon 1 found in the BCL-X gene; the proximal- 1A was identified first and is associated with CD40 ligand and NF-κB signalling, whilst the distal-1B is associated with E26 transformation-specific family (Ets) binding (figure 6.17) (Ban et al., 1998, Habens et al., 2007).

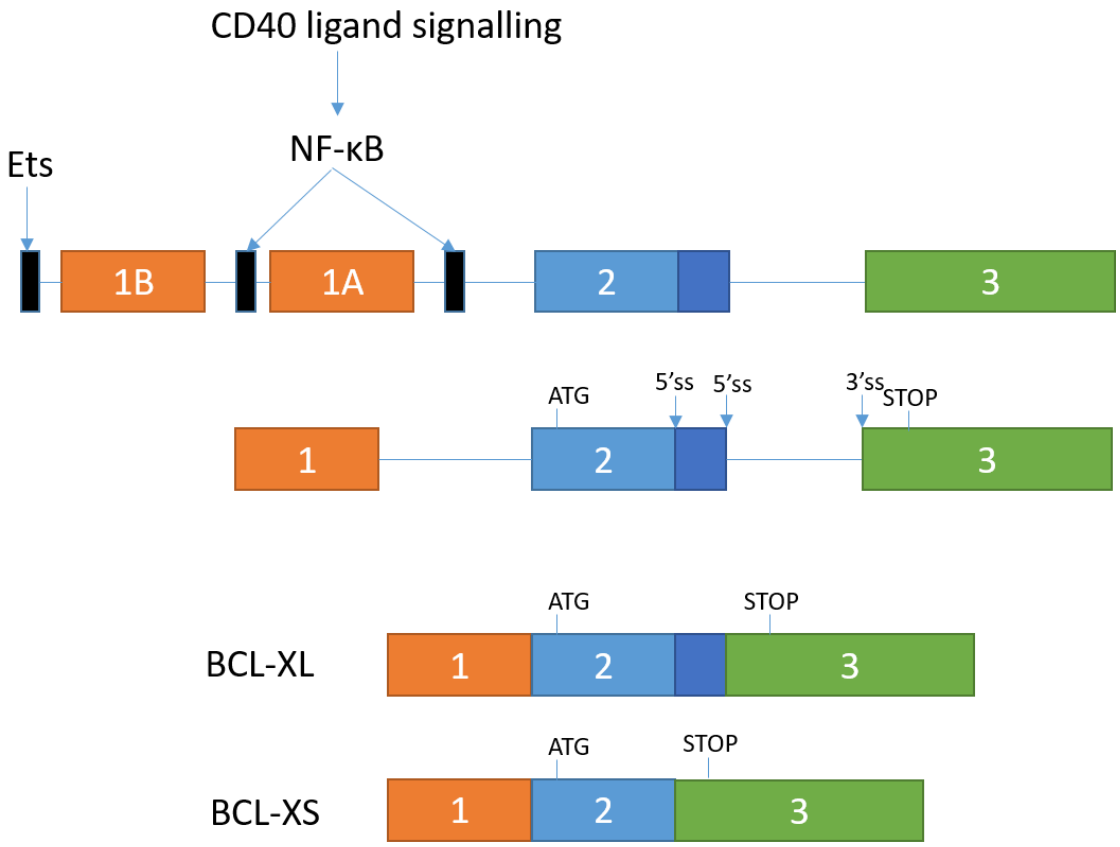

Figure 6.17 BC2L1 gene and BCL-X transcript. BCL-X has two versions of the first non-coding exons with separate promoters linked to Ets and NF-κB signalling. BCL-X pre-mRNA is alternatively spliced to form two different length sequences-known as BCL-XL and BCL-XS. Exons are numbered. Black boxes indicate transcription factor binding sites for E26 transformation-specific (Ets) and nuclear factor kappa-light-chain-enhancer of activated B cells (NF-κB) families. The translation start site (ATG) and stop site (STOP) are indicated, as are the 5' and 3' splice site (5'ss and 3'ss).

Alterations in the balance between anti and pro apoptotic factors towards the former could provide a mechanism of cell death avoidance in cancer cells. The use of drugs targeting apoptotic proteins has increased over the last few years with Venetoclax, a BCL2 inhibitor, approved for the treatment of 17p deleted CLL in 2016 and then for use in previously treated CLL in combination with Rituxan in 2018 and in newly diagnosed AML where standard induction therapy not appropriate in November 2018((FDA), 2018a, (FDA), 2018b).There are also ongoing trials in ALL. Whereas B-ALL showed high reliance on BCL2, only early T-cell precursor (ETP) showed this same pattern. More mature T-ALLs showed more BCL-X dependency (Chonghaile et al., 2014). Furthermore, knockdown of BCL-X_L in the T-ALL cell line CEM was synergistic with dexamethasone treatment (Broome et al., 2002).

6.7.3 mRNA expression with VXLD treatment

The mRNA expression of BCL-X (both the exon 1A and 1B form) was assessed in HPB-ALL and DND41 cells after 72 hours of treatment with a VXLD combination (figure 6.18). Expression was compared to cells treated with a solvent control. RNAs for BCL-X with exon 1A and RNAs with exon 1B were determined using separate primer sets.

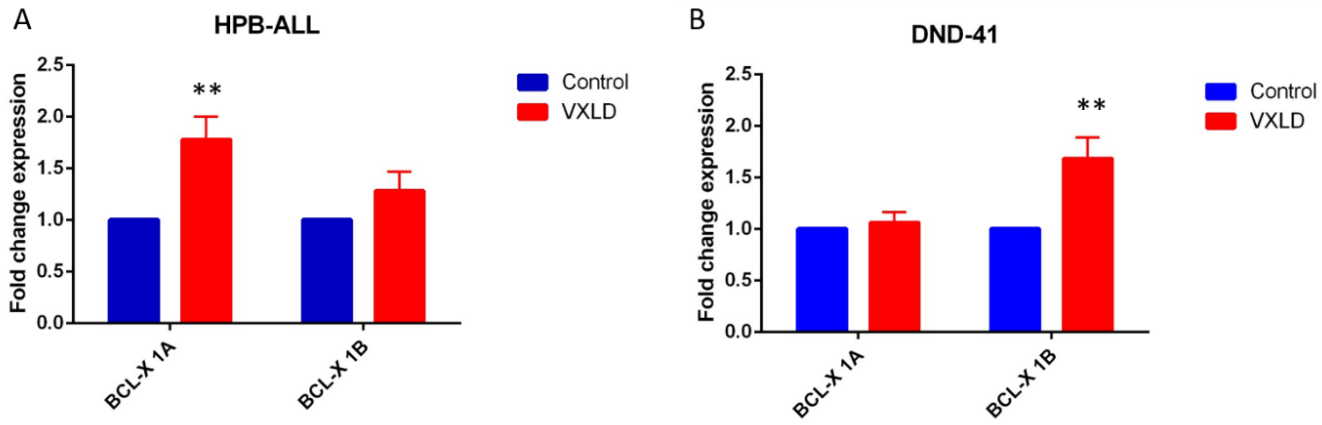

Figure 6.18 BCL-X 1A and 1B expression in HPB-All (A) and DND41 (B) with VXLD treatment at 72 hours. Significant increases in expression were detected by t-test (**p<0.01). Error bars represent standard error of the mean of 3 independent experiments.

Both HPB-ALL and DND41 showed significantly increased BCL-X expression after VXLD treatment, however the isoform that was increased varied with HPB-ALL

showing significant increase in RNA containing exon 1A and DND41 only showing significant increase of the alternate first exon 1B.

6.7.4 Treatment of HPB-ALL and DND41 with ABT-737

ABT-737 is a pan BCL2 family inhibitor that binds BCL2, BCL-W and BCL-X. ABT-737 was applied to HPB-ALL and DND41 cells in a dose dependant manner with and without a fixed VXLD dose. After 72 hours, the effect on cell numbers was measured as reduction in fluorescence in a resazurin assay compared to solvent treated control cells (figure 6.19).

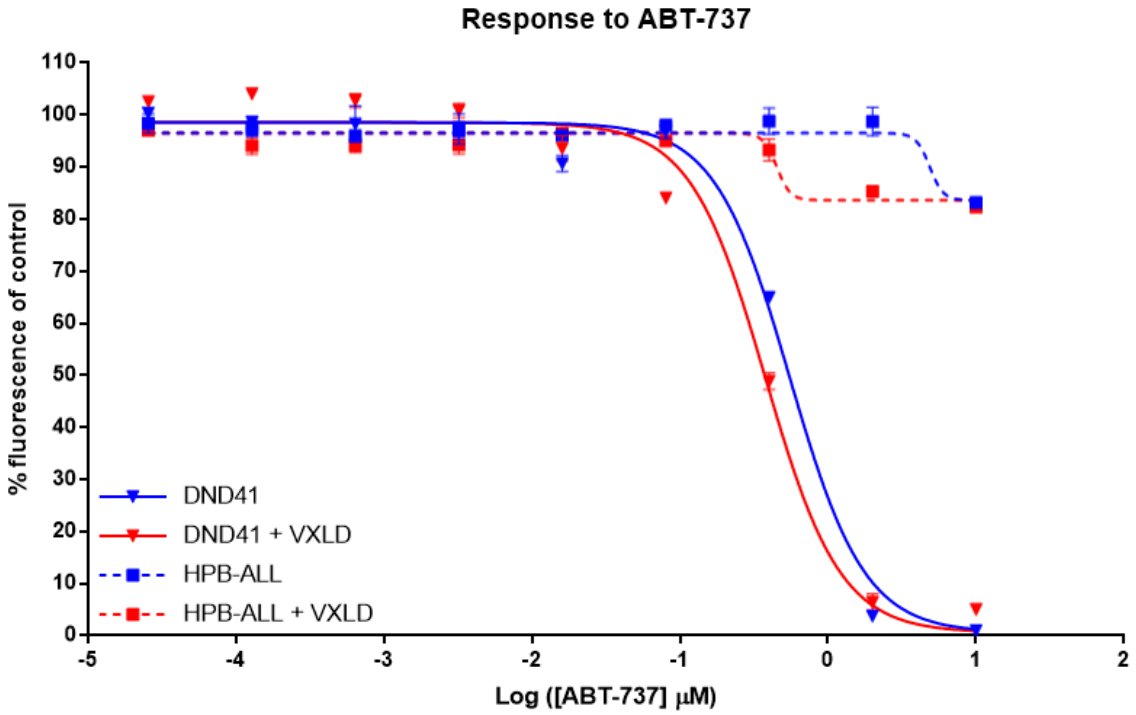

Figure 6.19 Dose response curves of HPB-ALL and DND41 to ABT-737 alone or with a fixed dose of VXLD treatment . For the control cells response is shown as percentage fluorescence of a solvent control well. For VXLD treated cells, results were normalised to fluorescence of cells treated with the fixed dose of VXLD alone (dex 50nM, dauno 33nM, vinc 1nM, asp 0.36mU/ml). EC50 shift analysis (performed in prism) shows curve shift ratio for HPB-ALL of 10.81 and for DND41 1.463.

The GI_{50} for ABT-737 as a single agent in DND41 cells was 0.7µM, with a fixed dose of VXLD it was lowered to 0.3µM (log inhibitor versus response). The curve shifts by a ratio of 1.46 is significant (EC50 curve shift ratio significantly different to 1 (no shift), p = 0.0001). HPB-ALL did not achieve greater than 20% reduction in fluorescence compared to a solvent control in a dose range up to 10 µM. However the addition of a fixed dose of VXLD to HPB-ALL did generate a curve shift (EC50 shift ratio of 10.81)

that was significantly different (EC50 curve shift ratio significantly different to 1 (no shift), $p < 0.0001$).

To identify if there was increased apoptosis upon treatment of HPB-ALL or DND41 with ABT-737 and annexin V assay was performed 24 hours of addition of drugs (figure 6.20).

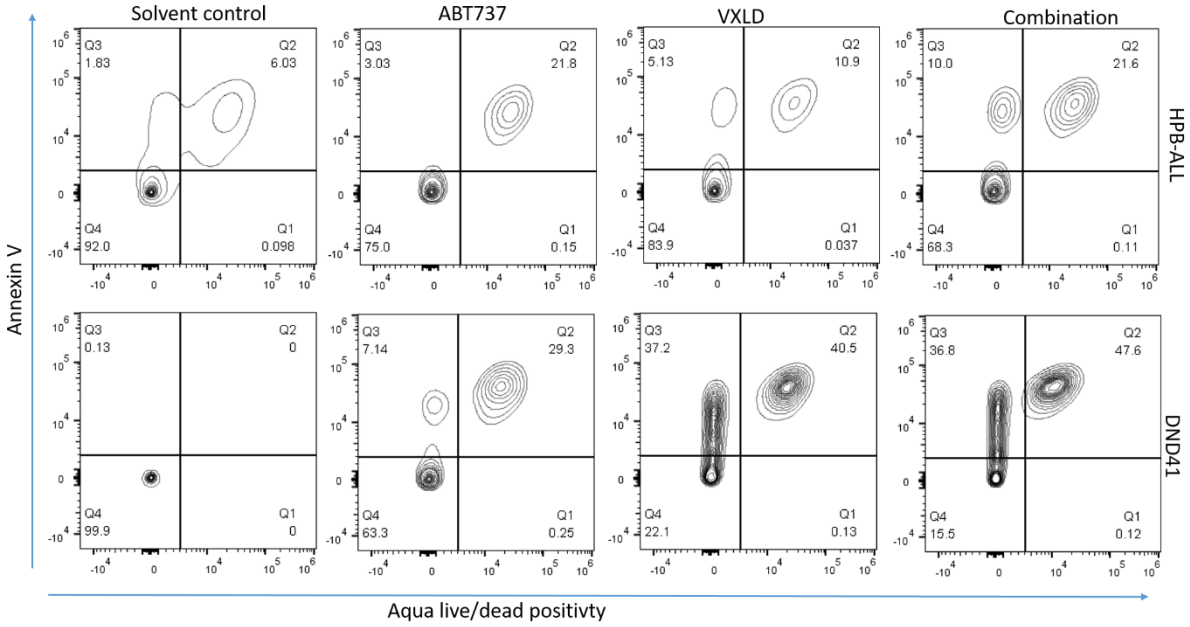

Figure 6.20 Annexin V assay for HPB-ALL and DND 41 treated with ABT-737 or VXLD or both ABT-737 and VXLD for 24 hours. The quadrants Q1, Q2, and Q4 represent live cells, early apoptotic cells, and dead cells respectively**.** N=1

The annexin V assay showed less than 10% of cells were apoptotic in HPB-ALL treated with ABT-737 (2µM) for 24 hours and there was no significant increase by combining ABT-737 with VXLD. DND41 showed 37% of cells were apoptotic with ABT-737 (0.4µM) and there was a non-significant increase in apoptosis by combining ABT-737 with VXLD in the DND41 cells.

6.7.5 Competitive assay

To establish if reduction in BCL-X led to decreased survival of HPB-ALL or DND41 cells, BCL-X was knocked down using a shRNA vector with a GFP tag. The shBCL-X reduced BCL-X expression in both HPB-ALL and DND41 at RNA level (figure 6.21). To directly compare the fitness of cells with BCL-X knockdown to cells without knockdown of BCXL-X, shBCL-X containing cells were mixed in a 1:1 ratio with cells transduced with a non-targeting control shRNA (shNTC) tagged with RFP657. The shBCL-X cell population was detected by GFP expression using flow cytometry and was compared to the RFP657 positive cells containing shNTC over time. The mixed cells were kept under standard culture conditions or were supplemented with VXLD. The percentage of cells is shown at the baseline (day of mixing) and after 1 week of culture (figure 6.22). To ensure the observed effect was not due to differential toxicity of 1 fluorochrome over another, a control assay was set up with two mixed non-targeting control constructs, one tagged with GFP (shNTC1) and another with RFP657 (shNTC2).

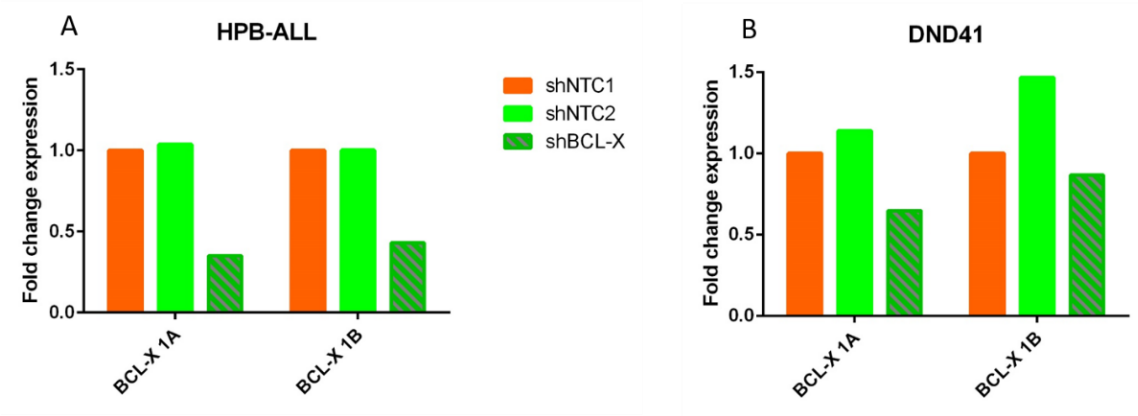

Figure 6.21 BCL-X expression after shRNA knockdown. RNA expression of BCL-X in HPB-ALL (A) and DND41 (B) is given as fold change compared cell transduced with a non-targeting control. N=1

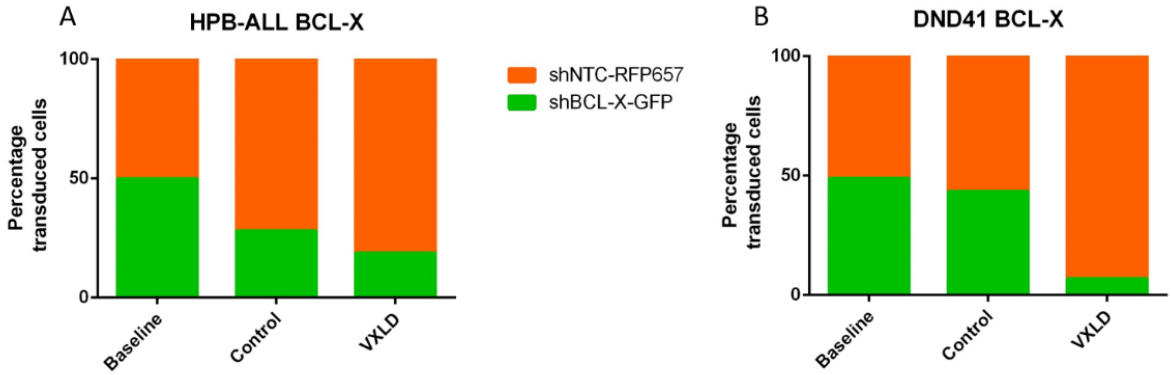

Figure 6.22 BCL-X knockdown competitive assay results. Relative proportions (percentage)of cells containing shBCLX-GFP or shNTC-RFP657 in HPB-ALL (A) and DND41 (B) cell lines at baseline and after 7 days in standard culture and after 7 days with VXLD treatment. N=1

BCL-X knockdown cells were competitively lost in HPB-ALL under standard culture conditions, with a further reduction in BCL-X knockdown cells after addition of VXLD chemotherapy. In DND41 cells BCL-X knockdown cells were not noticeably reduced in standard culture conditions compared to the NTC cells. However, upon VXLD treatment there was a dramatic reduction in BCL-X knockdown cells, with 95% of transduced cells now being shNTC. There was no change in the proportion of shNTC1-GFP cells and shNTC2-RFP657 cells in either condition.

6.7.6 BCL2L1 validation Summary

BCL2L1 was selected for validation, guides targeting *BCL2L1* were differentially depleted under VXLD treatment both *in vitro* and *in vivo. BCL2L1* encodes apoptotic regulators BCL-X_L (anti-apoptotic) and BCL-X_S (pro-apoptotic). The change in mRNA levels *of BCL-$X_{L/S}$* were assessed in two cell lines HPB-ALL and DND41 after 72 hour VXLD treatment. A BCL2 family member inhibitor ABT-737 inhibits BCL-X_L. Dose response to ABT-737 was established in HPB-ALL and DND41. The amount of apoptosis with VXLD and ABT-737 treatment was measured by annexin V assay. Lastly shRNA was used to knockdown BCL-X in HPB-ALL and DND41. The fitness of BCL-XL knockdown cells was compared to cells containing only a non-targeting shRNA in a competitive setting, including under the influence of VXLD treatment pressure.

Treatment with VXLD increased BCL-X mRNA level after 72 hours with a combination of vincristine, dexamethasone, asparaginase and daunorubicin. Different isoforms were significantly increased in the two tested cell lines, with 1A being significantly increased in HPB-ALL and 1B in DND41.

ABT-737 inhibits BCL2, BCL-X_L and BCL-W. HPB-ALL and DND41 cells were treated with ABT=737 with and without the presence of VXLD. ABT737 only reduced HPB-ALL cells by 20% at a 10µM concentration, the effect on HPB-ALL was not increased beyond 20% by addition of VXLD although a lower dose of ABT737 was required to produce the same 20% reduction. DND41 cells were more responsive to ABT-737 treatment with a GI50 of 0.7µM. Consistent with what was observed with HPB-ALL addition of VXLD generated a curve shift-with less ABT-737 required to generate the same effect. There was no greater annexin V positivity for HPB-ALL cells treated with 2µM of ABT-737 compared to a solvent control at 24 hours. The

treatment of DND41 cells with ABT-737 induced apoptosis as indicated by positive annexin V staining, but there was no increase in apoptosis with addition of VXLD chemotherapy at 24 hours, despite the significant curve shift by addition of VXLD at 72 hours.

Knockdown of *BCL-X$_{L/S}$* with shRNA in HPB-ALL showed that these cells have reduced fitness compared to cells without *BCL-X $_{L/S}$* knockdown. This effect was amplified by the addition of VXLD chemotherapy. In DND41 cells knockdown of *BCL-X* had only minimal effect on the fitness of the cells, until VXLD treatment was applied and, these knockdown cells were rapidly lost in a competitive assay.

6.8 The role of HECTD2 in TLX3 T-ALL cell lines

6.8.1 Introduction

Guides targeting HECTD2 were differentially depleted under VXLD treatment during both *in vitro* and *in vivo* screening. HECTD2 is involved in ubiquitination (chapter 6.8.2). Ubiquitination is of interest since proteasome inhibitors are being trialled in the treatment of ALL (Horton et al., 2019).

6.8.2 Background to HECTD2

HECTD2 is an E3 ubiquitin ligase, which ubiquitinates proteins and targets them for proteasome mediated degradation. HECTD2 has been shown to ubiquitinate the protein inhibitor of activated stat1 (PIAS1)(Coon et al., 2015). PIAS1 inhibits the ability of STAT1 to bind DNA and has also been shown to regulate NFkB signalling (Tahk et al., 2007, Liu et al., 2007, Vilimas et al., 2007). The interaction of PIAS1, HECTD2 and STAT1 is summarised in figure 6.23.

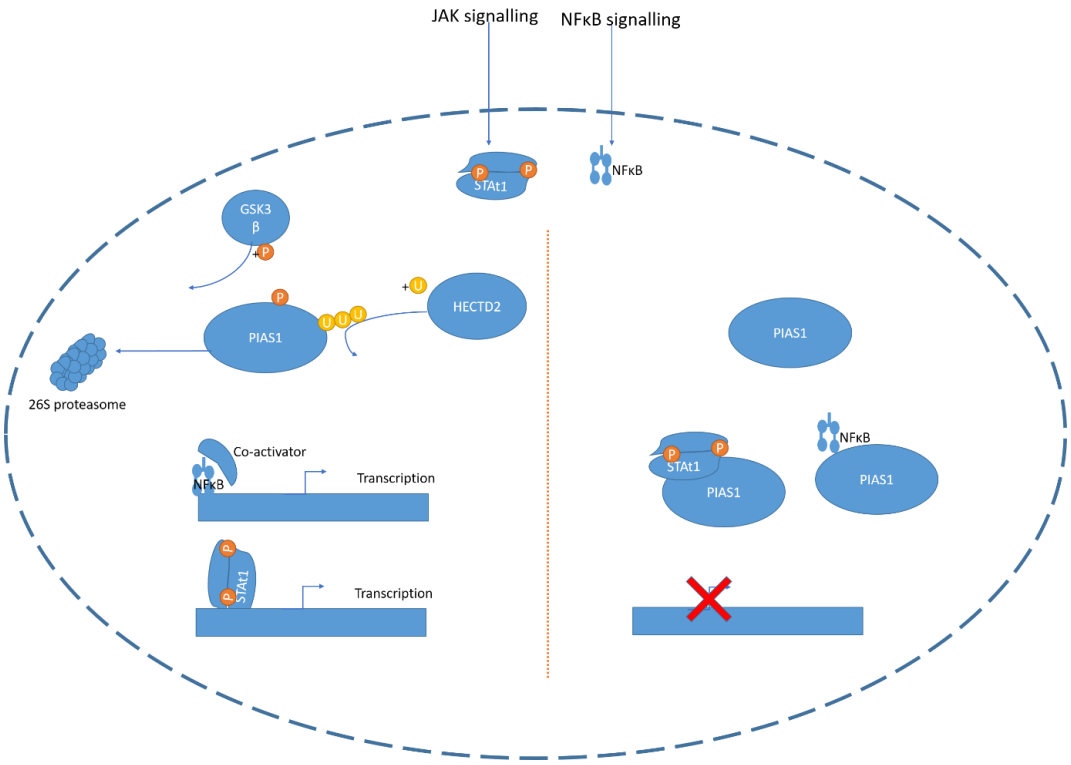

Figure 6.23 The interaction between HECTD2 and PIAS1 in JAK-STAT signalling and NF-κB signalling. PIAS1 binds to STAT1 in the nucleus and preventing binding to genes and activation of transcription. Similarly, PIAS1 binds NF-κB subunits preventing transcription of NF-κB target genes. HECTD2 acts to ubiquitinate PIAS1, this required phosphorylation of PIAS1, the ubiquitination of PIAS1 targets it for 26S proteasome mediated degradation.

6.8.3 mRNA expression of HECTD2 and PIAS1

The mRNA expression of *HECTD2* and the HECTD2 downstream target *PIAS1* was assessed in HPB-ALL and DND41 cells after 72 hours of treatment with a VXLD combination (figure 6.24). Expression was compared to cells treated with a solvent control.

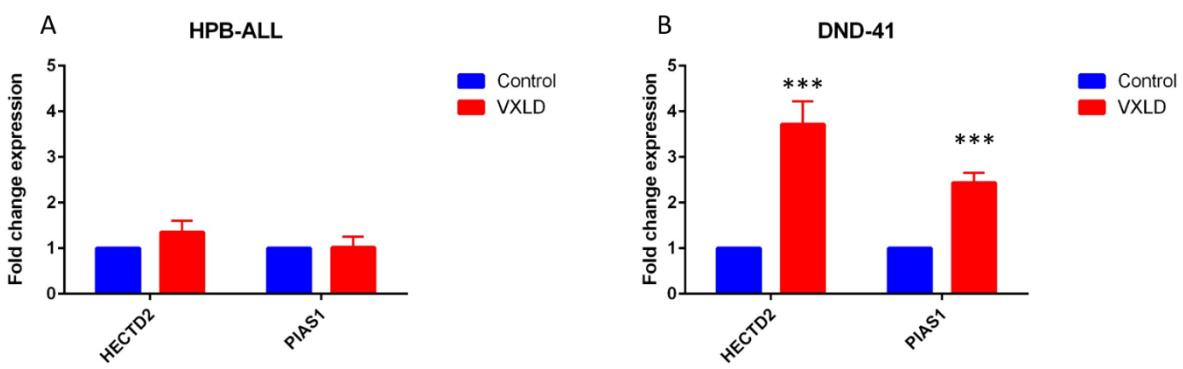

Figure 6.24 HECTD2 and PIAS1 gene expression in HPB-ALL and DND41 cells after 72 hours VXLD treatment. Significant differences in expression were detected by t-test (***p<0.001). Error bars represent standard error of the mean of 3 independent experiments.

There was no significant increase in *HECTD2* or *PIAS1* expression in HPB-ALL cells treated for 72 hours with VXLD. DND41 cells showed significant increase in both *HECTD2* and *PIAS1* expression after VXLD treatment.

6.8.4 Competitive assay

To establish if a reduction of HECTD2 gene expression led to decreased survival of HPB-ALL or DND41 cells, HECTD2 was knocked down using a shRNA vector with a GFP tag. Successful knockdown was confirmed at mRNA level with qRT-PCR, and the expression of PIAS1 was also measured upon HECTD2 knockdown (figure 6.25). To directly compare the fitness cells with BCL-X knockdown to cells without knockdown of HECTD2, shHECTD2 cells were mixed 1:1 with cells transduced with a non-targeting control shRNA (shNTC) tagged with RFP657. The shHECTD2 cell population was detected by GFP expression using flow cytometry and was compared to the RFP657 positive cells containing shNTC over time. The mixed cells were kept under standard culture conditions or were given VXLD. The percentage of cells is shown at the baseline (day of mixing) and after 1 week's culture (figure 6.26)

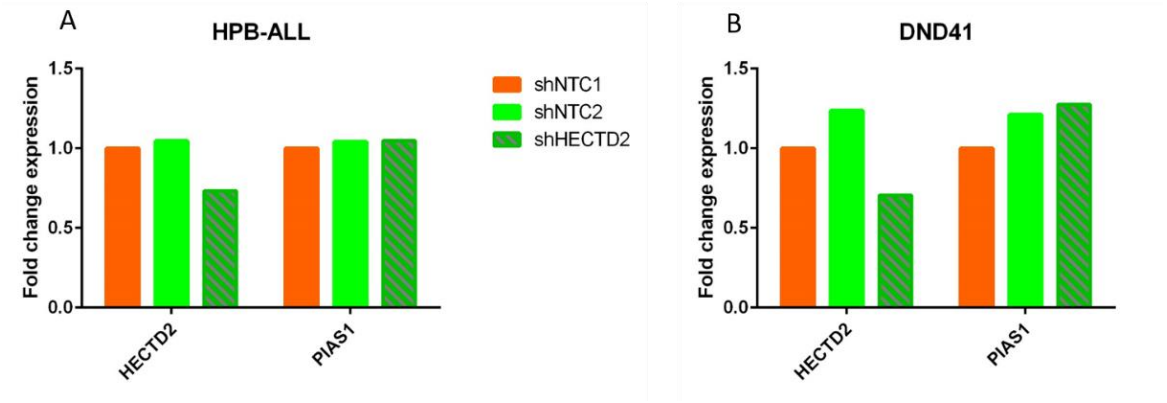

Figure 6.25 HECTD2 expression after knockdown with shRNA HECTD2 knockdown was confirmed by qRT-PCR in the HPB-ALL and DND41 cell lines. PIAS1 expression was measured in shHECTD2 transduced and shNTC cells. Results of a single experiment. N=1

HECTD2 expression was reduced in both DND41 and HPB-ALL but less than 2 fold. There was no change to PIAS1 expression in HPB-ALL after HECTD2 knockdown, but in DND41 an increase in PIAS1 expression was observed compared to shNTC1 cells. However, increased expression of PIAS1 was seen in shNTC2 cells.

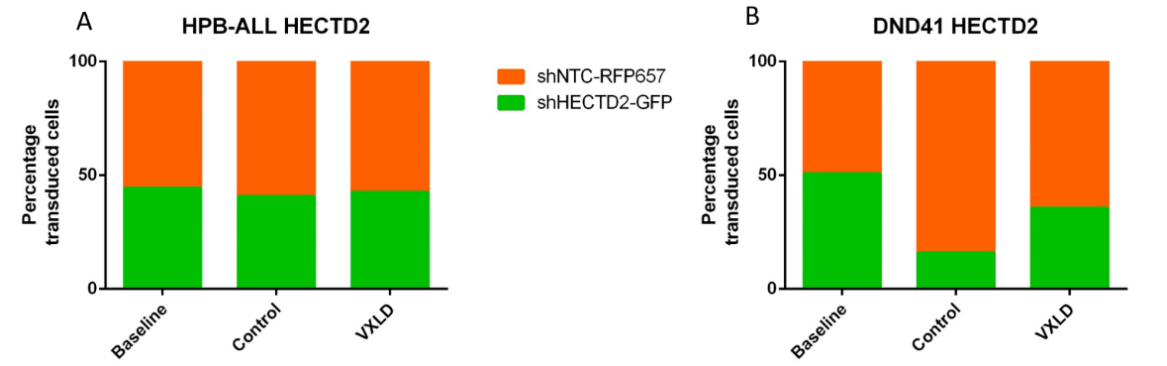

Figure 6.26 HECTD2 knockdown competitive assay results. Results of a competitive assay of HPB-ALL (A) and DND41 (B) cells with shHECTD2-GFP and shNTC-RFP657 at day of mixing and after 7 days standard culture (control) or with VXLD treatment (VXLD). N=1

There was no change in the relative abundance of shHECTD2 cells compared to shNTC cells in HPB-ALL in standard conditions or under VXLD chemotherapy. In DND41 shHECTD2 cells were competitively lost in both conditions, and to a greater extent under control conditions compared to VXLD treatment.

6.8.5 HECTD2 validation summary

HECTD2 was selected for further investigation based on screening data which demonstrated guides targeting *HECTD2* to be differentially depleted under VXLD treatment both *in vitro* and *in vivo. HECTD2* is a ubiquitin ligase, and ubquitinates *PIAS1.* The change in mRNA levels *of HECTD2* and *PIAS1* were assessed in two cell lines HPB-ALL and DND41 after 72 hours VXLD treatment. To check for a role for HECTD2 in T-ALL growth or survival under VXLD treatment and shRNA knockdown was performed. HECTD2 knockdown cells were compared directly with cells containing a non-targeting control shRNA both with the addition of VXLD chemotherapy and for comparison in standard culture conditions.

HPB-ALL did not show significant increase in *HECTD2* expression after 72 hours of treatment with VXLD. In DND41 cells I did observe a significant increase in *HECTD2* expression, which was accompanied by an increase in *PIAS1* expression.

DND41 and HPB-ALL also responded differently to HECTD2 knockdown despite a similar relative reduction in mRNA expression. No effect was seen in the fitness of HPB-ALL targeted with shHECTD2 compared to shNTC targeted cells, whereas there was a pronounced effect in shHECTD2 transduced DND41 cells which were competitively lost both with and without VXLD chemotherapy

6.9 Chapter discussion

This chapter has shown data derived from screen itself. To reflect the different sections of this chapter, the discussion has also been split into the following themes:

- the library coverage and read counts,
- how different genes identified fit into the context of important pathways,
- how genes were selected for preliminary validation,
- the conclusions from validation work for
    i. BCL2L1
    ii. HECTD2

6.9.1 Library coverage, read counts and data analysis

In vitro samples showed total library coverage ranging from 94.5 to 99.7% of the total library, demonstrating most of the library was retained from amplification of plasmid pool through various stages of screening including lentiviral, transduction and

puromycin selection. The screen was calculated to have 400 times coverage, a total of 31 million cells were taken for each time point-and ultimately around 31 million reads were required per sample. The two NextSeq runs were performed for the pooled samples giving a total of 800 million reads, split across the 26 samples this equates to nearly 31 million reads per sample. This did not account for any unmapped reads. Reads were only taken if they were an exact match, for each sample approximately 20% of reads were unmapped. Changing the stringency may increase total mapped reads, but since most of the library was covered this was unnecessary and the most stringent cut-off of exact sequences was used. The resulting data showed a guide distribution with a median read per guide of 200. Although below the recommended 400, this is still within what other similar screens report (Hart *et al*, 2017).

Each mouse received 2 million cells. When mice were harvested each mouse was treated as an individual sample, with enough PCR reactions to cover 31 million cells, equally nearly 31 million reads were performed for each barcoded mouse sample. There was substantial variation in the number of guides recovered from each mouse, some samples covered half the guides form the library where others had less than 5,000 guides. For this analysis all reads were summed across the same sample set, for future analysis it may be worth to cap some of the highest read counts for guides prior to pooling. Pooling the samples from treated mice and from control mice allowed the recovery of most of the guides from the library. It would be beneficial to do a subsampling analysis to see the optimum number of reads for the mouse samples when they are pooled, as with this strategy there is potential to drastically reduce PCR and sequencing costs.

6.9.2 Key genes/pathways implicated in VXLD chemo-resistance

Analysis of screening data highlighted roles for several different pathways including those depicted in figure 6.27- the proteasome, NFkB signalling, and the cell cycle. In addition to those depicted in figure 6.27: Ras signalling, the spliceosome and multidrug transporters were also identified.

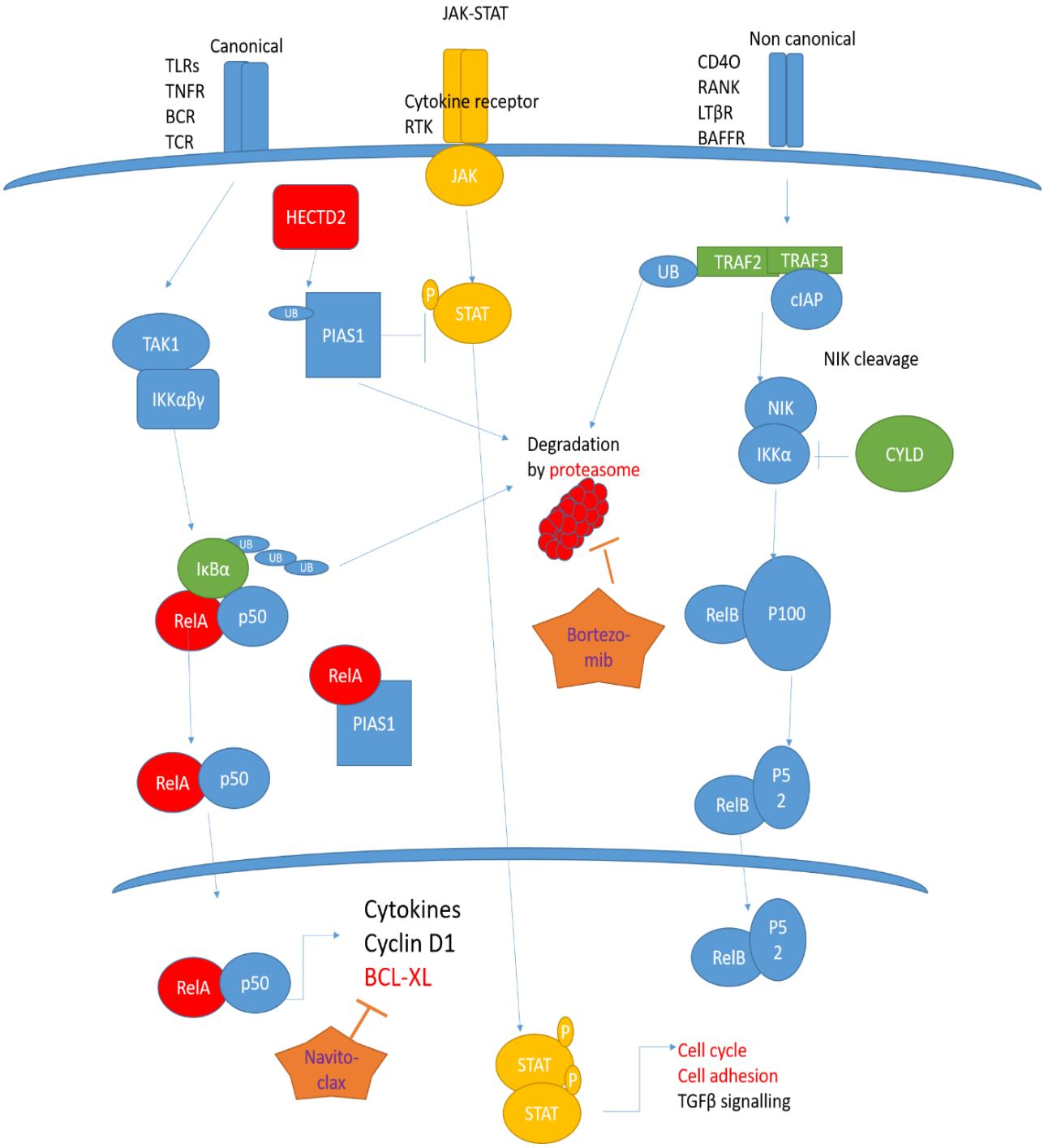

Figure 6.27 Summary of key targets differentially enriched and depleted under VXLD treatment The NF-κB (both canonical and non-canonical) and JAK signalling pathways and the genes that were found to be enriched or depleted with VXLD treatment. Genes with enriched guides are shown in green and genes with depleted guides in red. Downstream transcriptional targets are also indicated and coloured to indicate depletion. Potential drugs to inhibit these pathways are indicated in the orange boxes.

6.9.2.1 Multidrug transporter ABCC1

Guides targeting ATP Binding Cassette Subfamily C member 1 (ABCC1) were identified as differentially depleted during *in vitro* screening under VXLD treatment. Also known as multi-drug resistance protein 1, ABCC1 is known to confer resistance to many chemotherapeutics including daunorubicin and vincristine, and to contribute to progression of disease in T-ALL (Munoz et al., 2007, Winter et al., 2013). The identification of *ABCC1* provides support to the effectiveness of the screening approach taken to identify resistance mechanisms.

6.9.2.2 Cell cycle genes

Cell cycle pathways are mutated in 84% of T-ALL, mainly because of recurrent deletion of CDKN2A/B (Liu et al., 2017). P16 encoded by CDKN2A inhibits CDK4 and CDK6 , activating Rb proteins and block G1/S transition (Topacio et al., 2019). Several genes with known roles in cell cycle control were associated with resistance to VXLD therapy. The effectiveness of many drugs is cell cycle stage dependant. A simplified diagram indicating some of the key cyclins and kinase involved in the cell cycle is given in figure 6.27. Cell cycle arrest due to aberrant cell cycle control factors can generate resistance.

Cell cycle inhibitors such as Palbociclib (CDK4/6 inhibitor) are being used to treat a range of malignancies (Dickinson and Schwartz., 2009). Within my data, although CDK4 (cyclin dependent kinase 4) and 6 were depleted during screening they were not differentially depleted under VXLD therapy. On the contrary, a component of the anaphase promoting complex –Cell Division Cycle 26 (CDC26) and CCNA2 (cyclin A2, which binds CDK1 and CDK7)were differentially depleted , whereas *in vivo* as members of the mini chromosome maintenance complex (Marks et al.). MCM5, MCM6, MCM7 (which are involved in G1 to S progression) were differentially depleted. The different cell cycle phases these are found in may reflect differing drug pressures *in vitro* and *in vivo.* Work to clarify which phase of the cell cycle is most required for each of the chemotherapeutics used would be of benefit here.

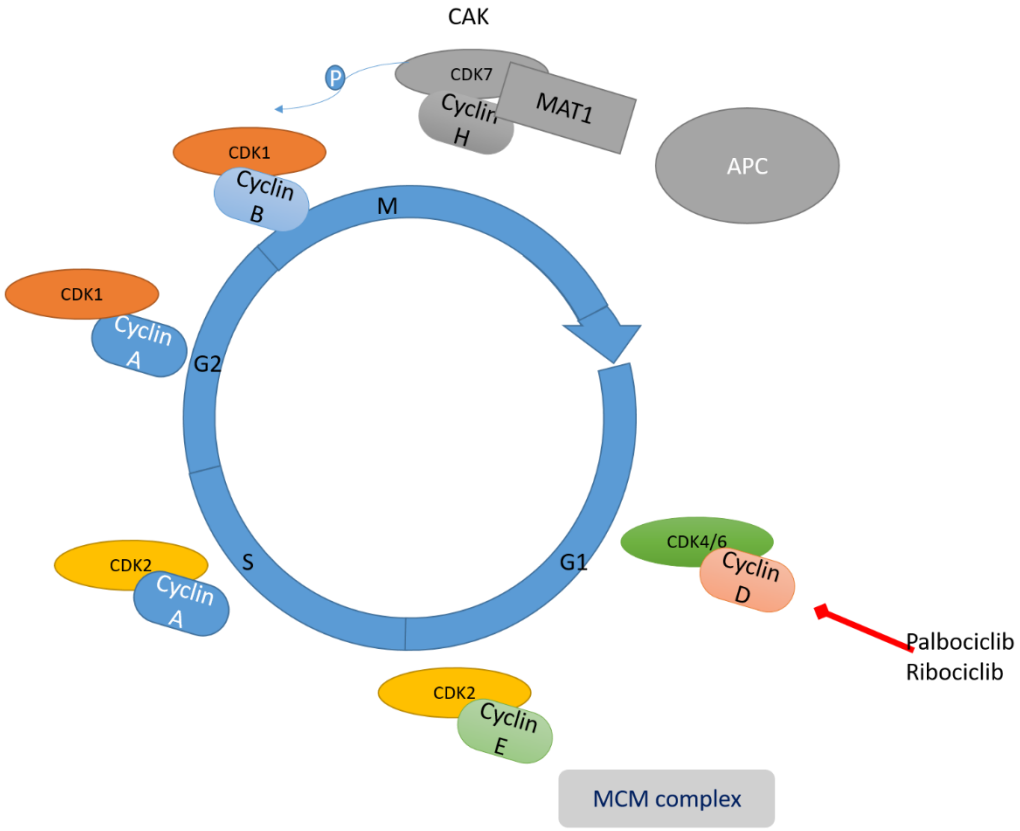

Figure 6.28 Simplified diagram of the cell cycle. The diagram highlights where the mini chromosome maintenance complex (MCM complex), cyclin A2 and cyclin dependant kinases (CDK) and cyclins appear in the cell cycle. During G1 the MCM complex acts as a scaffold for pre-replication complex. During the S phase the MCM complex forms part of a helicase responsible for unwinding DNA.

6.9.2.3 Ras signalling

DUSP4 scored as second highest differentially enriched guides in the *in vivo* screen (table 6.1). DUSP4 is a regulator of Ras signalling (Farooq and Zhou, 2004). As highlighted in the introduction-Ras signalling has already been implicated in chemo-resistance in T-ALL. Exome sequencing identified correlations between patients harbouring *KRAS* mutations and poor response to steroids (Li et al., 2016). In the same publication the authors show introduction of mutant NRAS into T-ALL cell lines alters steroid responsiveness. *KRAS* was also identified in this screen with *KRAS* targeting guides being differentially depleted with VXLD *in vivo*. The loss of guides targeting *KRAS* and enrichment of guides targeting negative regulator of Ras signalling DUSP4 indicate the importance of active Ras-signalling in driving resistance to VXLD therapy.

6.9.2.4 U2AF1 and splicing

U2AF1 was differential enriched in both *in vitro* and *in vivo* VXLD screening. U2AF1 encodes a component of the spliceosome. *U2AF1* mutations are associated with alternative splicing of inflammatory and immune related genes and ultimately are associated with a poor outcome in AML (Saygin et al., 2018) (Smith et al., 2019). Although *U2AF1* mutations are uncommon in ALL thousands of aberrant splicing events (compared to those in normal B-cells) have been detected in B-ALL, with many of the alternatively spliced genes being known cancer drivers (Smith et al., 2019). In T-ALL upregulation of H/ACA ribonucleoprotein assembly factor (SHQ1) which modifies spliceosomal small nuclear RNAs is important for cell survival (Su et al., 2016). T-ALLs express high levels of SHQ1 which is important in maintaining splicing of oncogenic driver MYC. Depletion of SHQ1 impaired widespread RNA splicing (including MYC) and induced T-ALL cell death (Su et al., 2016, Su et al., 2018).

Alternative splicing is also known to contribute to chemo resistance. For instance, alternate splicing of tumour protein p53 related proteins- tumour protein p63 and tumour protein p73 produces dominant negative forms that contribute to chemo resistance (Müller et al., 2006). Furthermore, alternative splicing of BCL-2 family member BCL-X produces long and short isoforms with opposing functions in apoptotic regulation (Chao and Korsmeyer, 1998). BCL-X_L is explored further in

section 6.7. The identification of U2AF1 prompts further investigation into the role of alternative splicing in resistance to VXLD therapy.

6.9.2.5 CYLD, HECTD2, the proteasome and ubiquitination

Many genes involved in the process of ubiquitination (and proteasomal degradation) have a role in carcinogenesis (Mansour, 2018). FBXW7 (the negative regulator of NOTCH1) for instance, is frequently mutated in T-ALL and is a ubiquitin ligase (O'Neil et al., 2007). Since the advent of proteasome inhibitors and their journey to the clinic there has been further interest into ubiquitination and the proteasome (Horton et al., 2006).

Guides targeting HECT Domain E3 Ubiquitin Protein Ligase 2 (*HECTD2)* were found to be only 1 of 6 differentially depleted both *in vitro* and *in vivo* and was of particular interest due to its ubiquitination function (Rotin and Kumar, 2009). HECTD2 was one of two genes selected for further validation (see section 6.8).

Guides targeting deubiquitinating enzyme *CYLD* were differentially enriched *in vitro*. *CYLD* originally identified in familial cylindromatosis is a known tumour suppressor (Bignell et al., 2000, Massoumi, 2010). CYLD regulates several signalling pathways by deubiquitinating Lysine 63 residues including TCR component leukocyte C-Terminal Src kinase and cell cycle regulator polo-like kinase 1 (PLK1) (Massoumi, 2010). Both of which that are implicated in leukaemia-genesis (Shi et al., 2020, Wang et al., 2015). CYLD is also a negative regulator of NF-κB signalling through deubiquitination of TNF receptor-associated factor 2 (TRAF2), TNF receptor-associated factor 6 (TRAF6) and NF-kappa-B essential modulator (NEMO) (Sun, 2010).

CYLD has been previously associated with sensitivity to various anti-cancer agents including histone deacetylate inhibitors and gemcitabine (Yin et al., 2016, Kotantaki and Mosialos, 2016). Of particular relevance it has been associated with 2 of the 4 induction regimen drugs: Daunorubcin (indirectly through its role in nuclear factor kappa-light-chain-enhancer of activated B cells (NFkB) regulation) and dexamethasone (Wang et al., 1996, Urbanik et al., 2011, Bonapace et al., 2010). Dexamethasone treatment of ALL cells triggered autophagy-dependent cell death, involving necroptosis, and this required CYLD and Receptor-interacting protein (RIP-1) kinase (Bonapace et al., 2010). My data suggests this may also be the case when dexamethasone is given as part of a 4-drug induction.

6.9.2.6 Nuclear factor kappa-light-chain-enhancer of activated B cells signalling components

CYLD was not the only NF-κB associated gene to be enriched under VXLD treatment. TNF receptor-associated factor 2 (*TRAF2*), TNF receptor-associated factor 3 (*TRAF3*) and NFKB Inhibitor Alpha (*NFKBIA) also* appear in the top 20 most differentially enriched with VXLD treatment *in vitro.* Elements of the NF-κB pathway are required for response to chemotherapeutics. NFKBIA an inhibitor of NF-κB mediated inflammation is induced by dexamethasone (Reddy et al., 2009). Altered regulation in NF-κB signalling could be responsible for resistance to the VXLD combination.

6.9.3 Selection of genes for validation

The relevance of *in vitro* only genes may not hold true in an *in vivo* setting and conversely *in vivo* only targets could make validation a lengthier process as it requires co-cultures or *in vivo* modelling. Therefore, the first targets taken forward for validation were identified both *in vitro* and *in vivo*. The key aim of the screen was to identify genes conferring resistance to chemotherapy, for this reason initially focus was on where guides were depleted with VXLD treatment. From the 6 genes that were depleted both *in vitro* and *in vivo*, the first gene selected was *BCL2L1*. *BCL2L1* represented a prime candidate for T-ALL therapy since it was a known apoptotic regulator and had many interactions with other differentially changed genes in STRING interaction analysis. The second gene selected was *HECTD2*. As a ubiquitin ligase it is likely to have connections with the proteasome pathways, which were enriched among depleted genes in VXLD screening.

6.9.4 Validation of BCL2L1

6.9.4.1 BCL-X mRNA expression after VXLD treatment

A single 72-hour treatment with VXLD treatment significantly increased mRNA levels of BCL-X in both HPB-ALL and DND41, this could indicate that in response to VXLD treatment cells are upregulating BCL-X_L expression in order to protect against drug induced cell death. It remains to be seen how mRNA levels change over the course of drug treatment. Since the primers used for qRT-PCR did not distinguish between long and short isoforms, it remains unproven whether the increase in transcript is due to increased BCL-X_L as opposed to the shorter pro-apoptotic form BCL-X_S. Specifically measuring levels of the short and long forms would help address this and give an idea of the balance of the two, and if this differs with drug treatment.

Transcript levels are not always reflective of protein levels, so moving forward protein levels should be analysed, potentially over a time course. Examining levels of BCL-$X_{L/S}$ in isolation may not be enough to fully understand the situation, a greater understanding of BCL-X and the interaction of BCL2 family members via BH3 profiling may give provide additional crucial information.

6.9.4.2 Treatment of HPB-ALL and DND41 with pan BCL2 inhibitor ABT-737

The maximum reduction in fluorescence by resazurin assay was less than 20% in HPB-ALL, although like in DND41 addition of VXLD shifted the dose response curve to the left. The shift in response in DND41 was small, based on screening data we may have anticipated a greater effect of combining BCL-XL inhibition with VXLD treatment. Extending the concentration range of VXLD in relation to ABT-737 might highlight a range with a larger increase in effect. Both DND41 an HPB-ALL were less sensitive to ABT-737 than murine Tel-Jak2 driven T-ALL (90% reduction cell viability at 0.5µM) (Waibel et al., 2013). ABT-737 treatment alone is not effective in sub micromolar range but VXLD treatment increases response to ABT-737.

The treatment of DND41 cells with ABT-737 induced apoptosis but there was no increase in apoptosis with addition of VXLD chemotherapy at 24 hours, despite the significant effect of VXLD addition indicated in resazurin assays. No apoptosis (above that seen in control) was observed in ABT-737 treated HPB-ALL. The lack of increase apoptosis when combining VXLD and ABT-737, despite dose response shift with VXLD could be due to:

- alternative methods of cell death are involved
- increased effect of VXLD is due to proliferative/cell cycle changes
- drugs act sequentially instead of concurrently
- we are not looking in the correct time window

It is possible that BCL-X_L is not being adequately inhibited by ABT-737. ABT-737 binds to BCL2, BCL-X_L and BCL-W, but displacement of BH3 only proteins by ABT-737 is lower in BCL-W and BCL-X compared to BCL2 (Rooswinkel et al., 2012). ABT-737 appears far more effective against BCL2, and it is suggested that BCL-X_L may even contribute to ABT-737 resistance (Rooswinkel et al., 2012). A BCL-X_L specific inhibitor such as A-1331852 should be assessed in combination with VXLD chemotherapy in T-ALL (Leverson et al., 2015).

Secondly, since it has been published in T-ALL that inhibition of mTORC1 lowered MCL-1 levels and sensitised cells to orally bioavailable form of ABT-737- ABT-263 (known as Navitoclax) (Dastur et al., 2019. Analysing the expression of MCL-1 and mTORC1 activity in HPB-ALL and DND41 may explain their response to ABT-737.

6.9.4.3 BCL-X knockdown impairs leukaemic cell fitness especially under VXLD treatment

Knockdown of BCL-X (both long and short isoforms) with shRNA in HPB-ALL showed that these cells have reduced fitness compared to cells without BCL-X knockdown. This effect was amplified by the addition of VXLD chemotherapy. In DND41 cells knockdown of BCL-X had only minimal effect on the fitness of the cells, until VXLD treatment was applied. Knockdown cells were rapidly lost in a competitive assay with VXLD treatment.

Since the ultimate goal would be to inhibit targets that drive chemo-resistance, a knockdown experiment was performed. As proof of principle induced overexpression of BCL-X_L and determining increasing resistance to VXLD (as a combination or individual agents) would help solidify the role of BCL-X_L in resistance to induction therapy

6.9.4.4 BCL2L1 validation summary

BCL-X knockdown impairs leukaemic cell fitness especially under VXLD treatment should biological replicates confirm this trend this would provide evidence for the role of BCL-X_L in cells surviving VXLD chemotherapy in HPB-ALL and in doing so confirm the validity as a true target identified through this work. Future work will see if inhibiting BCL-X_L across other T-ALL samples including patient and patient derived xenograft samples.

6.9.5 HECTD2 validation

6.9.5.1 HECTD2 transcript levels after VXLD treatment

HPB-ALL did not show significant increase in *HECTD2* expression after 72 hours of treatment with VXLD. In DND41 cells I did observe a significant increase in *HECTD2* expression, which was accompanied by an increase in *PIAS1* expression. It is still untested (due to time constraints) what occurs on a protein level. Protein levels of HECTD2 could be elevated through alternative means than mRNA upregulation for instance via increased protein stabilisation.

6.9.5.2 HECTD2 knockdown and competitive assay

DND41 and HPB-ALL responded differently to *HECTD2* knockdown despite a similar relative reduction in mRNA expression. Confirmation of protein level knockdown may shed light on this. If insufficient knockdown of HECTD2 remains a cause for concern an alternate method to reducing HECTD2 protein could be considered such as a CRISPR based approach. Generation of *HECTD2* CRISPR knockout in HPB-ALL and subsequent investigation into cell survival, proliferation and response to VXLD may be required to validate this target.

6.9.5.3 HECTD2 summary

At this point HECTD2 cannot be confirmed or ruled out as important in proliferation or maintenance of HPB-ALL cells, nor in the resistance of HPB-ALL to chemotherapy. If repetition of HECTD2 knockdown in DND41 confirmed the results achieved so far, we could infer a role of HECTD2 in DND41. Cell cycle and cell death should be assessed to identify why HECTD2 knockout cells were competitively lost.

HECTD2 is part of wider area of interest in ubiquitination and proteasome mediated degradation that was highlighted during screening as important in resistance to therapy.

6.10 **Chapter summary**

The aim was to identify genes that confer sensitivity or resistance to VXLD chemotherapy.

- Several genes were identified as having potential roles in resistance to chemotherapy
- *BCL2L1* and *HECTD2* were further investigated for their roles.
- *BCL2L1* validation work helped give further evidence towards its role in chemo resistance
- Pathways were identified as having potential roles to induction resistance

This screen has highlighted key genes in interconnecting signalling pathways that are of importance in response to chemotherapeutics. Some pathways were already implicated in resistance in T-ALL(such as Ras signalling and multidrug transporters) and the screen provides further support for their role, and some of which have not necessarily been studied in the context of T-ALL previously (like NFkB). By better

understanding these genes and pathways, we can learn more about how resistance develops, and therefore how to overcome it.

Chapter 7. Discussion

This final chapter takes an overview of the whole project. Several factors are addressed:

- how the work relates to similar studies and the unique parts afforded by the approach taken
- the importance and wider impacts of this work from both data that was generated, and the methodology used
- limitations to the approach and potential amendments
- how this work can be continued

Lastly the chapter and this thesis concludes by addressing the following question:

- have the project aims been met?

7.1 Comparison of this work to similar studies

There are different approaches used to identify drug resistance mechanism from screening-based approaches using RNAi or more recently with CRISPR technologies, to comparing RNA, protein or even chromatin in treated and non-treated settings. Identification of resistance mechanisms is often performed in the context of a single drug, and there are limited publications on such works in T-ALL. Three studies in T-ALL which focus on identification of drug resistance in T-ALL are discussed and how the approaches differ from the work presented in this thesis.

7.1.1 Exome and whole genome sequencing of patients and correlation with clinical steroid response

Exome and whole genome sequencing of T-ALL patients was performed in order to identify mutations. Mutation data was then put in context of clinical data and steroid responsiveness. This approach can identify pathways where mutations play a key role in resistance but may miss genes and pathways where resistance stems from transcriptional changes, splicing, methylation or protein stabilisation. They show JAK1 and KRAS mutations to be associated with steroid resistance and poor outcome (Li et al., 2016).Interestingly they also show steroid resistance to be associated with MEK-ERK activation , and upregulation of MCL1 and BCL-X_L(Li et al., 2016).These findings are in keeping with what I observe with both Ras signalling

and BCL-X_L being identified (see 6.7 and 6.9.2) taking what initially noted in the context of steroid response, and indicating a wider role in resistance to induction therapy.

7.1.2 Differential expression analysis from *in vivo* treated samples

A study published by Samuels et al describes the use of induction regimen drugs *in vivo* to produce resistance in patient derived xenograft material, and the subsequent identification of changes in gene expression compared to xenografts from non-treated animals (Samuels et al., 2014b). Gene expression profiling identified differences in lipid biosynthesis (particularly sterols) and carbohydrate metabolism. They then use simvastatin an inhibitor of 3-hydroxy-3-methyl-glutaryl-coenzyme A reductase (HMGCR -a rate-limiting enzyme in cholesterol synthesis) and a drug used in the treatment of high cholesterol to treat xenografts (Pietro et al., 1989). Although they study concluded simvastatin did not ultimately sensitise cells to VXLD treatment, lipid signalling may still play a role in resistance to VXLD therapy, and my data similarly showed sphingolipid signalling among pathways depleted with VXLD treatment.

Whilst I took inspiration from this work in the development of the *in vivo* induction regimen treatment, this approach to screening has many drawbacks. Generation of resistant cells was required for analysis and this was not achieved for all samples. Patient derived samples are potentially highly clonal, and you only determine average gene expression. Different clones can possess different mutational backgrounds with varying gene expression signatures, which can make establishing if changes in bulk RNA expression is due to different clonal representation or due to compensatory signalling in cells due to drug exposure. Gene expression was measured at a single timepoint, the levels of expression may however change during drug treatment, leading to issue about selecting an appropriate time window. This approach focuses on expressed genes, there are however many mechanisms of altering gene function. A CRISPR based approach has a much wider scope.

7.1.3 Genome wide CRISPR screen with asparaginase treatment

Perhaps the most similar screen to my work is the screen performed by Hinze et al, 2019. They aimed to identify pathways involved in resistance to one of the induction regimen agents, namely asparaginase. They performed a genome wide CRISPR screen on the asparaginase resistant T-ALL cell line CCRF-CEM with asparaginase

treatment to identify synthetically lethal targets. They identified depletion of negative regulators of Wnt signalling Naked cuticle 2 (NKD2) and Leucine Rich Repeat Containing G Protein-Coupled Receptor 6 (LGR6) under asparaginase treatment and concluded that Wnt pathway activation is required for sensitisation to asparaginase (Hinze et al., 2019).

Since my drug treatment also includes asparaginase, I checked to representation of Wnt pathway components to verify if any of the mentioned depleted genes in their study were similarly depleted with VXLD treatment. My findings were not consistent and neither Wnt pathway components nor Asparagine synthetase (ASNS) (used as a positive control in their study) appeared in my data. HPB-ALL is however sensitive to asparaginase. Hypermethylation of ASNS leads to decreased ASNS expression and greater asparaginase sensitivity (Touzart et al., 2019). HPB-ALL has been shown to have a highly methylated ASNS promoter and low ASNS levels (Serravalle et al., 2016). With an already highly methylated ASNS gene- no functional impact of knocking out ASNS is to be expected in this setting. They also present a role for the inhibition of proteasomal degradation in resistance to asparaginase, similarly in my work I observe a differential depletion under VXLD of guides targeting the proteasomal pathway.

The work presented within this thesis is differentiated from the work published by Hinze et al by one crucial factor- they present data from a single agent screen. This work is unique in that it uses multi-agent chemotherapy.

7.1.4 Unique points of this work

There are only a handful of screens published in the field of T-cell acute lymphoblastic leukaemia, and even fewer where the focus is on identification of mechanism of drug resistance. Using CRISPR technology over older technologies such as RNAi, allows for consideration of a much wider range of targets, not just those controlled by regulation of gene expression. The most crucial difference is the use of multi-agent chemotherapy which better reflects the clinical scenario for childhood ALL treatment as opposed to a single agent.

7.2 Contributions to our current understanding of T-ALL

The ultimate goal for treatment of relapse and refractory T-ALL is to identify an actionable target that can be used with concurrent chemotherapy. Although this is still a work in progress, through this project we have progressed our understanding of

resistance to induction therapy and identified potential targets of interest. The creation of a treatment regimen reflecting induction therapy combined with CRISPR screening has set a new standard for investigating resistant disease. Many essential steps have been accomplished towards a better understanding and hopefully ultimately a better treatment of T-ALL.

7.2.1 Pathways identified

Genes with a role in resistance to VXLD chemotherapy have been identified from the differential enrichment and depletions of sgRNAs under drug treatment. Lists of genes identified were also analysed to highlight pathways of interest. The wider impact of some of the pathways mentioned in the preceding chapter is given below.

7.2.1.1 Multi-drug transporters

Winter *et al* previously demonstrated that vincristine resistance was mediated by ABCC1, the upregulation of *ABCC1* also resulted in resistance to daunorubicin and prednisolone but not asparaginase (Winter et al., 2013). In cases of ABCC1 mediated resistance to chemotherapy- asparaginase could still be used in any new combinations and plays an ever more important role in conventional ALL regimens.

7.2.1.2 Cell cycle

Inhibitors of cell cycle control genes have entered the clinical arena. With the ongoing trial of a CDK4/6 inhibitor Palbociclib in KMT2A (MLL) re-arranged leukaemias, cell cycle inhibition has generated therapeutic interest (NIH, 2019). Palbociclib treatment of T-ALL cell lines dramatically reduced proliferation *in vitro* and delayed disease progression *in vivo* (Sawai et al., 2012). Another CDK4/6 inhibitor Ribociclib was investigated alongside chemotherapeutics in T-ALL samples. Ribociclib was an antagonist when given alongside asparaginase and doxorubicin, but synergistic with dexamethasone-highlighting the need to understand the role of the cell cycle under combination chemotherapy (Pikman et al., 2017).

The screen identified CCNA2 cyclin A2 (which binds CDK1 and CDK7). In this case- an inhibitor such as Dinaciclib (CDK1, CDK2, CDK5 and CDK9 inhibitor), may be more beneficial than CDK4/6 inhibitor Palbociclib.

7.2.1.3 Ras signalling

The identification of Ras signalling has direct relevance to the current treatment of relapsed and refractory T-ALL- due to the ongoing SeluDex trial. The SeluDex trial is

testing the safety and then the efficacy of selumetinib (a MEK inhibitor) with dexamethasone in relapsed and refractory ALL patients (children and adults) with Ras pathway mutations (NIH, 2019). This trials has stemmed from work showing *in vitro* and *in vivo* ALL samples with Ras pathway mutations are sensitive to MEK inhibition, and that a synergism if observed between selumetinib and dexamethasone (Matheson et al., 2019, Irving et al., 2014).

7.2.1.4 Proteasome and ubquitination

The reversible 26S proteasome inhibitor Bortezomib was first approved for treatment of multiple myeloma in 2003 (Field-Smith et al., 2006). Bortezomib has displayed synergism with dexamethasone and additivity with other chemotherapeutics in ALL *in vitro* and was recently trialled with re-induction therapy in high risk ALL patients at relapse (Horton et al., 2006) (Horton et al., 2019). The trial had encouraging response rates for T-ALL at 68% (Horton et al., 2019). The role of the proteasome in resistance therefore has direct relevance to the current clinical advances. The screening data would suggest that proteasome inhibition may overcome resistance to induction in T-ALL-which may explain the favourable response rates seen clinically. An ongoing trial will assess the benefit of adding Bortezomib to combination chemotherapy in newly diagnosed childhood T-ALL patients, it will be interesting to see if this will reduce the percentage of patients with high MRD at end of induction (NIH, 2019).

Unfortunately, promising results clinically has not been without toxicity. Substantial toxicity has been noticed with Bortezomib use with greater than 55% of patients having Grade 3 or 4 neutropaenia or thrombocytopaenia, non-haematological toxicities included gastrointestinal symptoms, metabolic abnormalities and infections (Horton et al., 2019). Development of inhibitors against specific ubiquitin ligases, could provide an alternative to proteasome inhibition and could help reduce toxicity. Using the generated screening data to devise a proteomic based approach to characterise ubiquitination in response to induction treatment could identify more specific targets, and provide alternatives to proteasome inhibition.

7.2.1.5 BCL-X_L

The apoptotic regulator BCL-X was identified through screening and has subsequently been shown to be important in helping cells survive VXLD treatment in two T-All cell lines. BCL-X_L is readily targetable with drugs, some of which have

already undergone clinical testing. Further investigations will test the hypothesis that concurrent treatment with BCL-X inhibitors can be used to treat induction regimen resistant T-ALL.

7.2.2 Methodology

This work has provided more than just the data output, it has set out a framework for similar studies.

We have seen how combinations of drugs can be selected *in vitro* via individual agent cytotoxicity assays and combination drug matrices. This work has demonstrated the complexity of selecting appropriate doses of chemotherapeutics when using them in combination therapies, and it shows the potential of being guided by clinical pharmacokinetics to select the optimum drug ratios.

We have established a VXLD treatment regimen in Rag2$^{-/-}$ gamma c$^{-/-}$ mice that reduces leukaemic burden and extends the lifespan of engrafted mice. The *in vivo* induction regimen model can be of great use in a range of different contexts from comparing VXLD backbone to new therapies, to generation of VXLD resistant samples.

We show an established screening protocol from introduction of library right through to next generation sequencing results. The screening stages and planning involved is of use to other future screens be they CRISPR or RNAi, genome wide or targeted.

7.3 Study limitations and suggested modifications

Despite the success of this work, one must remain mindful of the limitations to the work and of the changes that could improve the work further.

7.3.1 Replicates

One of the limitations of my study is the lack of replicates, since this limits the meaningful statistical analyses that can be performed and increases the risk of false positive results. Whilst this is rectifiable given additional time and funding *in vitro*, *in vivo* this requires the use of many additional animals- which is of concern from an ethical standpoint.

As our ability to model the complex interactions occurring between leukaemia and the niche, moving out of mice and into ex vivo models will allow a more ethical way of conducting large screens with replicates. An alternative strategy is to firstly perform

genome wide screening *in vitro* and follow this with a smaller targeted *in vivo* screen. Smaller libraries allow for easier library coverage and more replicates whilst keeping the number of animals required low. Individual animals can then be used as replicates and do not require combined analysis for coverage. The drawback of preforming *in vitro* screening initially is you risk missing out on niche specific targets. To mitigate this effect potential niche related targets should be derived from other sources (such as analysis of compartmental specific expression).

7.3.2 Interpretation of patient drug exposure

The second key consideration is the doses of each drug in VXLD used. Incorrect scaling of the drugs can lead to identification of resistance genes associated with a single predominating drug. Whilst we took time to try an appropriately select drug concentrations comparable to patient plasma C_{max} we did not consider total drug exposure (area under the curve). Adjusting dosing to better reflect the total drug exposure levels found clinically, could further improve our model of induction therapy.

7.3.3 Considering toxicity

We have yet to establish how the addition of drugs to a VXLD backbone may increase toxicity, both in our *in vivo* model and clinically. Drugs that have been trialled in a clinical setting will have known toxicity profiles and may have been used alongside chemotherapy, for these we can form predictions. For newer agents predicting toxicity (especially in combination therapy) may prove difficult. Integrating screening information on a range of non-malignant cells, could help us avoid targets with potential for high toxicity. Toxicity of new compounds could also be measured in combination with VXLD in our *in vivo* VXLD model.

7.4 Future work

The screen has generated vast amounts of data. Moving forward there are many alternate routes you could follow; I therefore present two key areas moving forward. Firstly, to conclude the validation work on BCL-XL to finalise had have a proven successful target. The second is to integrate the screen results with other data, which will help strengthen the current work and help focus future experiments.

7.4.1 Finalise validation of BCL-XL

To date, BCL-X knockdown and competitive assays have been performed in two T-ALL cell lines HPB-ALL and DND41, with expression measured at RNA level for

both. In addition, BCL-X expression should be assessed at a protein level. The effect of BCL-X specific inhibitor A-1331852 in HPB-ALL and DND41 will be assessed by resazurin assay and annexin v staining with and without VXLD. Thus far the effect of BCL-XL knockdown has been assessed, to help solidify the hypothesis that BCL-XL drives chemo-resistance the opposite should be performed. Overexpression and subsequent assessment of chemo-resistance should be performed.

After completion of validation in these two cell lines, the validation will be expanded with a panel of T-ALL cell lines of differing genetic backgrounds. Lastly, the role of BCL-X should be assessed in patient derived material. PDX material transduced with shRNA vectors against BCL-X and NTCs could be injected into mice and then *in vivo* VXLD treatment applied to determine if BCL-X deficient cells are outcompeted. Response to BCL-X inhibitors should also be assessed in an *in vivo* setting in combination with VXLD treatment.

BCL-X_L is part of a family of apoptotic regulators, although BCL2L1 targeting guides were the most differentially depleted in HPB-ALL cells this does not discount a role for of BCL2 family members. Expanding the research into other BCL2 family members would be of benefit, since not all T-ALLs may respond to BCL-X_L inhibition and this could also be of benefit when considering mechanism of resistance to pharmacological inhibition of BCL-X_L.

7.4.2 Integrate screen with other data

Many other successful screening strategies have benefitted from multiple data types feeding into the analysis and interpretation of results. The screen has generated vast amounts of data. To help filter and select potential drug targets, RNA sequencing of T-ALL patients will be used to identify changes in gene expression found in patients with relapsed and refractory ALL compared to those that respond well to induction therapy.

Many other successful screening strategies have benefitted from multiple data types feeding into the analysis and interpretation of results. The screen has generated vast amounts of data. To help filter and select potential drug targets, RNA sequencing of T-ALL patients will be used to identify changes in gene expression found in patients with relapsed and refractory ALL compared to those that respond well to induction therapy.

7.5 **Conclusions**

The key aims of all this work have been met and this work has made significant progress towards the goal to identify a therapeutically actionable target to treat relapsed and refractory T-ALL that can be implemented with concurrent chemotherapy. The aims were met as follows:

- HPB-ALL was identified as a suitable cell line for screening, it fits desired characteristics for a diploid cell line, with patient relevant genetic aberrations and engrafts in mice to produce a systemic disease (chapters 3 and 4)
- A matrix assay combined with clinical information regarding plasma C_{max} of drugs helped select appropriate doses of each induction drug in vitro (chapter 3)
- An *in vivo* VXLD dosing regimen that is tolerable and efficacious at reducing leukaemic burden was established (chapter 4)
- Each process in performing the screen from lentivirus generation through to cleaned pooled PCR product was checked and optimised (chapter 5)
- MAGEcKFlute was used to identify differential enrichment and depletion of guides under VXLD treatment, from which genes and pathways associated with resistance to VXLD chemotherapy were identified (chapter 6)

Overall, this CRISPR screen has provided much needed insight into resistance to induction therapy in T-ALL and is unique in its incorporation of all 4 induction regimen drugs.

Appendix A Intersected gene lists

Differentially enriched genes (intersection of *in vitro* and *in vivo* screening)

ACADSB ACOX1 ATXN7 BRD8 CAPN9 CHST13 COX17 CPD CXCR4 DLGAP2 EFCAB6 EIF4E FAM104A GPHB5 GRID1 GTPBP2 HEATR3 HIC2 IPO8 KCNC1 KLRG1 MARCH5 MIS18A NDUFS8 OR1L8 PAEP PDE6A POLE PPP1R1C PSMA6 RNF145 RPL38 RPS10 RYR3 SEC23IP SFMBT1 SLCO1B7 SNRPD3 SSR1 TAF5L TIRAP TRAP1 TXN U2AF1 UBA6 VAT1L VRK3

Differentially depleted genes (intersection of *in vitro* and *in vivo* screening)

BABAM1 BCL2L1 CTU1 GABBR2 HECTD2 ZFP69

Appendix B Published abstract

POSTER SESSION II: ACUTE LYMPHOBLASTIC LEUKEMIA – BIOLOGY & TRANSLATIONAL RESEARCH

PS933 DISCOVERING PATHWAYS INVOLVED IN RESISTANCE TO INDUCTION THERAPY IN T-ALL TO TREAT REFRACTORY AND RELAPSED DISEASE

Beckett, M.[1]; Shi, Y.[1]; Blair, H.[1]; Nakjang, S.[1]; Tirtakusuma, R.[1]; Szoltysek, K.[1]; Krippner-Heidenreich, A.[2]; Heidenreich, O.[2]; van Delft, F.W.[1]

[1]Northern Institute for cancer research, Newcastle University, Newcastle upon Tyne, United Kingdom

[2]Haemato-oncology, Prinses Máxima Centrum voor kinderoncologie, Utrecht, Netherlands

HemaSphere: June 2019 volume 3 Issue S1 p420

Background:

Survival for acute lymphoblastic leukaemia has increased over the last 50 years giving us around 80% survival in paediatric patients. These good results can be attributed to the refinement and response driven administration of intensive chemotherapy regimens. Despite the overall good survival, for patients with relapsed or refractory disease the outcome remains poor. Vincristine, Dexamethasone, Asparaginase and Daunorubicin (VXLD) form the cornerstones of T-ALL induction therapy. Response to induction therapy is predictive for outcome. Identifying pathways that contribute to resistance to induction chemotherapy will help identify novel drug targets that could improve the efficacy of treatment for patients with poor response to current therapy.

Aims:

We aim to identify new drug targets in pathways involved in resistance to improve remission rates and outcomes for patients with refractory and relapsed T-ALL.

Methods:

We use an orthotopic xenograft model of T-ALL and a four-drug treatment regimen based upon current T-ALL therapy to mimic the clinical setting. T-ALL cells were transduced with a genome wide knock out library prior to long term *in vitro* culture or intra-femoral injection into immunocompromised mice. T-ALL cells were harvested from cultured cells and from murine bone marrow to extract DNA for PCR amplification of guide containing regions. Next generation sequencing was used to determine representation of guides after VXLD treatment. The population of guides of cells retrieved from drug treated cells was compared to baseline samples and vehicle control treated mice in order to ascertain which guides are enriched or depleted by chemotherapeutic pressure.

Results:

We demonstrated the potential of identifying resistance mechanisms through combining the use of a clinically relevant multi agent chemotherapy regimen and concurrent CRISPR screening. Our pilot studies showed T-ALL induction therapy increases the survival of T-ALL engrafted mice and reduces leukemic burden. Relevant to the aim of this project, the administration of VXLD treatment resulted in differential sgRNA representation compared with control treatment, allowing us to explore mechanisms of drug resistance to conventional induction chemotherapy. We have already analysed the initial sequencing results which showed good quality reads as well as guide and library coverage. We observed enrichment of sgRNAs targeting the tumour suppressor PTEN in a cell line with wild type PTEN function suggesting that activation of PI3K/AKT/mTOR signalling provides proliferative advantage in this experimental setting. We also identify pathways associated with differentially expressed sgRNAs, including those linked to checkpoints in T-cell development. Their functional role and suitability as additional drug targets will be explored further.

Summary/Conclusion:

We used a genome wide knock out CRISPR library whilst applying chemotherapeutic pressure *in vitro* and *in vivo* conditions to identify pathways which may contribute to drug resistance to T-ALL induction therapy. Future work will focus on validation of differential sgRNA expression underlying these drug resistance mechanisms and ultimately improve efficacy and reduce toxicity of induction treatment.

Reference List

ADAMS, F. F., HECKL, D., HOFFMANN, T., TALBOT, S. R., KLOOS, A., THOL, F., HEUSER, M., ZUBER, J., SCHAMBACH, A. & SCHWARZER, A. 2017. An optimized lentiviral vector system for conditional RNAi and efficient cloning of microRNA embedded short hairpin RNA libraries. *Biomaterials,* 139**,** 102-115.

AGLIANO, A., MARTIN-PADURA, I., MANCUSO, P., MARIGHETTI, P., RABASCIO, C., PRUNERI, G., SHULTZ, L. D. & BERTOLINI, F. 2008. Human acute leukemia cells injected in NOD/LtSz-scid/IL-2Rgamma null mice generate a faster and more efficient disease compared to other NOD/scid-related strains. *Int J Cancer,* 123**,** 2222-7.

AL-AAMRI, H. M., KU, H., IRVING, H. R., TUCCI, J., MEEHAN-ANDREWS, T. & BRADLEY, C. 2019. Time dependent response of daunorubicin on cytotoxicity, cell cycle and DNA repair in acute lymphoblastic leukaemia. *BMC Cancer,* 19**,** 179.

ALKALAY, I., YARON, A., HATZUBAI, A., ORIAN, A., CIECHANOVER, A. & BEN-NERIAH, Y. 1995. Stimulation-dependent I kappa B alpha phosphorylation marks the NF-kappa B inhibitor for degradation via the ubiquitin-proteasome pathway. *Proc Natl Acad Sci U S A,* 92**,** 10599-603.

ALLAN, A. L. & KEENEY, M. 2010. Circulating Tumor Cell Analysis: Technical and Statistical Considerations for Application to the Clinic. *Journal of Oncology,* 2010**,** 10.

ANDERSON, N. M., HARROLD, I., MANSOUR, M. R., SANDA, T., MCKEOWN, M., NAGYKARY, N., BRADNER, J. E., LAN ZHANG, G., LOOK, A. T. & FENG, H. 2014. BCL2-specific inhibitor ABT-199 synergizes strongly with cytarabine against the early immature LOUCY cell line but not more-differentiated T-ALL cell lines. *Leukemia,* 28**,** 1145-1148.

ANGIOLILLO, A. L., SCHORE, R. J., DEVIDAS, M., BOROWITZ, M. J., CARROLL, A. J., GASTIER-FOSTER, J. M., HEEREMA, N. A., KEILANI, T., LANE, A. R., LOH, M. L., REAMAN, G. H., ADAMSON, P. C., WOOD, B., WOOD, C., ZHENG, H. W., RAETZ, E. A., WINICK, N. J., CARROLL, W. L. & HUNGER, S. P. 2014. Pharmacokinetic and Pharmacodynamic Properties of Calaspargase Pegol Escherichia coli L-Asparaginase in the Treatment of Patients With Acute Lymphoblastic Leukemia: Results From Children's Oncology Group Study AALL07P4. *Journal of Clinical Oncology,* 32**,** 3874-3882.

APLAN, P. D., LOMBARDI, D. P., REAMAN, G. H., SATHER, H. N., HAMMOND, G. D. & KIRSCH, I. R. 1992. Involvement of the putative hematopoietic transcription factor SCL in T-cell acute lymphoblastic leukemia. *Blood,* 79**,** 1327-33.

APPEL, I. M., DEN BOER, M. L., MEIJERINK, J. P. P., VEERMAN, A. J. P., RENIERS, N. C. M. & PIETERS, R. 2006. Up-regulation of asparagine synthetase expression is not linked to the clinical response l-asparaginase in pediatric acute lymphoblastic leukemia. *Blood,* 107**,** 4244-4249.

AREF, S., EL MENSHAWY, N., EL-GHONEMY, M. S., ZEID, T. A. & EL-BAIOMY, M. A. 2016. Clinicopathologic Effect of DNMT3A Mutation in Adult T-Cell Acute Lymphoblastic Leukemia. *Clin Lymphoma Myeloma Leuk,* 16**,** 43-8.

ASADA, N., TAKEISHI, S. & FRENETTE, P. S. 2017. Complexity of bone marrow hematopoietic stem cell niche. *International Journal of Hematology,* 106**,** 45-54.

ASLANIAN, A. M., FLETCHER, B. S. & KILBERG, M. S. 2001. Asparagine synthetase expression alone is sufficient to induce l-asparaginase resistance in MOLT-4 human leukaemia cells. *The Biochemical journal,* 357**,** 321-328.

ASSELIN, B. L., WHITIN, J. C., COPPOLA, D. J., RUPP, I. P., SALLAN, S. E. & COHEN, H. J. 1993. Comparative pharmacokinetic studies of three asparaginase preparations. *Journal of Clinical Oncology,* 11**,** 1780-1786.

AVRAMIS, V. I., SENCER, S., PERICLOU, A. P., SATHER, H., BOSTROM, B. C., COHEN, L. J., ETTINGER, A. G., ETTINGER, L. J., FRANKLIN, J., GAYNON, P. S., HILDEN, J. M., LANGE, B., MAJLESSIPOUR, F., MATHEW, P., NEEDLE, M., NEGLIA, J., REAMAN, G., HOLCENBERG, J. S. & STORK, L. 2002. A randomized comparison of native Escherichia coli asparaginase and polyethylene glycol conjugated asparaginase for treatment of children with newly diagnosed standard-risk acute lymphoblastic leukemia: a Children's Cancer Group study. *Blood,* 99**,** 1986-94.

AYROLDI, E. & RICCARDI, C. 2009. Glucocorticoid-induced leucine zipper (GILZ): a new important mediator of glucocorticoid action. *The FASEB Journal,* 23**,** 3649-3658.

BACHMANN, P. S., GORMAN, R., MACKENZIE, K. L., LUTZE-MANN, L. & LOCK, R. B. 2005. Dexamethasone resistance in B-cell precursor childhood acute lymphoblastic leukemia occurs downstream of ligand-induced nuclear translocation of the glucocorticoid receptor. *Blood,* 105**,** 2519-2526.

BALDUZZI, A., VALSECCHI, M. G., UDERZO, C., DE LORENZO, P., KLINGEBIEL, T., PETERS, C., STARY, J., FELICE, M. S., MAGYAROSY, E., CONTER, V., REITER, A., MESSINA, C., GADNER, H. & SCHRAPPE, M. 2005. Chemotherapy versus allogeneic transplantation for very-high-risk childhood acute lymphoblastic leukaemia in first complete remission: comparison by genetic randomisation in an international prospective study. *Lancet,* 366**,** 635-42.

BALKO, J. M., SCHWARZ, L. J., BHOLA, N. E., KURUPI, R., OWENS, P., MILLER, T. W., GÓMEZ, H., COOK, R. S. & ARTEAGA, C. L. 2013. Activation of MAPK Pathways due to DUSP4 Loss Promotes Cancer Stem Cell-like Phenotypes in Basal-like Breast Cancer. *Cancer Research,* 73**,** 6346-6358.

BAN, J., ECKHART, L., WENINGER, W., MILDNER, M. & TSCHACHLER, E. 1998. Identification of a human cDNA encoding a novel Bcl-x isoform. *Biochem Biophys Res Commun,* 248**,** 147-52.

BARRETINA, J., CAPONIGRO, G., STRANSKY, N., VENKATESAN, K., MARGOLIN, A. A., KIM, S., WILSON, C. J., LEHÁR, J., KRYUKOV, G. V., SONKIN, D., REDDY, A., LIU, M., MURRAY, L., BERGER, M. F., MONAHAN, J. E., MORAIS, P., MELTZER, J., KOREJWA, A., JANÉ-VALBUENA, J., MAPA, F. A., THIBAULT, J., BRIC-FURLONG, E., RAMAN, P., SHIPWAY, A., ENGELS, I. H., CHENG, J., YU, G. K., YU, J., ASPESI, P., DE SILVA, M., JAGTAP, K., JONES, M. D., WANG, L., HATTON, C., PALESCANDOLO, E., GUPTA, S., MAHAN, S., SOUGNEZ, C., ONOFRIO, R. C., LIEFELD, T., MACCONAILL, L., WINCKLER, W., REICH, M., LI, N., MESIROV, J. P., GABRIEL, S. B., GETZ, G., ARDLIE, K., CHAN, V., MYER, V. E., WEBER, B. L., PORTER, J., WARMUTH, M., FINAN, P., HARRIS, J. L., MEYERSON, M., GOLUB, T. R., MORRISSEY, M. P., SELLERS, W. R., SCHLEGEL, R. & GARRAWAY, L. A. 2012a. The Cancer Cell Line Encyclopedia enables predictive modelling of anticancer drug sensitivity. *Nature,* 483**,** 603.

BARRETINA, J., CAPONIGRO, G., STRANSKY, N., VENKATESAN, K., MARGOLIN, A. A., KIM, S., WILSON, C. J., LEHÁR, J., KRYUKOV, G. V., SONKIN, D., REDDY, A., LIU, M., MURRAY, L., BERGER, M. F., MONAHAN, J. E., MORAIS, P., MELTZER, J., KOREJWA, A., JANÉ-VALBUENA, J., MAPA, F. A., THIBAULT, J., BRIC-FURLONG, E., RAMAN, P., SHIPWAY, A., ENGELS, I. H., CHENG, J., YU, G. K., YU, J., ASPESI, P., JR., DE SILVA, M., JAGTAP, K., JONES, M. D., WANG, L., HATTON, C., PALESCANDOLO, E., GUPTA, S., MAHAN, S., SOUGNEZ, C., ONOFRIO, R. C., LIEFELD, T., MACCONAILL, L., WINCKLER, W., REICH, M., LI, N., MESIROV, J. P., GABRIEL, S. B., GETZ, G., ARDLIE, K., CHAN, V., MYER, V. E., WEBER, B. L., PORTER, J., WARMUTH, M., FINAN, P., HARRIS, J. L., MEYERSON, M., GOLUB, T. R., MORRISSEY, M. P., SELLERS, W. R., SCHLEGEL, R. & GARRAWAY, L. A. 2012b. The Cancer Cell Line Encyclopedia enables predictive modelling of anticancer drug sensitivity. *Nature,* 483**,** 603-607.

BEESLEY, A. H., WELLER, R. E., SENANAYAKE, S., WELCH, M. & KEES, U. R. 2009. Receptor mutation is not a common mechanism of naturally occurring glucocorticoid resistance in leukaemia cell lines. *Leukemia Research,* 33**,** 321-325.

BELDERBOS, M. E., KOSTER, T., AUSEMA, B., JACOBS, S., SOWDAGAR, S., ZWART, E., DE BONT, E., DE HAAN, G. & BYSTRYKH, L. V. 2017. Clonal selection and asymmetric distribution of human leukemia in murine xenografts revealed by cellular barcoding. *Blood,* 129**,** 3210.

BERGER, R., DASTUGUE, N., BUSSON, M., VAN DEN AKKER, J., PÉROT, C., BALLERINI, P., HAGEMEIJER, A., MICHAUX, L., CHARRIN, C., PAGES, M. P., MUGNERET, F., ANDRIEUX, J., TALMANT, P., HÉLIAS, C., MAUVIEUX, L., LAFAGE-POCHITALOFF, M., MOZZICONACCI, M. J., CORNILLET-LEFEBVRE, P., RADFORD, I., ASNAFI, V., BILHOU-NABERA, C., NGUYEN KHAC, F., LÉONARD, C., SPELEMAN, F., POPPE, B., BASTARD, C., TAVIAUX, S., QUILICHINI, B., HERENS, C., GRÉGOIRE, M. J., CAVÉ, H., BERNARD, O. A. & ON BEHALF OF THE GROUPE FRANÇAIS DE CYTOGÉNÉTIQUE, H. 2003. t(5;14)/HOX11L2-positive T-cell acute lymphoblastic leukemia. A collaborative study of the Groupe Français de Cytogénétique Hématologique (GFCH). *Leukemia,* 17**,** 1851-1857.

BERNARD, O. A., BUSSON-LECONIAT, M., BALLERINI, P., MAUCHAUFFE, M., DELLA VALLE, V., MONNI, R., NGUYEN KHAC, F., MERCHER, T., PENARD-LACRONIQUE, V., PASTURAUD, P., GRESSIN, L., HEILIG, R., DANIEL, M. T., LESSARD, M. & BERGER, R. 2001. A new recurrent and specific cryptic translocation, t(5;14)(q35;q32), is associated with expression of the Hox11L2 gene in T acute lymphoblastic leukemia. *Leukemia,* 15**,** 1495-504.

BERTAINA, A., VINTI, L., STROCCHIO, L., GASPARI, S., CARUSO, R., ALGERI, M., COLETTI, V., GURNARI, C., ROMANO, M., CEFALO, M. G., GIRARDI, K., TREVISAN, V., BERTAINA, V., MERLI, P. & LOCATELLI, F. 2017. The combination of bortezomib with chemotherapy to treat relapsed/refractory acute lymphoblastic leukaemia of childhood. *British Journal of Haematology,* 176**,** 629-636.

BHATLA, T., BLUM, R., WANG, J., JONES, C. L., MORRISON, D. J., RAETZ, E. A., BURKE, M. J., BROWN, P., HARVEY, R. C., WILLMAN, C. L., LOH, M., HUNGER, S. P. & CARROLL, W. L. 2014. Deciphering the Epigenetic Landscape of Relapsed Pediatric Acute Lymphoblastic Leukemia. *Blood,* 124**,** 612-612.

BHOJWANI, D. & PUI, C.-H. 2013. Relapsed childhood acute lymphoblastic leukaemia. *The Lancet Oncology,* 14**,** e205-e217.

BIGNELL, G. R., WARREN, W., SEAL, S., TAKAHASHI, M., RAPLEY, E., BARFOOT, R., GREEN, H., BROWN, C., BIGGS, P. J., LAKHANI, S. R., JONES, C., HANSEN, J., BLAIR, E., HOFMANN, B.,

SIEBERT, R., TURNER, G., EVANS, D. G., SCHRANDER-STUMPEL, C., BEEMER, F. A., VAN DEN OUWELAND, A., HALLEY, D., DELPECH, B., CLEVELAND, M. G., LEIGH, I., LEISTI, J. & RASMUSSEN, S. 2000. Identification of the familial cylindromatosis tumour-suppressor gene. *Nat Genet,* 25**,** 160-5.

BIONDI, A., SCHRAPPE, M., DE LORENZO, P., CASTOR, A., LUCCHINI, G., GANDEMER, V., PIETERS, R., STARY, J., ESCHERICH, G., CAMPBELL, M., LI, C.-K., VORA, A., ARICÒ, M., RÖTTGERS, S., SAHA, V. & VALSECCHI, M. G. 2012. Imatinib after induction for treatment of children and adolescents with Philadelphia-chromosome-positive acute lymphoblastic leukaemia (EsPhALL): a randomised, open-label, intergroup study. *The Lancet. Oncology,* 13**,** 936-945.

BLOMEN, V. A., MÁJEK, P., JAE, L. T., BIGENZAHN, J. W., NIEUWENHUIS, J., STARING, J., SACCO, R., VAN DIEMEN, F. R., OLK, N., STUKALOV, A., MARCEAU, C., JANSSEN, H., CARETTE, J. E., BENNETT, K. L., COLINGE, J., SUPERTI-FURGA, G. & BRUMMELKAMP, T. R. 2015. Gene essentiality and synthetic lethality in haploid human cells. *Science,* 350**,** 1092-1096.

BOEHMER, H. V. & FEHLING, H. J. 1997. STRUCTURE AND FUNCTION OF THE PRE-T CELL RECEPTOR. *Annual Review of Immunology,* 15**,** 433-452.

BOHANNON, R. A., MILLER, D. G. & DIAMOND, H. D. 1963. Vincristine in the Treatment of Lymphomas and Leukemias. *Cancer Research,* 23**,** 613-621.

BOLOTIN, A., QUINQUIS, B., SOROKIN, A. & EHRLICH, S. D. 2005. Clustered regularly interspaced short palindrome repeats (CRISPRs) have spacers of extrachromosomal origin. *Microbiology,* 151**,** 2551-61.

BOMKEN, S., BUECHLER, L., REHE, K., PONTHAN, F., ELDER, A., BLAIR, H., BACON, C. M., VORMOOR, J. & HEIDENREICH, O. 2013. Lentiviral marking of patient-derived acute lymphoblastic leukaemic cells allows in vivo tracking of disease progression. *Leukemia,* 27**,** 718-721.

BONAPACE, L., BORNHAUSER, B. C., SCHMITZ, M., CARIO, G., ZIEGLER, U., NIGGLI, F. K., SCHÄFER, B. W., SCHRAPPE, M., STANULLA, M. & BOURQUIN, J.-P. 2010. Induction of autophagy-dependent necroptosis is required for childhood acute lymphoblastic leukemia cells to overcome glucocorticoid resistance. *The Journal of clinical investigation,* 120**,** 1310-1323.

BOOS, J., WERBER, G., AHLKE, E., SCHULZE-WESTHOFF, P., NOWAK-GÖTTL, U., WÜRTHWEIN, G., VERSPOHL, E. J., RITTER, J. & JÜRGENS, H. 1996. Monitoring of asparaginase activity and asparagine levels in children on different asparaginase preparations. *European Journal of Cancer,* 32**,** 1544-1550.

BORTOLOZZI, R., BRESOLIN, S., RAMPAZZO, E., PAGANIN, M., MAULE, F., MARIOTTO, E., BOSO, D., MINUZZO, S., AGNUSDEI, V., VIOLA, G., TE KRONNIE, G., CAZZANIGA, G., BASSO, G. & PERSANO, L. 2018. AKR1C enzymes sustain therapy resistance in paediatric T-ALL. *British Journal of Cancer,* 118**,** 985-994.

BRAY, P. J. & COTTON, R. G. 2003. Variations of the human glucocorticoid receptor gene (NR3C1): pathological and in vitro mutations and polymorphisms. *Hum Mutat,* 21**,** 557-68.

BRESSANIN, D., EVANGELISTI, C., RICCI, F., TABELLINI, G., CHIARINI, F., TAZZARI, P. L., MELCHIONDA, F., BUONTEMPO, F., PAGLIARO, P., PESSION, A., MCCUBREY, J. A. &

MARTELLI, A. M. 2012. Harnessing the PI3K/Akt/mTOR pathway in T-cell acute lymphoblastic leukemia: eliminating activity by targeting at different levels. *Oncotarget,* 3**,** 811-823.

BROOME, H. E., YU, A. L., DICCIANNI, M., CAMITTA, B. M., MONIA, B. P. & DEAN, N. M. 2002. Inhibition of Bcl-xL expression sensitizes T-cell acute lymphoblastic leukemia cells to chemotherapeutic drugs. *Leukemia Research,* 26**,** 311-316.

BROOME, J. D. 1968. Studies on the mechanism of tumour inhbiiton by L-Asparginase. *Journal of Experimental Medicine*, 127**,** 1055-1072.

BROU, C., LOGEAT, F., GUPTA, N., BESSIA, C., LEBAIL, O., DOEDENS, J. R., CUMANO, A., ROUX, P., BLACK, R. A. & ISRAËL, A. 2000. A Novel Proteolytic Cleavage Involved in Notch Signaling: The Role of the Disintegrin-Metalloprotease TACE. *Molecular Cell,* 5**,** 207-216.

BURDEN, N., CHAPMAN, K., SEWELL, F. & ROBINSON, V. 2015. Pioneering better science through the 3Rs: an introduction to the national centre for the replacement, refinement, and reduction of animals in research (NC3Rs). *Journal of the American Association for Laboratory Animal Science : JAALAS,* 54**,** 198-208.

CALLIES, S., DE ALWIS, D. P., MEHTA, A., BURGESS, M. & AARONS, L. 2004. Population pharmacokinetic model for daunorubicin and daunorubicinol coadministered with zosuquidar.3HCl (LY335979). *Cancer Chemotherapy and Pharmacology,* 54**,** 39-48.

CHAN, W. K., HORVATH, T. D., TAN, L., LINK, T., HARUTYUNYAN, K. G., PONTIKOS, M. A., ANISHKIN, A., DU, D., MARTIN, L. A., YIN, E., REMPE, S. B., SUKHAREV, S., KONOPLEVA, M., WEINSTEIN, J. N. & LORENZI, P. L. 2019. Glutaminase activity of L-asparaginase contributes to durable preclinical activity against acute lymphoblastic leukemia. *Molecular Cancer Therapeutics***,** molcanther.1329.2018.

CHAO, D. T. & KORSMEYER, S. J. 1998. BCL-2 family: regulators of cell death. *Annu Rev Immunol,* 16**,** 395-419.

CHEN, B., JIANG, L., ZHONG, M. L., LI, J. F., LI, B. S., PENG, L. J., DAI, Y. T., CUI, B. W., YAN, T. Q., ZHANG, W. N., WENG, X. Q., XIE, Y. Y., LU, J., REN, R. B., CHEN, S. N., HU, J. D., WU, D. P., CHEN, Z., TANG, J. Y., HUANG, J. Y., MI, J. Q. & CHEN, S. J. 2018. Identification of fusion genes and characterization of transcriptome features in T-cell acute lymphoblastic leukemia. *Proc Natl Acad Sci U S A,* 115**,** 373-378.

CHEN, D., FREZZA, M., SCHMITT, S., KANWAR, J. & DOU, Q. P. 2011. Bortezomib as the first proteasome inhibitor anticancer drug: current status and future perspectives. *Current cancer drug targets,* 11**,** 239-253.

CHEN, S., SANJANA, N. E., ZHENG, K., SHALEM, O., LEE, K., SHI, X., SCOTT, D. A., SONG, J., PAN, J. Q., WEISSLEDER, R., LEE, H., ZHANG, F. & SHARP, P. A. 2015. Genome-wide CRISPR screen in a mouse model of tumor growth and metastasis. *Cell,* 160**,** 1246-1260.

CHEN, Y.-L., TANG, C., ZHANG, M.-Y., HUANG, W.-L., XU, Y., SUN, H.-Y., YANG, F., SONG, L.-L., WANG, H., MU, L.-L., LI, M.-H., ZHENG, W.-W., MIAO, Y., DING, L.-X., LI, B.-S., SHEN, S.-H., LIU, S.-L., LI, H., ZHU, Z.-Q., CHEN, H.-W., TANG, Z.-H., CHEN, J., HONG, D.-L., CHEN, H.-Z., DUAN, C.-W. & ZHOU, B.-B. S. 2019. Blocking ATM-dependent NF-κB pathway overcomes niche protection and improves chemotherapy response in acute lymphoblastic leukemia. *Leukemia*.

CHIARETTI, S., ZINI, G. & BASSAN, R. 2014. Diagnosis and subclassification of acute lymphoblastic leukemia. *Mediterranean journal of hematology and infectious diseases,* 6**,** e2014073-e2014073.

CHIEN, A. J. & MOASSER, M. M. 2008. Cellular Mechanisms of Resistance to Anthracyclines and Taxanes in Cancer: Intrinsic and Acquired. *Seminars in Oncology,* 35**,** S1-S14.

CHIEN, W.-W., LE BEUX, C., RACHINEL, N., JULIEN, M., LACROIX, C.-E., ALLAS, S., SAHAKIAN, P., CORNUT-THIBAUT, A., LIONNARD, L., KUCHARCZAK, J., AOUACHERIA, A., ABRIBAT, T. & SALLES, G. 2015. Differential mechanisms of asparaginase resistance in B-type acute lymphoblastic leukemia and malignant natural killer cell lines. *Scientific Reports,* 5**,** 8068.

CHITALE, D., GONG, Y., TAYLOR, B. S., BRODERICK, S., BRENNAN, C., SOMWAR, R., GOLAS, B., WANG, L., MOTOI, N., SZOKE, J., REINERSMAN, J. M., MAJOR, J., SANDER, C., SESHAN, V. E., ZAKOWSKI, M. F., RUSCH, V., PAO, W., GERALD, W. & LADANYI, M. 2009. An integrated genomic analysis of lung cancer reveals loss of DUSP4 in EGFR-mutant tumors. *Oncogene,* 28**,** 2773-2783.

CHIU, P. P. L., JIANG, H. & DICK, J. E. 2010. Leukemia-initiating cells in human T-lymphoblastic leukemia exhibit glucocorticoid resistance. *Blood,* 116**,** 5268-5279.

CHOI, B. Y., CHOI, H. S., KO, K., CHO, Y.-Y., ZHU, F., KANG, B. S., ERMAKOVA, S. P., MA, W.-Y., BODE, A. M. & DONG, Z. 2005. The tumor suppressor p16INK4a prevents cell transformation through inhibition of c-Jun phosphorylation and AP-1 activity. *Nature Structural & Molecular Biology,* 12**,** 699-707.

CHONGHAILE, T. N., RODERICK, J. E., GLENFIELD, C., RYAN, J., SALLAN, S. E., SILVERMAN, L. B., LOH, M. L., HUNGER, S. P., WOOD, B., DEANGELO, D. J., STONE, R., HARRIS, M., GUTIERREZ, A., KELLIHER, M. A. & LETAI, A. 2014. Maturation stage of T-cell acute lymphoblastic leukemia determines BCL-2 versus BCL-XL dependence and sensitivity to ABT-199. *Cancer discovery,* 4**,** 1074-1087.

CHOU, T.-C. & TALALAY, P. 1983. Analysis of combined drug effects: a new look at a very old problem. *Trends in Pharmacological Sciences,* 4**,** 450-454.

CHOW, L. M. & BAKER, S. J. 2006. PTEN function in normal and neoplastic growth. *Cancer Lett,* 241**,** 184-96.

CHU, E., CALLENDER, M. A., FARRELL, M. P. & SCHMITZ, J. C. 2003. Thymidylate synthase inhibitors as anticancer agents: from bench to bedside. *Cancer Chemotherapy and Pharmacology,* 52**,** 80-89.

CLAPPIER, E., GERBY, B., SIGAUX, F., DELORD, M., TOUZRI, F., HERNANDEZ, L., BALLERINI, P., BARUCHEL, A., PFLUMIO, F. & SOULIER, J. 2011. Clonal selection in xenografted human T cell acute lymphoblastic leukemia recapitulates gain of malignancy at relapse. *J Exp Med,* 208**,** 653-61.

COON, T. A., MCKELVEY, A. C., LEAR, T., RAJBHANDARI, S., DUNN, S. R., CONNELLY, W., ZHAO, J. Y., HAN, S., LIU, Y., WEATHINGTON, N. M., MCVERRY, B. J., ZHANG, Y. & CHEN, B. B. 2015. The proinflammatory role of HECTD2 in innate immunity and experimental lung injury. *Science translational medicine,* 7**,** 295ra109-295ra109.

COOPER, S. L. & BROWN, P. A. 2015. Treatment of pediatric acute lymphoblastic leukemia. *Pediatric clinics of North America,* 62**,** 61-73.

COWLEY, G. S., WEIR, B. A., VAZQUEZ, F., TAMAYO, P., SCOTT, J. A., RUSIN, S., EAST-SELETSKY, A., ALI, L. D., GERATH, W. F. J., PANTEL, S. E., LIZOTTE, P. H., JIANG, G., HSIAO, J., TSHERNIAK, A., DWINELL, E., AOYAMA, S., OKAMOTO, M., HARRINGTON, W., GELFAND, E., GREEN, T. M., TOMKO, M. J., GOPAL, S., WONG, T. C., LI, H., HOWELL, S., STRANSKY, N., LIEFELD, T., JANG, D., BISTLINE, J., HILL MEYERS, B., ARMSTRONG, S. A., ANDERSON, K. C., STEGMAIER, K., REICH, M., PELLMAN, D., BOEHM, J. S., MESIROV, J. P., GOLUB, T. R., ROOT, D. E. & HAHN, W. C. 2014. Parallel genome-scale loss of function screens in 216 cancer cell lines for the identification of context-specific genetic dependencies. *Scientific Data,* 1**,** 140035.

CRAWFORD, L. J., WALKER, B. & IRVINE, A. E. 2011. Proteasome inhibitors in cancer therapy. *Journal of cell communication and signaling,* 5**,** 101-110.

D'ALTRI, T., GONZALEZ, J., AIFANTIS, I., ESPINOSA, L. & BIGAS, A. 2011. Hes1 expression and CYLD repression are essential events downstream of Notch1 in T-cell leukemia. *Cell Cycle,* 10**,** 1031-6.

DADI, S., LE NOIR, S., PAYET-BORNET, D., LHERMITTE, L., ZACARIAS-CABEZA, J., BERGERON, J., VILLARESE, P., VACHEZ, E., DIK, W. A., MILLIEN, C., RADFORD, I., VERHOEYEN, E., COSSET, F. L., PETIT, A., IFRAH, N., DOMBRET, H., HERMINE, O., SPICUGLIA, S., LANGERAK, A. W., MACINTYRE, E. A., NADEL, B., FERRIER, P. & ASNAFI, V. 2012. TLX homeodomain oncogenes mediate T cell maturation arrest in T-ALL via interaction with ETS1 and suppression of TCRalpha gene expression. *Cancer Cell,* 21**,** 563-76.

DE KEERSMAECKER, K. & FERRANDO, A. A. 2011. TLX1-Induced T-cell Acute Lymphoblastic Leukemia. *Clinical Cancer Research,* 17**,** 6381-6386.

DE KEERSMAECKER, K., REAL, P. J., GATTA, G. D., PALOMERO, T., SULIS, M. L., TOSELLO, V., VAN VLIERBERGHE, P., BARNES, K., CASTILLO, M., SOLE, X., HADLER, M., LENZ, J., APLAN, P. D., KELLIHER, M., KEE, B. L., PANDOLFI, P. P., KAPPES, D., GOUNARI, F., PETRIE, H., VAN DER MEULEN, J., SPELEMAN, F., PAIETTA, E., RACEVSKIS, J., WIERNIK, P. H., ROWE, J. M., SOULIER, J., AVRAN, D., CAVE, H., DASTUGUE, N., RAIMONDI, S., MEIJERINK, J. P., CORDON-CARDO, C., CALIFANO, A. & FERRANDO, A. A. 2010. The TLX1 oncogene drives aneuploidy in T cell transformation. *Nat Med,* 16**,** 1321-7.

DE STROOPER, B., ANNAERT, W., CUPERS, P., SAFTIG, P., CRAESSAERTS, K., MUMM, J. S., SCHROETER, E. H., SCHRIJVERS, V., WOLFE, M. S., RAY, W. J., GOATE, A. & KOPAN, R. 1999. A presenilin-1-dependent gamma-secretase-like protease mediates release of Notch intracellular domain. *Nature,* 398**,** 518-22.

DEANGELO, D. J., YU, D., JOHNSON, J. L., COUTRE, S. E., STONE, R. M., STOPECK, A. T., GOCKERMAN, J. P., MITCHELL, B. S., APPELBAUM, F. R. & LARSON, R. A. 2007. Nelarabine induces complete remissions in adults with relapsed or refractory T-lineage acute lymphoblastic leukemia or lymphoblastic lymphoma: Cancer and Leukemia Group B study 19801. *Blood,* 109**,** 5136-42.

DEAR, T. N., SANCHEZ-GARCIA, I. & RABBITTS, T. H. 1993. The HOX11 gene encodes a DNA-binding nuclear transcription factor belonging to a distinct family of homeobox genes. *Proceedings of the National Academy of Sciences,* 90**,** 4431-4435.

DELGADO-MARTIN, C., MEYER, L. K., HUANG, B. J., SHIMANO, K. A., ZINTER, M. S., NGUYEN, J. V., SMITH, G. A., TAUNTON, J., WINTER, S. S., RODERICK, J. R., KELLIHER, M. A., HORTON, T.

M., WOOD, B. L., TEACHEY, D. T. & HERMISTON, M. L. 2017. JAK/STAT pathway inhibition overcomes IL7-induced glucocorticoid resistance in a subset of human T-cell acute lymphoblastic leukemias. *Leukemia,* 31**,** 2568-2576.

DELLA GATTA, G., PALOMERO, T., PEREZ-GARCIA, A., AMBESI-IMPIOMBATO, A., BANSAL, M., CARPENTER, Z. W., DE KEERSMAECKER, K., SOLE, X., XU, L., PAIETTA, E., RACEVSKIS, J., WIERNIK, P. H., ROWE, J. M., MEIJERINK, J. P., CALIFANO, A. & FERRANDO, A. A. 2012. Reverse engineering of TLX oncogenic transcriptional networks identifies RUNX1 as tumor suppressor in T-ALL. *Nature medicine,* 18**,** 436-440.

DENNISON, J. B., JONES, D. R., RENBARGER, J. L. & HALL, S. D. 2007. Effect of CYP3A5 expression on vincristine metabolism with human liver microsomes. *J Pharmacol Exp Ther,* 321**,** 553-63.

DI NOTTIA, M., MONTANARI, A., VERRIGNI, D., OLIVA, R., TORRACO, A., FERNANDEZ-VIZARRA, E., DIODATO, D., RIZZA, T., BIANCHI, M., CATTERUCCIA, M., ZEVIANI, M., DIONISI-VICI, C., FRANCISCI, S., BERTINI, E. & CARROZZO, R. 2017. Novel mutation in mitochondrial Elongation Factor EF-Tu associated to dysplastic leukoencephalopathy and defective mitochondrial DNA translation. *Biochimica et Biophysica Acta (BBA) - Molecular Basis of Disease,* 1863**,** 961-967.

DI VEROLI, G. Y., FORNARI, C., WANG, D., MOLLARD, S., BRAMHALL, J. L., RICHARDS, F. M. & JODRELL, D. I. 2016. Combenefit: an interactive platform for the analysis and visualization of drug combinations. *Bioinformatics,* 32**,** 2866-2868.

DOENCH, J. G., FUSI, N., SULLENDER, M., HEGDE, M., VAIMBERG, E. W., DONOVAN, K. F., SMITH, I., TOTHOVA, Z., WILEN, C., ORCHARD, R., VIRGIN, H. W., LISTGARTEN, J. & ROOT, D. E. 2016. Optimized sgRNA design to maximize activity and minimize off-target effects of CRISPR-Cas9. *Nature biotechnology,* 34**,** 184-191.

DORMON, K. L. 2017. Investigating the evolution of dexamethasone resistance in acute lymphoblastic leukaemia. PhD, Newcastle University.

DOWNING, J. R., WILSON, R. K., ZHANG, J., MARDIS, E. R., PUI, C.-H., DING, L., LEY, T. J. & EVANS, W. E. 2012. The Pediatric Cancer Genome Project. *Nature genetics,* 44**,** 619-622.

DREXLER, H. G., MACLEOD, R. A. F., NAGEL, S., DIRKS, W. G., UPHOFF, C. C., STEUBE, K. G. & QUENTMEIER, H. 2005. Guide to Leukemia-Lymphoma Cell Lines on CD. *Blood,* 106**,** 4340.

DUARTE, D., HAWKINS, E. D. & LO CELSO, C. 2018. The interplay of leukemia cells and the bone marrow microenvironment. *Blood,* 131**,** 1507.

EBEID, E. N., KAMEL, M. M. & ALI, B. A. 2008. Detection of anti-asparaginase antibodies during therapy with E.coli asparaginase in children with newly diagnosed acute lymphoblastic leukemia and lymphoma. *J Egypt Natl Canc Inst,* 20**,** 127-33.

ELDER, A., BOMKEN, S., WILSON, I., BLAIR, H. J., COCKELL, S., PONTHAN, F., DORMON, K., PAL, D., HEIDENREICH, O. & VORMOOR, J. 2017. Abundant and equipotent founder cells establish and maintain acute lymphoblastic leukaemia. *Leukemia,* 31**,** 2577.

ELLISEN, L. W., BIRD, J., WEST, D. C., SORENG, A. L., REYNOLDS, T. C., SMITH, S. D. & SKLAR, J. 1991. TAN-1, the human homolog of the Drosophila Notch gene, is broken by chromosomal translocations in T lymphoblastic neoplasms. *Cell,* 66**,** 649-661.

ESPINOSA, L., CATHELIN, S., D'ALTRI, T., TRIMARCHI, T., STATNIKOV, A., GUIU, J., RODILLA, V., INGLÉS-ESTEVE, J., NOMDEDEU, J., BELLOSILLO, B., BESSES, C., ABDEL-WAHAB, O., KUCINE, N., SUN, S.-C., SONG, G., MULLIGHAN, C. C., LEVINE, R. L., RAJEWSKY, K., AIFANTIS, I. & BIGAS, A. 2010. The Notch/Hes1 pathway sustains NF-κB activation through CYLD repression in T cell leukemia. *Cancer cell,* 18**,** 268-281.

FABER, A., GOESSLER, U. R., HOERMANN, K., SCHULTZ, J. D., UMBREIT, C. & STERN-STRAETER, J. 2013. SDF-1-CXCR4 axis: cell trafficking in the cancer stem cell niche of head and neck squamous cell carcinoma. *Oncol Rep,* 29**,** 2325-31.

FAROOQ, A. & ZHOU, M.-M. 2004. Structure and regulation of MAPK phosphatases. *Cellular Signalling,* 16**,** 769-779.

FDA, 2018a. FDA approves venetoclax for CLL or SLL, with or without 17 p deletion, after one prior therapy [Online]. Food and Drug Administration (FDA). [Accessed].

FDA,. 2018b. *FDA approves venetoclax in combination for AML in adults* [Online]. Food and Drug Administration (FDA). Available: https://www.fda.gov/drugs/fda-approves-venetoclax-combination-aml-adults [Accessed].

FERRANDO, A. A. 2009. The role of NOTCH1 signaling in T-ALL. *Hematology. American Society of Hematology. Education Program***,** 353-361.

FERRANDO, A. A., NEUBERG, D. S., STAUNTON, J., LOH, M. L., HUARD, C., RAIMONDI, S. C., BEHM, F. G., PUI, C. H., DOWNING, J. R., GILLILAND, D. G., LANDER, E. S., GOLUB, T. R. & LOOK, A. T. 2002. Gene expression signatures define novel oncogenic pathways in T cell acute lymphoblastic leukemia. *Cancer Cell,* 1**,** 75-87.

FIELD-SMITH, A., MORGAN, G. J. & DAVIES, F. E. 2006. Bortezomib (Velcadetrade mark) in the Treatment of Multiple Myeloma. *Therapeutics and clinical risk management,* 2**,** 271-279.
FULOP, G. M. & PHILLIPS, R. A. 1990. The scid mutation in mice causes a general defect in DNA repair. *Nature,* 347**,** 479-482.

FUNG, M. K. L. & CHAN, G. C.-F. 2017. Drug-induced amino acid deprivation as strategy for cancer therapy. *Journal of Hematology & Oncology,* 10**,** 144.

GANAPATHI, R. N. & GANAPATHI, M. K. 2013. Mechanisms regulating resistance to inhibitors of topoisomerase II. *Frontiers in pharmacology,* 4**,** 89-89.

GANDHI, V., KEATING, M. J., BATE, G. & KIRKPATRICK, P. 2006. Nelarabine. *Nature Reviews Drug Discovery,* 5**,** 17-18.

GAYNON, P. S., DESAI, A. A., BOSTROM, B. C., HUTCHINSON, R. J., LANGE, B. J., NACHMAN, J. B., REAMAN, G. H., SATHER, H. N., STEINHERZ, P. G., TRIGG, M. E., TUBERGEN, D. G. & UCKUN, F. M. 1997. Early response to therapy and outcome in childhood acute lymphoblastic leukemia. *Cancer,* 80**,** 1717-1726.

GAYNON, P. S., HARRIS, R. E., ALTMAN, A. J., BOSTROM, B. C., BRENEMAN, J. C., HAWKS, R., STEELE, D., ZIPF, T., STRAM, D. O., VILLALUNA, D. & TRIGG, M. E. 2006. Bone marrow transplantation versus prolonged intensive chemotherapy for children with acute lymphoblastic leukemia and an initial bone marrow relapse within 12 months of the completion of primary therapy: Children's Oncology Group study CCG-1941. *J Clin Oncol,* 24**,** 3150-6.

GENESCÀ, E., LAZARENKOV, A., MORGADES, M., BERBIS, G., RUÍZ-XIVILLÉ, N., GÓMEZ-MARZO, P., RIBERA, J., JUNCÀ, J., GONZÁLEZ-PÉREZ, A., MERCADAL, S., GUARDIA, R., ARTOLA, M. T., MORENO, M. J., MARTÍNEZ-LÓPEZ, J., ZAMORA, L., BARBA, P., GIL, C., TORMO, M., CLADERA, A., NOVO, A., PRATCORONA, M., NOMDEDEU, J., GONZÁLEZ-CAMPOS, J., ALMEIDA, M., CERVERA, J., MONTESINOS, P., BATLLE, M., VIVES, S., ESTEVE, J., FELIU, E., SOLÉ, F., ORFAO, A. & RIBERA, J. M. 2018. Frequency and clinical impact of CDKN2A/ARF/CDKN2B gene deletions as assessed by in-depth genetic analyses in adult T cell acute lymphoblastic leukemia. *Journal of Hematology & Oncology,* 11**,** 96.

GENG, Y., ZHAO, Y., SCHUSTER, L. C., FENG, B., LYNN, D. A., AUSTIN, K. M., STOKLOSA, J. D. & MORRISON, J. D. 2015. A Chemical Biology Study of Human Pluripotent Stem Cells Unveils HSPA8 as a Key Regulator of Pluripotency. *Stem cell reports,* 5**,** 1143-1154.

GERBY, B., TREMBLAY, C. S., TREMBLAY, M., ROJAS-SUTTERLIN, S., HERBLOT, S., HEBERT, J., SAUVAGEAU, G., LEMIEUX, S., LECUYER, E., VEIGA, D. F. & HOANG, T. 2014. SCL, LMO1 and Notch1 reprogram thymocytes into self-renewing cells. *PLoS Genet,* 10**,** e1004768.

GEWIRTZ, D. 1999. A critical evaluation of the mechanisms of action proposed for the antitumor effects of the anthracycline antibiotics adriamycin and daunorubicin. *Biochemical Pharmacology,* 57**,** 727-741.

GIANFELICI, V., CHIARETTI, S., DEMEYER, S., DI GIACOMO, F., MESSINA, M., LA STARZA, R., PERAGINE, N., PAOLONI, F., GEERDENS, E., PIERINI, V., ELIA, L., MANCINI, M., DE PROPRIS, M. S., APICELLA, V., GAIDANO, G., TESTI, A. M., VITALE, A., VIGNETTI, M., MECUCCI, C., GUARINI, A., COOLS, J. & FOÀ, R. 2016. RNA sequencing unravels the genetics of refractory/relapsed T-cell acute lymphoblastic leukemia. Prognostic and therapeutic implications. *Haematologica,* 101**,** 941-950.

GIDDING, C. E. M., KELLIE, S. J., KAMPS, W. A. & DE GRAAF, S. S. N. 1999. Vincristine revisited. *Critical Reviews in Oncology/Hematology,* 29**,** 267-287.

GILLET, J.-P., VARMA, S. & GOTTESMAN, M. M. 2013. The clinical relevance of cancer cell lines. *Journal of the National Cancer Institute,* 105**,** 452-458.

GIRARDI, T., VICENTE, C., COOLS, J. & DE KEERSMAECKER, K. 2017. The genetics and molecular biology of T-ALL. *Blood,* 129**,** 1113-1123.

GMEINER, W. H., DEBINSKI, W., MILLIGAN, C., CAUDELL, D. & PARDEE, T. S. 2016. The applications of the novel polymeric fluoropyrimidine F10 in cancer treatment: current evidence. *Future Oncol,* 12**,** 2009-20.

GOLDBERG, J. M., SILVERMAN, L. B., LEVY, D. E., DALTON, V. K., GELBER, R. D., LEHMANN, L., COHEN, H. J., SALLAN, S. E. & ASSELIN, B. L. 2003. Childhood T-Cell Acute Lymphoblastic Leukemia: The Dana-Farber Cancer Institute Acute Lymphoblastic Leukemia Consortium Experience. *Journal of Clinical Oncology,* 21**,** 3616-3622.

GOOSSENS, S. & VAN VLIERBERGHE, P. 2016. Overcoming Steroid Resistance in T Cell Acute Lymphoblastic Leukemia. *PLoS Med,* 13**,** e1002208.

GOULDEN, N. J., KIRKWOOD, A. A., MOPPETT, J., SAMARASINGHE, S., LAWSON, S., ROWNTREE, C., HOUGH, R., ATHWAL, R., KEARNS, P. R. & VORA, A. 2017. UKALL 2011: Randomised Trial Investigating a Short Induction Dexamethasone Schedule for Children and Young Adults with Acute Lymphoblastic Leukaemia. *Blood,* 130**,** 141-141.

GRABARCZYK, P., PRZYBYLSKI, G. K., DEPKE, M., VÖLKER, U., BAHR, J., ASSMUS, K., BRÖKER, B. M., WALTHER, R. & SCHMIDT, C. A. 2006. Inhibition of BCL11B expression leads to apoptosis of malignant but not normal mature T cells. *Oncogene,* 26**,** 3797.

GREM, J. L., DANENBERG, K. D., BEHAN, K., PARR, A., YOUNG, L., DANENBERG, P. V., NGUYEN, D., DRAKE, J., MONKS, A. & ALLEGRA, C. J. 2001. Thymidine Kinase, Thymidylate Synthase, and Dihydropyrimidine Dehydrogenase Profiles of Cell Lines of the National Cancer Institute's Anticancer Drug Screen. *Clinical Cancer Research,* 7**,** 999-1009.

GURYANOVA, O., SHANK, K., SPITZER, B., LUCIANI, L., P KOCHE, R., GARRETT-BAKELMAN, F., GANZEL, C., H DURHAM, B., MOHANTY, A., HOERMANN, G., A RIVERA, S., G CHRAMIEC, A., PRONIER, E., BASTIAN, L., D KELLER, M., TOVBIN, D., LOIZOU, E., R WEINSTEIN, A., RODRIGUEZ GONZALEZ, A. & L LEVINE, R. 2016. DNMT3A mutations promote anthracycline resistance in acute myeloid leukemia via impaired nucleosome remodeling. *Nature medicine,* 22.

GUTIERREZ, A., KENTSIS, A., SANDA, T., HOLMFELDT, L., CHEN, S.-C., ZHANG, J., PROTOPOPOV, A., CHIN, L., DAHLBERG, S. E., NEUBERG, D. S., SILVERMAN, L. B., WINTER, S. S., HUNGER, S. P., SALLAN, S. E., ZHA, S., ALT, F. W., DOWNING, J. R., MULLIGHAN, C. G. & LOOK, A. T. 2011. The BCL11B tumor suppressor is mutated across the major molecular subtypes of T-cell acute lymphoblastic leukemia. *Blood,* 118**,** 4169-4173.

GUTIERREZ, A., SANDA, T., GREBLIUNAITE, R., CARRACEDO, A., SALMENA, L., AHN, Y., DAHLBERG, S., NEUBERG, D., MOREAU, L. A., WINTER, S. S., LARSON, R., ZHANG, J., PROTOPOPOV, A., CHIN, L., PANDOLFI, P. P., SILVERMAN, L. B., HUNGER, S. P., SALLAN, S. E. & LOOK, A. T. 2009. High frequency of PTEN, PI3K, and AKT abnormalities in T-cell acute lymphoblastic leukemia. *Blood,* 114**,** 647-650.

HABENS, F., LAPHAM, A. S., DALLMAN, C. L., PICKERING, B. M., MICHELS, J., MARCUSSON, E. G., JOHNSON, P. W. M. & PACKHAM, G. 2007. Distinct promoters mediate constitutive and inducible Bcl-XL expression in malignant lymphocytes. *Oncogene,* 26**,** 1910-1919.

HAFT, D. H., SELENGUT, J., MONGODIN, E. F. & NELSON, K. E. 2005. A guild of 45 CRISPR-associated (Cas) protein families and multiple CRISPR/Cas subtypes exist in prokaryotic genomes. *PLoS Comput Biol,* 1**,** e60.

HAGENBEEK, T. J., NASPETTI, M., MALERGUE, F., GARÇON, F., NUNÈS, J. A., CLEUTJENS, K. B. J. M., TRAPMAN, J., KRIMPENFORT, P. & SPITS, H. 2004. The Loss of PTEN Allows TCR αβ Lineage Thymocytes to Bypass IL-7 and Pre-TCR–mediated Signaling. *The Journal of Experimental Medicine,* 200**,** 883-894.

HANAHAN, D. & WEINBERG, R. A. 2011. Hallmarks of cancer: the next generation. *Cell,* 144**,** 646-74.

HARSHA, B., CREATORE, C., KOK, C. Y., HATHAWAY, C., COLE, C. G., RAMSHAW, C. C., RYE, C. E., BEARE, D. M., DAWSON, E., BOUTSELAKIS, H., NOBLE, K., PONTING, L., BINDAL, N., FISH, P., CAMPBELL, P. J., STEFANCSIK, R., BAMFORD, S., THOMPSON, S. L., WARD, S., WANG, S., FORBES, S. A., JUPE, S. C., SONDKA, Z., TATE, J. G., JUBB, H. C. & SPEEDY, H. E. 2018. COSMIC: the Catalogue Of Somatic Mutations In Cancer. *Nucleic Acids Research,* 47**,** D941-D947.

HART, T., BROWN, K. R., SIRCOULOMB, F., ROTTAPEL, R. & MOFFAT, J. 2014. Measuring error rates in genomic perturbation screens: gold standards for human functional genomics. *Molecular Systems Biology,* 10**,** 733.

HART, T., CHANDRASHEKHAR, M., AREGGER, M., STEINHART, Z., BROWN, K. R., MACLEOD, G., MIS, M., ZIMMERMANN, M., FRADET-TURCOTTE, A., SUN, S., MERO, P., DIRKS, P., SIDHU, S., ROTH, F. P., RISSLAND, O. S., DUROCHER, D., ANGERS, S. & MOFFAT, J. 2015. High-Resolution CRISPR Screens Reveal Fitness Genes and Genotype-Specific Cancer Liabilities. *Cell,* 163**,** 1515-26.

HASKELL, C. M. & CANELLOS, G. P. 1969. l-asparaginase resistance in human leukemia--asparagine synthetase. *Biochem Pharmacol,* 18**,** 2578-80.

HAYASHI, K., YAMAGUCHI, T., YANO, S., KANAZAWA, I., YAMAUCHI, M., YAMAMOTO, M. & SUGIMOTO, T. 2009. BMP/Wnt antagonists are upregulated by dexamethasone in osteoblasts and reversed by alendronate and PTH: Potential therapeutic targets for glucocorticoid-induced osteoporosis. *Biochemical and Biophysical Research Communications,* 379**,** 261-266.

HE, K., GUO, X., LIU, Y., LI, J., HU, Y., WANG, D. & SONG, J. 2016. TUFM downregulation induces epithelial–mesenchymal transition and invasion in lung cancer cells via a mechanism involving AMPK-GSK3β signaling. *Cellular and Molecular Life Sciences,* 73**,** 2105-2121.

HEASMAN, S.-A., ZAITSEVA, L., BOWLES, K. M., RUSHWORTH, S. A. & MACEWAN, D. J. 2011. Protection of acute myeloid leukaemia cells from apoptosis induced by front-line chemotherapeutics is mediated by haem oxygenase-1. *Oncotarget,* 2**,** 658-668.

HEMPEL, G., RELLING, M. V., DE ROSSI, G., STARY, J., DE LORENZO, P., VALSECCHI, M. G., BARISONE, E., BOOS, J. & PIETERS, R. 2010a. Pharmacokinetics of daunorubicin and daunorubicinol in infants with leukemia treated in the interfant 99 protocol. *Pediatric Blood & Cancer,* 54**,** 355-360.

HEMPEL, G., RELLING, M. V., DE ROSSI, G., STARY, J., DE LORENZO, P., VALSECCHI, M. G., BARISONE, E., BOOS, J. & PIETERS, R. 2010b. Pharmacokinetics of daunorubicin and daunorubicinol in infants with leukemia treated in the interfant 99 protocol. *Pediatr Blood Cancer,* 54**,** 355-60.

HERMANOVA, I., ZALIOVA, M., TRKA, J. & STARKOVA, J. 2012. Low expression of asparagine synthetase in lymphoid blasts precludes its role in sensitivity to L-asparaginase. *Exp Hematol,* 40**,** 657-65.

HILLMANN, A. G., RAMDAS, J., MULTANEN, K., NORMAN, M. R. & HARMON, J. M. 2000. Glucocorticoid Receptor Gene Mutations in Leukemic Cells Acquired in Vitro and <em>in Vivo</em&gt. *Cancer Research,* 60**,** 2056.

HINZE, L., PFIRRMANN, M., KARIM, S., DEGAR, J., MCGUCKIN, C., VINJAMUR, D., SACHER, J., STEVENSON, K. E., NEUBERG, D. S., ORELLANA, E., STANULLA, M., GREGORY, R. I., BAUER, D. E., WAGNER, F. F., STEGMAIER, K. & GUTIERREZ, A. 2019. Synthetic Lethality of Wnt Pathway Activation and Asparaginase in Drug-Resistant Acute Leukemias. *Cancer Cell,* 35**,** 664-676.e7.

HOGAN, L. E., MEYER, J. A., YANG, J., WANG, J., WONG, N., YANG, W., CONDOS, G., HUNGER, S. P., RAETZ, E., SAFFERY, R., RELLING, M. V., BHOJWANI, D., MORRISON, D. J. & CARROLL, W. L. 2011. Integrated genomic analysis of relapsed childhood acute lymphoblastic leukemia reveals therapeutic strategies. *Blood,* 118**,** 5218-5226.

HOLMES, R. & ZUNIGA-PFLUCKER, J. C. 2009. The OP9-DL1 system: generation of T-lymphocytes from embryonic or hematopoietic stem cells in vitro. *Cold Spring Harb Protoc,* 2009**,** pdb.prot5156.

HOMMINGA, I., PIETERS, R., LANGERAK, A. W., DE ROOI, J. J., STUBBS, A., VERSTEGEN, M., VUERHARD, M., BUIJS-GLADDINES, J., KOOI, C., KLOUS, P., VAN VLIERBERGHE, P., FERRANDO, A. A., CAYUELA, J. M., VERHAAF, B., BEVERLOO, H. B., HORSTMANN, M., DE HAAS, V., WIEKMEIJER, A. S., PIKE-OVERZET, K., STAAL, F. J., DE LAAT, W., SOULIER, J., SIGAUX, F. & MEIJERINK, J. P. 2011. Integrated transcript and genome analyses reveal NKX2-1 and MEF2C as potential oncogenes in T cell acute lymphoblastic leukemia. *Cancer Cell,* 19**,** 484-97.

HOOFD, C., WANG, X., LAM, S., JENKINS, C., WOOD, B., GIAMBRA, V. & WENG, A. P. 2016. CD44 promotes chemoresistance in T-ALL by increased drug efflux. *Experimental Hematology,* 44**,** 166-171.e17.

HORTON, T., GANNAVARAPU, A., BLANEY, S., Z D'ARGENIO, D., PLON, S. & L BERG, S. 2006. Bortezomib interactions with chemotherapy agents in acute leukemia in vitro. *Cancer chemotherapy and pharmacology,* 58**,** 13-23.

HORTON, T., WHITLOCK, J., LU, X., M. O'BRIEN, M., BOROWITZ, M., DEVIDAS, M., RAETZ, E., A. BROWN, P., L. CARROLL, W. & P. HUNGER, S. 2019. Bortezomib reinduction chemotherapy in high-risk ALL in first relapse: a report from the Children's Oncology Group. *British Journal of Haematology,* 186.

HUSE, M. 2009. The T-cell-receptor signaling network. *Journal of Cell Science,* 122**,** 1269-1273.

HUTSON, R. G., KITOH, T., MORAGA AMADOR, D. A., COSIC, S., SCHUSTER, S. M. & KILBERG, M. S. 1997. Amino acid control of asparagine synthetase: relation to asparaginase resistance in human leukemia cells. *Am J Physiol,* 272**,** C1691-9.

IKEDA, M., KANAO, Y., YAMANAKA, M., SAKURABA, H., MIZUTANI, Y., IGARASHI, Y. & KIHARA, A. 2008. Characterization of four mammalian 3-hydroxyacyl-CoA dehydratases involved in very long-chain fatty acid synthesis. *FEBS Letters,* 582**,** 2435-2440.

IMAI, K., HAO, F., FUJITA, N., TSUJI, Y., OE, Y., ARAKI, Y., HAMASAKI, M., NODA, T. & YOSHIMORI, T. 2016. Atg9A trafficking through the recycling endosomes is required for autophagosome formation. *Journal of Cell Science,* 129**,** 3781-3791.

IRVING, J., MATHESON, E., MINTO, L., BLAIR, H., CASE, M., HALSEY, C., SWIDENBANK, I., PONTHAN, F., KIRSCHNER-SCHWABE, R., GROENEVELD-KRENTZ, S., HOF, J., ALLAN, J., HARRISON, C., VORMOOR, J., VON STACKELBERG, A. & ECKERT, C. 2014. Ras pathway mutations are prevalent in relapsed childhood acute lymphoblastic leukemia and confer sensitivity to MEK inhibition. *Blood,* 124**,** 3420-30.

ISHIKAWA, F., YASUKAWA, M., LYONS, B., YOSHIDA, S., MIYAMOTO, T., YOSHIMOTO, G., WATANABE, T., AKASHI, K., SHULTZ, L. D. & HARADA, M. 2005. Development of functional human blood and immune systems in NOD/SCID/IL2 receptor {gamma} chain(null) mice. *Blood,* 106**,** 1565-73.

IWAMOTO, S., MIHARA, K., DOWNING, J. R., PUI, C.-H. & CAMPANA, D. 2007. Mesenchymal cells regulate the response of acute lymphoblastic leukemia cells to asparaginase. *The Journal of clinical investigation,* 117**,** 1049-1057.

JACKSON, R. 2017. Personalisation of dexamethasone in childhood acute lymphoblastic leukaemia. Doctor of Philosophy (PhD), Newcastle University.

JACKSON, R. K., IRVING, J. A. E. & VEAL, G. J. 2016a. Abstract CT115: Pharmacokinetics of standard versus short high-dose dexamethasone therapy in childhood acute lymphoblastic leukemia: results from the UKALL 2011 trial. *Cancer Research,* 76**,** CT115-CT115.

JACKSON, R. K., IRVING, J. A. E. & VEAL, G. J. 2016b. Personalization of dexamethasone therapy in childhood acute lymphoblastic leukaemia. *British Journal of Haematology,* 173**,** 13-24.

JACOBY, E., CHIEN, C. D. & FRY, T. J. 2014. Murine models of acute leukemia: important tools in current pediatric leukemia research. *Frontiers in oncology,* 4**,** 95-95.

JANAS, M. L. & TURNER, M. 2010. Stromal cell-derived factor 1a and CXCR4: newly defined requirements for efficient thymic b selection. *Trends in Immunology,* 31**,** 370-376.

JANSEN, R., EMBDEN, J. D., GAASTRA, W. & SCHOULS, L. M. 2002. Identification of genes that are associated with DNA repeats in prokaryotes. *Mol Microbiol,* 43**,** 1565-75.

JINEK, M., CHYLINSKI, K., FONFARA, I., HAUER, M., DOUDNA, J. A. & CHARPENTIER, E. 2012. A programmable dual-RNA-guided DNA endonuclease in adaptive bacterial immunity. *Science (New York, N.Y.),* 337**,** 816-821.

JOHNSON, I. S., ARMSTRONG, J. G., GORMAN, M. & BURNETT, J. P. 1963. The Vinca Alkaloids: A New Class of Oncolytic Agents. *Cancer Research,* 23**,** 1390-1427.

KAMB, A., GRUIS, N., WEAVER-FELDHAUS, J., LIU, Q., HARSHMAN, K., TAVTIGIAN, S., STOCKERT, E., DAY, R., JOHNSON, B. & SKOLNICK, M. 1994. A cell cycle regulator potentially involved in genesis of many tumor types. *Science,* 264**,** 436-440.

KANG, X., LI, M., ZHU, H., LU, X., MIAO, J., DU, S., XIA, X. & GUAN, W. 2017. DUSP4 promotes doxorubicin resistance in gastric cancer through epithelial-mesenchymal transition. *Oncotarget,* 8.

KASPERS, G. J. L. 2019. Acute myeloid leukaemia niche regulates response to L-asparaginase. *British Journal of Haematology*.

KASTNER, P. & CHAN, S. 2011. Role of Ikaros in T-cell acute lymphoblastic leukemia. *World journal of biological chemistry,* 2**,** 108-114.

KATAYAMA, A., OGINO, T., BANDOH, N., NONAKA, S. & HARABUCHI, Y. 2005. Expression of CXCR4 and its down-regulation by IFN-gamma in head and neck squamous cell carcinoma. *Clin Cancer Res,* 11**,** 2937-46.

KENNEDY, M. A., GONZALEZ-SARMIENTO, R., KEES, U. R., LAMPERT, F., DEAR, N., BOEHM, T. & RABBITTS, T. H. 1991. HOX11, a homeobox-containing T-cell oncogene on human chromosome 10q24. *Proceedings of the National Academy of Sciences of the United States of America,* 88**,** 8900-8904.

KIM, H., JANG, S. M., AHN, H., SIM, J., YI, K., CHUNG, Y., HAN, H., REHMAN, A., CHUNG, M. S., JANG, K. & PAIK, S. S. 2015. Clinicopathological significance of dual-specificity protein phosphatase 4 expression in invasive ductal carcinoma of the breast. *Journal of breast cancer,* 18**,** 1-7.

KIRKPATRICK, D. S., DENISON, C. & GYGI, S. P. 2005. Weighing in on ubiquitin: the expanding role of mass-spectrometry-based proteomics. *Nat Cell Biol,* 7**,** 750-7.

KLUMPER, E., PIETERS, R., VEERMAN, A., R HUISMANS, D., LOONEN, A. H., HÄHLEN, K., KASPERS, G. J. L., R VAN WERING, E., HARTMANN, R. & HENZE, G. 1995. In vitro cellular resistance in children with relapsed/refractory acute lymphoblastic leukemia. *Blood,* 86**,** 3861-8.

KNOECHEL, B., RODERICK, J. E., WILLIAMSON, K. E., ZHU, J., LOHR, J. G., COTTON, M. J., GILLESPIE, S. M., FERNANDEZ, D., KU, M., WANG, H., PICCIONI, F., SILVER, S. J., JAIN, M., PEARSON, D., KLUK, M. J., OTT, C. J., SHULTZ, L. D., BREHM, M. A., GREINER, D. L., GUTIERREZ, A., STEGMAIER, K., KUNG, A. L., ROOT, D. E., BRADNER, J. E., ASTER, J. C., KELLIHER, M. A. & BERNSTEIN, B. E. 2014. An epigenetic mechanism of resistance to targeted therapy in T cell acute lymphoblastic leukemia. *Nature Genetics,* 46**,** 364.

KONERMANN, S., BRIGHAM, M. D., TREVINO, A. E., JOUNG, J., ABUDAYYEH, O. O., BARCENA, C., HSU, P. D., HABIB, N., GOOTENBERG, J. S., NISHIMASU, H., NUREKI, O. & ZHANG, F. 2015. Genome-scale transcriptional activation by an engineered CRISPR-Cas9 complex. *Nature,* 517**,** 583-8.

KOSZTYU, P., BUKVOVA, R., DOLEZEL, P. & MLEJNEK, P. 2014. Resistance to daunorubicin, imatinib, or nilotinib depends on expression levels of ABCB1 and ABCG2 in human leukemia cells. *Chemico-Biological Interactions,* 219**,** 203-210.

KOTANTAKI, P. & MOSIALOS, G. 2016. The expression of tumor suppressor gene Cyld is upregulated by histone deacetylace inhibitors in human hepatocellular carcinoma cell lines. *Cell Biochem Funct,* 34**,** 465-468.

KRAJINOVIC, M., COSTEA, I. & CHIASSON, S. 2002. Polymorphism of the thymidylate synthase gene and outcome of acute lymphoblastic leukaemia. *The Lancet,* 359**,** 1033-1034.

KREJCI, O., STARKOVA, J., OTOVA, B., MADZO, J., KALINOVA, M., HRUSAK, O. & TRKA, J. 2004. Upregulation of asparagine synthetase fails to avert cell cycle arrest induced by L-asparaginase in TEL/AML1-positive leukaemic cells. *Leukemia,* 18**,** 434-41.

KUMAR, S. K., LAPLANT, B., CHNG, W. J., ZONDER, J., CALLANDER, N., FONSECA, R., FRUTH, B., ROY, V., ERLICHMAN, C., STEWART, A. K. & MAYO PHASE, C. 2015. Dinaciclib, a novel CDK inhibitor, demonstrates encouraging single-agent activity in patients with relapsed multiple myeloma. *Blood,* 125**,** 443-448.

KUO, L. J. & YANG, L. X. 2008. Gamma-H2AX - a novel biomarker for DNA double-strand breaks. *In Vivo,* 22**,** 305-9.

LANGENAU, D. M., FENG, H., BERGHMANS, S., KANKI, J. P., KUTOK, J. L. & LOOK, A. T. 2005. Cre/lox-regulated transgenic zebrafish model with conditional myc-induced T cell acute lymphoblastic leukemia. *Proceedings of the National Academy of Sciences,* 102**,** 6068-6073.

LANGENAU, D. M., TRAVER, D., FERRANDO, A. A., KUTOK, J. L., ASTER, J. C., KANKI, J. P., LIN, S., PROCHOWNIK, E., TREDE, N. S., ZON, L. I. & LOOK, A. T. 2003. Myc-Induced T Cell Leukemia in Transgenic Zebrafish. *Science,* 299**,** 887-890.

LARANJEIRA, A. B. A., DE VASCONCELLOS, J. F., SODEK, L., SPAGO, M. C., FORNAZIM, M. C., TONE, L. G., BRANDALISE, S. R., NOWILL, A. E. & YUNES, J. A. 2011. IGFBP7 participates in the reciprocal interaction between acute lymphoblastic leukemia and BM stromal cells and in leukemia resistance to asparaginase. *Leukemia,* 26**,** 1001.

LEE, J., KANG, S., WANG, X., ROSALES, J. L., GAO, X., BYUN, H.-G., JIN, Y., FU, S., WANG, J. & LEE, K.-Y. 2019. HAP1 loss confers L-asparaginase resistance in ALL by downregulating the calpain-1-Bid-caspase-3/12 pathway. *Blood***,** blood-2018-12-890236.

LEGHA, S. S. 1986. Vincristine Neurotoxicity: Pathophysiology and Management. *Medical Toxicology,* 1**,** 421-427.

LEIBNIZ-INSTITUT. Deutsche Sammlung von Mikroorganismen und Zellkulturen [Online]. [Accessed 2019].

LEONG, K. G. & KARSAN, A. 2006. Recent insights into the role of Notch signaling in tumorigenesis. *Blood,* 107**,** 2223-2233.

LEVERSON, J. D., PHILLIPS, D. C., MITTEN, M. J., BOGHAERT, E. R., DIAZ, D., TAHIR, S. K., BELMONT, L. D., NIMMER, P., XIAO, Y., MA, X. M., LOWES, K. N., KOVAR, P., CHEN, J., JIN, S., SMITH, M., XUE, J., ZHANG, H., OLEKSIJEW, A., MAGOC, T. J., VAIDYA, K. S., ALBERT, D. H., TARRANT, J. M., LA, N., WANG, L., TAO, Z. F., WENDT, M. D., SAMPATH, D., ROSENBERG, S. H., TSE, C., HUANG, D. C., FAIRBROTHER, W. J., ELMORE, S. W. & SOUERS, A. J. 2015. Exploiting selective BCL-2 family inhibitors to dissect cell survival dependencies and define improved strategies for cancer therapy. *Sci Transl Med,* 7**,** 279ra40.

LI, J., LAW, H. K. W., LAU, Y. L. & CHAN, G. C. F. 2004. Differential damage and recovery of human mesenchymal stem cells after exposure to chemotherapeutic agents. *British Journal of Haematology,* 127**,** 326-334.

LI, J., POI, M. J. & TSAI, M.-D. 2011. Regulatory mechanisms of tumor suppressor P16(INK4A) and their relevance to cancer. *Biochemistry,* 50**,** 5566-5582.

LI, W., XU, H., XIAO, T., CONG, L., LOVE, M. I., ZHANG, F., IRIZARRY, R. A., LIU, J. S., BROWN, M. & LIU, X. S. 2014. MAGeCK enables robust identification of essential genes from genome-scale CRISPR/Cas9 knockout screens. *Genome Biology,* 15**,** 554.

LI, Y., BUIJS-GLADDINES, J. G. C. A. M., CANTÉ-BARRETT, K., STUBBS, A. P., VROEGINDEWEIJ, E. M., SMITS, W. K., VAN MARION, R., DINJENS, W. N. M., HORSTMANN, M., KUIPER, R. P., BUIJSMAN, R. C., ZAMAN, G. J. R., VAN DER SPEK, P. J., PIETERS, R. & MEIJERINK, J. P. P. 2016. IL-7 Receptor Mutations and Steroid Resistance in Pediatric T cell Acute Lymphoblastic Leukemia: A Genome Sequencing Study. *PLOS Medicine,* 13**,** e1002200.

LISTON, D. R. & DAVIS, M. 2017. Clinically Relevant Concentrations of Anticancer Drugs: A Guide for Nonclinical Studies. *Clinical Cancer Research,* 23**,** 3489.
LIU, B., LIAO, J., RAO, X., KUSHNER, S. A., CHUNG, C. D., CHANG, D. D. & SHUAI, K. 1998. Inhibition of Stat1-mediated gene activation by PIAS1. *Proceedings of the National Academy of Sciences of the United States of America,* 95**,** 10626-10631.

LIU, B., YANG, Y., CHERNISHOF, V., LOO, R. R. O., JANG, H., TAHK, S., YANG, R., MINK, S., SHULTZ, D., BELLONE, C. J., LOO, J. A. & SHUAI, K. 2007. Proinflammatory Stimuli Induce IKKα-Mediated Phosphorylation of PIAS1 to Restrict Inflammation and Immunity. *Cell,* 129**,** 903-914.

LIU, Y., EASTON, J., SHAO, Y., MACIASZEK, J., WANG, Z., WILKINSON, M. R., MCCASTLAIN, K., EDMONSON, M., POUNDS, S. B., SHI, L., ZHOU, X., MA, X., SIOSON, E., LI, Y., RUSCH, M., GUPTA, P., PEI, D., CHENG, C., SMITH, M. A., AUVIL, J. G., GERHARD, D. S., RELLING, M. V., WINICK, N. J., CARROLL, A. J., HEEREMA, N. A., RAETZ, E., DEVIDAS, M., WILLMAN, C. L.,

HARVEY, R. C., CARROLL, W. L., DUNSMORE, K. P., WINTER, S. S., WOOD, B. L., SORRENTINO, B. P., DOWNING, J. R., LOH, M. L., HUNGER, S. P., ZHANG, J. & MULLIGHAN, C. G. 2017. The genomic landscape of pediatric and young adult T-lineage acute lymphoblastic leukemia. *Nature Genetics,* 49**,** 1211.

LIU, Y., ZHANG, Y.-D., GUO, L., HUANG, H.-Y., ZHU, H., HUANG, J.-X., LIU, Y., ZHOU, S.-R., DANG, Y.-J., LI, X. & TANG, Q.-Q. 2013. Protein Inhibitor of Activated STAT 1 (PIAS1) Is Identified as the SUMO E3 Ligase of CCAAT/Enhancer-Binding Protein β (C/EBPβ) during Adipogenesis. *Molecular and Cellular Biology,* 33**,** 4606-4617.

LONNERHOLM, G., FROST, B. M., ABRAHAMSSON, J., BEHRENDTZ, M., CASTOR, A., FORESTIER, E., HEYMAN, M., UGES, D. R. & DE GRAAF, S. S. 2008. Vincristine pharmacokinetics is related to clinical outcome in children with standard risk acute lymphoblastic leukemia. *Br J Haematol,* 142**,** 616-21.

LUSTOSA DE SOUSA, D. W., DE ALMEIDA FERREIRA, F. V., CAVALCANTE FÉLIX, F. H. & DE OLIVEIRA LOPES, M. V. 2015. Acute lymphoblastic leukemia in children and adolescents: prognostic factors and analysis of survival. *Revista Brasileira de Hematologia e Hemoterapia,* 37**,** 223-229.

MACLEOD, R. A., NAGEL, S., KAUFMANN, M., JANSSEN, J. W. & DREXLER, H. G. 2003. Activation of HOX11L2 by juxtaposition with 3'-BCL11B in an acute lymphoblastic leukemia cell line (HPB-ALL) with t(5;14)(q35;q32.2). *Genes Chromosomes Cancer,* 37**,** 84-91.

MACPHAIL, S. H., BANATH, J. P., YU, Y., CHU, E. & OLIVE, P. L. 2003. Cell cycle-dependent expression of phosphorylated histone H2AX: reduced expression in unirradiated but not X-irradiated G1-phase cells. *Radiat Res,* 159**,** 759-67.

MALI, P., YANG, L., ESVELT, K. M., AACH, J., GUELL, M., DICARLO, J. E., NORVILLE, J. E. & CHURCH, G. M. 2013. RNA-guided human genome engineering via Cas9. *Science (New York, N.Y.),* 339**,** 823-826.

MANSOUR, M. R., ABRAHAM, B. J., ANDERS, L., BEREZOVSKAYA, A., GUTIERREZ, A., DURBIN, A. D., ETCHIN, J., LAWTON, L., SALLAN, S. E., SILVERMAN, L. B., LOH, M. L., HUNGER, S. P., SANDA, T., YOUNG, R. A. & LOOK, A. T. 2014. Oncogene regulation. An oncogenic super-enhancer formed through somatic mutation of a noncoding intergenic element. *Science (New York, N.Y.),* 346**,** 1373-1377.

MARINELLO, J., DELCURATOLO, M. & CAPRANICO, G. 2018. Anthracyclines as Topoisomerase II Poisons: From Early Studies to New Perspectives. *Int J Mol Sci,* 19.

MARKS, D. I., PAIETTA, E. M., MOORMAN, A. V., RICHARDS, S. M., BUCK, G., DEWALD, G., FERRANDO, A., FIELDING, A. K., GOLDSTONE, A. H., KETTERLING, R. P., LITZOW, M. R., LUGER, S. M., MCMILLAN, A. K., MANSOUR, M. R., ROWE, J. M., TALLMAN, M. S. & LAZARUS, H. M. 2009. T-cell acute lymphoblastic leukemia in adults: Clinical features, immunophenotype, cytogenetics, and outcome from the large randomized prospective trial (UKALL XII/ECOG 2993). *Blood,* 114**,** 5136-5145.

MARTELLI, M. A., PAGANELLI, F., FAZIO, A., BAZZICHETTO, C., CONCIATORI, F. & MCCUBREY, A. J. 2019. The Key Roles of PTEN in T-Cell Acute Lymphoblastic Leukemia Development, Progression, and Therapeutic Response. *Cancers,* 11.

MARTINO, E., CASAMASSIMA, G., CASTIGLIONE, S., CELLUPICA, E., PANTALONE, S., PAPAGNI, F., RUI, M., SICILIANO, A. M. & COLLINA, S. 2018. Vinca alkaloids and analogues as anti-

cancer agents: Looking back, peering ahead. *Bioorganic & Medicinal Chemistry Letters,* 28**,** 2816-2826.

MASSOUMI, R. 2010. Ubiquitin chain cleavage: CYLD at work. *Trends Biochem Sci,* 35**,** 392-9.

MATHESON, E. C., THOMAS, H., CASE, M., BLAIR, H., JACKSON, R. K., MASIC, D., VEAL, G., HALSEY, C., NEWELL, D. R., VORMOOR, J. & IRVING, J. A. E. 2019. Glucocorticoids and selumetinib are highly synergistic in RAS pathway mutated childhood acute lymphoblastic leukemia through upregulation of BIM. *Haematologica***,** haematol.2017.185975.

MAVRAKIS, K. J., VAN DER MEULEN, J., WOLFE, A. L., LIU, X., METS, E., TAGHON, T., KHAN, A. A., SETTY, M., RONDOU, P., VANDENBERGHE, P., DELABESSE, E., BENOIT, Y., SOCCI, N. B., LESLIE, C. S., VAN VLIERBERGHE, P., SPELEMAN, F. & WENDEL, H.-G. 2011. A cooperative microRNA-tumor suppressor gene network in acute T-cell lymphoblastic leukemia (T-ALL). *Nature Genetics,* 43**,** 673.

MAVRAKIS, K. J., WOLFE, A. L., ORICCHIO, E., PALOMERO, T., DE KEERSMAECKER, K., MCJUNKIN, K., ZUBER, J., JAMES, T., KHAN, A. A., LESLIE, C. S., PARKER, J. S., PADDISON, P. J., TAM, W., FERRANDO, A. & WENDEL, H.-G. 2010. Genome-wide RNA-mediated interference screen identifies miR-19 targets in Notch-induced T-cell acute lymphoblastic leukaemia. *Nature Cell Biology,* 12**,** 372.

MCCORMACK, M. P., YOUNG, L. F., VASUDEVAN, S., DE GRAAF, C. A., CODRINGTON, R., RABBITTS, T. H., JANE, S. M. & CURTIS, D. J. 2010. The Lmo2 Oncogene Initiates Leukemia in Mice by Inducing Thymocyte Self-Renewal. *Science,* 327**,** 879.

MCGOWAN, J. V., CHUNG, R., MAULIK, A., PIOTROWSKA, I., WALKER, J. M. & YELLON, D. M. 2017. Anthracycline Chemotherapy and Cardiotoxicity. *Cardiovasc Drugs Ther,* 31**,** 63-75.
MEDICINE, N. L. O. 2019. *ClinicalTrials.gov* [Online]. National Institutes of Health (NIH). Available: https://clinicaltrials.gov/ [Accessed 2019].

MEIBOHM, B. & DERENDORF, H. 1997. Basic concepts of pharmacokinetic/pharmacodynamic (PK/PD) modelling. *Int J Clin Pharmacol Ther,* 35**,** 401-13.

MESSINGER, Y. H., GAYNON, P. S., SPOSTO, R., VAN DER GIESSEN, J., ECKROTH, E., MALVAR, J. & BOSTROM, B. C. 2012. Bortezomib with chemotherapy is highly active in advanced B-precursor acute lymphoblastic leukemia: Therapeutic Advances in Childhood Leukemia & Lymphoma (TACL) Study. *Blood,* 120**,** 285.

MESTAS, J. & HUGHES, C. C. 2004. Of mice and not men: differences between mouse and human immunology. *J Immunol,* 172**,** 2731-8.

MEYERS, R. M., BRYAN, J. G., MCFARLAND, J. M., WEIR, B. A., SIZEMORE, A. E., XU, H., DHARIA, N. V., MONTGOMERY, P. G., COWLEY, G. S., PANTEL, S., GOODALE, A., LEE, Y., ALI, L. D., JIANG, G., LUBONJA, R., HARRINGTON, W. F., STRICKLAND, M., WU, T., HAWES, D. C., ZHIVICH, V. A., WYATT, M. R., KALANI, Z., CHANG, J. J., OKAMOTO, M., STEGMAIER, K., GOLUB, T. R., BOEHM, J. S., VAZQUEZ, F., ROOT, D. E., HAHN, W. C. & TSHERNIAK, A. 2017. Computational correction of copy number effect improves specificity of CRISPR–Cas9 essentiality screens in cancer cells. *Nature Genetics,* 49**,** 1779.

MITCHELL, C., PAYNE, J., WADE, R., VORA, A., KINSEY, S., RICHARDS, S. & EDEN, T. 2009. The impact of risk stratification by early bone-marrow response in childhood lymphoblastic

leukaemia: results from the United Kingdom Medical Research Council trial ALL97 and ALL97/99. *British Journal of Haematology,* 146**,** 424-436.

MOORE, A. S., NORRIS, R., PRICE, G., NGUYEN, T., NI, M., GEORGE, R., VAN BREDA, K., DULEY, J., CHARLES, B. & PINKERTON, R. 2011a. Vincristine pharmacodynamics and pharmacogenetics in children with cancer: A limited-sampling, population modelling approach. *Journal of Paediatrics and Child Health,* 47**,** 875-882.

MOORE, A. S., NORRIS, R., PRICE, G., NGUYEN, T., NI, M., GEORGE, R., VAN BREDA, K., DULEY, J., CHARLES, B. & PINKERTON, R. 2011b. Vincristine pharmacodynamics and pharmacogenetics in children with cancer: a limited-sampling, population modelling approach. *J Paediatr Child Health,* 47**,** 875-82.

MOORE, C. B., GUTHRIE, E. H., HUANG, M. T.-H. & TAXMAN, D. J. 2010. Short hairpin RNA (shRNA): design, delivery, and assessment of gene knockdown. *Methods in molecular biology (Clifton, N.J.),* 629**,** 141-158.

MOORMAN AV, I. J., ENSHAEI A, PARKER CA, SUTTON R, KUIPER R, ERHORN A, MINTO L, VENN NC, LAW T, YU J, SCHWAB C, DAVIES R, SONNEVELD E, DEN BOER ML, LOVE SB, HARRISON CJ, HOOGERBRUGGE PM, REVESZ T, SAHA V. Composite Index for Risk Prediction in Relapsed Childhood Acute Lymphoblastic Leukaemia. 20th Congress of the European Hematology Association, 21/05/2015 2015. Ferrata Storti Foundation, 195-196.

MUKHERJEE, D. & ZHAO, J. 2013. The Role of chemokine receptor CXCR4 in breast cancer metastasis. *American journal of cancer research,* 3**,** 46-57.

MÜLLER, H.-J., BEIER, R., LÖNING, L., BLÜTTERS-SAWATZKI, R., DÖRFFEL, W., MAASS, E., MÜLLER-WEIHRICH, S., SCHEEL-WALTER, H.-G., SCHERER, F., STAHNKE, K., SCHRAPPE, M., HORN, A., LÜMKEMANN, K. & BOOS, J. 2001. Pharmacokinetics of native Escherichia coli asparaginase (Asparaginase medac) and hypersensitivity reactions in ALL-BFM 95 reinduction treatment. *British Journal of Haematology,* 114**,** 794-799.

MÜLLER, M., SCHLEITHOFF, E. S., STREMMEL, W., MELINO, G., KRAMMER, P. H. & SCHILLING, T. 2006. One, two, three—p53, p63, p73 and chemosensitivity. *Drug Resistance Updates,* 9**,** 288-306.

MULLIGHAN, C. G., PHILLIPS, L. A., SU, X., MA, J., MILLER, C. B., SHURTLEFF, S. A. & DOWNING, J. R. 2008. Genomic analysis of the clonal origins of relapsed acute lymphoblastic leukemia. *Science (New York, N.Y.),* 322**,** 1377-1380.

MUNOZ, M., HENDERSON, M., HABER, M. & NORRIS, M. 2007. Role of the MRP1/ABCC1 Multidrug Transporter Protein in Cancer. *IUBMB Life,* 59**,** 752-757.

MURDOCH, C. 2000. CXCR4: chemokine receptor extraordinaire. *Immunol Rev,* 177**,** 175-84.

NAGEL, S., SCHERR, M., KEL, A., HORNISCHER, K., CRAWFORD, G. E., KAUFMANN, M., MEYER, C., DREXLER, H. G. & MACLEOD, R. A. 2007. Activation of TLX3 and NKX2-5 in t(5;14)(q35;q32) T-cell acute lymphoblastic leukemia by remote 3'-BCL11B enhancers and coregulation by PU.1 and HMGA1. *Cancer Res,* 67**,** 1461-71.

NAIR, A. B. & JACOB, S. 2016. A simple practice guide for dose conversion between animals and human. *Journal of basic and clinical pharmacy,* 7**,** 27-31.

NEUMANN, M., VOSBERG, S., SCHLEE, C., HEESCH, S., SCHWARTZ, S., GOKBUGET, N., HOELZER, D., GRAF, A., KREBS, S., BARTRAM, I., BLUM, H., BRUGGEMANN, M., HECHT, J.,

BOHLANDER, S. K., GREIF, P. A. & BALDUS, C. D. 2015. Mutational spectrum of adult T-ALL. *Oncotarget,* 6**,** 2754-66.

NIEMEYER, C. M. & GERMLINE, C. B. L. 2010. mutations cause developmental abnormalities and predispose to juvenile myelomonocytic leukemia. *Nat. Genet.,* 42**,** 794-800.

NIH. 2019. *ClinicalTrials.gov* [Online]. National Institutes of Health (NIH). Available: https://clinicaltrials.gov/ [Accessed 2019].

NISHIWAKI, E., TURNER, S. L., HARJU, S., MIYAZAKI, S., KASHIWAGI, M., KOH, J. & SERIZAWA, H. 2000. Regulation of CDK7-carboxyl-terminal domain kinase activity by the tumor suppressor p16(INK4A) contributes to cell cycle regulation. *Molecular and cellular biology,* 20**,** 7726-7734.

NITISS, J. L. 2009. Targeting DNA topoisomerase II in cancer chemotherapy. *Nature Reviews Cancer,* 9**,** 338-350.

O'BOYLE, G., SWIDENBANK, I., MARSHALL, H., BARKER, C. E., ARMSTRONG, J., WHITE, S. A., FRICKER, S. P., PLUMMER, R., WRIGHT, M. & LOVAT, P. E. 2013. Inhibition of CXCR4-CXCL12 chemotaxis in melanoma by AMD11070. *British journal of cancer,* 108**,** 1634-1640.

O'CONNOR, D., MOORMAN, A., WADE, R., HANCOCK, J., TAN, R., BARTRAM, J., MOPPETT, J., SCHWAB, C., PATRICK, K., HARRISON, C., HOUGH, R., GOULDEN, N., VORA, A. & SAMARASINGHE, S. 2017. Use of Minimal Residual Disease Assessment to Redefine Induction Failure in Pediatric Acute Lymphoblastic Leukemia. *Journal of clinical oncology : official journal of the American Society of Clinical Oncology,* 35**,** JCO2016696278.

O'DOHERTY, U., SWIGGARD, W. J. & MALIM, M. H. 2000. Human immunodeficiency virus type 1 spinoculation enhances infection through virus binding. *J Virol,* 74**,** 10074-80.

O'NEIL, J., GRIM, J., STRACK, P., RAO, S., TIBBITTS, D., WINTER, C., HARDWICK, J., WELCKER, M., MEIJERINK, J. P., PIETERS, R., DRAETTA, G., SEARS, R., CLURMAN, B. E. & LOOK, A. T. 2007. FBW7 mutations in leukemic cells mediate NOTCH pathway activation and resistance to gamma-secretase inhibitors. *J Exp Med,* 204**,** 1813-24.

OAKLEY, R. H. & CIDLOWSKI, J. A. 2013. The biology of the glucocorticoid receptor: new signaling mechanisms in health and disease. *The Journal of allergy and clinical immunology,* 132**,** 1033-1044.

OLLENSCHLAGER, G., ROTH, E., LINKESCH, W., JANSEN, S., SIMMEL, A. & MODDER, B. 1988. Asparaginase-induced derangements of glutamine metabolism: the pathogenetic basis for some drug-related side-effects. *Eur J Clin Invest,* 18**,** 512-6.

OLSON, T. S. & LEY, K. 2002. Chemokines and chemokine receptors in leukocyte trafficking. *American Journal of Physiology-Regulatory, Integrative and Comparative Physiology,* 283**,** R7-R28.

PACI, A., VEAL, G., BARDIN, C., LEVÊQUE, D., WIDMER, N., BEIJNEN, J., ASTIER, A. & CHATELUT, E. 2014. Review of therapeutic drug monitoring of anticancer drugs part 1 – Cytotoxics. *European Journal of Cancer,* 50**,** 2010-2019.

PALOMERO, T., BARNES, K. C., REAL, P. J., GLADE BENDER, J. L., SULIS, M. L., MURTY, V. V., COLOVAI, A. I., BALBIN, M. & FERRANDO, A. A. 2006. CUTLL1, a novel human T-cell

lymphoma cell line with t(7;9) rearrangement, aberrant NOTCH1 activation and high sensitivity to gamma-secretase inhibitors. *Leukemia,* 20**,** 1279-87.

PANG, B., QIAO, X., JANSSEN, L., VELDS, A., GROOTHUIS, T., KERKHOVEN, R., NIEUWLAND, M., OVAA, H., ROTTENBERG, S., VAN TELLINGEN, O., JANSSEN, J., HUIJGENS, P., ZWART, W. & NEEFJES, J. 2013. Drug-induced histone eviction from open chromatin contributes to the chemotherapeutic effects of doxorubicin. *Nature Communications,* 4**,** 1908.

PANOSYAN, E. H., SEIBEL, N. L., MARTIN-ARAGON, S., GAYNON, P. S., AVRAMIS, I. A., SATHER, H., FRANKLIN, J., NACHMAN, J., ETTINGER, L. J., LA, M., STEINHERZ, P., COHEN, L. J., SIEGEL, S. E. & AVRAMIS, V. I. 2004. Asparaginase antibody and asparaginase activity in children with higher-risk acute lymphoblastic leukemia: Children's Cancer Group Study CCG-1961. *J Pediatr Hematol Oncol,* 26**,** 217-26.

PARKER, C., WATERS, R., LEIGHTON, C., HANCOCK, J., SUTTON, R., MOORMAN, A. V., ANCLIFF, P., MORGAN, M., MASUREKAR, A., GOULDEN, N., GREEN, N., RÉVÉSZ, T., DARBYSHIRE, P., LOVE, S. & SAHA, V. 2010. Effect of mitoxantrone on outcome of children with first relapse of acute lymphoblastic leukaemia (ALL R3): An open-label randomised trial. *The Lancet,* 376**,** 2009-2017.

PARNAS, O., JOVANOVIC, M., EISENHAURE, THOMAS M., HERBST, REBECCA H., DIXIT, A., YE, CHUN J., PRZYBYLSKI, D., PLATT, RANDALL J., TIROSH, I., SANJANA, NEVILLE E., SHALEM, O., SATIJA, R., RAYCHOWDHURY, R., MERTINS, P., CARR, STEVEN A., ZHANG, F., HACOHEN, N. & REGEV, A. 2015. A Genome-wide CRISPR Screen in Primary Immune Cells to Dissect Regulatory Networks. *Cell,* 162**,** 675-686.

PASSARO, D., IRIGOYEN, M., CATHERINET, C., GACHET, S., DA COSTA DE JESUS, C., LASGI, C., TRAN QUANG, C. & GHYSDAEL, J. 2015. CXCR4 Is Required for Leukemia-Initiating Cell Activity in T Cell Acute Lymphoblastic Leukemia. *Cancer Cell,* 27**,** 769-779.

PATEL, B., DEY, A., CASTLETON, A. Z., SCHWAB, C., SAMUEL, E., SIVAKUMARAN, J., BEATON, B., ZAREIAN, N., ZHANG, C. Y., RAI, L., ENVER, T., MOORMAN, A. V. & FIELDING, A. K. 2014. Mouse xenograft modeling of human adult acute lymphoblastic leukemia provides mechanistic insights into adult LIC biology. *Blood,* 124**,** 96-105.

PATRICK, K., WADE, R., GOULDEN, N., MITCHELL, C., MOORMAN, A. V., ROWNTREE, C., JENKINSON, S., HOUGH, R. & VORA, A. 2014. Outcome for children and young people with Early T-cell precursor acute lymphoblastic leukaemia treated on a contemporary protocol, UKALL 2003. *British Journal of Haematology,* 166**,** 421-424.

PAUGH, S. W., BONTEN, E. J., SAVIC, D., RAMSEY, L. B., THIERFELDER, W. E., GURUNG, P., MALIREDDI, R. K. S., ACTIS, M., MAYASUNDARI, A., MIN, J., COSS, D. R., LAUDERMILK, L. T., PANETTA, J. C., MCCORKLE, J. R., FAN, Y., CREWS, K. R., STOCCO, G., WILKINSON, M. R., FERREIRA, A. M., CHENG, C., YANG, W., KAROL, S. E., FERNANDEZ, C. A., DIOUF, B., SMITH, C., HICKS, J. K., ZANUT, A., GIORDANENGO, A., CRONA, D., BIANCHI, J. J., HOLMFELDT, L., MULLIGHAN, C. G., DEN BOER, M. L., PIETERS, R., JEHA, S., DUNWELL, T. L., LATIF, F., BHOJWANI, D., CARROLL, W. L., PUI, C.-H., MYERS, R. M., GUY, R. K., KANNEGANTI, T.-D., RELLING, M. V. & EVANS, W. E. 2015. NALP3 inflammasome upregulation and CASP1 cleavage of the glucocorticoid receptor cause glucocorticoid resistance in leukemia cells. *Nature Genetics,* 47**,** 607.

PEAR, W. S., ASTER, J. C., SCOTT, M. L., HASSERJIAN, R. P., SOFFER, B., SKLAR, J. & BALTIMORE, D. 1996. Exclusive development of T cell neoplasms in mice transplanted with

bone marrow expressing activated Notch alleles. *The Journal of Experimental Medicine,* 183**,** 2283-2291.

PIETERS, R., DE LORENZO, P., ANCLIFFE, P., AVERSA, L. A., BRETHON, B., BIONDI, A., CAMPBELL, M., ESCHERICH, G., FERSTER, A., GARDNER, R. A., KOTECHA, R. S., LAUSEN, B., LI, C. K., LOCATELLI, F., ATTARBASCHI, A., PETERS, C., RUBNITZ, J. E., SILVERMAN, L. B., STARY, J., SZCZEPANSKI, T., VORA, A., SCHRAPPE, M. & VALSECCHI, M. G. 2019. Outcome of Infants Younger Than 1 Year With Acute Lymphoblastic Leukemia Treated With the Interfant-06 Protocol: Results From an International Phase III Randomized Study. *J Clin Oncol,* 37**,** 2246-2256.

PIETRO, D. A., ALEXANDER, S., MANTELL, G., STAGGERS, J. E. & COOK, T. J. 1989. Effects of simvastatin and probucol in hypercholesterolemia (simvastatin multicenter study group II). *The American Journal of Cardiology,* 63**,** 682-686.

PIKMAN, Y., ALEXE, G., ROTI, G., CONWAY, A. S., FURMAN, A., LEE, E. S., PLACE, A. E., KIM, S., SARAN, C., MODISTE, R., WEINSTOCK, D. M., HARRIS, M., KUNG, A. L., SILVERMAN, L. B. & STEGMAIER, K. 2017. Synergistic Drug Combinations with a CDK4/6 Inhibitor in T-cell Acute Lymphoblastic Leukemia. *Clinical Cancer Research,* 23**,** 1012-1024.

PIOVAN, E., YU, J., TOSELLO, V., HERRANZ, D., AMBESI-IMPIOMBATO, A., DA SILVA, ANA C., SANCHEZ-MARTIN, M., PEREZ-GARCIA, A., RIGO, I., CASTILLO, M., INDRACCOLO, S., CROSS, JUSTIN R., DE STANCHINA, E., PAIETTA, E., RACEVSKIS, J., ROWE, JACOB M., TALLMAN, MARTIN S., BASSO, G., MEIJERINK, JULES P., CORDON-CARDO, C., CALIFANO, A. & FERRANDO, ADOLFO A. 2013. Direct Reversal of Glucocorticoid Resistance by AKT Inhibition in Acute Lymphoblastic Leukemia. *Cancer Cell,* 24**,** 766-776.

POGLIO, S., LEWANDOWSKI, D., CALVO, J., CAYE, A., GROS, A., LAHARANNE, E., LEBLANC, T., LANDMAN-PARKER, J., BARUCHEL, A., SOULIER, J., BALLERINI, P., CLAPPIER, E. & PFLUMIO, F. 2016. Speed of leukemia development and genetic diversity in xenograft models of T cell acute lymphoblastic leukemia. *Oncotarget,* 7**,** 41599-41611.

POLAK, R., DE ROOIJ, B., PIETERS, R. & DEN BOER, M. L. 2014. Primary Acute Lymphoblastic Leukemia Cells Create a Drug-Resistant Niche By Tunneling Nanotube Signaling with Mesenchymal Stromal Cells. *Blood,* 124**,** 64-64.

PORCU, M., GIELEN, O., COOLS, J. & DE KEERSMAECKER, K. 2009. JAK1 mutation analysis in T-cell acute lymphoblastic leukemia cell lines. *Haematologica,* 94**,** 435-437.

PRABST, K., ENGELHARDT, H., RINGGELER, S. & HUBNER, H. 2017. Basic Colorimetric Proliferation Assays: MTT, WST, and Resazurin. *Methods Mol Biol,* 1601**,** 1-17.

PRATT, W. B. & TOFT, D. O. 1997. Steroid receptor interactions with heat shock protein and immunophilin chaperones. *Endocrine reviews,* 18**,** 306-360.

PRESCOTT, M. J. & LIDSTER, K. 2017. Improving quality of science through better animal welfare: the NC3Rs strategy. *Lab Anim (NY),* 46**,** 152-156.

QIN, J.-Z., ZIFFRA, J., STENNETT, L., BODNER, B., BONISH, B. K., CHATURVEDI, V., BENNETT, F., POLLOCK, P. M., TRENT, J. M., HENDRIX, M. J. C., RIZZO, P., MIELE, L. & NICKOLOFF, B. J. 2005. Proteasome Inhibitors Trigger NOXA-Mediated Apoptosis in Melanoma and Myeloma Cells. *Cancer Research,* 65**,** 6282-6293.

QIU, S., ADEMA, C. M. & LANE, T. 2005. A computational study of off-target effects of RNA interference. *Nucleic acids research,* 33**,** 1834-1847.

QUECKENBERG, C., WACHALL, B., ERLINGHAGEN, V., DI GION, P., TOMALIK-SCHARTE, D., TAWAB, M., GERBETH, K. & FUHR, U. 2011. Pharmacokinetics, Pharmacodynamics, and Comparative Bioavailability of Single, Oral 2-mg Doses of Dexamethasone Liquid and Tablet Formulations: A Randomized, Controlled, Crossover Study in Healthy Adult Volunteers. *Clinical Therapeutics,* 33**,** 1831-1841.

RAETZ, E. A., BOROWITZ, M. J., DEVIDAS, M., LINDA, S. B., HUNGER, S. P., WINICK, N. J., CAMITTA, B. M., GAYNON, P. S. & CARROLL, W. L. 2008. Reinduction platform for children with first marrow relapse of acute lymphoblastic Leukemia: A Children's Oncology Group Study[corrected]. *J Clin Oncol,* 26**,** 3971-8.

RAHMAN, A. M., YUSUF, S. W. & EWER, M. S. 2007. Anthracycline-induced cardiotoxicity and the cardiac-sparing effect of liposomal formulation. *International journal of nanomedicine,* 2**,** 567-583.

RAMDAS, J., LIU, W. & HARMON, J. M. 1999. Glucocorticoid-induced Cell Death Requires Autoinduction of Glucocorticoid Receptor Expression in Human Leukemic T Cells. *Cancer Research,* 59**,** 1378-1385.

RAPPA, G., LORICO, A., FLAVELL, R. A. & SARTORELLI, A. C. 1997. Evidence That the Multidrug Resistance Protein (MRP) Functions as a Co-Transporter of Glutathione and Natural Product Toxins. *Cancer Research,* 57**,** 5232-5237.

RATAJCZAK, M. Z., ZUBA-SURMA, E., KUCIA, M., RECA, R., WOJAKOWSKI, W. & RATAJCZAK, J. 2006. The pleiotropic effects of the SDF-1–CXCR4 axis in organogenesis, regeneration and tumorigenesis. *Leukemia,* 20**,** 1915-1924.

RATEI, R., BASSO, G., DWORZAK, M., GAIPA, G., VELTRONI, M., RHEIN, P., BIONDI, A., SCHRAPPE, M., LUDWIG, W. D. & KARAWAJEW, L. 2008. Monitoring treatment response of childhood precursor B-cell acute lymphoblastic leukemia in the AIEOP-BFM-ALL 2000 protocol with multiparameter flow cytometry: predictive impact of early blast reduction on the remission status after induction. *Leukemia,* 23**,** 528.

REDDY, T. E., PAULI, F., SPROUSE, R. O., NEFF, N. F., NEWBERRY, K. M., GARABEDIAN, M. J. & MYERS, R. M. 2009. Genomic determination of the glucocorticoid response reveals unexpected mechanisms of gene regulation. *Genome research,* 19**,** 2163-2171.

RIBEIRO, D., MELÃO, A. & BARATA, J. T. 2013. IL-7R-mediated signaling in T-cell acute lymphoblastic leukemia. *Advances in Biological Regulation,* 53**,** 211-222.

RIDGES, S., HEATON, W. L., JOSHI, D., CHOI, H., EIRING, A., BATCHELOR, L., CHOUDHRY, P., MANOS, E. J., SOFLA, H., SANATI, A., WELBORN, S., AGARWAL, A., SPANGRUDE, G. J., MILES, R. R., COX, J. E., FRAZER, J. K., DEININGER, M., BALAN, K., SIGMAN, M., MÜSCHEN, M., PEROVA, T., JOHNSON, R., MONTPELLIER, B., GUIDOS, C. J., JONES, D. A. & TREDE, N. S. 2012. Zebrafish screen identifies novel compound with selective toxicity against leukemia. *Blood,* 119**,** 5621-5631.

RIZOS, H., MCKENZIE, H. A., AYUB, A. L., WOODRUFF, S., BECKER, T. M., SCURR, L. L., STAHL, J. & KEFFORD, R. F. 2006. Physical and Functional Interaction of the p14ARF Tumor Suppressor with Ribosomes. *Journal of Biological Chemistry,* 281**,** 38080-38088.

RIZZARI, C., ZUCCHETTI, M., CONTER, V., DIOMEDE, L., BRUNO, A., GAVAZZI, L., PAGANINI, M., SPARANO, P., LO NIGRO, L., ARICÒ, M., MILANI, M. & D'LNCALCI, M. 2000. l-asparagine depletion and l-asparaginase activity in children with acute lymphoblastic leukemia receiving i.m. or i.v. Erwinia C. or E. colil-asparaginase as first exposure. *Annals of Oncology,* 11**,** 189-193.

ROOSWINKEL, R. W., VAN DE KOOIJ, B., VERHEIJ, M. & BORST, J. 2012. Bcl-2 is a better ABT-737 target than Bcl-xL or Bcl-w and only Noxa overcomes resistance mediated by Mcl-1, Bfl-1, or Bcl-B. *Cell Death &Amp; Disease,* 3**,** e366.

ROSE, A. & MAYOR, T. 2018. Exploring the Rampant Expansion of Ubiquitin Proteomics. *Methods Mol Biol,* 1844**,** 345-362.

ROSENTHAL, S. & KAUFMAN, S. 1974. Vincristine neurotoxicity. *Annals of Internal Medicine,* 80**,** 733-737.

ROSEWICZ, S., R MCDONALD, A., MADDUX, B., D GOLDFINE, I., L MIESFELD, R. & LOGSDON, C. 1988. *Mechanism of glucocorticoid receptor down-regulation by glucocorticoids*.

ROTIN, D. & KUMAR, S. 2009. Physiological functions of the HECT family of ubiquitin ligases. *Nat Rev Mol Cell Biol,* 10**,** 398-409.

ROTS, M. G., WILLEY, J. C., JANSEN, G., VAN ZANTWIJK, C. H., NOORDHUIS, P., DEMUTH, J. P., KUIPER, E., VEERMAN, A. J., PIETERS, R. & PETERS, G. J. 2000. mRNA expression levels of methotrexate resistance-related proteins in childhood leukemia as determined by a standardized competitive template-based RT-PCR method. *Leukemia,* 14**,** 2166-75.
SAIGUSA, S., INOUE, Y., TANAKA, K., TOIYAMA, Y., OKUGAWA, Y., SHIMURA, T., HIRO, J., UCHIDA, K., MOHRI, Y. & KUSUNOKI, M. 2013. Decreased expression of DUSP4 is associated with liver and lung metastases in colorectal cancer. *Medical oncology (Northwood, London, England),* 30**,** 620.

SAITO, Y., AOKI, Y., MURAMATSU, H., MAKISHIMA, H., MACIEJEWSKI, J. P., IMAIZUMI, M., RIKIISHI, T., SASAHARA, Y., KURE, S., NIIHORI, T., TSUCHIYA, S., KOJIMA, S. & MATSUBARA, Y. 2012. Casitas B-cell lymphoma mutation in childhood T-cell acute lymphoblastic leukemia. *Leukemia Research,* 36**,** 1009-1015.

SAMUELS, A. L., BEESLEY, A. H., YADAV, B. D., PAPA, R. A., SUTTON, R., ANDERSON, D., MARSHALL, G. M., COLE, C. H., KEES, U. R. & LOCK, R. B. 2014a. A pre-clinical model of resistance to induction therapy in pediatric acute lymphoblastic leukemia. *Blood Cancer J,* 4**,** e232.

SAMUELS, A. L., BEESLEY, A. H., YADAV, B. D., PAPA, R. A., SUTTON, R., ANDERSON, D., MARSHALL, G. M., COLE, C. H., KEES, U. R. & LOCK, R. B. 2014b. A pre-clinical model of resistance to induction therapy in pediatric acute lymphoblastic leukemia. *Blood Cancer Journal,* 4**,** e232.

SANADA, M., SUZUKI, T., SHIH, L.-Y., OTSU, M., KATO, M., YAMAZAKI, S., TAMURA, A., HONDA, H., SAKATA-YANAGIMOTO, M., KUMANO, K., ODA, H., YAMAGATA, T., TAKITA, J., GOTOH, N., NAKAZAKI, K., KAWAMATA, N., ONODERA, M., NOBUYOSHI, M., HAYASHI, Y., HARADA, H., KUROKAWA, M., CHIBA, S., MORI, H., OZAWA, K., OMINE, M., HIRAI, H., NAKAUCHI, H., KOEFFLER, H. P. & OGAWA, S. 2009. Gain-of-function of mutated C-CBL tumour suppressor in myeloid neoplasms. *Nature,* 460**,** 904.

SANDA, T., TYNER, J. W., GUTIERREZ, A., NGO, V. N., GLOVER, J., CHANG, B. H., YOST, A., MA, W., FLEISCHMAN, A. G., ZHOU, W., YANG, Y., KLEPPE, M., AHN, Y., TATAREK, J., KELLIHER, M. A., NEUBERG, D. S., LEVINE, R. L., MORIGGL, R., MÜLLER, M., GRAY, N. S., JAMIESON, C. H. M., WENG, A. P., STAUDT, L. M., DRUKER, B. J. & LOOK, A. T. 2013. TYK2–STAT1–BCL2 Pathway Dependence in T-cell Acute Lymphoblastic Leukemia. *Cancer Discovery,* 3**,** 564-577.

SANDLER, S. G., TOBIN, W. & HENDERSON, E. S. 1969. Vincristine-induced neuropathy: A clinical study of fifty leukemic patients. *Neurology,* 19**,** 367-374.

SANJANA, N. E., SHALEM, O. & ZHANG, F. 2014. Improved vectors and genome-wide libraries for CRISPR screening. *Nature methods,* 11**,** 783-784.

SANSON, K. R., HANNA, R. E., HEGDE, M., DONOVAN, K. F., STRAND, C., SULLENDER, M. E., VAIMBERG, E. W., GOODALE, A., ROOT, D. E., PICCIONI, F. & DOENCH, J. G. 2018. Optimized libraries for CRISPR-Cas9 genetic screens with multiple modalities. *Nature Communications,* 9**,** 5416.

SASSA, T., SUTO, S., OKAYASU, Y. & KIHARA, A. 2012. A shift in sphingolipid composition from C24 to C16 increases susceptibility to apoptosis in HeLa cells. *Biochim Biophys Acta,* 1821**,** 1031-7.

SATO, A., KLAUNBERG, B. & TOLWANI, R. 2004. In vivo bioluminescence imaging. *Comp Med,* 54**,** 631-4.

SAWAI, C. M., FREUND, J., OH, P., NDIAYE-LOBRY, D., BRETZ, JAMIESON C., STRIKOUDIS, A., GENESCA, L., TRIMARCHI, T., KELLIHER, MICHELLE A., CLARK, M., SOULIER, J., CHEN-KIANG, S. & AIFANTIS, I. 2012. Therapeutic Targeting of the Cyclin D3:CDK4/6 Complex in T Cell Leukemia. *Cancer Cell,* 22**,** 452-465.

SAYGIN, C., HIRSCH, C., PRZYCHODZEN, B., SEKERES, M. A., HAMILTON, B. K., KALAYCIO, M., CARRAWAY, H. E., GERDS, A. T., MUKHERJEE, S., NAZHA, A., SOBECKS, R., GOEBEL, C., ABOUNADER, D., MACIEJEWSKI, J. P. & ADVANI, A. S. 2018. Mutations in DNMT3A, U2AF1, and EZH2 identify intermediate-risk acute myeloid leukemia patients with poor outcome after CR1. *Blood Cancer Journal,* 8**,** 4.

SCHARF, S. H., LIEBL, C., BINDER, E. B., SCHMIDT, M. V. & MÜLLER, M. B. 2011. Expression and Regulation of the Fkbp5 Gene in the Adult Mouse Brain. *PLOS ONE,* 6**,** e16883.

SCHEER, N., ROSS, J., KAPELYUKH, Y., RODE, A. & WOLF, C. R. 2010. In Vivo Responses of the Human and Murine Pregnane X Receptor to Dexamethasone in Mice. *Drug Metabolism and Disposition,* 38**,** 1046-1053.

SCHMID, C. A., ROBINSON, M. D., SCHEIFINGER, N. A., MÜLLER, S., COGLIATTI, S., TZANKOV, A. & MÜLLER, A. 2015. DUSP4 deficiency caused by promoter hypermethylation drives JNK signaling and tumor cell survival in diffuse large B cell lymphoma. *The Journal of experimental medicine,* 212**,** 775-792.

SCHMIDT, M. H. H. & DIKIC, I. 2005. The Cbl interactome and its functions. *Nature Reviews Molecular Cell Biology,* 6**,** 907-918.

SCHMIDT, S., IRVING, J. A. E., MINTO, L., MATHESON, E., NICHOLSON, L., PLONER, A., PARSON, W., KOFLER, A., AMORT, M., ERDEL, M., HALL, A. & KOFLER, R. 2006. Glucocorticoid resistance in two key models of acute lymphoblastic leukemia occurs at the level of the glucocorticoid receptor. *The FASEB Journal,* 20**,** 2600-2602.

SCHRAPPE, M., HUNGER, S. P., PUI, C.-H., SAHA, V., GAYNON, P. S., BARUCHEL, A., CONTER, V., OTTEN, J., OHARA, A., VERSLUYS, A. B., ESCHERICH, G., HEYMAN, M., SILVERMAN, L. B., HORIBE, K., MANN, G., CAMITTA, B. M., HARBOTT, J., RIEHM, H., RICHARDS, S., DEVIDAS, M. & ZIMMERMANN, M. 2012. Outcomes after Induction Failure in Childhood Acute Lymphoblastic Leukemia. *New England Journal of Medicine,* 366**,** 1371-1381.

SEIBEL, N. L., STEINHERZ, P. G., SATHER, H. N., NACHMAN, J. B., DELAAT, C., ETTINGER, L. J., FREYER, D. R., MATTANO, L. A., HASTINGS, C. A., RUBIN, C. M., BERTOLONE, K., FRANKLIN, J. L., HEEREMA, N. A., MITCHELL, T. L., PYESMANY, A. F., LA, M. K., EDENS, C. & GAYNON, P. S. 2008. Early postinduction intensification therapy improves survival for children and adolescents with high-risk acute lymphoblastic leukemia: a report from the Children's Oncology Group. *Blood,* 111**,** 2548-2555.

SERIZAWA, H. 1998. Cyclin-dependent Kinase Inhibitor p16INK4A Inhibits Phosphorylation of RNA Polymerase II by General Transcription Factor TFIIH. *The Journal of biological chemistry,* 273**,** 5427-30.

SERRANO, M., HANNON, G. J. & BEACH, D. 1993. A new regulatory motif in cell-cycle control causing specific inhibition of cyclin D/CDK4. *Nature,* 366**,** 704-707.

SERRAVALLE, S., BERTUCCIO, S. N., ASTOLFI, A., MELCHIONDA, F. & PESSION, A. 2016. Synergistic Cytotoxic Effect of L-Asparaginase Combined with Decitabine as a Demethylating Agent in Pediatric T-ALL, with Specific Epigenetic Signature. *BioMed Research International,* 2016**,** 6.

SHALEM, O., SANJANA, N. E., HARTENIAN, E., SHI, X., SCOTT, D. A., MIKKELSON, T., HECKL, D., EBERT, B. L., ROOT, D. E., DOENCH, J. G. & ZHANG, F. 2014. Genome-scale CRISPR-Cas9 knockout screening in human cells. *Science,* 343**,** 84-87.

SHAPIRO, G. I., EDWARDS, C. D., KOBZIK, L., GODLESKI, J., RICHARDS, W., SUGARBAKER, D. J. & ROLLINS, B. J. 1995. Reciprocal Rb inactivation and p16INK4 expression in primary lung cancers and cell lines. *Cancer Res,* 55**,** 505-9.

SHAPOSHNIKOV, V. L. 1979. Distribution of bone marrow cells in the mouse skeleton. *Bulletin of Experimental Biology and Medicine,* 87**,** 510-512.

SHARMA, A., SINGH, K. & ALMASAN, A. 2012. Histone H2AX phosphorylation: a marker for DNA damage. *Methods Mol Biol,* 920**,** 613-26.

SHENG, X., TUCCI, J., PARMENTIER, J. H., JI, L., BEHAN, J. W., HEISTERKAMP, N. & MITTELMAN, S. D. 2016. Adipocytes cause leukemia cell resistance to daunorubicin via oxidative stress response. *Oncotarget,* 7**,** 73147-73159.

SHI, J., WANG, E., MILAZZO, J. P., WANG, Z., KINNEY, J. B. & VAKOC, C. R. 2015. Discovery of cancer drug targets by CRISPR-Cas9 screening of protein domains. *Nature biotechnology,* 33**,** 661-667.

SHULTZ, L. D., LYONS, B. L., BURZENSKI, L. M., GOTT, B., CHEN, X., CHALEFF, S., KOTB, M., GILLIES, S. D., KING, M., MANGADA, J., GREINER, D. L. & HANDGRETINGER, R. 2005. Human lymphoid and myeloid cell development in NOD/LtSz-scid IL2R gamma null mice engrafted with mobilized human hemopoietic stem cells. *J Immunol,* 174**,** 6477-89.

SILVEIRA, A. B., LARANJEIRA, A. B. A., RODRIGUES, G. O. L., LEAL, P. C., CARDOSO, B. A., BARATA, J. T., YUNES, R. A., ZANCHIN, N. I. T., BRANDALISE, S. R. & YUNES, J. A. 2015. PI3K

inhibition synergizes with glucocorticoids but antagonizes with methotrexate in T-cell acute lymphoblastic leukemia. *Oncotarget,* 6**,** 13105-13118.

SIMONIAN, P. L., GRILLOT, D. A. M. & NUÑEZ, G. 1997. Bcl-2 and Bcl-XL can differentially block chemotherapy-induced cell death. *Blood,* 90**,** 1208-1216.

SKOVSGAARD, T. 1978. Mechanism of Cross-Resistance between Vincristine and Daunorubicin in Ehrlich Ascites Tumor Cells. *Cancer Research,* 38**,** 4722-4727.

SMITH, M. A., CHOUDHARY, G. S., PELLAGATTI, A., CHOI, K., BOLANOS, L. C., BHAGAT, T. D., GORDON-MITCHELL, S., VON AHRENS, D., PRADHAN, K., STEEPLES, V., KIM, S., STEIDL, U., WALTER, M., FRASER, I. D. C., KULKARNI, A., SALOMONIS, N., KOMUROV, K., BOULTWOOD, J., VERMA, A. & STARCZYNOWSKI, D. T. 2019. U2AF1 mutations induce oncogenic IRAK4 isoforms and activate innate immune pathways in myeloid malignancies. *Nature Cell Biology,* 21**,** 640-650.

SMITH, M. A. & HOUGHTON, P. 2013. A Proposal Regarding Reporting of In Vitro Testing Results. *Clinical Cancer Research,* 19**,** 2828-2833.

STAMS, W. A., DEN BOER, M. L., HOLLEMAN, A., APPEL, I. M., BEVERLOO, H. B., VAN WERING, E. R., JANKA-SCHAUB, G. E., EVANS, W. E. & PIETERS, R. 2005. Asparagine synthetase expression is linked with L-asparaginase resistance in TEL-AML1-negative but not TEL-AML1-positive pediatric acute lymphoblastic leukemia. *Blood,* 105**,** 4223-5.

STROBER, W. 2001. Trypan blue exclusion test of cell viability. *Curr Protoc Immunol,* Appendix 3**,** Appendix 3B.

STYCZYNSKI, J., WYSOCKI, M., BALWIERZ, W., ROKICKA-MILEWSKA, R., MATYSIAK, M., BALCERSKA, A., KOWALCZYK, A., WACHOWIAK, J., SOŃTA-JAKIMCZYK, D. & CHYBICKA, A. 2002. In vitro comparative antileukemic activity of various glucocorticoids in childhood acute leukemia. *Neoplasma,* 49**,** 178-83.

STYCZYNSKI, J., WYSOCKI, M., DEBSKI, R., CZYZEWSKI, K., KOLODZIEJ, B., RAFINSKA, B., KUBICKA, M., KOŁTAN, S., KOLTAN, A., POGORZALA, M., KURYLAK, A., OLSZEWSKA-SŁONINA, D., BALWIERZ, W., JURASZEWSKA, E., WIECZOREK, M., OLEJNIK, I., KRAWCZUK-RYBAK, M., KUZMICZ, M., KOWALCZYK, J. & MACIEJKA-KAPUŚCIŃSKA, L. 2007a. Predictive value of multidrug resistance proteins and cellular drug resistance in childhood relapsed acute lymphoblastic leukemia. *Journal of cancer research and clinical oncology,* 133**,** 875-93.

STYCZYNSKI, J., WYSOCKI, M., DEBSKI, R., CZYZEWSKI, K., KOLODZIEJ, B., RAFINSKA, B., KUBICKA, M., KOLTAN, S., KOLTAN, A., POGORZALA, M., KURYLAK, A., OLSZEWSKA-SLONINA, D., BALWIERZ, W., JURASZEWSKA, E., WIECZOREK, M., OLEJNIK, I., KRAWCZUK-RYBAK, M., KUZMICZ, M., KOWALCZYK, J., STEFANIAK, J., BADOWSKA, W., SONTA-JAKIMCZYK, D., SZCZEPANSKI, T., MATYSIAK, M., MALINOWSKA, I. & STANCZAK, E. 2007b. Predictive value of multidrug resistance proteins and cellular drug resistance in childhood relapsed acute lymphoblastic leukemia. *Journal of Cancer Research and Clinical Oncology,* 133**,** 875-893.

SU, H., HU, J., HUANG, L., YANG, Y., THENOZ, M., KUCHMIY, A., HU, Y., LI, P., FENG, H., ZHOU, Y., TAGHON, T., VAN VLIERBERGHE, P., QING, G., CHEN, Z. & LIU, H. 2018. SHQ1 regulation of RNA splicing is required for T-lymphoblastic leukemia cell survival. *Nature Communications,* 9**,** 4281.

SU, H., HU, Y., JIANG, J., CHEN, Z. & LIU, H. 2016. SHQ1 Regulates MYC mRNA Splicing and Promotes T Cell Leukemogenesis. *Blood,* 128**,** 440-440.

SU, N., PAN, Y. X., ZHOU, M., HARVEY, R. C., HUNGER, S. P. & KILBERG, M. S. 2008. Correlation between asparaginase sensitivity and asparagine synthetase protein content, but not mRNA, in acute lymphoblastic leukemia cell lines. *Pediatr Blood Cancer,* 50**,** 274-9.

SUN, S. C. 2010. CYLD: a tumor suppressor deubiquitinase regulating NF-kappaB activation and diverse biological processes. *Cell Death Differ,* 17**,** 25-34.

SUI, H., FAN, Z. Z. & LI, Q. 2012. Signal transduction pathways and transcriptional mechanisms of ABCB1/Pgp-mediated multiple drug resistance in human cancer cells. *The Journal of international medical research,* 40**,** 426-435.

SUZUKI, A., DE LA POMPA, J. L., STAMBOLIC, V., ELIA, A. J., SASAKI, T., DEL BARCO BARRANTES, I., HO, A., WAKEHAM, A., ITIE, A., KHOO, W., FUKUMOTO, M. & MAK, T. W. 1998. High cancer susceptibility and embryonic lethality associated with mutation of the PTEN tumor suppressor gene in mice. *Curr Biol,* 8**,** 1169-78.

SWERDLOW, S., MCCOLL, K., RONG, Y., LAM, M., GUPTA, A. & DISTELHORST, C. W. 2008. Apoptosis inhibition by Bcl-2 gives way to autophagy in glucocorticoid-treated lymphocytes. *Autophagy,* 4**,** 612-620.

SZYMANSKA, B., WILCZYNSKA-KALAK, U., KANG, M. H., LIEM, N. L. M., CAROL, H., BOEHM, I., GROEPPER, D., REYNOLDS, C. P., STEWART, C. F. & LOCK, R. B. 2012a. Pharmacokinetic modeling of an induction regimen for in vivo combined testing of novel drugs against pediatric acute lymphoblastic leukemia xenografts. *PloS one,* 7**,** e33894-e33894.

SZYMANSKA, B., WILCZYNSKA-KALAK, U., KANG, M. H., LIEM, N. L. M., CAROL, H., BOEHM, I., GROEPPER, D., REYNOLDS, C. P., STEWART, C. F. & LOCK, R. B. 2012b. Pharmacokinetic Modeling of an Induction Regimen for In Vivo Combined Testing of Novel Drugs against Pediatric Acute Lymphoblastic Leukemia Xenografts. *PLOS ONE,* 7**,** e33894.

TAHK, S., LIU, B., CHERNISHOF, V., WONG, K. A., WU, H. & SHUAI, K. 2007. Control of specificity and magnitude of NF-κB and STAT1-mediated gene activation through PIASy and PIAS1 cooperation. *Proceedings of the National Academy of Sciences,* 104**,** 11643-11648.

TALLEN, G., RATEI, R., MANN, G., KASPERS, G., NIGGLI, F., KARACHUNSKY, A., EBELL, W., ESCHERICH, G., SCHRAPPE, M., KLINGEBIEL, T., FENGLER, R., HENZE, G. & VON STACKELBERG, A. 2010. Long-Term Outcome in Children With Relapsed Acute Lymphoblastic Leukemia After Time-Point and Site-of-Relapse Stratification and Intensified Short-Course Multidrug Chemotherapy: Results of Trial ALL-REZ BFM 90. *Journal of Clinical Oncology,* 28**,** 2339-2347.

TAN, T. K., ZHANG, C. & SANDA, T. 2019. Oncogenic transcriptional program driven by TAL1 in T-cell acute lymphoblastic leukemia. *International Journal of Hematology,* 109**,** 5-17.

TASIAN, S. K., BORNHAUSER, M. & RUTELLA, S. 2018. Targeting Leukemia Stem Cells in the Bone Marrow Niche. *Biomedicines,* 6.

TEICHER, B. A. & FRICKER, S. P. 2010. CXCL12 (SDF-1)/CXCR4 pathway in cancer. *Clin Cancer Res,* 16**,** 2927-31.

TEUFFEL, O., KUSTER, S. P., HUNGER, S. P., CONTER, V., HITZLER, J., ETHIER, M. C., SHAH, P. S., BEYENE, J. & SUNG, L. 2011. Dexamethasone versus prednisone for induction therapy in childhood acute lymphoblastic leukemia: a systematic review and meta-analysis. *Leukemia,* 25**,** 1232.

THOMPSON, B. J., BUONAMICI, S., SULIS, M. L., PALOMERO, T., VILIMAS, T., BASSO, G., FERRANDO, A. & AIFANTIS, I. 2007. The SCFFBW7 ubiquitin ligase complex as a tumor suppressor in T cell leukemia. *The Journal of experimental medicine,* 204**,** 1825-1835.

THOMPSON, P., WHEELER, H. E., DELANEY, S. M., LORIER, R., BROECKEL, U., DEVIDAS, M., REAMAN, G. H., SCORSONE, K., SUNG, L., DOLAN, M. E. & BERG, S. L. 2014. Pharmacokinetics and pharmacogenomics of daunorubicin in children: a report from the Children's Oncology Group. *Cancer chemotherapy and pharmacology,* 74**,** 831-838.

TOMLINSON, E. S., LEWIS, D. F. V., MAGGS, J. L., KROEMER, H. K., PARK, B. K. & BACK, D. J. 1997. In vitro metabolism of dexamethasone (DEX) in human liver and kidney: The involvement of CYP3a4 and CYP17 (17,20 LYASE) and molecular modelling studies. *Biochemical Pharmacology,* 54**,** 605-611.

TOSELLO, V. & FERRANDO, A. A. 2013. The NOTCH signaling pathway: role in the pathogenesis of T-cell acute lymphoblastic leukemia and implication for therapy. *Therapeutic advances in hematology,* 4**,** 199-210.

TOUZART, A., LENGLINÉ, E., LATIRI, M., BELHOCINE, M., SMITH, C., THOMAS, X., SPICUGLIA, S., PUTHIER, D., PFLUMIO, F., LEGUAY, T., GRAUX, C., CHALANDON, Y., HUGUET, F., LEPRÊTRE, S., IFRAH, N., DOMBRET, H., MACINTYRE, E., HUNAULT, M., BOISSEL, N. & ASNAFI, V. 2019. Epigenetic Silencing Affects l-Asparaginase Sensitivity and Predicts Outcome in T-ALL. *Clinical Cancer Research,* 25**,** 2483-2493.

TOWNSEND, D. M. & TEW, K. D. 2003. The role of glutathione-S-transferase in anti-cancer drug resistance. *Oncogene,* 22**,** 7369-7375.

TRAGGIAI, E., CHICHA, L., MAZZUCCHELLI, L., BRONZ, L., PIFFARETTI, J.-C., LANZAVECCHIA, A. & MANZ, M. G. 2004. Development of a Human Adaptive Immune System in Cord Blood Cell-Transplanted Mice. *Science,* 304**,** 104-107.

TSHERNIAK, A., VAZQUEZ, F., MONTGOMERY, P. G., WEIR, B. A., KRYUKOV, G., COWLEY, G. S., GILL, S., HARRINGTON, W. F., PANTEL, S., KRILL-BURGER, J. M., MEYERS, R. M., ALI, L., GOODALE, A., LEE, Y., JIANG, G., HSIAO, J., GERATH, W. F. J., HOWELL, S., MERKEL, E., GHANDI, M., GARRAWAY, L. A., ROOT, D. E., GOLUB, T. R., BOEHM, J. S. & HAHN, W. C. 2017. Defining a Cancer Dependency Map. *Cell,* 170**,** 564-576.e16.

UEDA, K., OKAMURA, N., HIRAI, M., TANIGAWARA, Y., SAEKI, T., KIOKA, N., KOMANO, T. & HORI, R. 1992. Human P-glycoprotein transports cortisol, aldosterone, and dexamethasone, but not progesterone. *J Biol Chem,* 267**,** 24248-52.

UENO, T., OHTAWA, K., MITSUI, K., KODERA, Y., HIROTO, M., MATSUSHIMA, A., INADA, Y. & NISHIMURA, H. 1997. Cell cycle arrest and apoptosis of leukemia cells induced by L-asparaginase. *Leukemia,* 11**,** 1858-61.

URBANIK, T., KOEHLER, B. C., JOHANNA BOGER, R., ALEXANDER WÖRNS, M., HEEGER, S., OTTO, G., HÖVELMEYER, N., ROBERT GALLE, P., SCHUCHMANN, M., WAISMAN, A. & SCHULZE-BERGKAMEN, H. 2011. Down-regulation of CYLD as a trigger for NF-κB activation and a mechanism of apoptotic resistance in hepatocellular carcinoma cells. *International journal of oncology,* 38**,** 121-31.

VAN DER ZWET, J. C. G., CORDO, V., CANTE-BARRETT, K. & MEIJERINK, J. P. P. 2019. Multi-omic approaches to improve outcome for T-cell acute lymphoblastic leukemia patients. *Adv Biol Regul,* 74**,** 100647.

VAN TELLINGEN, O., BUCKLE, T., JONKER, J. W., VAN DER VALK, M. A. & BEIJNEN, J. H. 2003. P-glycoprotein and Mrp1 collectively protect the bone marrow from vincristine-induced toxicity in vivo. *British Journal of Cancer,* 89**,** 1776-1782.

VILIMAS, T., MASCARENHAS, J., PALOMERO, T., MANDAL, M., BUONAMICI, S., MENG, F., THOMPSON, B., SPAULDING, C., MAKAROUN, S., ALEGRE, M.-L., L KEE, B., FERRANDO, A., MIELE, L. & AIFANTIS, I. 2007. Targeting the NF-κB signaling pathway in Notch1-induced T-cell leukemia. *Nature medicine,* 13**,** 70-7.

VORA, A., GOULDEN, N., MITCHELL, C., HANCOCK, J., HOUGH, R., ROWNTREE, C., MOORMAN, A. V. & WADE, R. 2014. Augmented post-remission therapy for a minimal residual disease-defined high-risk subgroup of children and young people with clinical standard-risk and intermediate-risk acute lymphoblastic leukaemia (UKALL 2003): a randomised controlled trial. *The Lancet Oncology,* 15**,** 809-818.

VORA, A., GOULDEN, N., WADE, R., MITCHELL, C., HANCOCK, J., HOUGH, R., ROWNTREE, C. & RICHARDS, S. 2013. Treatment reduction for children and young adults with low-risk acute lymphoblastic leukaemia defined by minimal residual disease (UKALL 2003): a randomised controlled trial. *The Lancet Oncology,* 14**,** 199-209.

WAIBEL, M., SOLOMON, V. S., KNIGHT, D. A., RALLI, R. A., KIM, S.-K., BANKS, K.-M., VIDACS, E., VIRELY, C., SIA, K. C. S., BRACKEN, L. S., COLLINS-UNDERWOOD, R., DRENBERG, C., RAMSEY, L. B., MEYER, S. C., TAKIGUCHI, M., DICKINS, R. A., LEVINE, R., GHYSDAEL, J., DAWSON, M. A., LOCK, R. B., MULLIGHAN, C. G. & JOHNSTONE, R. W. 2013. Combined targeting of JAK2 and Bcl-2/Bcl-xL to cure mutant JAK2-driven malignancies and overcome acquired resistance to JAK2 inhibitors. *Cell reports,* 5**,** 1047-1059.

WANG, C.-Y., MAYO, M. W. & BALDWIN, A. S. 1996. TNF- and Cancer Therapy-Induced Apoptosis: Potentiation by Inhibition of NF-κB. *Science,* 274**,** 784-787.

WANG, C., WANG, G., FENG, X., SHEPHERD, P., ZHANG, J., TANG, M., CHEN, Z., SRIVASTAVA, M., MCLAUGHLIN, M. E., NAVONE, N. M., HART, G. T. & CHEN, J. 2019. Genome-wide CRISPR screens reveal synthetic lethality of RNASEH2 deficiency and ATR inhibition. *Oncogene,* 38**,** 2451-2463.

WANG, X., JIN, D.-Y., WONG, H. L., FENG, H., WONG, Y.-C. & TSAO, S. W. 2003. MAD2-induced sensitization to vincristine is associated with mitotic arrest and Raf/Bcl-2 phosphorylation in nasopharyngeal carcinoma cells. *Oncogene,* 22**,** 109-116.

WANG, Y., XIE, Y. & OUPICKÝ, D. 2016. Potential of CXCR4/CXCL12 Chemokine Axis in Cancer Drug Delivery. *Current Pharmacology Reports,* 2**,** 1-10.

WENG, A. P., FERRANDO, A. A., LEE, W., MORRIS, J. P., SILVERMAN, L. B., SANCHEZ-IRIZARRY, C., BLACKLOW, S. C., LOOK, A. T. & ASTER, J. C. 2004a. Activating Mutations of NOTCH1 in Human T Cell Acute Lymphoblastic Leukemia. *Science,* 306**,** 269-271.

WENG, A. P., FERRANDO, A. A., LEE, W., MORRIS, J. P. T., SILVERMAN, L. B., SANCHEZ-IRIZARRY, C., BLACKLOW, S. C., LOOK, A. T. & ASTER, J. C. 2004b. Activating mutations of NOTCH1 in human T cell acute lymphoblastic leukemia. *Science,* 306**,** 269-71.

WHITEHURST, A. W., BODEMANN, B. O., CARDENAS, J., FERGUSON, D., GIRARD, L., PEYTON, M., MINNA, J. D., MICHNOFF, C., HAO, W., ROTH, M. G., XIE, X.-J. & WHITE, M. A. 2007. Synthetic lethal screen identification of chemosensitizer loci in cancer cells. *Nature,* 446**,** 815.

WILLIMOTT, S., MERRIAM, T. & WAGNER, S. D. 2011. Apoptosis induces Bcl-XS and cleaved Bcl-XL in chronic lymphocytic leukaemia. *Biochemical and Biophysical Research Communications,* 405**,** 480-485.

WINTER, S. S., DUNSMORE, K. P., DEVIDAS, M., WOOD, B. L., ESIASHVILI, N., CHEN, Z., EISENBERG, N., BRIEGEL, N., HAYASHI, R. J., GASTIER-FOSTER, J. M., CARROLL, A. J., HEEREMA, N. A., ASSELIN, B. L., GAYNON, P. S., BOROWITZ, M. J., LOH, M. L., RABIN, K. R., RAETZ, E. A., ZWEIDLER-MCKAY, P. A., WINICK, N. J., CARROLL, W. L. & HUNGER, S. P. 2018. Improved Survival for Children and Young Adults With T-Lineage Acute Lymphoblastic Leukemia: Results From the Children's Oncology Group AALL0434 Methotrexate Randomization. *J Clin Oncol,* 36**,** 2926-2934.

WINTER, S. S., RICCI, J., LUO, L., LOVATO, D. M., KHAWAJA, H. M., SERNA-GALLEGOS, T., DEBASSIGE, N. & LARSON, R. S. 2013. ATP Binding Cassette C1 (ABCC1/MRP1)-mediated drug efflux contributes to disease progression in T-lineage acute lymphoblastic leukemia. *Health,* 5**,** 41-50.

WOJCIK, C. 1999. Proteasomes in apoptosis: villains or guardians? *Cell Mol Life Sci,* 56**,** 908-17.

WOO, M. H., HAK, L. J., STORM, M. C., EVANS, W. E., SANDLUND, J. T., RIVERA, G. K., WANG, B., PUI, C. H. & RELLING, M. V. 1998. Anti-asparaginase antibodies following E. coli asparaginase therapy in pediatric acute lymphoblastic leukemia. *Leukemia,* 12**,** 1527-33.

WORKMAN, P., ABOAGYE, E. O., BALKWILL, F., BALMAIN, A., BRUDER, G., CHAPLIN, D. J., DOUBLE, J. A., EVERITT, J., FARNINGHAM, D. A. H., GLENNIE, M. J., KELLAND, L. R., ROBINSON, V., STRATFORD, I. J., TOZER, G. M., WATSON, S., WEDGE, S. R., ECCLES, S. A. & AN AD HOC COMMITTEE OF THE NATIONAL CANCER RESEARCH, I. 2010. Guidelines for the welfare and use of animals in cancer research. *British Journal Of Cancer,* 102**,** 1555.

WU, G., LYAPINA, S., DAS, I., LI, J., GURNEY, M., PAULEY, A., CHUI, I., DESHAIES, R. J. & KITAJEWSKI, J. 2001. SEL-10 is an inhibitor of notch signaling that targets notch for ubiquitin-mediated protein degradation. *Molecular and cellular biology,* 21**,** 7403-7415.

WU, J., SALVA, K. A. & WOOD, G. S. 2015. c-CBL E3 ubiquitin ligase is overexpressed in cutaneous T-cell lymphoma: its inhibition promotes activation-induced cell death. *J Invest Dermatol,* 135**,** 861-868.

XIRODIMAS, D. P., CHISHOLM, J., DESTERRO, J. M. S., LANE, D. P. & HAY, R. T. 2002. P14ARF promotes accumulation of SUMO-1 conjugated (H)Mdm2. *FEBS Letters,* 528**,** 207-211.

YAMAGUCHI, H., HSU, J. & HUNG, M.-C. 2012. Regulation of Ubiquitination-Mediated Protein Degradation by Survival Kinases in Cancer. *Frontiers in Oncology,* 2.

YANG, L., PANETTA, J. C., CAI, X., YANG, W., PEI, D., CHENG, C., KORNEGAY, N., PUI, C.-H. & RELLING, M. V. 2008. Asparaginase May Influence Dexamethasone Pharmacokinetics in Acute Lymphoblastic Leukemia. *Journal of Clinical Oncology,* 26**,** 1932-1939.

YIN, L., LIU, S., LI, C., DING, S., BI, D., NIU, Z., HAN, L., LI, W., GAO, D., LIU, Z. & LU, J. 2016. CYLD downregulates Livin and synergistically improves gemcitabine chemosensitivity and decreases migratory/invasive potential in bladder cancer: the effect is autophagy-associated. *Tumour Biol,* 37**,** 12731-12742.

ZHANG, C., COOPER, D. E., GREVENGOED, T. J., LI, L. O., KLETT, E. L., EATON, J. M., HARRIS, T. E. & COLEMAN, R. A. 2014. Glycerol-3-phosphate acyltransferase-4-deficient mice are protected from diet-induced insulin resistance by the enhanced association of mTOR and rictor. *Am J Physiol Endocrinol Metab,* 307**,** E305-15.

ZHANG, Y., YANG, S.-H. & GUO, X.-L. 2017. New insights into Vinca alkaloids resistance mechanism and circumvention in lung cancer. *Biomedicine & Pharmacotherapy,* 96**,** 659-666.

ZLOTNIK, A. & YOSHIE, O. 2000. Chemokines: a new classification system and their role in immunity. *Immunity,* 12**,** 121-7.

ZONCU, R., EFEYAN, A. & SABATINI, D. M. 2010. mTOR: from growth signal integration to cancer, diabetes and ageing. *Nature Reviews Molecular Cell Biology,* 12**,** 21.

ZUURBIER, L., PETRICOIN, E. F., 3RD, VUERHARD, M. J., CALVERT, V., KOOI, C., BUIJS-GLADDINES, J. G. C. A. M., SMITS, W. K., SONNEVELD, E., VEERMAN, A. J. P., KAMPS, W. A., HORSTMANN, M., PIETERS, R. & MEIJERINK, J. P. P. 2012. The significance of PTEN and AKT aberrations in pediatric T-cell acute lymphoblastic leukemia. *Haematologica,* 97**,** 1405-1413.

ZWAAN, C. M., KOWALCZYK, J., SCHMITT, C., BIELORAI, B., RUSSO, M. W., WOESSNER, M., RANGANATHAN, S. & LEVERGER, G. 2017. Safety and efficacy of nelarabine in children and young adults with relapsed or refractory T-lineage acute lymphoblastic leukaemia or T-lineage lymphoblastic lymphoma: results of a phase 4 study. *British Journal of Haematology,* 179**,** 284-293.